Design, Scale-up and Optimization of Double Emulsion Processes

Behnam Khadem Hamedani

▶ To cite this version:

THESE de DOCTORAT DE L'UNIVERSITE DE LYON
opérée au sein de
Université Claude Bernard Lyon 1

Ecole Doctorale N° ED 206
(ECOLE DOCTORALE DE CHIMIE)

Spécialité de doctorat : Génie des procédés
Discipline : (Génie des procédés)

Soutenue publiquement le 15/07/2019, par :
Behnam KHADEM-HAMEDANI

Design, Scale-up and Optimization of Double Emulsion Processes

Devant le jury composé de :

BOLZINGER, Marie-Alexandrine, Professor, Université Claude Bernard Lyon 1, Présidente

NOPENS, Ingmar, Professor, Ghent University, Rapporteur

MORCHAIN, Jérôme, Maître de Conférences, INSA Toulouse, Rapporteur

LIAN, Guoping, Professor, University of Surrey, Examinateur

SHEIBAT – OTHMAN, Nida, Directrice de Recherche CNRS, Université Claude Bernard Lyon 1, Directrice de thèse

Acknowledgements

The culmination of the journey of PhD, climbing the high peak of which required encouragement, difficulty, learning, trust and frustration, is a thesis with one's name on the top while it wouldn't be accessible without the help and support of a great many people to whom this page is devoted.

The first and foremost gratitude is for my supervisor, Dr. Nida SHEIBAT-OTHMAN, who entrusted me since the first day of this PhD. I am indebted to her for the great support and encouragement I received in every moment of this challenging project. Her immense knowledge, motivation and patience have given me more power and spirit to excel in this research. The interesting and long-lasting scientific chats having made this PhD achievable are hard to forget throughout my life.

I would like to express my gratitude to Prof. Marie-Alexandrine BOLZINGER for giving the encouragement and sharing insightful suggestions since the first thesis evaluation to the defense.

I would like to thank Prof. Guoping LIAN (Unilever) who has assessed my work since the beginning and has provided me with invaluable advices and remarks.

I am pleased to thank Dr. Jérôme MORCHAIN (INSA de Toulouse) for accepting the evaluation of my PhD work and making my dissertation stronger.

This is of my pleasure to thank Prof. Ingmar NOPENS (Ghent University) for his assessment of my PhD work to make a more valuable thesis.

Many thanks to Dr. Yves CHEVALIER for everyday chats and guidance that helped me throughout the PhD research and in writing the thesis.

Saying thanks to Dr. Adel MHAMDI is a pleasure for guiding and supporting me at RWTH Aachen university. I am grateful to thank Dr. Mahir OZDEMIR and Dr. Sami Othman for their encouragement and support.

A special "thank you" to Dr. Giovanna LOLLO for her every encouragement. Another "thank you" to Dr. Noureddine LEBAZ for the interesting scientific conversations. I am also glad to thank Nadia CHAPEL for her support and for being such a nice person.

I wish to express the gratitude to rest of the team both at LAGEPP and ModLife: Prof. Stéphanie BRIANCON, Dr. Claire BORDES, Prof. Gürkan SIN, Prof. Alexander MITSOS, Prof. Krist GERNAEY, Géraldine, Quentin, Jean-Pierre and Sebastien.

I won't forget to thank my dear friends who helped me in all aspects. I wish I could write about each of them one by one, but it would make another complete PhD manuscript. So, for all the inspiration, happiness, and support that they have brought about for me, I deeply thank Denise, Margaux, Pedro, Francisco, Annalisa, Mohamad, Saeed, Behnaz, Amid, Mina, Shabnam, Payam, Sabrina, Sabrine, Manis, Geoffrey Alexis, Andrea, Joël, Océan, Eduardo, Frederico, Simon, Joris, Daniele, Amenda, Chryssa, Romain, Laura, Maya, Marouane, Antonio, Mark, Lukasz, Sasha, Sonia and Soheil.

I am always grateful to my parents, brother and sister who support me through all ups and downs of life, no matter what. Being here at this point is undoubtedly thanks to them.

Words would never say how grateful I am to my fantastic wife, Elena, for her love, constant support, and understanding which have helped me to stand at this point.

Summary

Double emulsions can nowadays be found in a number of applications in different domains, like food, cosmetics, chemicals or biochemical. In food for instance, double emulsions may allow to encapsulate flavors or reduce the fat content. Yet, the literature is still lacking a comprehensive understanding of these systems. Modelling may improve the understanding of a system and allow optimizing the operating conditions in order to improve the product quality. In these systems, the product quality is determined by the encapsulation efficiency and the inner and outer droplet size distribution, which may affect the physical stability during storage. The objective of this work is to handle theoretical and experimental investigations of the phenomena occurring during both the preparation and the storage of double emulsions. The contribution of the work can therefore be divided into two parts. First of all, investigations of the parameters affecting the preparation step of double emulsions are handled, and models are proposed to describe them. Three processes were considered for the emulsification of the double emulsions, ultrasonication, Ultra-Turrax and a stirred vessel. The model is based on a population balance model of the outer droplets, including the kernels of breakage and coalescence combined with a leakage model of the inner droplets. The leakage of inner droplets is assumed to be governed by the breakage of the outer droplets. In order to be applicable in the different processes, the breakage models were adapted to different scales of turbulence, the dissipation subrange for ultrasonication and the inertial subrange for the Ultra-Turrax. The second contribution of the work concerns the investigation of the phenomena taking place during the storage of the double emulsions, including swelling and release. In this case, two population balance models of the inner and outer droplets were considered, including the phenomena of swelling of the inner, and so of the outer, droplets as well as the escape of the inner droplets by diffusion and coalescence with the external continuous phase. The swelling model takes into account the Laplace pressure that counterbalances the osmotic pressure which is the driving force for swelling. In the different steps of preparation or storage, the developed models allow the prediction of the droplet size distributions and the release rate.

De nos jours, les émulsions doubles se trouvent dans de nombreuses applications dans différents domaines, tels que le domaine alimentaire, les produits cosmétiques, les produits chimiques ou biochimiques. Dans les produits alimentaires par exemple, les émulsions doubles peuvent permettre d'encapsuler des arômes ou de réduire la teneur en matières grasses. La littérature manque cependant de compréhension globale de ces systèmes. La modélisation peut améliorer la compréhension d'un système et permettre d'optimiser les conditions de fonctionnement afin d'améliorer la qualité du produit. Dans ces systèmes, la qualité du produit est déterminée par l'efficacité de l'encapsulation et la distribution de la taille des gouttes internes et externes, qui peuvent affecter la stabilité physique pendant le stockage. L'objectif de ce travail est de réaliser une étude théorique et expérimentale approfondie des phénomènes intervenant à la fois lors de la préparation et du stockage des émulsions doubles. La contribution du travail peut donc être divisée en deux parties. Dans un premier temps, nous étudions les paramètres affectant l'étape de préparation des émulsions doubles et nous proposons des modèles pour les décrire. Trois procédés ont été considérés pour l'émulsification des émulsions doubles, l'ultra-sonication, l'Ultra-Turrax et un réacteur agité. Le modèle est basé sur un modèle de bilan de population des gouttelettes externes, incluant les phénomènes de rupture et de coalescence, associé à un modèle de relargage des gouttes internes. Le relargage des gouttes internes est supposé être régi par la rupture des gouttes externes. Pour être applicables aux différents procédés, les modèles de rupture ont été adaptés aux différentes échelles de turbulence, de dissipation pour ultra-sonication et inertielle pour Ultra-Turrax. La deuxième contribution de ce travail concerne l'étude des phénomènes ayant lieu lors du stockage des émulsions doubles, notamment le gonflement et le relargage des gouttes. Dans ce cas, deux modèles de bilan de population des gouttelettes internes et externes ont été développés, comprenant les phénomènes de gonflement des gouttelettes internes, et donc externes, ainsi que le relagage des gouttelettes internes par diffusion et coalescence avec la phase continue externe. Le modèle de gonflement prend en compte la pression de Laplace qui contrebalance le gradient de pression osmotique et arrête le gonflement. Dans les différentes étapes de préparation ou de stockage, les modèles développés permettent de prédire les distributions de la taille des gouttelettes et le taux de libération.

Contents

Introduction

Double emulsions are emulsions in which the dispersed phase itself is an emulsion. They are used in a wide range of domains including foods, cosmetics, pharmaceutical, chemical, petrochemical, polymer, and wastewater treatment. The quality of the final product is controlled by the inner and outer droplet size and the encapsulation efficiency. These properties are function of the process parameters, including the viscosities and densities of the different phases, the fractions of the different phases (internal phase, primary emulsion, and encapsulated substance) and the dispersing energy and duration. Developing a model that relates these operating conditions to the product quality is essential in order to allow for a better comprehension of the phenomena taking place during preparation and storage, and to be able to optimize the product quality.

Due to the wide size of the inner and outer droplets, the approach of population balance models (PBMs) are employed in this work. These models describe the different phenomena taking place during preparation and storage and allow the prediction of the inner and outer droplet size and the release rate. Different mixing devices were considered: ultrasonication, rotor-stators and stirred vessels, and the models were adapted to the different scales of turbulence. Indeed, emulsification in ultrasonication takes place in the dissipation subrange while the emulsification in the rotor-stator or the stirred vessel is mainly taking place in the inertial subrange of turbulence.

In the first chapter, an overview of the whole work is given, with an introduction to double emulsions and the phenomena that may take place during preparation and storage. The chapter includes an experimental section with the choice of materials and devices.

The second chapter is related to the preparation of dilute water-in-oil-in water (W/O/W) double emulsions (1 %) in a stirred vessel. This chapter is mainly experimental, with an extensive review of the literature related to the preparation and stability investigations of double emulsions. Monitoring the release and the swelling rates during preparation and storage was handled to highlight the key process parameters (namely, the emulsification time, stirring rate, the fractions of primary emulsion, internal phase and salt) affecting the encapsulation efficiency and the double emulsion stability. This is done using *in situ* online video and conductivity probes that were inserted into the vessel combined to offline measurements like granulometry and optical microscopy. During preparation, the outer droplets undergo breakage and coalescence, but Ostwald ripening is negligible in this system. The main cause of release is found to be the breakage of the outer droplets, since molecular diffusion is slow due to the low solubility of salt in oil. During storage, the release is found to be governed by inner droplet escape, i.e. by coalescence with the external phase through the surface of the outer droplets. Negligible inner-inner or outer-outer droplet coalescence occurs during storage in this system, but the droplets swell due to the osmotic gradient between the internal and external water phases, which increases their size. This leads to overswelling-breakdown which causes breakage of the outer droplets and an abrupt release of the inner droplets.

The third chapter is related to modelling the preparation of double emulsions under high shear stirring (rotor-stator) in the turbulent inertial subrange, with more concentrated double emulsions (10 %). The PBM of the outer droplets, including the breakage and coalescence kernels, is coupled with a novel leakage model of the inner droplets. The leakage is defined as the release of inner droplets due to the breakage of the outer droplets. The breakage kernel of Alopaeus et al. [1] and the coalescence kernel of Coulaloglou and Tavlarides [2] were incorporated into the outer PBM using the apparent viscosity and density of the outer droplets (i.e. the properties that account for the presence of inner droplets). The modelling results were validated with the experimental data under different ranges of parameter variations (internal phase fraction, stirring rate and emulsification time).

In the fourth chapter, modelling the preparation of double emulsions using ultrasonication is considered. Due to the fast process, equilibrium correlations were considered rather than transient PBMs. Two different comprehensive correlations were developed to predict the mean diameter of the outer droplets in the dissipation subrange of turbulence, based on Taylor [3,4] and Hinze [5] approaches. The effect of salt, which is specific to double emulsions, and the effect of time were incorporated in these correlations. A model connecting the leakage to the droplet size is proposed as well. Indeed, similarly to emulsification in the rotor-stator (chapter three), the release is assumed to be mainly due to the breakage of the outer droplets. The results were validated by the experimental data where both the internal and external emulsions were prepared by ultrasound emulsification.

In chapter five, modelling the evolution of the double emulsions during storage is considered. In this chapter, two coupled PBMs of the inner and outer droplets were developed. While during preparation the main phenomena taking place are droplet breakage, coalescence and leakage (i.e., escape due to breakage), during storage the main phenomena taking place are inner (and so outer) droplet swelling and inner droplet escape. Sub-models describing these phenomena are therefore inserted in the PBMs, based on the permeability model of membranes to describe the swelling and the dewetting model of Kang et al. [6] to describe the frequency of inner droplet escape. In this case, a coupled inner-outer 2-PBM approach is necessary. The model allows the prediction of the size distribution of the inner and outer droplets as well as the release rate, until the onset of the overswelling-breakdown phenomenon.

Chapter six is related to inner droplet size measurement using the pulsed field gradient nuclear magnetic resonance (PFG-NMR) technique and by employing the Gaussian phase distribution (GPD) approach. An improvement is proposed by using a bimodal lognormal distribution instead of a monomodal distribution. The results are compared to the swelling model results (chapter five) during storage of double emulsion. Conclusions and perspectives of the work are presented after the main chapters.

Three appendices are available. Appendix one is about modelling pure escape in a silicone oil double emulsion during storage for different conditions: viscosity of the oil phase and size of the inner and outer droplets. Appendix two presents the analytical solution of the dewetting model of Kang et al. [1], which is used to determine the escape time in this study. Appendix

three is a short summary describing the interest of using dynamic optimization to optimize the product properties by manipulating the operating conditions.

Chapter 1. Overview

1.1. Double emulsions

Water-in-oil-in-water (W/O/W) or oil-in-water-in-oil (O/W/O) are the two major types of double emulsions. They appear in a wide range of domains including foods, cosmetics, pharmaceutical, chemical, petrochemical, polymer, and wastewater treatment. Some applications of double emulsions are low-fat food products [7], drug delivery [8], compounds extraction [9].

Double emulsions were firstly observed by Seifriz et al. (1925) [10]. While there have been some attempts to produce double emulsions in one-step, the most common way of their preparation is the two-step method [11]. The two-step method was introduced independently by Li (1968) [12] as liquid membranes for extraction processes, and by Matsumoto et al. (1976) [13] for the formation of double emulsions. As shown in Fig. 1.1, this method consists of the preparation of a first simple emulsion (i.e., primary emulsion) under high energy to produce small size inner (also called micro-) droplets in a first step. Then, this primary emulsion is dispersed in an external phase under a lower energy to prevent the release of the internal phase which leads to the production of bigger outer droplets (also called macro-droplets or globules) [14,15].
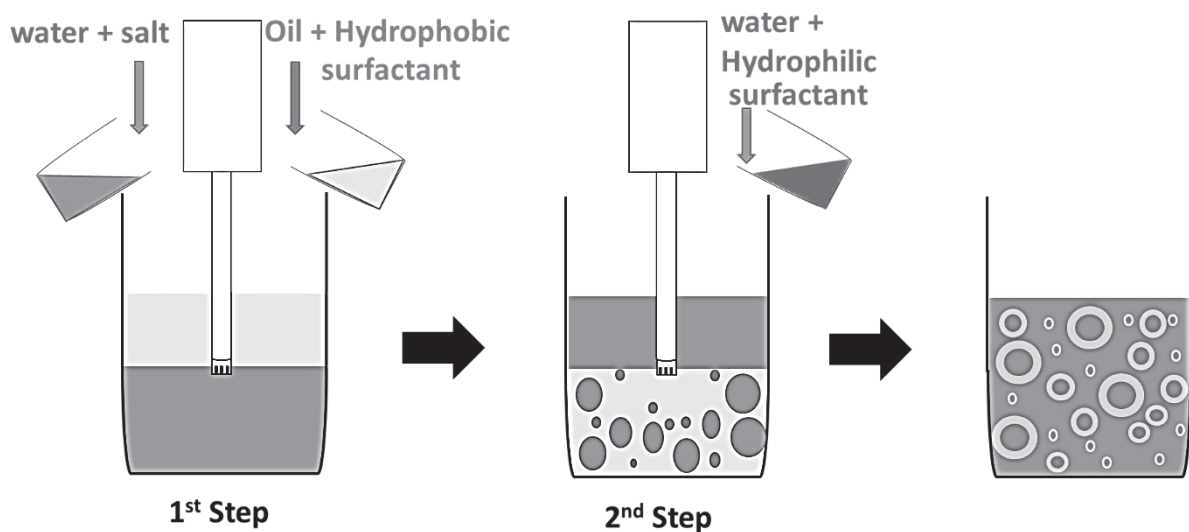
Fig. 1.1. *Double emulsion preparation by the two-step method.*

The quality of the final product in double emulsions, such as shelf stability and physical appearance, is controlled by the inner and outer droplet size distribution and the encapsulation efficiency, which themselves are function of the process parameters including the viscosities, densities, the fraction of the internal phase, the fraction of the primary emulsion, the fraction of the encapsulated substance (e.g., salt or glucose), the dispersing energy and the duration of the preparation steps.
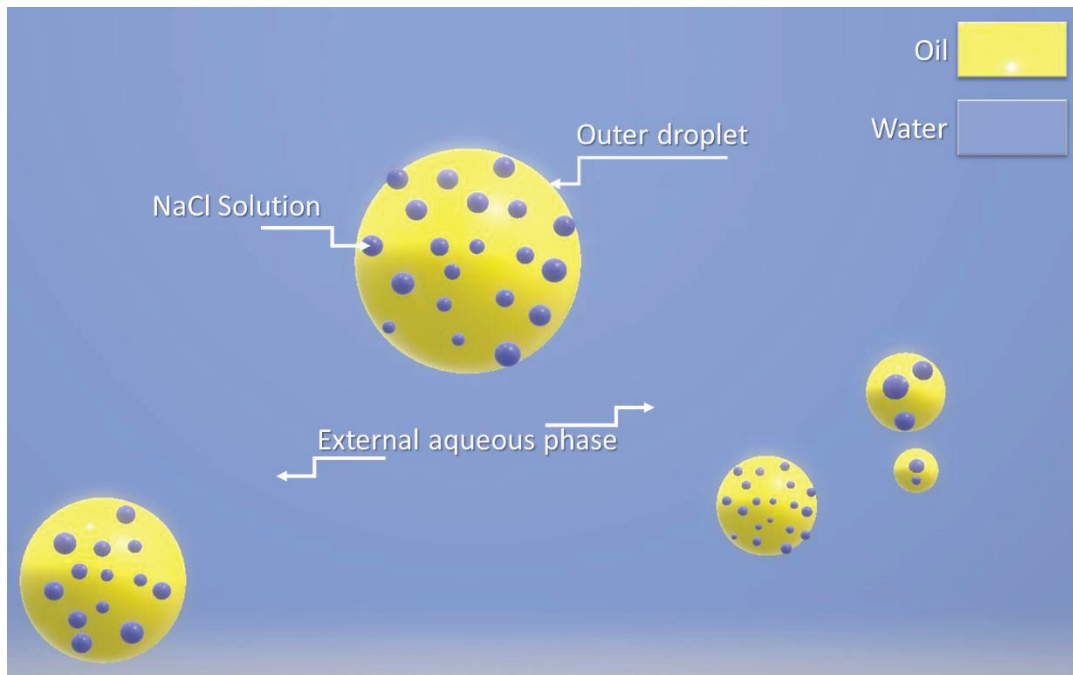
Fig. 1.2. *Double emulsion scheme*

During this work, W/O/W double emulsions are produced, and salt is encapsulated in the internal water phase as the active substance (see Fig. 1.2), the release of which to the external aqueous phase through the oil phase to be controlled.

1.2. Phenomena occurring during preparation and storage of double emulsions

A number of phenomena occur during the second preparation step or during storage of the double emulsions [16–22]. During the second preparation step, the possible pathways are mainly:

- Breakage and coalescence of the outer droplets due to the shear force (usually a turbulent regime is employed).
- Leakage of the inner droplets to the external phase as a result of outer droplet breakage (by coalescence to the external phase, and film rupture of the outer droplet).
- Release of the encapsulated substance through the outer layer without film rupture, by molecular diffusion. This phenomenon is negligible in this work due to the low solubility of the used salt in oil.
- Shrinkage or swelling of the inner, and so of the outer, droplets due to osmotic pressure gradient. This phenomenon is also found to be negligible during preparation in this work, due to the short preparation time.
- Adsorption of surfactant on the new generated surface. In this work, a high amount of surfactant is employed (higher than the surface coverage area of the droplets), and the surface tension is assumed to be constant during preparation.

During storage, the phenomena that may take place are:

- Coalescence of the outer droplets due to Brownian motion (i.e., outer-outer droplets coalescence). The coalescence rate is found to be negligible in diluted systems (up to 10 %) and were a high amount of surfactant is used. This was validated experimentally.

- Coalescence of the inner droplets (i.e., inner-inner droplets coalescence). This phenomenon was also neglected in this work, due to the high oil viscosity, which reduces the droplets collision frequency.
- Release of the encapsulated substance through the outer layer without film rupture.
- Escape of the inner droplets by coalescence with the external phase.
- Shrinkage or swelling of the inner, and so of the outer droplets, due to osmotic pressure gradient.
- Overswelling-breakdown, which leads to important escape of the inner droplets and breakage of the outer droplets.
- Rheological evolutions may appear due to the swelling or release phenomena (for instance change of the outer layer viscosity).

Therefore, the phenomena taking place in this work – shown in Fig. 1.3 – during the second preparation step are limited to:

- Breakage and coalescence of the outer droplets due to the shear force (both inertial and dissipation subranges of turbulence are employed).
- Leakage of the inner droplets to the external phase as a result of outer droplets' breakage (by coalescence to the external phase, and film rupture of the outer droplet).

During storage, the phenomena that may take place in the present system are:

- Escape of the inner droplets by coalescence with the external phase.
- Swelling of the inner, and so of the outer droplets, due to osmotic pressure gradient.
- Overswelling-breakdown, which leads to important escape of the inner droplets and breakage of the outer droplets.
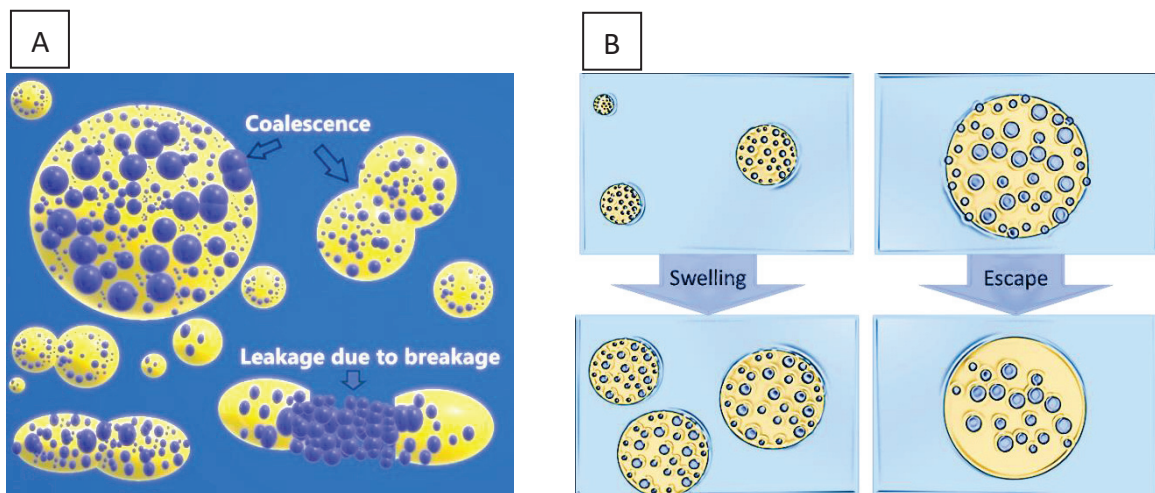
Fig. 1.3. *phenomena taking place in this work during (A) the second step of preparation of double emulsion and (B) the storage of double emulsion.*

The following notations should not be confused:

- Release: Indicates the release of the encapsulated substance through the outer layer without film rupture of the outer droplet, by molecular diffusion.

- Escape: Indicates the release of the full inner droplet to the external phase due to its Brownian motion (by coalescence to the external phase, and film rupture of the outer droplet). So, the term "escape" is used when there is no breakage of the outer droplet.
- Leakage: Indicates the escape of the full inner droplet to the external continuous phase as a result of outer droplet breakage (by coalescence to the external phase, and film rupture of the outer droplet).
- Overswelling-breakdown: This term is used to describe the simultaneous breakage of the outer droplet and the abrupt leakage of inner droplet due to the extent of the swelling phenomenon.

1.3. Modelling double emulsions

As the phenomena taking place during preparation and storage are different, different models need to be developed for the two stages. The main properties to be estimated by the model are the droplet size and the release rate (or the encapsulation efficiency). The models need to be based on the properties of the different phases and operating conditions that have an impact on the key properties to be estimated.

1.3.1. Modelling the droplet size

For single emulsions, a number of works treated modelling the evolution of the droplet size during preparation, either by predicting the mean diameter using stationary model approaches [5,23,24] or by predicting the full distribution using PBMs [25,26]. Some correlations of single emulsions were applied to double emulsions [27–30], but the correct adoption of the different properties (i.e., viscosity, density, and interfacial tension) is still lacking.

PBM provides a framework to describe the dynamics of distributed properties [31]. Since in double emulsions there are two size distributions involving different simultaneous with coupled phenomena, the PBMs of the inner and outer droplets should be solved simultaneously, which represents a big challenge due to a number of reasons, some important of which are solving a great many equations simultaneously, defining the corresponding kernels, and validating the results of the PBMs [31]. During the second preparation step, the phenomena that take place, which are estimated to be of significance in this work, are the breakage and coalescence of the outer droplets and leakage of the inner droplets. The available breakage and coalescence models of single emulsions [25,26] can be adopted for double emulsions by taking into account the apparent properties (densities, viscosities, surface tension). But there is a need to define a leakage model to be included in the PBM of the inner droplets. As the driving force of leakage is defined to be the breakage of the outer droplets, the leakage model should be related to the breakage kernel.

During storage, the phenomena taking place are mainly inner droplet swelling and escape. Coalescence of inner-inner and outer-outer droplets may also take place during storage, due to their Brownian motion, but were found to be negligible in this work. In case of the existence of such phenomena, a possible option can be the well-known model of Smoluchowski [32]. Regarding the available models of swelling of double emulsions, the permeability model is

usually employed by considering a mean droplet size [22,33–37]. However, the mean droplet size is not a good characteristic for a system with polydisperse inner and outer droplets. Therefore, there is a need to consider the full droplet size distributions (DSD) in the swelling model. Moreover, the available works neglected the effect of Laplace pressure, which means that the swelling continues until osmotic equilibrium. However, the Laplace pressure may counterbalance the osmotic pressure gradient and stop swelling before osmotic equilibrium. This observation was highlighted in the literature, when very small inner droplets were found to keep their small size while bigger droplets swell. Neglecting the effect of Laplace pressure is valid only in case of big inner aqueous droplet size or very high amounts of salt. Therefore, it will be accounted for in this work.

1.3.2. Modelling the release rate

The encapsulated substance may release by two ways: i) molecular diffusion of salt through the oil layer to the external phase, or ii) full escape of the inner droplet to the external phase by coalescence on the surface of the outer droplet. Depending on the composition of the double emulsion, the release will be mainly driven by one of these phenomena. Therefore, models for both categories were proposed in the literature.

Among the models developed for the first category, Ho et al. (1982) [38] proposed a diffusion model considering uniform sizes of inner and outer droplets. This approach was used in some works regarding extraction in liquid membrane systems where the extracted material can diffuse with a higher rate within the membrane phase [38,39].

In the present work, the encapsulated substance (i.e., NaCl) has a very low solubility in the oil phase and the release due to diffusion is negligible compared to inner droplet escape. Therefore, only release by inner droplet escape is modelled. During storage, the rate of escape is governed by the Brownain motion of the droplets, while during preparation the escape is found to be proportional to the breakage of the outer droplets and is called leakage.

Inner droplet escape (without breakage of the outer droplet). Generally, inner droplet escape can occur during storage (or under simple shear that does not lead to breakage of the outer droplet), which leads to a decrease in the number of inner droplets causing the release of encapsulated substance to the external phase and the volumetric decrease of the outer droplet size. The escape rate is based on three key parameters to be identified: (a) the escape frequency Ω_{Es}, (b) the number of inner droplets in the region at the vicinity of the surface of the outer droplet from which the escape may occur, which will be called critical region hereafter, α_{cr} and the coalescence probability P. The rate of inner droplet escape is therefore $R_{Es} = \alpha_{cr}.P.\Omega_{Es}$.

Some models were proposed to estimate these key parameters in the literature (all models assumed uniform size of inner and outer droplets):

    a. The escape model of Pays et al. (2001) [40]: this work proposes a method to estimate α_{cr}, during storage. An adsorption isotherm is employed to estimate the number of inner droplets adsorbed on the surface of the outer droplet, which are prone to release. The escape frequency Ω_{Es} was fitted experimentally and the probability

assumed $P = 1$ (or assumed regrouped with the fitted frequency, $P.\Omega_{ES}$). This model will not be used in this work as α_{cr} will be identified by fitting to experimental data, but we will similarly assume $P = 1$ (i.e., similarly it will be regrouped with the experimentally identified critical region, $P.\alpha_{cr}$).

b. The escape model of Chávez-Páez et al. (2012) [41]: this work proposes a method to estimate $\alpha_{cr} \times \Omega_{ES}$, during storage. It is based on 3D simulation of the Brownian motion of the inner droplets and predicts their collision frequency with the surface of the outer droplet. The escape probability P was assumed to be estimated by an independent method. Such calculation is heavy to handle and therefore it is not adopted in this work.

c. The dwetting model of Kang et al. (2016) [6]: This model allows to predict the escape frequency Ω_{ES}, during storage. It is based on the Stokes flow and energy and momentum conservation of inner and outer droplets. This model will be employed in this work to estimate the escape frequency Ω_{ES}. Note that this model does not include the salt effect on the forces or on the viscosities of the different phases.

d. The escape model of Klahn et al. (2002) [42] in presence of simple shear: this work provides a method to estimate both the escape frequency Ω_{ES} (based on the internal circulation streamlines) and probability P (based on the film drainage theory). This model is valid only under simple shear. The fraction of the critical region prone to escape, α_{cr}, was fitted experimentally.

Inner droplet leakage (i.e. escape joining the breakage of the outer droplet). During preparation, outer droplet breakage appears to be the driving force for inner droplet escape. This can be explained by the fact that the outer droplet breakage process implies oscillations of the droplet (so an enhanced motion within it) and the creation of a new surface by elongation and breakup (which increases the escape probability). In this regard, Shere and Cheung (1988) [43] proposed a model based on the probability of the rupture of outer droplets as the main cause of the leakage of inner droplets. Okazaki et al. (1992) [44] also proposed a correlation for a leakage coefficient as a function of energy dissipation, oil viscosity, membrane thickness and osmotic pressure. Both works consider a mean droplet size. In this work, a leakage model will be proposed using equilibrium correlations based on the mean size as well as using PBM.

1.3.3. Population balance models of inner and outer droplets

Most of the abovementioned models are developed for the case of uniform or mean sizes of inner and outer droplets that may fail to give a full insight into the system. To generalize the models and take into account the full DSD, the key phenomena need to be incorporated into the PBM.

There are two ways of considering population balance modelling of double emulsions:

1) Considering two separate PBMs of inner and outer droplets (though connected and solved simultaneously). This allows to account for the evolution in the sizes and number of the inner and outer droplets due to the several phenomena of swelling,

escape, breakage and coalescence. However, in this approach, outer droplets of different sizes are assumed to have the same density of inner droplets.

2) Another method would be to consider one PBM of the outer droplets with two inner coordinates: the outer droplet size and the concentration of inner droplets. By this way, the outer droplets may contain different densities of inner droplets, for instance depending on the outer droplet size. However, this method has the drawback of not being able to predict the changes in the size of the inner droplets due to swelling, since the coordinate that can represent the inner droplet size is not available in this method. It would be applicable during preparation, where only inner droplet escape occurs besides breakage and coalescence of the outer droplets. Generally, this approach is applied in liquid-liquid extraction methods were the main focus is to predict the mass transfer rate.

Based on this analysis, it was decided to proceed by developing two PBMs for the inner and outer droplets.

The general PBM form of the inner droplets (n_μ) is the following:

$$\frac{\partial n_\mu(t, v_\mu)}{\partial t} + \underbrace{\frac{\partial \left(\mathbb{S}_\mu(t, v_\mu) n_\mu(t, v_\mu) \right)}{\partial v_\mu}}_{\substack{\text{swelling (or shrinkage) of} \\ \text{inner droplets (mainly \textbf{during storage})}}} + \underbrace{\frac{\partial \left(G_\mu(t, v_\mu) n_\mu(t, v_\mu) \right)}{\partial v_\mu}}_{\substack{\text{gowth by Ostwald ripening of} \\ \text{inner droplets}}} \qquad 1.1$$

$$= \underbrace{\mathfrak{R}_{Co}^\mu}_{\substack{\text{Coalescence of} \\ \text{inner droplets} \\ \text{(due to shear collision} \\ \textbf{during preparation} \text{ or} \\ \text{due to Brownian motion} \\ \textbf{during storage})}} + \underbrace{\mathfrak{R}_{Leak}}_{\substack{\text{Leakage of} \\ \text{inner droplets due to} \\ \text{breakage of outer droplets} \\ (\textbf{during preparation} \text{ or} \\ \text{overswelling–breakdown} \\ \text{of outer droplets} \\ \textbf{during storage})}}$$

$$+ \underbrace{\mathfrak{R}_{ES}}_{\substack{\text{Escape of} \\ \text{inner droplets to} \\ \text{the external phase} \\ \text{through the surface} \\ \text{of outer droplets} \\ (\textbf{during storage} \\ \textbf{or preparation} \text{ under} \\ \text{simple shear flow})}}$$

The general PBM form of the outer droplets (n_M) is the following:

$$\frac{\partial n_{\mathrm{M}}(t, v_{\mathrm{M}})}{\partial t} + \underbrace{\frac{\partial\big(\mathbb{S}_{\mathrm{M}}(t, v_{\mathrm{M}})n_{\mathrm{M}}(t, v_{\mathrm{M}})\big)}{\partial v_{\mathrm{M}}}} \qquad\qquad 1.2$$

Change in the size of the outer droplets due to swelling or shrinkage of
the inner droplets (mainly **During storage**)

$$+ \qquad \underbrace{\frac{\partial\big(G_{\mathrm{M}}(t, v_{\mathrm{M}})n_{\mathrm{M}}(t, v_{\mathrm{M}})\big)}{\partial v_{\mathrm{M}}}}$$

Change in the size of the outer droplets due to Ostwald ripening

$$+ \qquad \underbrace{\frac{\partial\big(Q_{\mathrm{es,M}}(t, v_{\mathrm{M}})n_{\mathrm{M}}(t, v_{\mathrm{M}})\big)}{\partial v_{\mathrm{M}}}}$$

Change in the size of the outer droplets due to escape of the inner droples **during storage**

$$= \qquad \underbrace{\mathfrak{R}_{\mathrm{Br}}}_{} \qquad + \qquad \underbrace{\mathfrak{R}_{\mathrm{Co}}^{\mathrm{M}}}_{} \qquad + \qquad \underbrace{\mathfrak{R}_{\mathrm{OSB}}}_{}$$

Breakage of	Coalescence of	Breakage of
the outer droplets	the outer droplets	the outer droplets
(**during preparation**)	(**during preparation** or **during storage**)	due to overswelling (**during storage**)

where n is the number density of the droplets (i.e., number per m^{-3} of droplet size), t (s) the time, v (m^3) the volume, $\mathbb{S}$ (m^3.s^{-1}) the rate of the swelling or shrinkage, G (m^3.s^{-1}) the growth by Ostwald ripening, $Q_{\mathrm{es,M}}$ (m^3.s^{-1}) the volumetric change of the outer droplets due to escape of the inner droplets, $\mathfrak{R}_{\mathrm{Co}}$ (m^{-3}.s^{-1}) the coalescence rate, $\mathfrak{R}_{\mathrm{Leak}}$ (m^{-3}.s^{-1}) the leakage rate of the inner droplets, $\mathfrak{R}_{\mathrm{Es}}$ (m^{-3}.s^{-1}) the escape rate of the inner droplets, $\mathfrak{R}_{\mathrm{Br}}$ (m^{-3}.s^{-1}) the breakage rate of the outer droplets due to shear, and $\mathfrak{R}_{\mathrm{OSB}}$ (m^{-3}.s^{-1}) is the breakage rate of the outer droplets as a result of overswelling. All over the work, the properties of the inner droplets are indicated with the subscript μ (or sometimes m) and the ones of the outer droplets with M.

The breakage and coalescence kernels or equilibrium correlations of the droplet size are usually developed for a particular scale of turbulence. Therefore, the following section introduces some useful notations about the scales of turbulence.

1.3.4. Turbulent scales

Based on the droplet deformation theory of Taylor, a droplet with diameter d and interfacial tension σ does not break below a critical value of the generalized Weber group ($N_{\mathrm{We}} = \frac{\tau d}{\sigma}$) [5]. In this relation, the external stress (i.e., force per unit area) acting on the droplet surface, τ, depends on the type of the flow regime around the droplet [5].

Considering the kinematic viscosity ($v = \frac{\text{dynamic viscosity}}{\text{density}} = \frac{\mu}{\rho}$) and the energy dissipation rate (ε), Kolmogorov (1941) defined the length scale of the smallest vortices as $\eta = \left(\frac{v^3}{\varepsilon}\right)^{1/4}$, known as Kolmogorov length scale, based on three hypotheses [45,46]. Kolmogorov arguments indicate that unlike the turbulence of the anisotropic large scale vortices that depends on the geometry, the turbulence of the small scales are statistically isotropic and independent of the

geometry [45,46]. With regards to the Kolmogorov length scale and the largest vortices (L), two general ranges can be defined for sufficiently high Reynolds numbers [46,47]: The energy containing range ($L/6 \ll \lambda \ll L$) and the universal equilibrium range. Based on the three hypothesis of Kolmogorov, the universal subrange can be divided into two different subranges summarized in Fig. 1.4 [46,47]:

(1) Over the range of $60\,\eta \ll \lambda \ll L/6$, the subrange is called the inertial subrange, where the motion is controlled only by the energy dissipation rate. In this subrange, an eddy of size λ can fluctuate by the mean velocity of $\overline{u_\lambda^2} \propto \varepsilon^{\frac{2}{3}} \lambda^{\frac{2}{3}}$ creating the stress of $\tau = \rho_c\,\overline{u_\lambda^2}$ on the surface of the droplet, which transforms the generalized Weber group to the Webber number of the form $N_{We} = We = \frac{\rho_c\,\overline{u_\lambda^2}\,d}{\sigma}$ [5,48].

(2) Over the range of $\eta \ll \lambda \ll 60\,\eta$, the subrange is named the dissipation or viscous subrange, in which both the energy dissipation and the kinematic viscosity govern the motion leading to a velocity of $\overline{u_\lambda^2} \propto \frac{\varepsilon\lambda^2}{\nu}$ and an external stress of $\tau = \mu_c\frac{\partial \overline{u_\lambda}}{\partial \lambda}$. This transfers the generalized Weber group to the form of Capillary number, $N_{We} = Ca = \frac{\mu_c\,d}{\sigma}\frac{\partial u_\lambda}{\partial \lambda}$ [5,49].

There are a number of works regarding the equilibrium mean droplet size in the inertial subrange [2,5,23,48,50,51] while there are only few works, such as Nazarzadeh and Sajjadi (2010) [52] and Gupta et al. (2016) [53], that consider the dissipation subrange for the mean droplet size of Nano-emulsions. Similarly, most of the breakage and coalescence kernels employed in PBMs are valid for the inertial subrange.
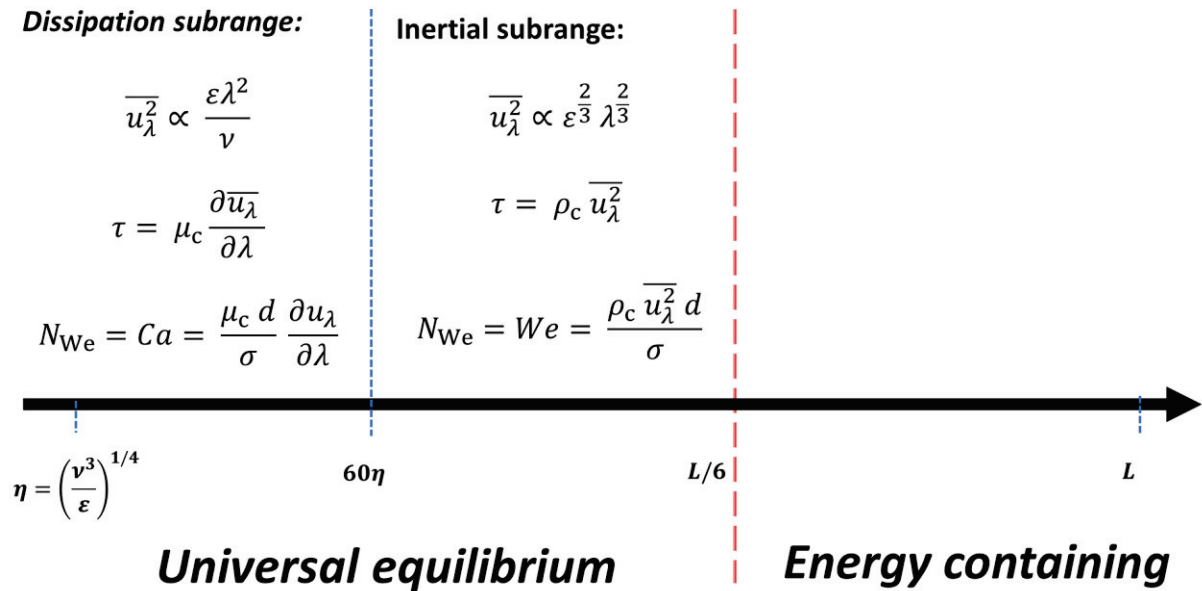
Fig. 1.4. *Scales of the turbulent energy (adopted from Andersson (2011) [46] and modified)*

1.3.5. Double emulsion considerations

Since the dispersed phase of a double emulsion itself is an emulsion, some properties of the outer phase (i.e., viscosity, density, and interfacial tension) undergo alteration due to the existence of the inner phase.

The viscosity (μ) and density (ρ) of the outer droplets can be simply calculated by employing the well-known models of Vermeulen (1955)[54] and Miller and Mann (1944)[55] respectively, which are typically used for single emulsions:

$$\mu_M = \frac{\mu_c}{1-\phi}\left(1 + 1.5\,\phi\,\frac{\mu_d}{\mu_d + \mu_c}\right) \qquad\qquad 1.3$$

$$\rho_M = \phi\,\rho_d + (1-\phi)\,\rho_c \qquad\qquad 1.4$$

Where "d" and "c" are the representative of dispersed and continuous phases, respectively, and ϕ is the fraction of the dispersed phase.

The surface tension can also be altered, since the change in the work required to strain a pure droplet (W) and the work required for a droplet containing other droplets (W_M) are different and given by Michaut et al. (2004) [56]. Considering W/O/W double emulsions:

$$W \approx \gamma\,P_L\,v \approx \gamma\,\sigma\,r^2 \qquad\qquad 1.5$$

$$W_M \approx \gamma\,(\sigma_{oil-out}\,r_M^2 + N_\mu\sigma_{\mu-M}\,r_\mu^2)$$

where γ is the shear frequency, P_L is the Laplace pressure, r is the droplet radius, $N_\mu = \phi_\mu\dfrac{d_M^3}{d_\mu^3}$ is the total number of inner droplets in an outer droplet, and σ is the surface tension. Thus, the interfacial tension of the outer droplets can be affected by the presence of inner droplets as follows:

$$\sigma_{M-out} = \sigma_{oil-out} + \sigma_{\mu-M}\,\phi_\mu\frac{d_M}{d_\mu} \qquad\qquad 1.6$$

However, our calculation indicated that the effect of the inner droplets (~ 1 µm) on the surface tension of the outer droplets is negligible. Thus, one may consider the surface tension of the oil/water single emulsion instead of the surface tension of outer droplet, i.e., $\sigma_{M-out} \approx \sigma_{oil-out}$. However, the employment of the inner emulsifier importantly affects the surface tension, therefore the used value should be that of the oil droplet (in which a hydrophobic emulsifier is dissolved) that is dispersed in water (in which a hydrophilic emulsifier is dissolved).

1.4. Experimental

1.4.1. Emulsification devices

Different devices – namely impellers, high speed rotor-stators, high pressure homogenizers, micro-fluidic devices, membranes, or ultrasonicators – can be used to produce double emulsions [57–59]. However, the encapsulation efficiency was found to be governed mainly by the size of the inner and outer droplets, and less by the emulsification device itself [57]. Therefore, in this work, three different devices were employed to vary the size of the droplets over a wide range.

a) Mechanically stirred vessel: Stirred vessels are typically equipped with an impeller (e.g., three bladed impeller) and baffles. In this work, their use was opted in order to allow online and *in-situ* records of different properties such as conductivity and video images. As the online video probe and image treatment are more efficient for dilute systems, a double emulsion of

1 % is prepared in the stirred vessel. The type of the mixing element controls the flow type and the energy dissipation rate governs the breakage mechanism. In such devices, the energy dissipation rate is in the range of 0.1 $m^2.s^{-3}$ – 100 $m^2.s^{-3}$, which allows producing droplet sizes of 20 μm – 500 μm in single emulsions [60]. In the used stirred vessel of this study, equipped with a three pitched blades impeller, the mean energy dissipation is around 0.5 $m^2.s^{-3}$ and the obtained outer mean droplet diameters are of the order of 40 μm.

b) High speed rotor-stators: Rotor-stators are composed of a fixed element (i.e., the stator) and a driven mixing element (i.e., the high-speed rotor). The rotating part has a tip velocity range of 10 to 50 $m.s^{-1}$, thus creating a higher local energy dissipation than the mechanically stirred vessels. The local energy dissipation rate is usually in the range of 1000 $m^2.s^{-3}$– 100,000 $m^2.s^{-3}$ producing droplet sizes in the range of 0.5 μm – 100 μm [60]. In this study, using Ultra-Turrax, the mean diameter of the outer droplets in double emulsions is approximately 20 μm and the mean energy dissipation is of the order of 3.2 $m^2.s^{-3}$ – i.e., local energy dissipation (the estimation is given by [61,62]) is of the order of 100,000 $m^2.s^{-3}$. Here, a more concentrated double emulsion is produced (10 % in chapters 3 and 6 and Appendix 1).

c) Ultrasonicators: Ultrasonication is very convenient for the preparation of very small droplets in a very short time scale. The energy dissipation rate is associated with acoustic cavitation that erupts the dispersed phase, as droplets, into the continuous phase following by very high local shear that breaks the formed droplets into very fine droplets [59,63–66]. In such systems, the local energy dissipation can be around 10^9 $m^2.s^{-3}$, so forming droplets in the size range of 0.2 μm – 0.5 μm [60]. Based on the experimental results of this study, the mean outer droplet size of the double emulsions was found to be slightly bigger than 0.35 μm with the mean energy dissipation of the order of 1000 $m^2.s^{-3}$. Here also a more concentrated double emulsion is produced (10 %).

The chosen devices have different energy inputs that change the turbulent scales from viscous to inertial sub-range, and time scales from seconds for Ultrasonicator, to few minutes for the rotor-stator, to hours for the stirred tank.

1.4.2. Materials and fractions

The choice of the materials is usually defined by the application, and the fractions are usually optimized in order to maximize the encapsulation rate and the stability of the double emulsion during storage. Table 1.1 shows the effect of the different fractions of materials used for the preparation of double emulsions in the literature.

Table 1.1. *Effect of different parameters on the formation of double emulsions (selected works).*

		↑ ϕ_{inner}	↑ ϕ_{outer}	↑ ϕ_{ions}	↑ $\phi_{emulsifier}^{in}$	↑ $\phi_{emulsifier}^{out}$
EE	↑	[13,67,68]	[13,14]	[67,69]	[13,70]	-
	↓	[14,71]	-	[68]	-	[13,72]
d_{outer}	↑	[67,71,73,74]	[75]	[69]	-	-
	↓	-	-	[76]	-	[72]

ϕ: fraction, EE: encapsulation efficiency, and d: droplet diameter (m), inner: internal phase, outer: outer droplet or primary emulsion phase, in: inside, out: outside, ↑: increase, ↓: decrease.

The materials and fractions employed in this work were adopted from the work of Schmidts et al. (2009) [77] as follows: Mineral oil (Fisher Scientific™), fluid paraffin oil (Cooper, France), Marcol 82 (ExxonMobil) and Marcol 52 (ExxonMobil) are the used oils. Span 80 (Alfa Aesar) is the hydrophobic emulsifier and Tween 80 (Fisher Scientific™) the hydrophilic emulsifier. Sodium Chloride is used as tracer. The used water, all over the work, is Millipore water with resistivity ≈ 18.2 mΩ.cm.

In some preliminary experimental manipulations, the used oil was silicon oil, a wider viscosity of which was available, to investigate the effect of the oil viscosity on the pure escape of inner droplets to the external phase during storage (see Appendix A1). The used emulsifiers were similarly Span 80 and Tween 80. The properties of the different mineral and silicon oils, which are used in this study, are listed in Table 1.2.

Table 1.2. Properties of the used oils

Oil	Name/Indicator	Viscosity (mPa.s)	Density (kg.m^{-3})	Interfacial tension (mN.m^{-1}) between oil + span 80 and water
Mineral / paraffin oil	Macro 52	6	825	~ 5
	Macrol 82	22	835	
	Fluid Paraffil oil	32	842	
	Mineral oil	42	850	
Silicon oil	V50	50	958.4	~ 5.4
	V100	100	964.4	
	V350	350	967.6	

The concentrations of the inner and outer emulsifiers were calculated in a way to ensure full coverage of the inner and outer droplets after emulsification and were not varied in this study, while the other fractions were varied (salt, inner water, primary emulsion).

It is to be noted that, besides the Hydrophilic–Lipophilic Balance (HLB) which is a numeric system to describe the degree of being hydrophilic or lipophilic for a non-ionic surfactant [78], the chemical compatibility of the two used emulsifiers (i.e., lipophilic and hydrophilic) is important to validate [77], and the ratio of lipophilic to hydrophilic emulsifiers are important parameters affecting the stability of W/O/W double emulsions. Frenkel et al. (1983) [79] linked the effect of the two emulsifiers by a "'weighted HLB" term that is found to be useful to calculate the fractions of the two emulsifiers [77]:

$$\text{Weighted HLB} = \frac{\text{HLB}_l \times \phi_M \times X_l + \text{HLB}_h \times X_h}{\phi_M \times X_l + X_h} \qquad 1.7$$

Where, ϕ_M is the volume fraction of primary emulsion in double emulsion, X is the percent by weight of the emulsifier, and l and h are respectively the indicators of the lipophilic and hydrophilic emulsifiers in W/O/W double emulsions. On this basis, the weighted HLB is suggested to be lower than 10 and lower than the required HLB of the oil phase [79]. Also, Matsumoto et al. (1976) [13] reported a ratio of the concentration of the lipophilic to hydrophilic emulsifier (i.e., X_l/X_h) of higher than 10 to be considered for making stable double emulsions, the value of which is respected to be 10 in this study.

1.4.3. Droplet size measurement

Tree common off-line techniques were employed to evaluate the size of the droplets:

a) Dynamic light scattering (e.g. Malvern Zetasizer Nano ZS®) for inner droplets (valid for the range of 0.3 nm to 10 μm).
b) Laser diffraction technique (e.g. Malvern Mastersizer 3000®) for outer droplets (valid for the range of 0.01 μm to 3500 μm).
c) Optical microscopic observations (e.g. Leica© DM2000 LED, with resolution of 0.2 μm) for validating the formation of double emulsion and verifying the mean droplet sizes. Optical microscopic visualization is limited to the droplets with size bigger than 1 μm for light microscopes (and bigger than 750 nm for confocal fluorescence microscopes) [80].

The most critical concern of using the laser diffraction and dynamic light scattering techniques is the necessity of dilution which may alter the droplet size due to surfactant redistribution (which may cause droplet coalescence). Moreover, in the laser diffraction method the double emulsion is pumped into the detecting area, which may cause further droplet breakage. Moreover, in the laser diffraction method, where the double emulsion is analyzed, it is required to choose the refractive index of the dispersed phase. While the outer droplets consist of oil and water, it is reasonable to use the refractive index of the oil (e.g., 1.467 for mineral oil) that corresponds to the main material in the droplet especially in the outer layer. This assumption was also verified by Schmidts et al. [81] who compared measurements of the outer droplets from Mastersizer and microscopic observations. Microscopic observations were also handled in this work.

Besides off-line measurements, an *in-situ* video probe (EZ Probe-D25® designed in our laboratory LAGEPP) is selected and installed in a stirred rector [82]. The real time 2D recorded videos were then transformed into picture frames allowing the size determination in a delayed time based on the circular Hough transform [82]. This probe was not used in the ultrasonication or rotor-stator systems, due to the smaller volume of the sample and to the higher concentration of the double emulsion.

Inner droplet size measurement. Since inner droplets are very small and covered by oil layer, their size is challenging to measure after the production of the double emulsions. The two techniques were suggested in the literature to overcome this difficulty are:

- Pulsed-field gradient nuclear magnetic resonance (PFG-NMR) [80,83–88]. PFG-NMR is based on the molecular displacements due to diffusion that provides the signal attenuation of the specific matter. Taking into account this signal attenuation and based on the three known modelling approaches – i.e., short gradient pulse (SGP), Gaussian Phase Distribution (GPD) and block gradient pulse approximation (BGP) – suggested in the literature [80,89], it is possible to estimate the inner droplet size [80,83–88]. This method was investigated in this work and found to be comparable to the results from the model of swelling (Chapter 6).
- Confocal laser scanning microscopy (CLSM) [85,86,90]. CLSM, is based on using an appropriate fluorescence marker which creates a high contrast between the two

phases (i.e., inner and outer). The captured image can then be processed using software to determine the inner and outer droplet sizes [90].

However, microscopic observations in this study and the results by [88] indicate that the size of inner droplets do not evolve importantly during the short emulsification time of the second step of preparation. Thus, the sizes of inner droplets measured right after the primary emulsion preparation (i.e., before the second step) can be considered as their approximate representative scale after the formation of double emulsion. This information was used as an input to the swelling model for instance.

1.5. Objectives of the PhD

The objective of this PhD work is to investigate the phenomena taking place during the preparation and the storage of double emulsions, both experimentally and by fundamental modelling.

Two different stages are considered:

(a) During preparation under turbulence where the outer droplets may undergo breakage and coalescence and the inner droplets may escape to the external phase. Distinguishing between the different turbulent subranges is critical, since different size ranges of droplets, produced with different systems, lead to shift from a subrange to another. Two approaches are employed here: an equilibrium correlation is employed in the ultrasonication system due to the short preparation time while a population balance model is employed in the rotor-stator system.

(b) During storage, the identified possible pathways of instability are the release of the encapsulated ingredient (by coalescence with the external continuous phase) and swelling of the inner, and thus the outer droplets, and overswelling-breakdown of the outer droplets leading to leakage of the inner phase and reduction in the size of the outer droplets.

References

[1] V. Alopaeus, J. Koskinen, K. I. Keskinen, J. Majander, Simulation of the population balances for liquid–liquid systems in a nonideal stirred tank. Part 2—parameter fitting and the use of the multiblock model for dense dispersions, Chem. Eng. Sci. 57 (2002) 1815–1825. doi:10.1016/S0009-2509(02)00067-2.

[2] C.A. Coulaloglou, L.L. Tavlarides, Description of interaction processes in agitated liquid-liquid dispersions, Chem. Eng. Sci. 32 (1977) 1289–1297. doi:10.1016/0009-2509(77)85023-9.

[3] G.I. Taylor, The Viscosity of a Fluid Containing Small Drops of Another Fluid, Proc. R. Soc. Math. Phys. Eng. Sci. 138 (1932) 41–48. doi:10.1098/rspa.1932.0169.

[4] G.I. Taylor, The Formation of Emulsions in Definable Fields of Flow, Proc. R. Soc. Math. Phys. Eng. Sci. 146 (1934) 501–523. doi:10.1098/rspa.1934.0169.

[5] J.O. Hinze, Fundamentals of the hydrodynamic mechanism of splitting in dispersion processes, AIChE J. 1 (1955) 289–295. doi:10.1002/aic.690010303.

[6] Z. Kang, P. Zhu, T. Kong, L. Wang, A Dewetting Model for Double-Emulsion Droplets, Micromachines. 7 (2016) 196. doi:10.3390/mi7110196.

[7] G. Muschiolik, Multiple emulsions for food use, Curr. Opin. Colloid Interface Sci. 12 (2007) 213–220. doi:10.1016/j.cocis.2007.07.006.

[8] A. Aserin, ed., Multiple emulsions: technology and applications, Wiley-Interscience, Hoboken, N.J, 2008.

[9] W.S.W. Ho, K.K. Sirkar, eds., Membrane Handbook, Springer US, Boston, MA, 1992. doi:10.1007/978-1-4615-3548-5.

[10] W. Seifriz, Studies in Emulsions. I-II, J. Phys. Chem. 29 (1924) 587–600. doi:10.1021/j150251a008.

[11] J. Khurana, S. Singh, A.K. Dash, Multiple emulsions an overview and pharmaceutical applications, in: Colloids Drug Deliv., CRC Press, 2016: pp. 177–202.

[12] N.N. Li, Separating hydrocarbons with liquid membranes, Google Patents, 1968.

[13] S. Matsumoto, Y. Kita, D. Yonezawa, An attempt at preparing water-in-oil-in-water multiple-phase emulsions, J. Colloid Interface Sci. 57 (1976) 353–361. doi:10.1016/0021-9797(76)90210-1.

[14] T.S.H. Leong, M. Zhou, N. Kukan, M. Ashokkumar, G.J.O. Martin, Preparation of water-in-oil-in-water emulsions by low frequency ultrasound using skim milk and sunflower oil, Food Hydrocoll. 63 (2017) 685–695. doi:10.1016/j.foodhyd.2016.10.017.

[15] K. Lindenstruth, B.W. Müller, W/O/W multiple emulsions with diclofenac sodium, Eur. J. Pharm. Biopharm. 58 (2004) 621–627. doi:10.1016/j.ejpb.2004.04.003.

[16] S.S. Davis, A.S. Burbace, Electron micrography of water-in-oil-in-water emulsions, J. Colloid Interface Sci. 62 (1977) 361–363. doi:10.1016/0021-9797(77)90134-5.

[17] S.S. Davis, A.S. Burbage, The Particle Size Analysis of Multiple Emulsions (Water-in-Oil-in-Water), in: Part. Size Anal. Proc. Conf. Organ. Anal. Div. Chem. Soc. Held Univ. Salford 12-15 Sept. 1977, Heyden & Son, 1978: p. 395.

[18] D. Whitehill, A.T. Florence, Mechanisms of instability in W/O/W multiple emulsions, J. Pharm. Pharmacol. 31 (1979) 3P-3P.

[19] A.T. Florence, D. Whitehill, The formulation and stability of multiple emulsions, Int. J. Pharm. 11 (1982) 277–308.

[20] M.-F. Ficheux, L. Bonakdar, F. Leal-Calderon, J. Bibette, Some Stability Criteria for Double Emulsions, Langmuir. 14 (1998) 2702–2706. doi:10.1021/la971271z.

[21] I. Terrisse, M. Seiller, J.L. Grossiord, A. Magnet, C. Le Hen-Ferrenbach, Application of rheological analysis to W/O/W multiple emulsions: Effect of the incorporation of a

coemulsifier, Colloids Surf. Physicochem. Eng. Asp. 91 (1994) 121–128. doi:10.1016/0927-7757(94)02790-0.

[22] S. Matsumoto, M. Kohda, The viscosity of W/O/W emulsions: an attempt to estimate the water permeation coefficient of the oil layer from the viscosity changes in diluted systems on aging under osmotic pressure gradients, J. Colloid Interface Sci. 73 (1980) 13–20.

[23] J.T. Davies, Drop sizes of emulsions related to turbulent energy dissipation rates, Chem. Eng. Sci. 40 (1985) 839–842. doi:10.1016/0009-2509(85)85036-3.

[24] J. Zhang, S. Xu, W. Li, High shear mixers: A review of typical applications and studies on power draw, flow pattern, energy dissipation and transfer properties, Chem. Eng. Process. Process Intensif. 57–58 (2012) 25–41. doi:10.1016/j.cep.2012.04.004.

[25] P.J. Becker, F. Puel, R. Henry, N. Sheibat-Othman, Investigation of Discrete Population Balance Models and Breakage Kernels for Dilute Emulsification Systems, Ind. Eng. Chem. Res. 50 (2011) 11358–11374. doi:10.1021/ie2006033.

[26] Y. Liao, D. Lucas, A literature review on mechanisms and models for the coalescence process of fluid particles, Chem. Eng. Sci. 65 (2010) 2851–2864. doi:10.1016/j.ces.2010.02.020.

[27] T. Kataoka, T. Nishiki, Dispersed mean drop sizes of (W/O)/W emulsions in a stirred tank., J. Chem. Eng. Jpn. 19 (1986) 408–412. doi:10.1252/jcej.19.408.

[28] T. Ohtake, T. Hano, K. Takagi, F. Nakashio, Effects of viscosity on drop diameter of W/O emulsion dispersed in a stirred tank., J. Chem. Eng. Jpn. 20 (1987) 443–447. doi:10.1252/jcej.20.443.

[29] R. Rautenbach, O. Machhammer, Modeling of liquid membrane separation processes, J. Membr. Sci. 36 (1988) 425–444. doi:10.1016/0376-7388(88)80034-6.

[30] T. Gallego-Lizon, E.S. Pérez de Ortiz, Drop Sizes in Liquid Membrane Dispersions, Ind. Eng. Chem. Res. 39 (2000) 5020–5028. doi:10.1021/ie000016y.

[31] I. Nopens, E. Torfs, J. Ducoste, P.A. Vanrolleghem, K.V. Gernaey, Population balance models: a useful complementary modelling framework for future WWTP modelling, Water Sci. Technol. 71 (2015) 159–167. doi:10.2166/wst.2014.500.

[32] M. v. Smoluchowski, Grundriß der Koagulationskinetik kolloider Lösungen, Kolloid-Z. 21 (1917) 98–104. doi:10.1007/BF01427232.

[33] N. Jager-Lezer, I. Terrisse, F. Bruneau, S. Tokgoz, L. Ferreira, D. Clausse, M. Seiller, J.-L. Grossiord, Influence of lipophilic surfactant on the release kinetics of water-soluble molecules entrapped in a W/O/W multiple emulsion, J. Controlled Release. 45 (1997) 1–13. doi:10.1016/S0168-3659(96)01507-6.

[34] S. Matsumoto, P. Sherman, A PRELIMINARY STUDY OF W/O/W EMULSIONS WITH A VIEW TO POSSIBLE FOOD APPLICATIONS, J. Texture Stud. 12 (1981) 243–257. doi:10.1111/j.1745-4603.1981.tb01234.x.

[35] J. Yan, R. Pal, Isotonic swelling behavior of W/O/W emulsion liquid membranes under agitation conditions, J. Membr. Sci. 213 (2003) 1–12. doi:10.1016/S0376-7388(02)00501-X.

[36] N. Garti, S. Magdassi, D. Whitehill, Transfer phenomena across the oil phase in water-oil-water multiple emulsions evaluated by Coulter counter: 1. Effect of emulsifier 1 on water permeability, J. Colloid Interface Sci. 104 (1985) 587–591.

[37] J. Bahtz, D.Z. Gunes, E. Hughes, L. Pokorny, F. Riesch, A. Syrbe, P. Fischer, E.J. Windhab, Decoupling of Mass Transport Mechanisms in the Stagewise Swelling of Multiple Emulsions, Langmuir. 31 (2015) 5265–5273. doi:10.1021/acs.langmuir.5b01138.

[38] W.S. Ho, T.A. Hatton, E.N. Lightfoot, N.N. Li, Batch extraction with liquid surfactant membranes: A diffusion controlled model, AIChE J. 28 (1982) 662–670. doi:10.1002/aic.690280419.

[39] M. Chakraborty, C. Bhattacharya, S. Datta, Emulsion Liquid Membranes, in: Liq. Membr., Elsevier, 2010: pp. 141–199. doi:10.1016/B978-0-444-53218-3.00004-0.

[40] K. Pays, J. Giermanska-Kahn, B. Pouligny, J. Bibette, F. Leal-Calderon, Coalescence in Surfactant-Stabilized Double Emulsions, Langmuir. 17 (2001) 7758–7769. doi:10.1021/la010735x.

[41] M. Chávez-Páez, C.M. Quezada, L. Ibarra-Bracamontes, H.O. González-Ochoa, J.L. Arauz-Lara, Coalescence in Double Emulsions, Langmuir. 28 (2012) 5934–5939. doi:10.1021/la205144g.

[42] J.K. Klahn, J.J.M. Janssen, G.E.J. Vaessen, R. de Swart, W.G.M. Agterof, On the escape process during phase inversion of an emulsion, Colloids Surf. Physicochem. Eng. Asp. 210 (2002) 167–181. doi:10.1016/S0927-7757(02)00376-X.

[43] A.J. Shere, H.M. Cheung, MODELING OF LEAKAGE IN LIQUID SURFACTANT MEMBRANE SYSTEMS, Chem. Eng. Commun. 68 (1988) 143–164. doi:10.1080/00986448808940403.

[44] S. Okazaki, M. Imai, M. Shimizu, Leakage Suppressing Oe W/O Emulsion Using High Viscous Solvent, in: Process Metall., Elsevier, 1992: pp. 1487–1492. doi:10.1016/B978-0-444-88677-4.50064-7.

[45] A.N. Kolmogorov, The local structure of turbulence in incompressible viscous fluid for very large Reynolds numbers, in: Dokl Akad Nauk SSSR, 1941: pp. 299–303.

[46] B. Andersson, R. Andersson, L. Håkansson, M. Mortensen, R. Sudiyo, B. Van Wachem, Computational fluid dynamics for engineers, Cambridge University Press, 2011.

[47] M. Karimi, R. Andersson, An exploratory study on fluid particles breakup rate models for the entire spectrum of turbulent energy, Chem. Eng. Sci. 192 (2018) 850–863. doi:10.1016/j.ces.2018.08.016.

[48] Andrey Kolmogorov, On the breakage of drops in a turbulent flow, Dokl Akad Navk SSSR. 66 (1949).

[49] R. Shinnar, On the behaviour of liquid dispersions in mixing vessels, J. Fluid Mech. 10 (1961) 259. doi:10.1017/S0022112061000214.

[50] P.H. CALDERBANK, Physical Rate Processes in Industrial Fermentations Part I : The Interfacial Area in Gas-Liquid Contacting with Mechanical Agitation, Trans Inst Chem Engrs. 36 (1958) 443–463.

[51] P.H. Chen, Factors influencing methane fermentation of microalgae, PhD Thesis, California Univ., Berkeley, USA, 1987.

[52] E. Nazarzadeh, S. Sajjadi, Viscosity effects in miniemulsification via ultrasound, AIChE J. 56 (2010) 2751–2755. doi:10.1002/aic.12133.

[53] A. Gupta, H.B. Eral, T.A. Hatton, P.S. Doyle, Controlling and predicting droplet size of nanoemulsions: scaling relations with experimental validation, Soft Matter. 12 (2016) 1452–1458. doi:10.1039/C5SM02051D.

[54] Theodore Vermeulen, Interfacial area in liquid-liquid and gas-liquid agitation, Chem. Eng. Progr. 51 (1955) 85F-94F.

[55] S.A. Miller, C.A. Mann, Agitation of Two-Phase Systems of Immiscible Liquids, Trans. Am. Inst. Chem. Engrs. (1944) 709–743.

[56] F. Michaut, P. Perrin, P. Hébraud, Interface Composition of Multiple Emulsions: Rheology as a Probe, Langmuir. 20 (2004) 8576–8581. doi:10.1021/la048715t.

[57] A. Schuch, J. Wrenger, H.P. Schuchmann, Production of W/O/W double emulsions. Part II: Influence of emulsification device on release of water by coalescence, Colloids Surf. Physicochem. Eng. Asp. 461 (2014) 344–351. doi:10.1016/j.colsurfa.2013.11.044.

[58] T.S.H. Leong, G.J.O. Martin, M. Ashokkumar, Ultrasonic encapsulation – A review, Ultrason. Sonochem. 35 (2017) 605–614. doi:10.1016/j.ultsonch.2016.03.017.

[59] T.S.H. Leong, S. Manickam, G.J.O. Martin, W. Li, M. Ashokkumar, Ultrasonic Production of Nano-emulsions for Bioactive Delivery in Drug and Food Applications, Springer International Publishing, Cham, 2018. doi:10.1007/978-3-319-73491-0.

[60] E.L. Paul, V.A. Atiemo-Obeng, S.M. Kresta, Handbook of industrial mixing: science and practice, John Wiley & Sons, 2004.

[61] L. Fradette, B. Brocart, P.A. Tanguy, Comparison of Mixing Technologies for the Production of Concentrated Emulsions, Chem. Eng. Res. Des. 85 (2007) 1553–1560. doi:10.1205/cherd06015.

[62] B. Brocart, P.A. Tanguy, C. Magnin, J. Bousquet, Design of In-Line Emulsification Processes for Water-in-Oil Emulsions, J. Dispers. Sci. Technol. 23 (2002) 45–53. doi:10.1080/01932690208984188.

[63] M.K. Li, H.S. Fogler, Acoustic emulsification. Part 1. The instability of the oil-water interface to form the initial droplets, J. Fluid Mech. 88 (1978) 499. doi:10.1017/S0022112078002232.

[64] M.K. Li, H.S. Fogler, Acoustic emulsification. Part 2. Breakup of the large primary oil droplets in a water medium, J. Fluid Mech. 88 (1978) 513. doi:10.1017/S0022112078002244.

[65] A. Shanmugam, M. Ashokkumar, Ultrasonic Preparation of Food Emulsions, in: M. Villamiel, A. Montilla, J.V. García-Pérez, J.A. Cárcel, J. Benedito (Eds.), Ultrasound Food Process., John Wiley & Sons, Ltd, Chichester, UK, 2017: pp. 287–310. doi:10.1002/9781118964156.ch10.

[66] T. Leong, M. Ashokkumar, S. Kentish, The fundamentals of power ultrasound-A review, (2011).

[67] B. Khadem, N. Sheibat-Othman, Modeling of double emulsions using population balance equations, Chem. Eng. J. 366 (2019) 587–597. doi:10.1016/j.cej.2019.02.092.

[68] A. Cárdenas, E. Castro, Breaking of multiple emulsions under osmotic pressure and the effect of W1/O relation, Interciencia. 28 (2003) 534–538.

[69] T. Hino, Y. Kawashima, S. Shimabayashi, Basic study for stabilization of w/o/w emulsion and its application to transcatheter arterial embolization therapy, Adv. Drug Deliv. Rev. 45 (2000) 27–45. doi:10.1016/S0169-409X(00)00098-3.

[70] S. Matsumoto, Y. Ueda, Y. Kita, D. Yonezawa, Preparation of Water-in-Olive Oil-in-Water Multiple-phase Emulsions in an Eatable Form, Agric. Biol. Chem. 42 (1978) 739–743. doi:10.1080/00021369.1978.10863054.

[71] A. Schuch, P. Deiters, J. Henne, K. Köhler, H.P. Schuchmann, Production of W/O/W (water-in-oil-in-water) multiple emulsions: droplet breakup and release of water, J. Colloid Interface Sci. 402 (2013) 157–164. doi:10.1016/j.jcis.2013.03.066.

[72] E. Dickinson, Double Emulsions Stabilized by Food Biopolymers, Food Biophys. 6 (2011) 1–11. doi:10.1007/s11483-010-9188-6.

[73] A. Sharma, A.N. Goswami, B.S. Rawat, Drop size prediction in liquid membrane systems, J. Membr. Sci. 60 (1991) 261–274. doi:10.1016/S0376-7388(00)81539-2.

[74] T. Ohtake, T. Hano, K. Takagi, F. Nakashio, Analysis of water entrainment into dispersed W/O emulsion drops., J. Chem. Eng. Jpn. 21 (1988) 272–276. doi:10.1252/jcej.21.272.

[75] T. Gallego-Lizon, E.S. Pérez de Ortiz, Drop Sizes in Liquid Membrane Dispersions, Ind. Eng. Chem. Res. 39 (2000) 5020–5028. doi:10.1021/ie000016y.

[76] T. Schmidts, D. Dobler, P. Schlupp, C. Nissing, H. Garn, F. Runkel, Development of multiple W/O/W emulsions as dermal carrier system for oligonucleotides: Effect of additives on emulsion stability, Int. J. Pharm. 398 (2010) 107–113. doi:10.1016/j.ijpharm.2010.07.037.

[77] T. Schmidts, D. Dobler, C. Nissing, F. Runkel, Influence of hydrophilic surfactants on the properties of multiple W/O/W emulsions, J. Colloid Interface Sci. 338 (2009) 184–192. doi:10.1016/j.jcis.2009.06.033.

[78] W.C. Griffin, Classification of surface-active agents by" HLB", J Soc Cosmet Chem. 1 (1949) 311–326.

[79] M. Frenkel, R. Shwartz, N. Garti, Multiple emulsions, J. Colloid Interface Sci. 94 (1983) 174–178. doi:10.1016/0021-9797(83)90247-3.

[80] F. Wolf, L. Hecht, H.P. Schuchmann, E.H. Hardy, G. Guthausen, Preparation of W_1/O/W$_2$ emulsions and droplet size distribution measurements by pulsed-field gradient nuclear magnetic resonance (PFG-NMR) technique, Eur. J. Lipid Sci. Technol. 111 (2009) 730–742. doi:10.1002/ejlt.200800272.

[81] T. Schmidts, D. Dobler, A.-C. Guldan, N. Paulus, F. Runkel, Multiple W/O/W emulsions—Using the required HLB for emulsifier evaluation, Colloids Surf. Physicochem. Eng. Asp. 372 (2010) 48–54. doi:10.1016/j.colsurfa.2010.09.025.

[82] A. Khalil, F. Puel, Y. Chevalier, J.-M. Galvan, A. Rivoire, J.-P. Klein, Study of droplet size distribution during an emulsification process using in situ video probe coupled with an automatic image analysis, Chem. Eng. J. 165 (2010) 946–957. doi:10.1016/j.cej.2010.10.031.

[83] J.P. Hindmarsh, J. Su, J. Flanagan, H. Singh, PFG–NMR Analysis of Intercompartment Exchange and Inner Droplet Size Distribution of W/O/W Emulsions, Langmuir. 21 (2005) 9076–9084. doi:10.1021/la051626b.

[84] X. Guan, K. Hailu, G. Guthausen, F. Wolf, R. Bernewitz, H.P. Schuchmann, PFG-NMR on W1/O/W2-emulsions: Evidence for molecular exchange between water phases, Eur. J. Lipid Sci. Technol. 112 (2010) 828–837. doi:10.1002/ejlt.201000022.

[85] R. Bernewitz, F. Dalitz, K. Köhler, H.P. Schuchmann, G. Guthausen, Characterisation of multiple emulsions by NMR spectroscopy and diffusometry, Microporous Mesoporous Mater. 178 (2013) 69–73. doi:10.1016/j.micromeso.2013.02.049.

[86] R. Bernewitz, U.S. Schmidt, H.P. Schuchmann, G. Guthausen, Structure of and diffusion in O/W/O double emulsions by CLSM and NMR–comparison with W/O/W, Colloids Surf. Physicochem. Eng. Asp. 458 (2014) 10–18. doi:10.1016/j.colsurfa.2014.01.002.

[87] L. Vermeir, P. Sabatino, M. Balcaen, A. Declerck, K. Dewettinck, J.C. Martins, G. Guthausen, P. Van der Meeren, Effect of molecular exchange on water droplet size analysis as determined by diffusion NMR: The W/O/W double emulsion case, J. Colloid Interface Sci. 475 (2016) 57–65. doi:10.1016/j.jcis.2016.04.029.

[88] I. Lönnqvist, B. Håkansson, B. Balinov, O. Söderman, NMR Self-Diffusion Studies of the Water and the Oil Components in a W/O/W Emulsion, J. Colloid Interface Sci. 192 (1997) 66–73. doi:10.1006/jcis.1997.4966.

[89] M.A. Voda, J. van Duynhoven, Characterization of food emulsions by PFG NMR, Trends Food Sci. Technol. 20 (2009) 533–543. doi:10.1016/j.tifs.2009.07.001.

[90] S. Schuster, R. Bernewitz, G. Guthausen, J. Zapp, A.M. Greiner, K. Köhler, H.P. Schuchmann, Analysis of W1/O/W2 double emulsions with CLSM: Statistical image processing for droplet size distribution, Chem. Eng. Sci. 81 (2012) 84–90. doi:10.1016/j.ces.2012.06.059.

Chapter 2. Investigating Swelling-Breakdown in Double Emulsions

Dilute water-in-oil-in water double emulsions are prepared to investigate the release and swelling phenomena during preparation and storage. During storage, a specific attention is paid to detect the overswelling-breakdown phenomenon that is due to overswelling of the outer droplets which causes their breakage and abrupt release of the inner droplets. A swelling ratio of the outer droplets is defined and is found useful to identify the effect of different parameters on the swelling behavior of the double emulsions. Yet, the investigation of the full droplet size distribution is also necessary. Before overswelling-breakdown, the escape is governed by the Brownian motion of the inner droplets and their coalescence with the external phase through the surface of the outer droplets. The swelling rate is governed by the osmotic gradient between the internal and external water phases.

2.1. Introduction

To produce double emulsions, typically, a primary emulsion is prepared in a first step under high shear to disperse an internal phase in an intermediate phase. In a second step, this primary emulsion is dispersed in an external phase while mixing under a lower shear rate. Both water-in-oil-in-water (W/O/W) and oil-in-water-in-oil (O/W/O) double emulsions can be produced. This two-step method was firstly introduce by Li (1968) [1] for the purpose of extraction (O/W/O) and the term liquid membranes was employed. A first hydrophobic phase was emulsified within an aqueous surfactant solution to produce oil droplets coated with a thin membrane of surfactant and water, which was then dispersed into another hydrophobic phase to be washed by permeation through the membrane. Then, Matsumoto et al. (1976) [2] introduced this method for the formation of double emulsions, which is still the most common way of producing double emulsions. A higher shear is employed in the first step in order to produce small inner (i.e., micro) droplets and a lower shear is employed in the second step with the aim of preventing the release of inner droplets and thus bigger outer (i.e., macro) droplets are formed. The outer droplets are sometimes also called globules. The droplet size of both the inner and outer droplets and the encapsulation rate have a major effect on the quality of double emulsion products [3].

The preparation and stability of double emulsions have been the subject of many studies. On one hand, during the second preparation step, the outer droplets may undergo breakage, coalescence, and Oswald ripening while the inner droplets may undergo coalescence, growth by Oswald ripening or escape to the external phase [1,2,4–9]. On the other hand, during storage, different possible destabilization pathways of the double emulsion may occur, namely inner-inner and outer-outer droplet coalescence, expulsion of the inner droplets (i.e. inner droplet coalescence with the outer phase), Oswald ripening, swelling/shrinkage of the inner (and so of the outer) droplets (i.e. diffusion of water/solvent) and molecular diffusion of dissolved ingredients between the phases [8,10–19]. The swelling phenomena may ultimately

lead to swelling-breakdown, i.e. gradual expulsion of the inner droplets out of the outer droplet [11,19–21], or to a more abrupt expulsion [11,19–21], here called over-swelling breakdown. The later phenomenon may cause breakage of the outer droplet that joins the important escape of the inner droplets. These different phenomena impact the encapsulation efficiency and the droplet size that has a direct influence on the stability of the double emulsions.

Parameters affecting the preparation of double emulsions. During preparation, the operating conditions were found to have the following effects in W/O/W double emulsions: An increase in the encapsulation efficiency was observed when increasing the fraction of the primary emulsion [2,22,23] and the fraction of lipophilic (i.e. internal) emulsifier [2,24]. A decrease in the encapsulation efficiency was observed when increasing the hydrophilic (i.e. external) emulsifier concentration [2,25], the emulsification time [5,6,23,24,26–28] and the stirring rate (or energy) in the second emulsification step [5,22,25,27,29,30]. The effects of increasing the stirring time and rate on the encapsulation efficiency can be explained by an increased inner droplet escape rate [28], which in turn is enhanced by the increased outer droplet deformation and breakage [1,24,27]. The encapsulation efficiency also depends on the sizes of the inner and outer droplets. It increases with bigger outer droplets [5,9,28,31] and with smaller inner droplets or with a reduced inner-to-outer droplet size ratio [32]. A comparative study over various devices (i.e., colloid mill, tooth rim dispersing machine, high pressure homogenizer, and rotating membrane device) for the preparation of double emulsions was handled by Schuch et al. (2014) who indicated the encapsulation efficiency to mainly depend on the outer droplet size but not on the device [9]. The size of the outer droplets is itself defined by the operating conditions, and it was found to decrease for higher stirring rates (or energy) [5,7,9,31,33,34], longer emulsification times [5,23,28] and higher hydrophilic (i.e. external) emulsifier concentrations [25], while bigger outer droplets were produced with higher internal phase fraction [5,7,34,35] and/or higher primary emulsion fraction [23,33].

Frenkel et al. (1983) [36] introduced a weighted HLB expression to define the effects of both lipophilic and hydrophilic surfactants on the preparation of double emulsions. They outlined that the formation of double emulsion can occur only if both the criteria of (a) weighted-HLB < 10, and (b) weighted-HLB < desired HLB of the oil phase, are realized, and, the size of the outer droplets should be big enough (> 5 µm in their study) to be able to contain the inner droplets of a certain size. Schmidts et al. (2009 and 2010) [37,38] indicated that, other than the HLB value, the chemical composition of the hydrophilic surfactant needs to be compatible with the oil and lipophilic surfactant type and amount.

Other operating conditions were found to have more complex effects and sometimes contradictory effects appear in the literature. For instance, increasing the internal phase fractions were found to decrease the encapsulation efficiency by [22,35] and to increase it by [2,5,26]. This is partly due to the fact that when increasing the inner phase fraction, the concentration of ions is also changes. Indeed, the ions (e.g. NaCl, MgSO4, glucose, dissolved in the inner phase) are usually employed to enhance the stability of the double emulsion. Schmidts et al. (2009 and 2010) [37,38] observed that the characteristics of the system – both

right after preparation and during storage – were affected by the concentration and nature of the osmotic additives. The use of ions was found to have complex effects. For higher NaCl fractions in the inner phase, an increase in the outer droplet size was observed by [23,39] while a decrease was observed by [38]. Similarly, increasing the NaCl fraction in the inner phase was found to increase the encapsulation efficiency by [5,23,39] but to decrease it by [26]. Increasing the fractions of MgSO4 in the inner phase showed an increase or a decrease depending on the amount of hydrophilic emulsifiers [38].

Parameters affecting the stability of double emulsions during storage. Double emulsions were monitored by optical or electronic microscopy during storage in order to investigate their evolution during storage in terms of size and number of the inner and outer droplets. The outer droplet size was found to decrease at the beginning of storage which was assumed to be due the release of inner droplets [16,18] and to increase with time which was assumed to be due to droplet coalescence [16]. Ficheux et al. (1998) [40], identified two types of instabilities: inner-inner and inner droplet coalescence with the outer continuous phase (i.e., escape), and indicated that they were determined by the concentration of hydrophilic surfactant in the external aqueous phase in W/O/W double emulsions. Pays et al. (2001) [12] identified two types of release: molecular release of the encapsulated substance and inner droplet escape by coalescence with the outer phase. They proposed a behavioural curve as a function of the hydrophilic surfactant and inner phase fractions in order to define the border of these two types of release.

Besides inner-inner coalescence, molecular diffusion and inner droplet escape, swelling or shrinkage were also observed to occur in double emulsions containing ions in the inner or outer phases. The first swelling study was reported by Matsumoto and Kohda (1980) [41], regarding water transfer through the oil layer in W/O/W double emulsions. A mechanism of diffusion through the intermediate oil membrane was described considering by the osmotic pressure gradient between the inner and outer water phases as a driving force (i.e., $L_\mathrm{p} A_\mu \Delta\Pi$), and the swelling rate was assumed to be governed by the permeation coefficient (L_p) and the surface of inner droplets (A_μ). The osmotic pressure gradient is proportional to the ions concentration gradient, $\Delta\Pi \propto \Delta C$.

In subsequent works, the permeation coefficient of the oil phase and the swelling rate were investigated by varying the oil type or viscosity, where a decrease in the swelling rate was observed when increasing the oil viscosity [10,41–43]. Increasing the lipophilic surfactant concentration (i.e. internal emulsifier) showed an increase in the swelling rate in some works [11,15,44] and a decrease in others [41]. The swelling rate was found to be higher with higher osmotic pressure gradients [15,41,43] and lower for higher inner phase fractions [15].

Terrisse et al. (1994) [45], observed that the swelling was followed by a rupture in the oil membrane, which was later called swelling-breakdown [11]. This phenomenon represents the expulsion of inner droplets, through their coalescence with the outer phase. As it is enhanced by swelling, it may lead to the breakage of the outer droplet. This behaviour was also observed by Raynal et al. (1993) [21] who indicated that it can be tuned through the osmotic pressure gradient. Jager-Lezer (1997) [11] and Geiger et al. (1998) [20] reported that the swelling-

breakdown was the main cause of release in their case while the diffusion was negligible. They indicated the swelling-breakdown to be controlled by the swelling capacity of the outer droplet (i.e. the oil layer resistance against breakdown) and that having higher lipophilic emulsifier leads to higher swelling capacities of W/O/W double emulsions (also observed by [15,44]). This was explained by the fact that increasing the surface of inner droplets, as a consequence of swelling, required an increasing amount of lipophilic surfactant. Similarly, Mezzenga et al. (2004) [46] stated that increasing the lipophilic surfactant fraction decreases the interfacial tension, which in turn decreases the Laplace pressure, leading to an increased swelling ratio. The overswelling-breakdown phenomenon was recently employed as a way to form hydrogel microfibers with precise length, where the swelling was induced via an alternating current electric field [47]. By investigating single drop-in-drop double emulsions Bahtz et al. (2015) [43] observed a lag stage (of about tens of minutes) at the beginning of storage, during which the swelling rate was very slow, as also reported by [11]. They indicated the lag duration to be higher for more viscous oil layers and lower for a higher inner phase fraction, while the osmotic pressure did not show any effect on the lag time duration [43].

In summary, the release of the encapsulated substance can generally be of different types: (a) Molecular diffusion of the encapsulated substance through the oil layer (without film rupture) which is generally slow if the encapsulated substance has a low solubility in the intermediate layer [11,13], (b) leakage of inner droplets due to breakage of the outer droplets through inner droplet coalescence with the outer phase (only during preparation) [5,6,23,30], (c) escape of inner droplets due to their Brownian motion (during storage), by coalescence of inner droplets to the external continuous phase through the surface of the outer droplets [12,14]; this phenomenon might be enhanced if there is a simple shear applied on the double emulsion, without necessarily breaking the outer droplets [28] (d) swelling of the inner (and so of the outer) droplets may enhance the escape of inner droplets, which is in this case called swelling-breakdown [11], e) extreme swelling may lead to over swelling-breakdown where a burst escape of inner droplets is observed causing breakage of the outer droplet.

It appears from the literature review that the preparation of double emulsions and their stability during storage are governed by a number of operating conditions that need further investigation. More precisely, the swelling and overswelling-breakdown phenomena need quantification. Also, correlations between the operating parameters and the properties just after preparation as well as during storage are required.

Objectives. The objective of this work is to investigate the effect of different operating conditions on the properties of the double emulsions during preparation and storage. During preparation, the breakage of the outer droplets and leakage of inner droplets are investigated. During storage, the escape and swelling-breakdown phenomena are investigated to determine their original causes. A specific attention is paid to investigate the full size distribution of the inner and outer droplets (DSD). A number of key process parameters were varied, namely the fraction of internal water, the stirring rate in the second preparation step, the fraction of salt, and the fraction of primary emulsions. The first preparation step is done using ULTRA-TURRAX®. The second emulsification step is done in a 1-L stirred vessel that is

equipped with an in situ online video probe and a conductivity probe. The inner droplet size was measured right after the first step of preparation. The outer droplet size and the conductivity of the double emulsions (which is indicative of the release rate) were monitored during the second preparation step using both online and offline measurements, and during storage using offline measurements.

2.2. Experimental

2.2.1 Materials

W/O/W double emulsions are prepared using Mineral oil (Fisher ScientificTM), Span 80 (Alfa Aesar) as hydrophobic internal emulsifier, Tween 80 (Fisher ScientificTM) as hydrophilic external emulsifier, Sodium Chloride as tracer and Millipore water (resistivity $\approx 18.2\ m\Omega.cm$).

2.2.2 Double emulsion preparation

A two-step method was used to produce W/O/W double emulsions at room temperature. First, a primary emulsion was prepared by dispersing the NaCl aqueous solution in the oil phase – oil containing Span 80 – using an IKA T 25 digital ULTRA-TURRAX® at 12 000 rpm for 4 min. Second, the double emulsion was produced by dispersing the primary emulsion in an external aqueous phase – water containing Tween 80 – in a 1-L vessel stirred at 300–500 rpm for 70 min (Fig. 1). The fractions of these materials can be seen in Table 2.1.

***Table 2.1**. Experimental conditions*

	First preparation step Fractions (wt. %)				Operating parameters		Second preparation step Fractions (wt. %)			Operating parameters	
	Water	Mineral oil	NaCl	Span 80	t_1 (min)	ω_{RS} (rpm)	Primary	Water	Tween 80	t_2 (min)	ω_R (rpm)
Set 1: ϕ_{outer}	40	50	0.05	9.95	4	12000	1 2 3 4	98 97 96 95	1	70	400
Set 2: ϕ_{NaCl}	40	50	0.05 0.14 0.19 0.24	9.95	4	12000	1	98	1	70	400
Set 3: ϕ_{inner}	40 30 20 10	50 60 70 80	0.05	9.95	4	12000	1	98	1	70	400
Set 4: ω_R	40	50	0.05	9.95	4	12000	1	98	1	70	300 350 400 500

Symbols: ϕ_{outer}: Outer phase fraction, ϕ_{NaCl}: Salt fraction, ϕ_{inner}: Inner phase fraction, ω_R: stirring rate in the vessel, and ω_{RS}: stirring rate by the Ultra-Turrax.
The total mass in the second step is 1 kg.

The 1-L stirred vessel is equipped with a three-bladed stainless-steel impeller and four baffles (Fig. 2.1). The vessel is equipped with an in situ video probe to online monitor the outer droplet size while the release rate of salt is monitored by a conductivity probe.
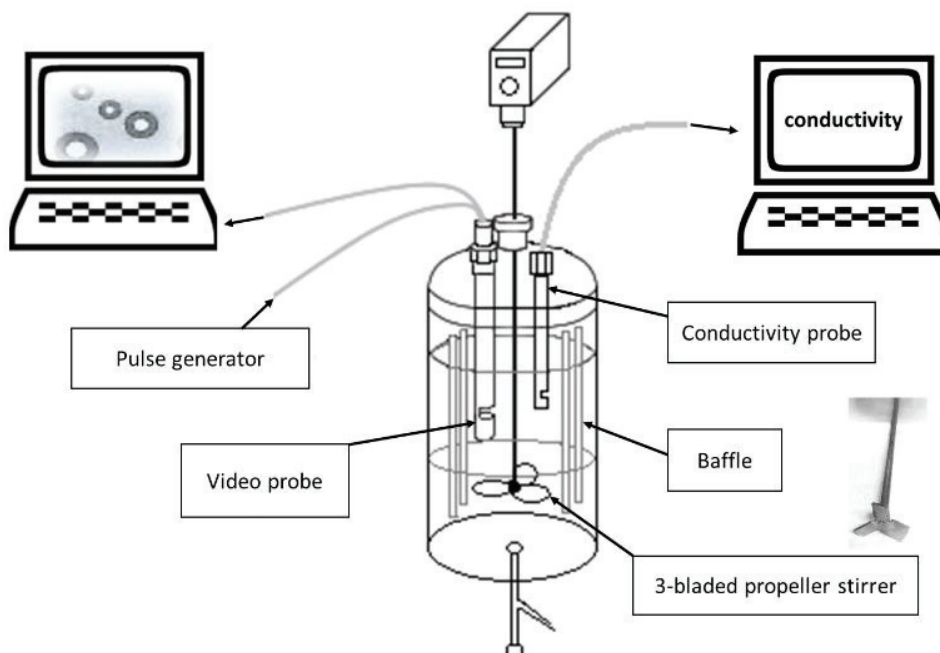
Fig. 2.1. *Set-up for the second step of double emulsion preparation in a 1-L reactor.*

2.2.3 Conductivity measurements

The conductivity measurement was performed using a CDM210 Conductivity Meter (MeterLab®) during the second preparation step. The conductivity data then allowed to predict the released amount of salt using a predetermined calibration curve, by dissolving different salt concentration in pure water, or in a single O/W emulsion, were the two methods were found equivalent for the calibration. The samples were kept at controlled room temperature of 20°C.

2.2.4 Droplet size measurement

The size of the inner droplets was measured right after the first preparation step by means of dynamic light scattering (Malvern Zetasizer Nano ZS®). The samples were diluted approximately 1:1000 in mineral oil and the analysis was repeated twice.

The size of the outer droplets was measured by two techniques. First, an offline laser diffraction technique was employed (Malvern Mastersizer 3000®). Samples were regularly taken during the second preparation step and during storage. The refractive index of the outer droplets was considered to be that of oil (i.e. 1.467), which represents the main component of these droplets, especially close to the surface. Second, an in situ video probe EZ Probe-D25® was employed to take videos of the emulsion (Fig. 1), followed by image processing and reconstruction of a number density distribution. The probe was located 5 cm above the stirrer and close to the stirring shaft as suggested by [48]. The video probe has a CCD camera with a recording rate of 50 frames per second. Each video recording duration was 30 s, from which 300 frames – of size 720×576 pixels – were selected. Image processing was then done offline using a MATLAB® program based on the circular Hough transform [48]. Besides these two quantitative methods, double emulsions were observed with an optical microscope to provide a visual analysis of inner and outer droplets (Leica© DM2000 LED).

2.3. Results and discussions

2.3.1 Evidence of over swelling and overswelling-breakdown

An example of the obtained inner droplet size distribution, measured by dynamic light scattering after the first preparation step is shown in Fig. 2.2. In general, inner droplets with a monomodal distribution around 1 μm in mean diameter are obtained. After the production of the double emulsion (and during storage), quantitative measurement of the inner droplet's size distribution represents a big challenge. Recent investigations involve the use of pulsed field gradient NMR technique (PFG-NMR) [8,49–54], and confocal laser scanning microscopy (CLSM) [50,51,55,56], which are promising but they have different constraints and require mathematical treatments. In this work, a qualitative measurement is obtained by optical microscopy.
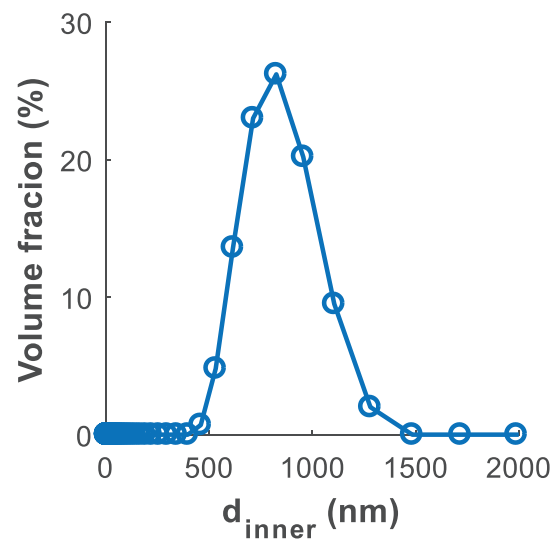
Fig. 2.2. *An example of the size distribution of inner droplets (i.e., the primary W/O emulsion), prepared with ω_{RS} = 12000 rpm, ϕ_{inner} = 40 % and ϕ_{NaCl} = 0.05 %.*

Regarding the outer droplets, two techniques were employed to measure the DSD. Indeed, while laser diffraction is nowadays a well-established method to measure the size of single emulsions, it is worthy to validate that the inner droplets do not impact the measurement of the outer droplets and eliminate possible effects of the dilution and pumping procedure in the Mastersizer (e.g. breakage or coalescence). Therefore, besides offline measurement using the master sizer, a video probe was inserted into the stirred vessel and the images were treated to predict the outer DSD.

Fig. 2.3 shows an example of one 2-D image of the outer droplets taken in situ during the second emulsification step. The image processing treatment allows the detection of the outer droplets that are surrounded by circles, where most of them appear to be correctly detected. A comparison between the two techniques is shown in Fig. 2.4. In order to compare the results of the two methods, the size distributions were first converted into number densities then the real volume fractions, which are a better representative of the system, were determined. It can be seen that the video probe has a limited capacity to detect very small droplets that are

30

better captured by the master sizer. However, while the lower number of droplets in the on-line method makes a less smooth curve, a fairly similar DSD is obtained by both methods. It can be concluded that the inner emulsion does not influence the measurement in laser diffraction and that the double emulsion is stable during the measurement. Since the results from the Mastersizer are based on a bigger number of droplets and give smoother curves, in the rest of the paper only these measurements are shown.
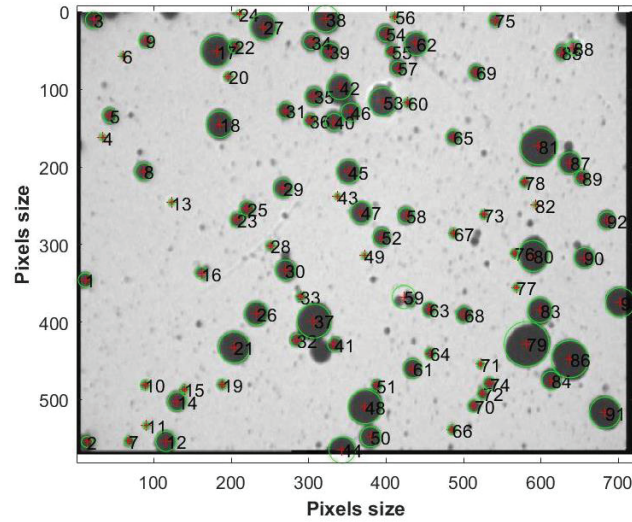
Fig. 2.3. *An image extracted from the video probe measurement with the outer droplets detected by image processing, for the sample prepared with ϕ_{inner} = 40 %, ϕ_{NaCl} = 0.05 %, ϕ_{outer} = 1 %, and ω_R = 300 rpm.*
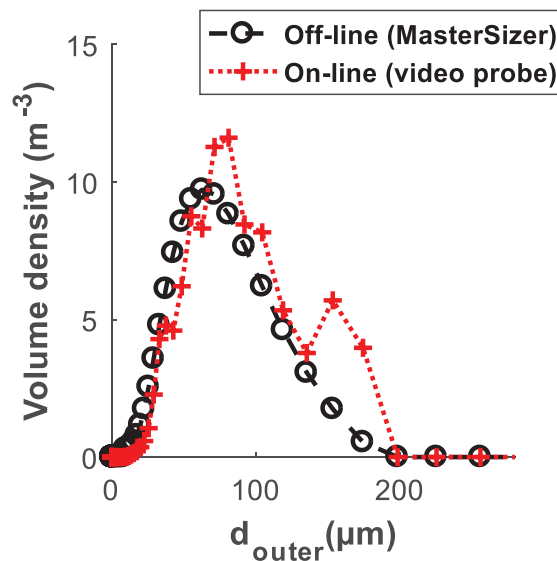
Fig. 2.4. *A comparison of the outer droplet size distribution measured by MasterSizer and the video probe, for the sample prepared with ϕ_{inner} = 40 %, ϕ_{NaCl} = 0.05 %, ϕ_{outer} = 1 %, and ω_R = 300 rpm.*

The DSD of the outer droplets were also qualitatively validated by optical microscopy. Besides, the microscopy represents the only available method in this work to investigate the evolution of the inner droplets after the production of the double emulsions.

50 μm

30,41 μm

40,18 μm

60,99 μm

47,76 μm

A

50 μm

B

50 μm

29,41 μm

36,83 μm

C

20 μm

12,95 μm

9,72 μm

11,38 μm

11,01 μm

D
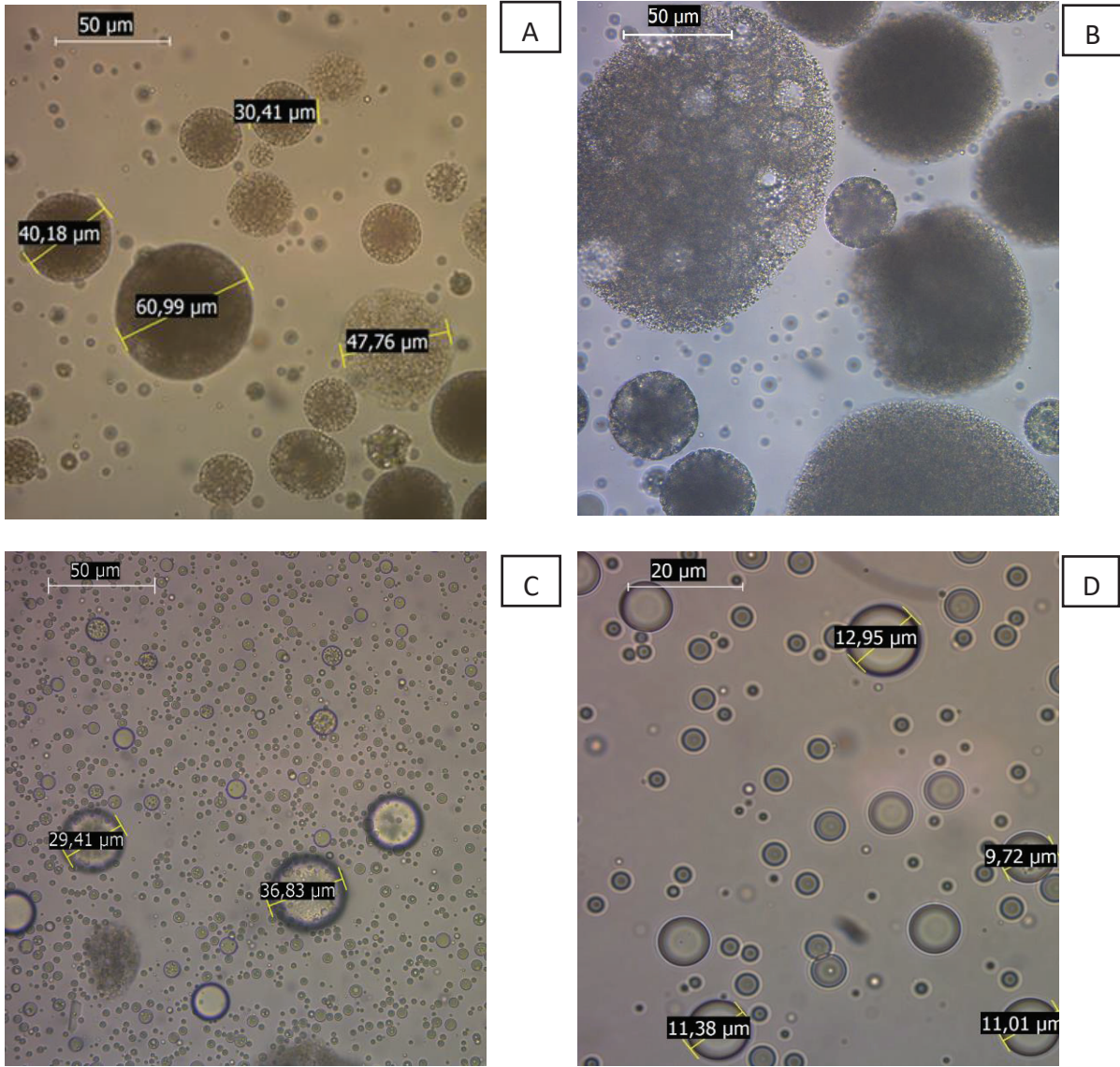
Fig. 2.5. *Microscopic images, for the sample prepared with* ϕ_{inner} *= 40 %,* ϕ_{outer} *= 1 %, and* ω_R *= 400 rpm: A) Right after preparation (Day 0), B) Day 6, C) Day 9, and D) Day 50.*

Fig. 2.5 shows few examples of microscopic images made during storage. At day 0, right after the preparation of the double emulsion, both the inner and outer droplets clearly appear and their sizes are coherent with the measurements given in Figs 2.2–2.4. It can be seen that the inner and outer droplets importantly swell at day 6 (Fig. 2.5B), then breakdown at day 9 and decrease importantly in size (Fig. 2.5C). Full escape does not justify such a decrease in the size, which reveals the occurrence of breakage of the outer droplets. It appears that the outer droplets reach a maximum swelling capacity (here observed at day 6). This causes their breakdown (here observed at day 9), resulting in fast inner droplets escape to the external phase and outer droplet breakage. Fig. 2.5C shows that few inner droplets remain inside the outer droplets at day 9. These inner droplet did not over-swell, certainly due to their initial smaller size and so higher Laplace pressure that counterbalances the osmotic pressure. They continue to release to the external phase via diffusion to the surface of the outer droplet and coalescence to the external phase. At day 50 all the outer droplets appear to be empty from

the inner droplets (Fig. 2.5D, note that the zoom bare is reduced in this figure to 20 μm to confirm that the outer droplets are empty).

Other than swelling, the increase in the outer droplet size during storage could be due to outer-outer droplet coalescence or Ostwald ripening. However, a single O/W emulsion ($\phi_{\text{Mineral oil + Span 80}}$ = 1 %, $\phi_{\text{Tween 80}}$ = 1 % and ϕ_{Water} = 98 %) was prepared and stored at similar conditions as the double emulsion and the increase in the size by coalescence or Oswald ripening was found to be negligible over 3 weeks. A comparison between this O/W emulsion and a W/O/W double emulsion after one week of storage is shown in Fig. 2.6. It can be seen that the initial sizes of both the single and double emulsion are comparable, and therefore they may be expected to undergo similar coalescence rates. After one week of storage, the droplet size of the O/W emulsion increased only very slightly due to droplet coalescence, while the outer droplet size of the W/O/W double emulsion increased importantly. This indicates that the main increase in the W/O/W double emulsion is due to swelling, which is driven by the osmotic pressure gradient caused by the presence of salt in the inner phase.
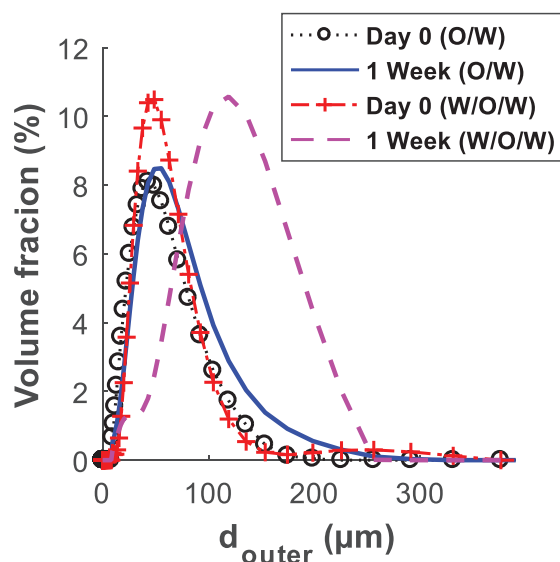
Fig. 2.6. Comparison between DSD of single O/W emulsion and outer DSD of W/O/W double emulsion during one week of storage. O/W is prepared with $\phi_{\text{oil phase}}$ = 1 % and ω_R = 400 rpm. W/O/W is prepared with ϕ_{inner} = 40 %, ϕ_{NaCl} = 0.05 %, ϕ_{outer} = 1 % and ω_R = 400 rpm

Fig. 2.7 shows an example of the evolution of the outer DSD over three weeks. Two stages can be distinguished from the figure: a) During the first week, the outer droplets get bigger in size due to swelling until reaching a maximum swelling (observed here at day 8), and b) during the following weeks, a decrease in their size is observed due to overswelling-breakdown. After three weeks, the final size of the outer droplets is smaller than the initial outer droplet size. Such a decrease could not be explained by the escape of the internal phase alone. Indeed, the theoretical final mean droplet size was calculated, based on the initial droplet size and the inner fraction, by assuming only escape (Fig. 2.8). It can be seen that the measured final size is smaller than the predicted one if only escape occurs. This confirms the occurrence of breakage of the outer droplets during the overswelling-breakdown phenomenon.
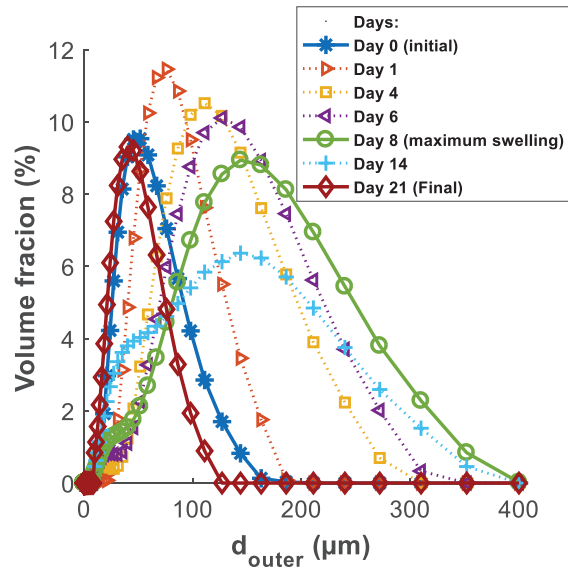
Fig. 2.7. *Evolution of the outer droplet size distribution for the sample prepared with ϕ_{inner} = 40 %, ϕ_{NaCl} = 0.05 %, ϕ_{outer} = 2 % and ω_R = 400 rpm.*
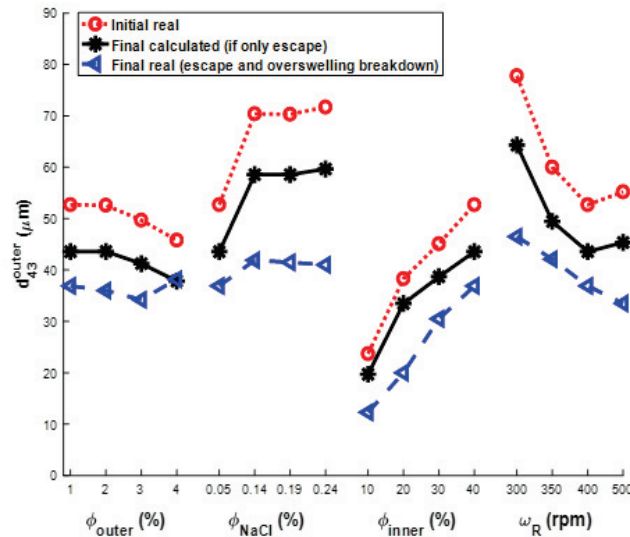

Fig. 2.8. *Mean outer droplets diameter: Real initial d_{43}, real final d_{43} and final predicted d_{43} calculated assuming full escape (initial outer droplet volume - inner droplets volume).*

In the following sections, the effect of different key process parameters on the outer DSD and release rate, during preparation and storage, are investigated and discussed: the fraction of internal water, the stirring rate in the second preparation step, the fraction of salt, and the fraction of primary emulsion.

2.3.2. Effect of the primary emulsion fraction (ϕ_{outer})

The primary emulsion was prepared with 40 % inner phase and 0.05 % salt. Different amounts of this emulsion were then introduced in the stirred vessel under 400 rpm for 70 min (Table 2.1).

During preparation, increasing the dispersed phase fraction may enhance droplet coalescence and reduce the breakage efficiency due to the damping effect of the energy dissipation [57]. Indeed, the energy dissipation rate ε (W.kg-1) in a stirred tank can be calculated using the general power equation, $\varepsilon = \frac{N_P \, \omega_R^3 \, D_R^5}{V}$, where the power number of the employed three blade Mixel TT propeller is $N_P = 0.8$, ω_R (rev.s-1) is the stirring rate, $D_R = 0.088$ m is the impeller diameter and V (m3) is the volume of the material in the reactor. This gives $\varepsilon = 1.25$ W.kg-1 with a mixing rate of 400 rpm. For a two-phase system, a dampening effect was highlighted where the effective energy dissipation rate becomes $\varepsilon_{eff} = \frac{\varepsilon}{(1+\phi_{outer})^3}$ (with ϕ_{outer} the fraction of the outer phase) [5,56]. This gives $\varepsilon_{eff} = 1.21$, 1.18, 1.14, and 1.11 for $\phi_{outer} = 1$, 2, 3, and 4 %, respectively. Therefore, increasing the outer phase fraction from 1 % to 4 % slightly lowers the effective energy dissipation rate. From Fig. 2.9A, it can be seen that increasing ϕ_{outer} leads to slightly larger distributions and bigger droplets, except with $\phi_{outer} = 4$ %. However, the effect is not significant which can be explained by the fact that the emulsions are dilute and to the use of a big amount of surfactant. A slight increase in the outer droplet size with increasing ϕ_{outer} of dilute emulsions (i.e. $\phi_{outer} = 2\text{–}7$ %) was reported by [33]. Fig. 2.9B shows the released fraction calculated from the conductivity measurements. Similar release rates are obtained with most of the fractions, except the one with $\phi_{outer} = 1$ % that led to a slightly higher release during preparation, indicating a slightly higher escape of inner droplets by the shear-induced breakage of the outer droplets [2,5,6,30]. A lower release (i.e., higher encapsulation efficiency) was reported when increasing ϕ_{outer} by [2] for more concentrated double emulsions (i.e., $\phi_{outer} = 10\text{–}50$ %). In the present system, the solubility of salt in the oil phase is low and it leads to negligible release by molecular diffusion, during preparation and storage. Thus, leakage due to breakage is the main cause of release [5,23].

The samples were then stored at room temperature and the size and release were monitored during three weeks. A swelling ratio was calculated, as the ratio between the outer droplet mean diameter d_{43} during storage to the initial diameter obtained right after the preparation [15]. Fig. 2.9C shows that the swelling ratio reaches a maximum between one to two weeks then starts decreasing. The ratio appears to be higher for higher primary emulsion fractions. Fig. 2.9D shows the release profile during storage. The presented released fraction is the part released during storage and is not cumulated with the released amount during preparation. Initially, the release rate is lower and is governed by the escape of inner droplets, due to their Brownian motion followed by inner droplet coalescence with the outer phase. This is in agreement with previous findings, where the release mechanism was found to be controlled by escape for an W/O/W double emulsion containing over 100 CMC of hydrophilic emulsifier with HLB < 30 (e.g. Tween 80) [12,13]. Then, a burst release is observed between one to two weeks, which corresponds to the time where the maximum swelling ratio is reached and overswelling-breakdown occurs. This phenomenon is caused by exceeding the swelling capacity of the double emulsion. This causes faster inner droplet escape and outer droplet breakage. Fig. 2.9D shows that the samples with lower swelling have higher release rates, which was also observed by [11].
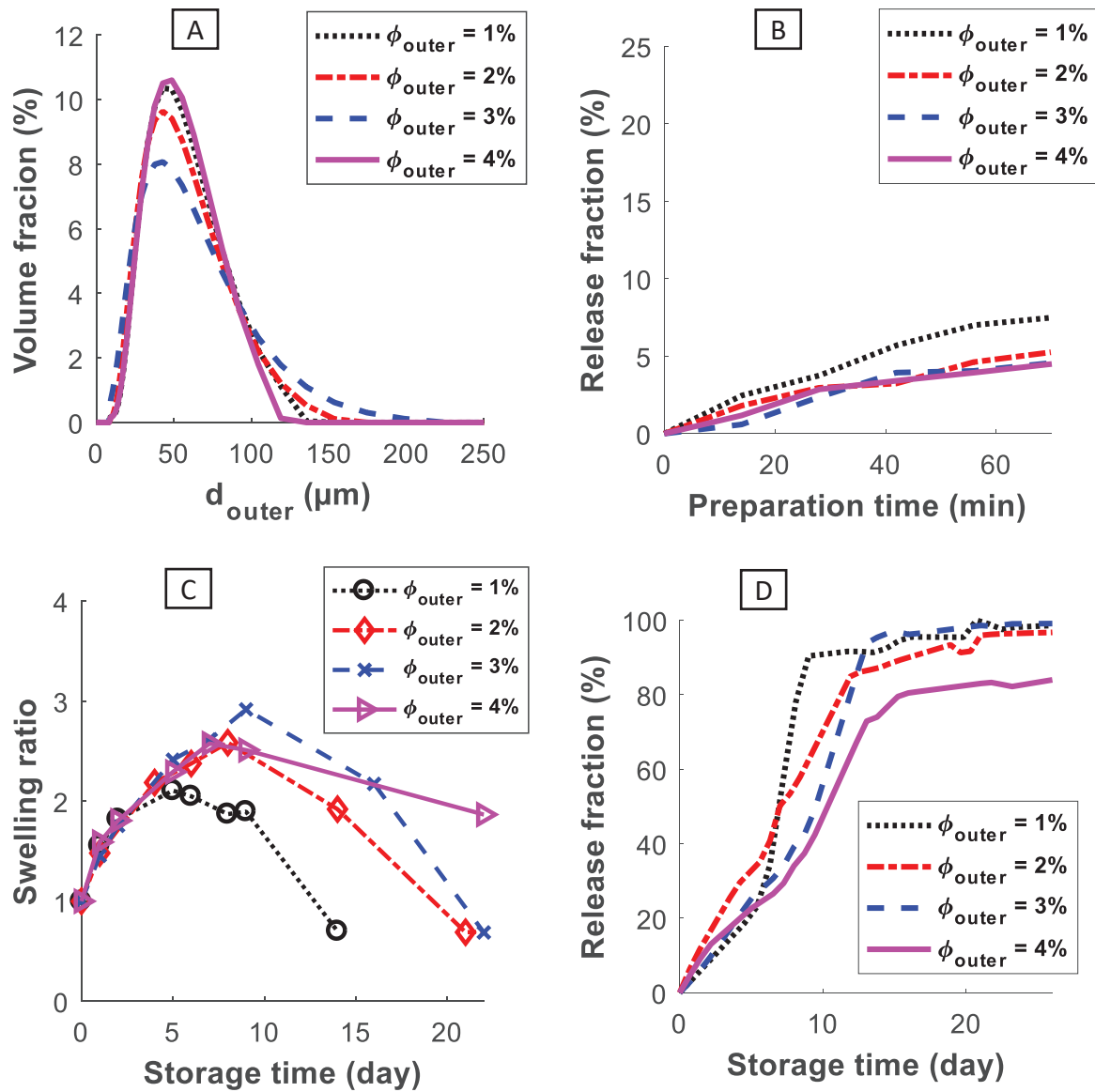
Fig. 2.9. *Effect of the fraction of primary emulsion (ϕ$_{outer}$) on the: A) size distribution during preparation, B) release during preparation, C) swelling ratio during storage (i.e. the ratio of the mean diameter d$_{43}$ after and before swelling), and D) release*
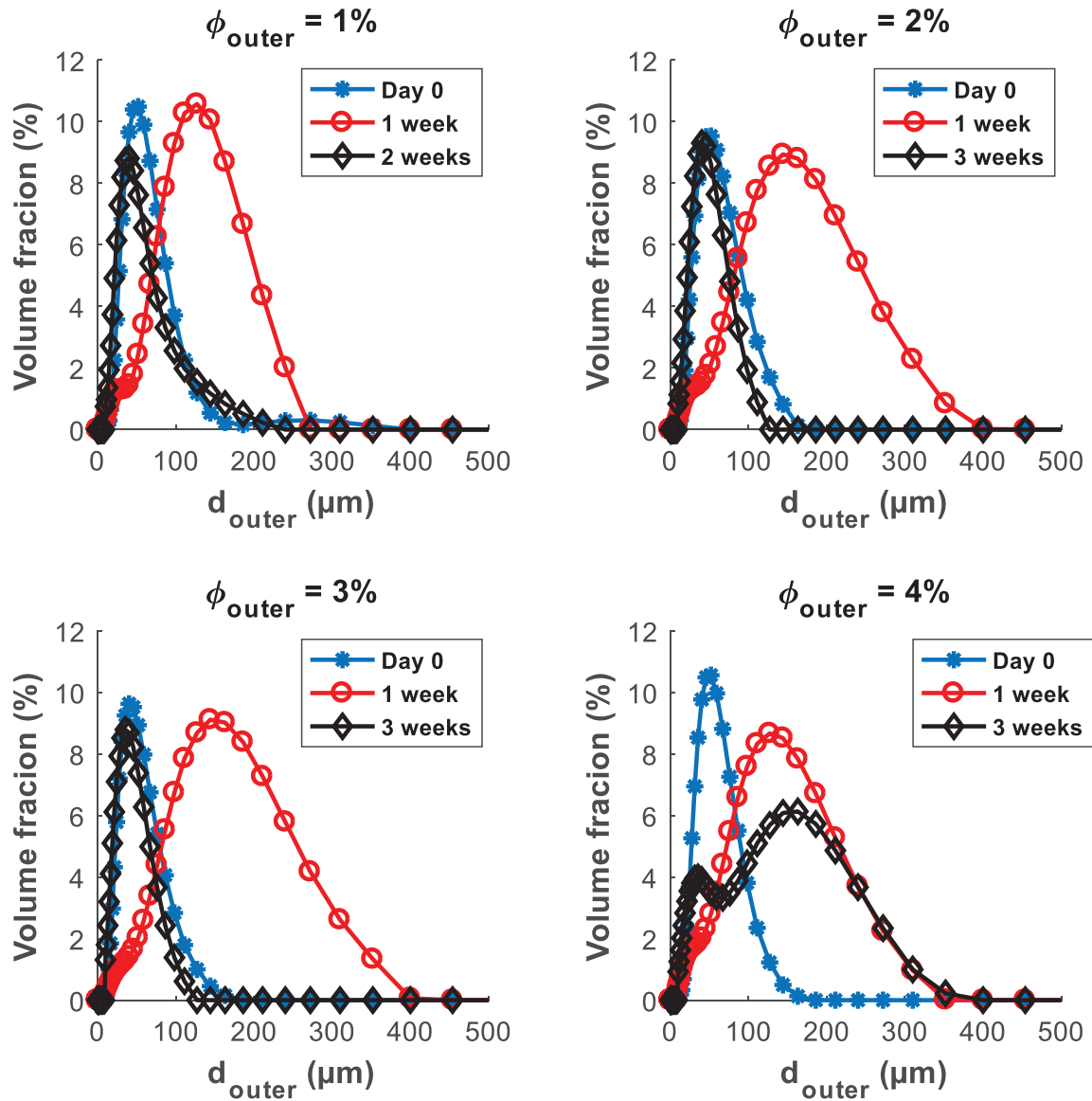
Fig. 2.10. *Effect of primary emulsion fraction (ϕ_{outer}) on size distribution during storage.*

Fig. 2.10 shows the initial, maximum swollen and final broken-down DSD of the outer droplets measured during storage for the different primary emulsion fractions. The full distribution is shown, which gives supplementary information compared to the swelling ratio that is based on a mean diameter that may not be representative of the full distribution. It can be seen that the occurrence of the overswelling breakdown is slightly delayed when increasing the primary emulsion fraction. Namely, the experiment with $\phi_{outer} = 4\ \%$ is bimodal where part of the droplets are still at their maximum swelling capacity while others have brokendown to small sizes.

2.3.3. Effect of the salt fraction (ϕ_{NaCl})

In this set, the fraction of salt in the internal phase was varied over the range of 0.05, 0.14, 0.19 and 0.24 %. The primary emulsions – consisting of 40 % of the inner phase fraction – were used to produce double emulsions at a fraction of $\phi_{outer} = 1\ \%$.
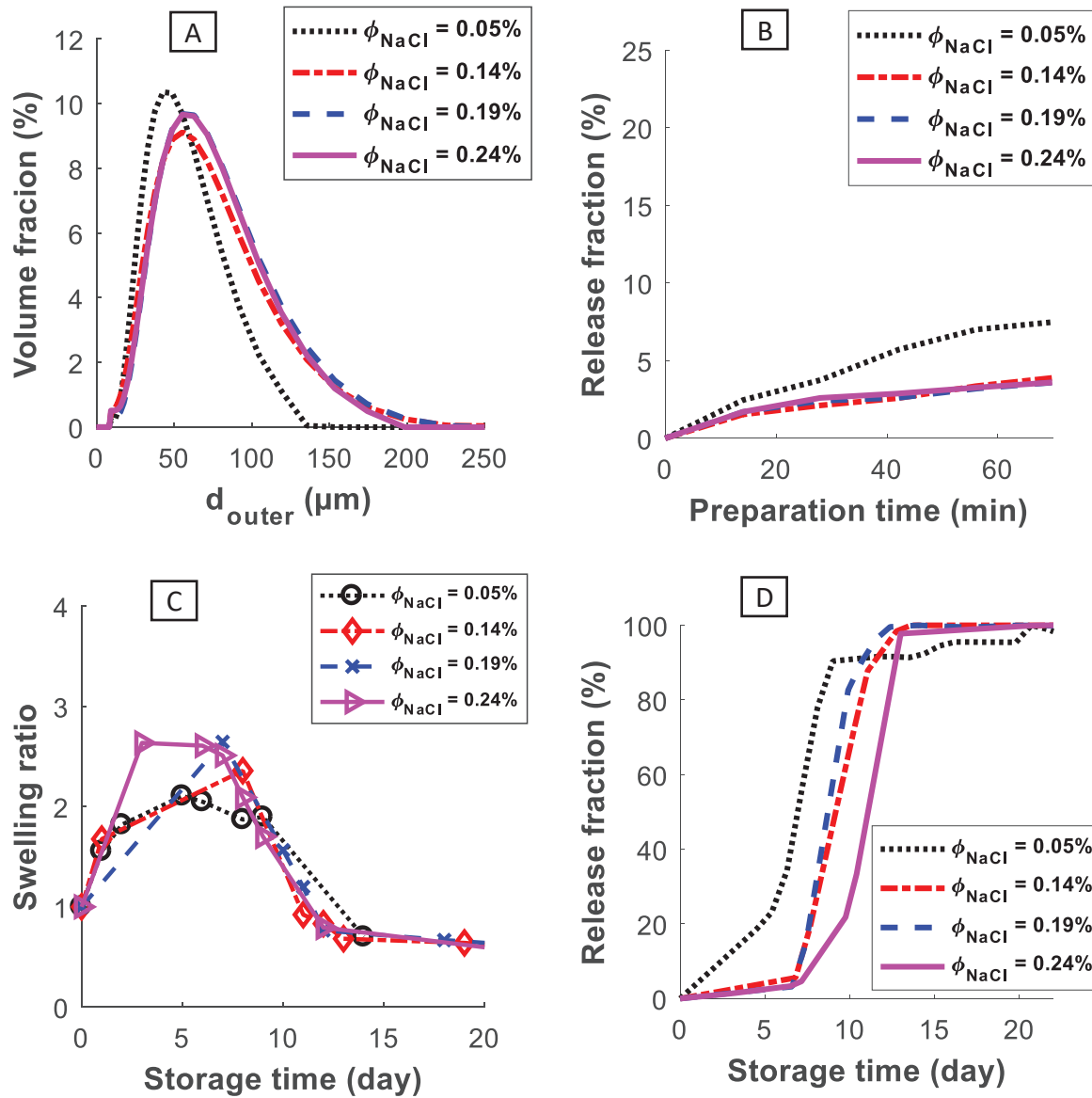
Fig. 2.11. *Effect of salt fraction (ϕ_{NaCl}) on: A) size distribution during preparation, B) release during preparation, C) swelling ratio during storage, and D) release during storage.*

Fig. 2.11A indicates that similar DSD are obtained with the different salt fractions except the one at the lowest salt fraction (ϕ_{NaCl} = 0.05 %) that leads to the formation of much smaller outer droplets during the second preparation step. The presence of ions was found in the literature to play a complex role, thus affecting surfactant spreading and the rheology of the oil layer, which may explain this observation. This measurement is in line with the release profiles (Fig. 2.11B), where a higher release rate is observed with the salt fraction of ϕ_{NaCl} = 0.05 %. This may be due to the higher breakage events and surface area generated during the preparation of this experiment (that has smaller outer droplets), which leads to an enhanced escape of the inner droplets. During storage, the swelling ratio increased slightly when increasing the salt fraction, mainly at the maximum swelling capacity (Fig. 2.11C). In addition, overswelling-breakdown appeared faster for higher salt fractions, respectively at days 14, 13, 12 and 12 for ϕ_{NaCl} = 0.05, 0.14, 0.19 and 0.24 %. This can be explained by the increase in the osmotic gradient. The released fraction follows the pathway observed before where a slow

release due to inner droplets escape first takes placed, then a fast release is observed when overswelling-breakdown occurs (Fig. 2.11D). A lower release rate is observed when higher swelling occurs (i.e., for higher salt fractions). Fig. 2.12 shows the full DSD of the outer droplets with the different salt fractions during storage. The samples with higher salt fractions (i.e., higher osmotic pressure) swell more, which is in line with previous works [15,41,43].
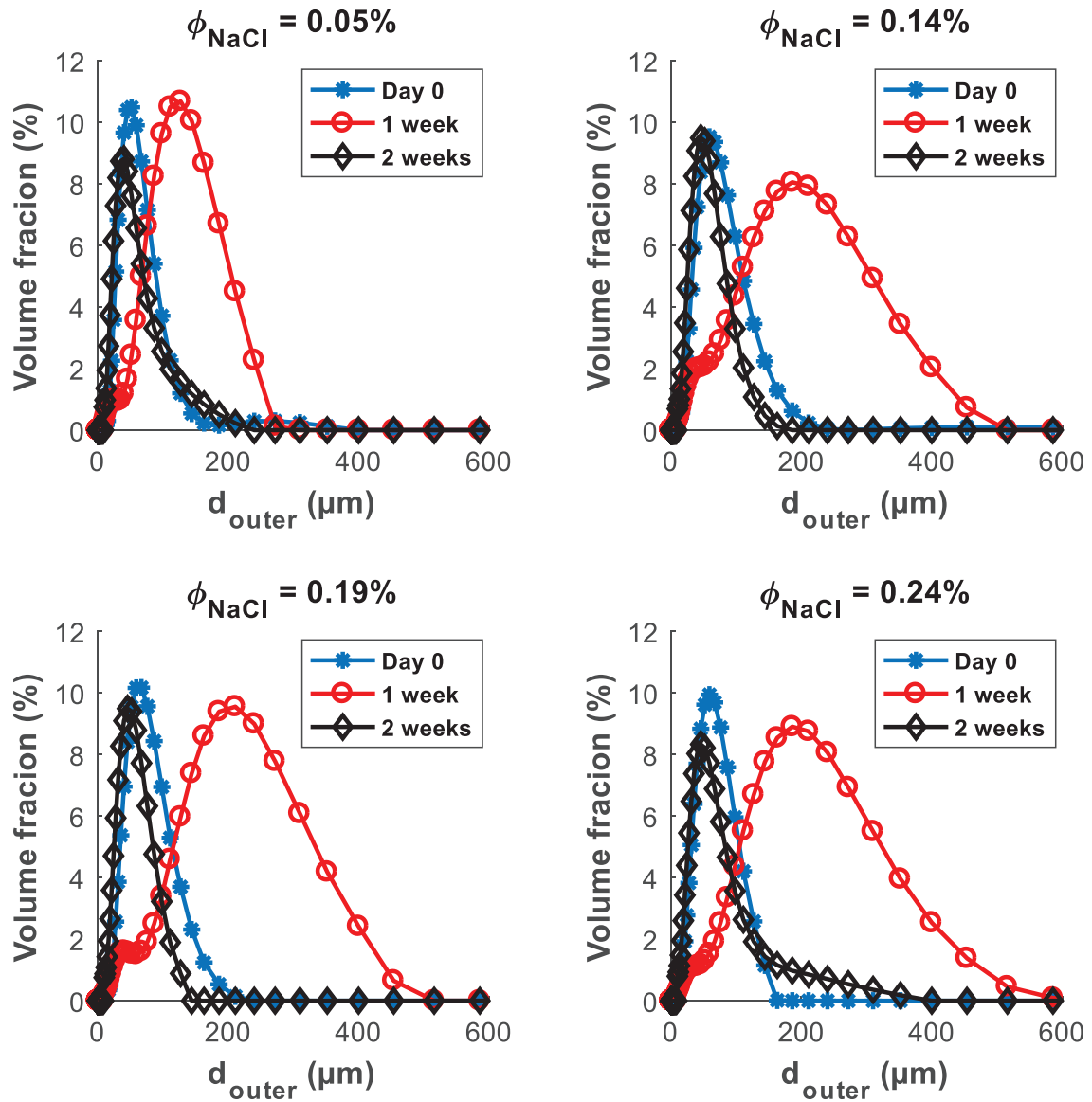
Fig. 2.12. *Effect of the salt fraction (ϕ_{NaCl}) on the outer droplet size distribution during storage.*

2.3.4. Effect of the inner phase fraction (ϕ_{inner})

In this set of experiments, the salt fraction was kept at 0.05 % while the internal phase fraction was varied over the range of ϕ_{inner} = 10, 20, 30 and 40 % in the primary emulsion. The double emulsions were prepared using 1 % of primary emulsion.
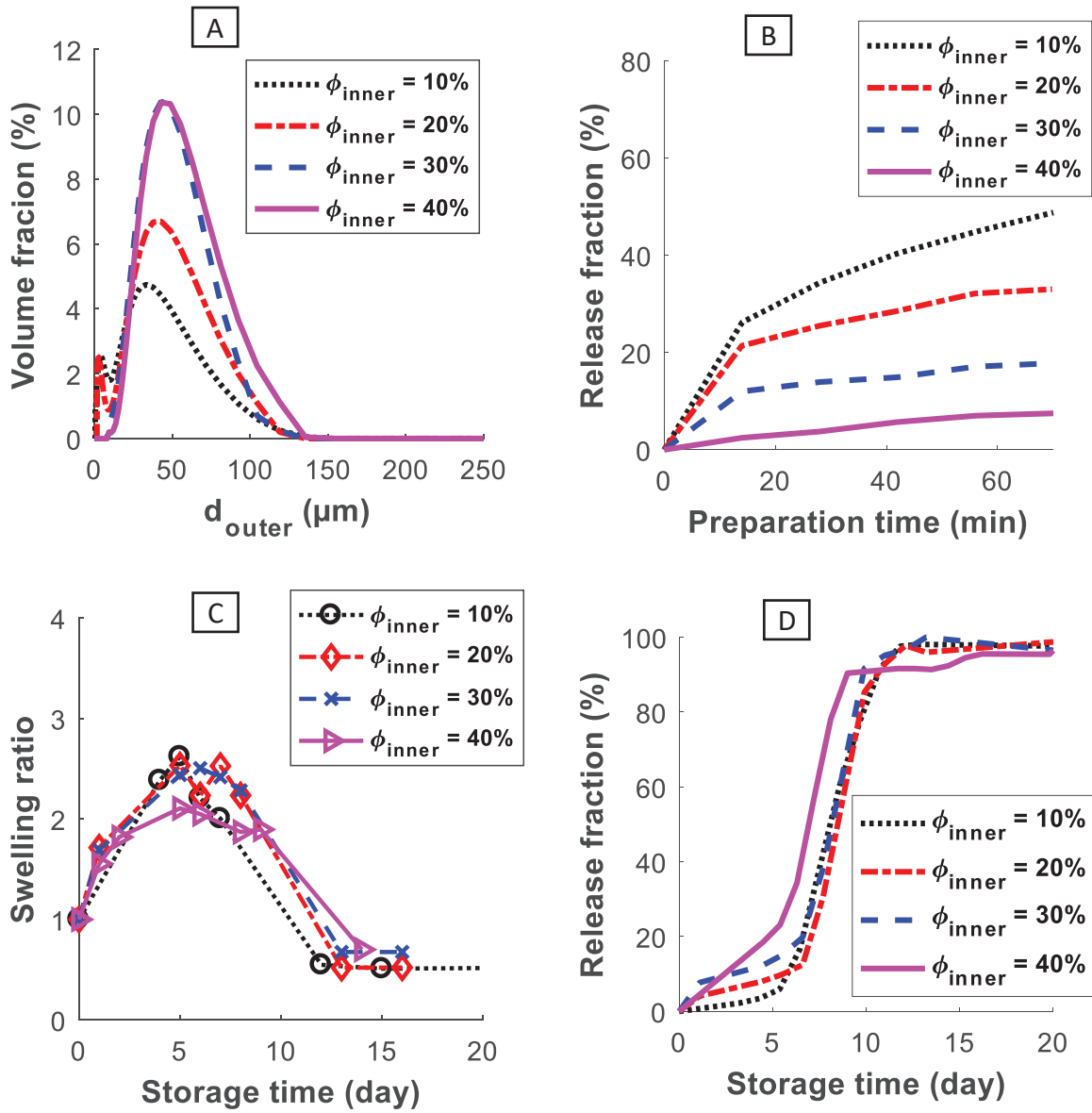
Fig. 2.13. *Effect of the internal phase (ϕ_{inner}) on: A) the outer droplet size distribution during preparation, B) the release during preparation, C) the swelling ratio during storage, and D) the release of salt during storage.*

It can be seen that increasing ϕ_{inner} leads to an increase in the outer droplet size (Fig. 2.13A) and a reduced released fraction (Fig. 2.13B). Similar findings appear, where for higher ϕ_{inner} bigger droplets were observed [5,7,34,35] and higher encapsulation efficiencies were reported [2,5,26], while a lower encapsulation efficiency was observed by [22,35]. The increase in the size and encapsulation efficiency can be explained by the viscosity change in double emulsions. Indeed, changing the internal water fraction changes the viscosity of the outer droplets (μ_{outer}) following the viscosity model of dispersions, for instance the model of Vermeulen (1955) [58], $\mu_{outer} = \frac{\mu_{oil}}{1-\phi_{inner}}\left(1 + 1.5\ \phi_{inner}\frac{\mu_{inner}}{\mu_{inner}+\mu_{oil}}\right)$. Considering mineral oil with viscosity, μ_{oil} =55 mPa.s, the viscosity of the outer phase calculated based on the model of Vermeulen gives μ_{outer} = 61.11, 68.75, 78.57, and 91.67 mPa.s for ϕ_{inner} = 10, 20, 30 and 40 %, respectively. This model indicates that increasing the inner droplet fraction (ϕ_{inner}) increases the viscosity of the outer droplets. Higher viscous outer droplets resist the

40

deformation and breakage during preparation, thus leading to lower inner droplet leakage [5,59]. During storage, Fig. 2.13C shows that the maximum swelling ratio is slightly lower for the sample with the highest inner fractions, so the highest viscous outer droplets, and a negligible effect for the other samples. Bahtz et al. [43] observed a negligible effect of ϕ_{inner} while Yan and Pal [15] observed a decrease in the swelling ratio when increasing the internal phase fraction. Fig. 2.13D shows a similar behavior of the released fraction for all inner fractions, except for the highest ϕ_{inner} where a higher release is observed. This confirms the previous observation of lower release for higher swelling.
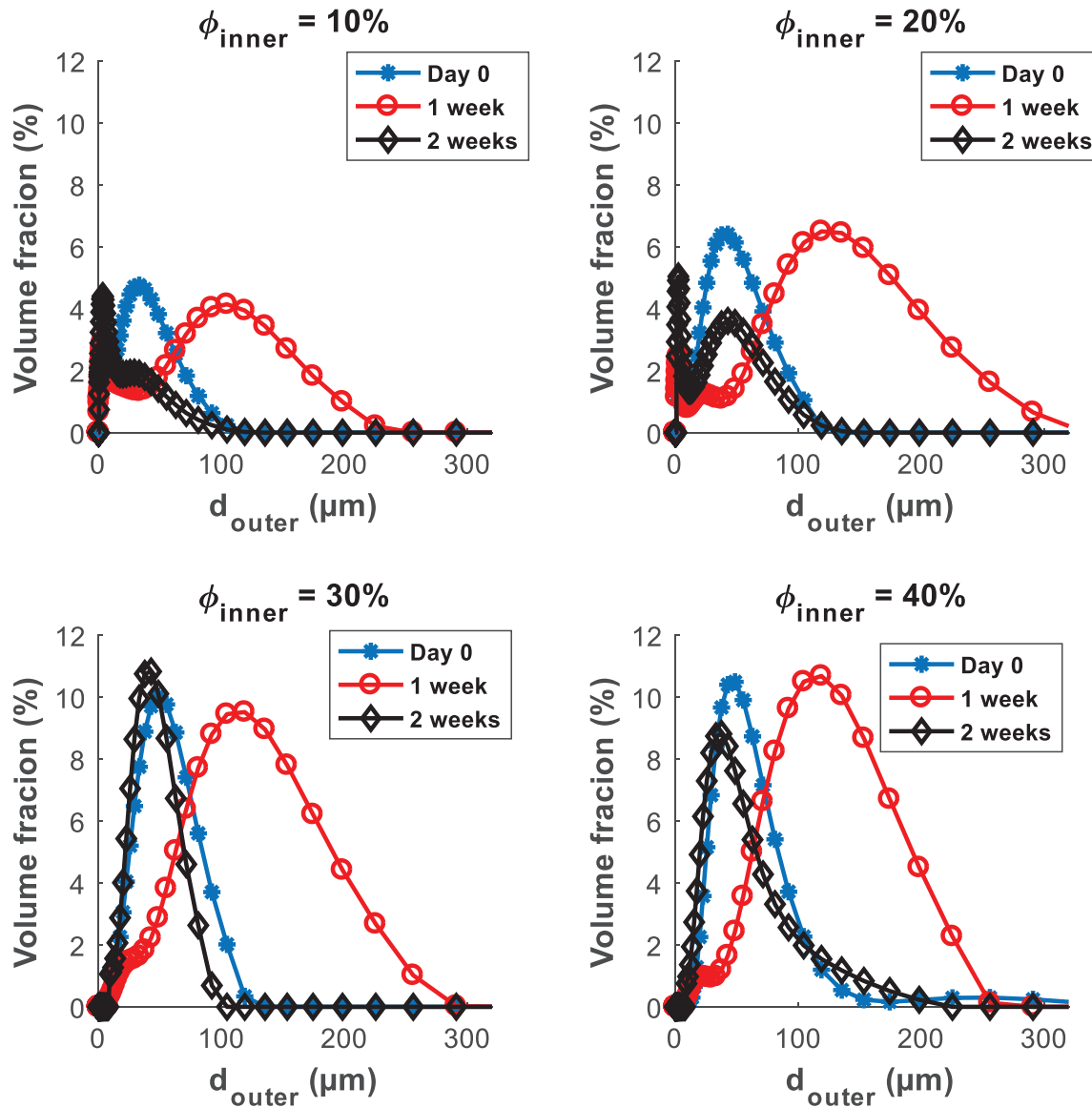
Fig. 2.14. *Effect of internal phase fraction (ϕ_{inner}) on size distribution during storage.*

Fig. 2.14 shows the full outer DSD of the experiments with different ϕ_{inner}. The overswelling breakdown occurs at about two weeks for all the inner fractions, and so viscosities. The peak of very small droplets created after overswelling breakdown for the experiments with the lowest ϕ_{inner} (10 and 20 %) reveal a greater breakup due to the lower viscosity of these experiments (Fig. 2.14A and 14B). This information is not clearly visible on the swelling ratio as the mean size used to calculate the swelling ratio may not be influenced by this peak.

2.3.5. Effect of the stirring rate (ω_R)

The internal phase and salt fractions were respectively kept at 40 % and 0.05 % in the primary emulsion. Then, the double emulsions were prepared using 1 % of primary emulsion fraction under different stirring rates: ω_R= 300, 350, 400 and 500 rpm.
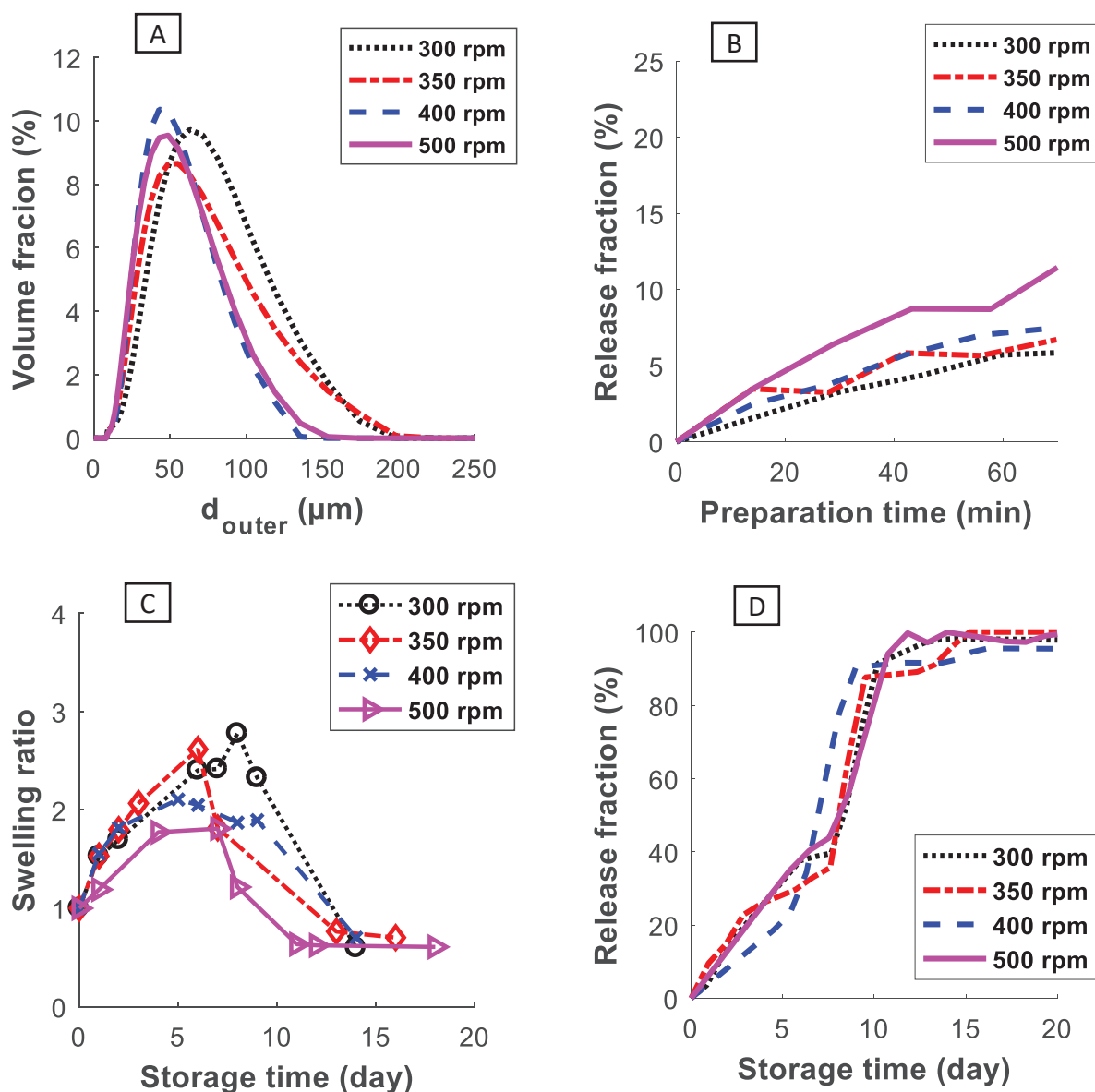
Fig. 2.15. *Effect of the stirring rate (ω_R) on: A) the outer droplet size distribution during preparation, B) the release during preparation, C) the swelling ratio during storage, and D) the release of salt during storage.*

The energy dissipation was calculated for the different stirring rates as explained above leading to ε = 0.53, 0.84, 1.25, and 2.44 (W.kg-1) for ω_R= 300, 350, 400 and 500 rpm, respectively. Therefore, During the second preparation step, increasing the stirring rate leads to a decrease in the outer droplet mean size and to a narrower distribution (Fig. 2.15A). Besides, an acceleration of inner droplet escape rate is observed (Fig. 2.15B). This is due to the higher breakage events taking place under higher stirring rates and the joint escape of inner droplets [5]. Indeed, the release is governed by the shear-induced breakage of the outer

droplets during preparation [5,6,30]. Similar observations were previously highlighted for the effect of stirring rate (or energy) on the outer droplet diameter [5,7,9,31,33,34] and the encapsulation efficiency [5,22,25,27,29,30].

From Fig. 2.15C it can be seen that the swelling ratio is higher for the samples prepared with lower stirring rates, 300 and 350 rpm (i.e., bigger initial sizes). This is confirmed on Fig. 2.16 showing the full DSDs, where big outer droplets can be observed for the samples prepared under 300 and 350 rpm. This is partly due to their initial bigger size besides the fact that these double emulsions have a higher initial salt fraction (i.e., lower release during preparation). The overswelling breakdown of the outer droplets occurs at around 2 weeks for all the samples showing that the initial size of the outer droplets does not have a direct effect on the oil layer rheology. As a consequence, the released fractions are all identical (Fig. 2.15D).
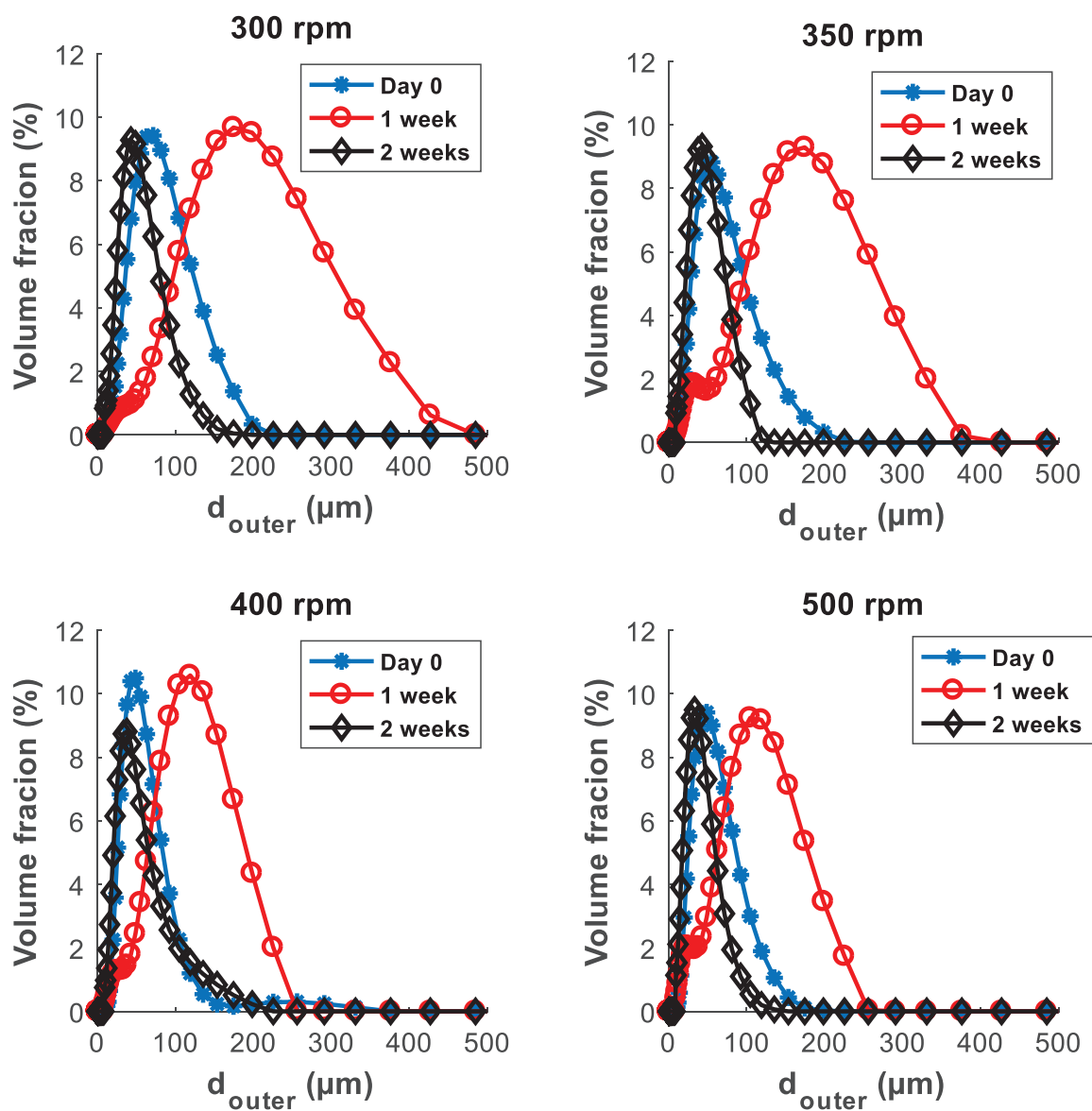
Fig. 2.16. *Effect of the stirring rate (ω_R) on the outer droplet size distribution during storage.*

2.4. Conclusions

The evolution of the outer droplet size and release rate in dilute double emulsions during the second step of preparation and storage was studied by varying different key process parameters.

During preparation, the breakage governs the size of the outer droplets and the release rate (leakage). It was found that varying the primary emulsion fractions from 1 to 4 % did not affect the size of outer droplets nor the release. Increasing the salt fraction from 0.05 to 0.14 % led to more swelling and lower release. Increasing the internal phase fraction generated more viscous outer droplets with higher resistivity against breakage leading to bigger outer droplets and lower release rates. Increasing the stirring rate – the main cause of breakage – allowed to create smaller sizes and led to higher release fractions.

During the storage time, two periods can be distinguished. A first period, of about one to two weeks, corresponds to swelling of the inner, and so of the outer droplets, and escape of inner droplets by Brownian motion through their coalescence with the external phase through the surface of the outer droplet. The second period appears once the maximum swelling capacity is reached and overswelling-breakdown occurs. In this case, a faster inner droplet escape is observed. Moreover, it appears that the outer droplet size is smaller than the initial one (before swelling) and smaller than the theoretical size when assuming full inner droplet escape. This indicates that the overswelling-breakdown causes breakage of the outer droplets, not only full release of inner droplets. Investigating the effect of the different key process parameters indicated that higher primary emulsion fractions resulted in more swelling and so less release and delayed breakdown. The samples with high salt fractions reached very high swelling ratios. Increasing the internal phase fractions slightly lowered the maximum swelling ratio, due to the increased overall viscosity of the outer droplets. Bigger initial outer droplets, prepared with lower stirring rates, swelled more due to their higher initial salt fractions (i.e. lower release during preparation).

It appears that the system having 40 % inner and 4 % outer phase fractions, 0.14 % salt fraction, and 400 rpm stirring rate would lead to a final product having smaller outer droplets and lower release, which represent the main indicators of quality products. Besides, this system proves a longer delay in undesired overswelling-breakdown while keeping salt and stirring rate at low value.

This detailed study provides an important insight in the preparation of double emulsions and on the overswelling-breakdown phenomenon during storage. The results can be useful for formulation of more stable quality products.

References

[1] N.N. Li, Separating hydrocarbons with liquid membranes, Google Patents, 1968.

[2] S. Matsumoto, Y. Kita, D. Yonezawa, An attempt at preparing water-in-oil-in-water multiple-phase emulsions, J. Colloid Interface Sci. 57 (1976) 353–361. doi:10.1016/0021-9797(76)90210-1.

[3] G. Muschiolik, I. Scherze, P. Preissler, J. Weiß, A. Knoth, A. Fechner, Multiple Emulsions - Preparation and Stability, in: 13th World Congr. Food Sci. Technol., EDP Sciences, Nantes, France, 2006. doi:10.1051/IUFoST:20060043.

[4] L. Zeng, Y. Zhang, C. Bukirwa, W. Li, Y. Yang, Study of mean diameter and drop size distribution of emulsion drops in a modified rotating disc contactor for an emulsion liquid membrane system, RSC Adv. 5 (2015) 89959–89970. doi:10.1039/C5RA16267J.

[5] B. Khadem, N. Sheibat-Othman, Modeling of double emulsions using population balance equations, Chem. Eng. J. 366 (2019) 587–597. doi:10.1016/j.cej.2019.02.092.

[6] A.J. Shere, H.M. Cheung, MODELING OF LEAKAGE IN LIQUID SURFACTANT MEMBRANE SYSTEMS, Chem. Eng. Commun. 68 (1988) 143–164. doi:10.1080/00986448808940403.

[7] T. Ohtake, T. Hano, K. Takagi, F. Nakashio, Analysis of water entrainment into dispersed W/O emulsion drops., J. Chem. Eng. Jpn. 21 (1988) 272–276. doi:10.1252/jcej.21.272.

[8] X. Guan, K. Hailu, G. Guthausen, F. Wolf, R. Bernewitz, H.P. Schuchmann, PFG-NMR on W1/O/W2-emulsions: Evidence for molecular exchange between water phases, Eur. J. Lipid Sci. Technol. 112 (2010) 828–837. doi:10.1002/ejlt.201000022.

[9] A. Schuch, J. Wrenger, H.P. Schuchmann, Production of W/O/W double emulsions. Part II: Influence of emulsification device on release of water by coalescence, Colloids Surf. Physicochem. Eng. Asp. 461 (2014) 344–351. doi:10.1016/j.colsurfa.2013.11.044.

[10] S. Mataumoto, W.W. Kang, FORMATION AND APPLICATIONS OF MULTIPLE EMULSIONS, J. Dispers. Sci. Technol. 10 (1989) 455–482. doi:10.1080/01932698908943184.

[11] N. Jager-Lezer, I. Terrisse, F. Bruneau, S. Tokgoz, L. Ferreira, D. Clausse, M. Seiller, J.-L. Grossiord, Influence of lipophilic surfactant on the release kinetics of water-soluble molecules entrapped in a W/O/W multiple emulsion, J. Controlled Release. 45 (1997) 1–13. doi:10.1016/S0168-3659(96)01507-6.

[12] K. Pays, J. Giermanska-Kahn, B. Pouligny, J. Bibette, F. Leal-Calderon, Coalescence in Surfactant-Stabilized Double Emulsions, Langmuir. 17 (2001) 7758–7769. doi:10.1021/la010735x.

[13] K. Pays, Double emulsions: how does release occur?, J. Controlled Release. 79 (2002) 193–205. doi:10.1016/S0168-3659(01)00535-1.

[14] M. Chávez-Páez, C.M. Quezada, L. Ibarra-Bracamontes, H.O. González-Ochoa, J.L. Arauz-Lara, Coalescence in Double Emulsions, Langmuir. 28 (2012) 5934–5939. doi:10.1021/la205144g.

[15] J. Yan, R. Pal, Osmotic swelling behavior of globules of W/O/W emulsion liquid membranes, J. Membr. Sci. 190 (2001) 79–91.

[16] S.S. Davis, A.S. Burbage, The Particle Size Analysis of Multiple Emulsions (Water-in-Oil-in-Water), in: Part. Size Anal. Proc. Conf. Organ. Anal. Div. Chem. Soc. Held Univ. Salford 12-15 Sept. 1977, Heyden & Son, 1978: p. 395.

[17] D. Whitehill, A.T. Florence, Mechanisms of instability in W/O/W multiple emulsions, J. Pharm. Pharmacol. 31 (1979) 3P-3P.

[18] A.T. Florence, D. Whitehill, The formulation and stability of multiple emulsions, Int. J. Pharm. 11 (1982) 277–308.

[19] A.T. Florence, D. Whitehill, Some features of breakdown in water-in-oil-in-water multiple emulsions, J. Colloid Interface Sci. 79 (1981) 243–256. doi:10.1016/0021-9797(81)90066-7.

[20] S. Geiger, S. Tokgoz, A. Fructus, N. Jager-Lezer, M. Seiller, C. Lacombe, J.-L. Grossiord, Kinetics of swelling–breakdown of a W/O/W multiple emulsion: possible mechanisms for the lipophilic surfactant effect, J. Controlled Release. 52 (1998) 99–107. doi:10.1016/S0168-3659(97)00202-2.

[21] S. Raynal, J.L. Grossiord, M. Seiller, D. Clausse, A topical W/O/W multiple emulsion containing several active substances: formulation, characterization and study of release, J. Controlled Release. 26 (1993) 129–140. doi:10.1016/0168-3659(93)90112-I.

[22] T.S.H. Leong, M. Zhou, N. Kukan, M. Ashokkumar, G.J.O. Martin, Preparation of water-in-oil-in-water emulsions by low frequency ultrasound using skim milk and sunflower oil, Food Hydrocoll. 63 (2017) 685–695. doi:10.1016/j.foodhyd.2016.10.017.

[23] B. Khadem, N. Sheibat-Othman, Theoretical and experimental investigations of double emulsion preparation by ultrasonication, Ind. Eng. Chem. Res. (2019). doi:10.1021/acs.iecr.9b00556.

[24] S. Matsumoto, Y. Ueda, Y. Kita, D. Yonezawa, Preparation of Water-in-Olive Oil-in-Water Multiple-phase Emulsions in an Eatable Form, Agric. Biol. Chem. 42 (1978) 739–743. doi:10.1080/00021369.1978.10863054.

[25] E. Dickinson, Double Emulsions Stabilized by Food Biopolymers, Food Biophys. 6 (2011) 1–11. doi:10.1007/s11483-010-9188-6.

[26] A. Cárdenas, E. Castro, Breaking of multiple emulsions under osmotic pressure and the effect of W1/O relation, Interciencia. 28 (2003) 534–538.

[27] T.P. Martin, G.A. Davies, The extraction of copper from dilute aqueous solutions using a liquid membrane process, Hydrometallurgy. 2 (1977) 315–334. doi:10.1016/0304-386X(77)90040-8.

[28] J.K. Klahn, J.J.M. Janssen, G.E.J. Vaessen, R. de Swart, W.G.M. Agterof, On the escape process during phase inversion of an emulsion, Colloids Surf. Physicochem. Eng. Asp. 210 (2002) 167–181. doi:10.1016/S0927-7757(02)00376-X.

[29] H. Okochi, M. Nakano, Preparation and evaluation of w/o/w type emulsions containing vancomycin, Adv. Drug Deliv. Rev. 45 (2000) 5–26. doi:10.1016/S0169-409X(00)00097-1.

[30] S. Okazaki, M. Imai, M. Shimizu, Leakage Suppressing Oe W/O Emulsion Using High Viscous Solvent, in: Process Metall., Elsevier, 1992: pp. 1487–1492. doi:10.1016/B978-0-444-88677-4.50064-7.

[31] V. Muguet, M. Seiller, G. Barratt, D. Clausse, J.P. Marty, J.L. Grossiord, W/O/W Multiple Emulsions Submitted to a Linear Shear Flow: Correlation between Fragmentation and Release, J. Colloid Interface Sci. 218 (1999) 335–337. doi:10.1006/jcis.1999.6374.

[32] K. Lindenstruth, B.W. Müller, W/O/W multiple emulsions with diclofenac sodium, Eur. J. Pharm. Biopharm. 58 (2004) 621–627. doi:10.1016/j.ejpb.2004.04.003.

[33] T. Gallego-Lizon, E.S. Pérez de Ortiz, Drop Sizes in Liquid Membrane Dispersions, Ind. Eng. Chem. Res. 39 (2000) 5020–5028. doi:10.1021/ie000016y.

[34] A. Sharma, A.N. Goswami, B.S. Rawat, Drop size prediction in liquid membrane systems, J. Membr. Sci. 60 (1991) 261–274. doi:10.1016/S0376-7388(00)81539-2.

[35] A. Schuch, P. Deiters, J. Henne, K. Köhler, H.P. Schuchmann, Production of W/O/W (water-in-oil-in-water) multiple emulsions: droplet breakup and release of water, J. Colloid Interface Sci. 402 (2013) 157–164. doi:10.1016/j.jcis.2013.03.066.

[36] M. Frenkel, R. Shwartz, N. Garti, Multiple emulsions, J. Colloid Interface Sci. 94 (1983) 174–178. doi:10.1016/0021-9797(83)90247-3.

[37] T. Schmidts, D. Dobler, C. Nissing, F. Runkel, Influence of hydrophilic surfactants on the properties of multiple W/O/W emulsions, J. Colloid Interface Sci. 338 (2009) 184–192. doi:10.1016/j.jcis.2009.06.033.

[38] T. Schmidts, D. Dobler, P. Schlupp, C. Nissing, H. Garn, F. Runkel, Development of multiple W/O/W emulsions as dermal carrier system for oligonucleotides: Effect of additives on emulsion stability, Int. J. Pharm. 398 (2010) 107–113. doi:10.1016/j.ijpharm.2010.07.037.

[39] T. Hino, Y. Kawashima, S. Shimabayashi, Basic study for stabilization of w/o/w emulsion and its application to transcatheter arterial embolization therapy, Adv. Drug Deliv. Rev. 45 (2000) 27–45. doi:10.1016/S0169-409X(00)00098-3.

[40] M.-F. Ficheux, L. Bonakdar, F. Leal-Calderon, J. Bibette, Some Stability Criteria for Double Emulsions, Langmuir. 14 (1998) 2702–2706. doi:10.1021/la971271z.

[41] S. Matsumoto, M. Kohda, The viscosity of W/O/W emulsions: an attempt to estimate the water permeation coefficient of the oil layer from the viscosity changes in diluted systems on aging under osmotic pressure gradients, J. Colloid Interface Sci. 73 (1980) 13–20.

[42] S. Matsumoto, T. Inoue, M. Kohda, K. Ikura, Water permeability of oil layers in W/O/W emulsions under osmotic pressure gradients, J. Colloid Interface Sci. 77 (1980) 555–563.

[43] J. Bahtz, D.Z. Gunes, E. Hughes, L. Pokorny, F. Riesch, A. Syrbe, P. Fischer, E.J. Windhab, Decoupling of Mass Transport Mechanisms in the Stagewise Swelling of Multiple Emulsions, Langmuir. 31 (2015) 5265–5273. doi:10.1021/acs.langmuir.5b01138.

[44] N. Garti, S. Magdassi, D. Whitehill, Transfer phenomena across the oil phase in water-oil-water multiple emulsions evaluated by Coulter counter: 1. Effect of emulsifier 1 on water permeability, J. Colloid Interface Sci. 104 (1985) 587–591.

[45] I. Terrisse, M. Seiller, J.L. Grossiord, A. Magnet, C. Le Hen-Ferrenbach, Application of rheological analysis to W/O/W multiple emulsions: Effect of the incorporation of a coemulsifier, Colloids Surf. Physicochem. Eng. Asp. 91 (1994) 121–128. doi:10.1016/0927-7757(94)02790-0.

[46] R. Mezzenga, B.M. Folmer, E. Hughes, Design of Double Emulsions by Osmotic Pressure Tailoring, Langmuir. 20 (2004) 3574–3582. doi:10.1021/la036396k.

[47] X. Deng, Y. Ren, L. Hou, W. Liu, Y. Jia, H. Jiang, Electric Field-Induced Cutting of Hydrogel Microfibers with Precise Length Control for Micromotors and Building Blocks, ACS Appl. Mater. Interfaces. 10 (2018) 40228–40237. doi:10.1021/acsami.8b12597.

[48] A. Khalil, F. Puel, Y. Chevalier, J.-M. Galvan, A. Rivoire, J.-P. Klein, Study of droplet size distribution during an emulsification process using in situ video probe coupled with an automatic image analysis, Chem. Eng. J. 165 (2010) 946–957. doi:10.1016/j.cej.2010.10.031.

[49] R. Bernewitz, E. Caro, D. Topgaard, H.P. Schuchmann, G. Guthausen, Double Emulsion Character with PFG-NMR- Methods: WOW and OWO, in: F. Capozzi, L. Laghi, P.S. Belton (Eds.), Spec. Publ., Royal Society of Chemistry, Cambridge, 2015: pp. 120–126. http://ebook.rsc.org/?DOI=10.1039/9781782622741-00120 (accessed June 27, 2016).

[50] R. Bernewitz, U.S. Schmidt, H.P. Schuchmann, G. Guthausen, Structure of and diffusion in O/W/O double emulsions by CLSM and NMR–comparison with W/O/W, Colloids Surf. Physicochem. Eng. Asp. 458 (2014) 10–18. doi:10.1016/j.colsurfa.2014.01.002.

[51] R. Bernewitz, F. Dalitz, K. Köhler, H.P. Schuchmann, G. Guthausen, Characterisation of multiple emulsions by NMR spectroscopy and diffusometry, Microporous Mesoporous Mater. 178 (2013) 69–73. doi:10.1016/j.micromeso.2013.02.049.

[52] J.P. Hindmarsh, J. Su, J. Flanagan, H. Singh, PFG–NMR Analysis of Intercompartment Exchange and Inner Droplet Size Distribution of W/O/W Emulsions, Langmuir. 21 (2005) 9076–9084. doi:10.1021/la051626b.

[53] I. Lönnqvist, B. Håkansson, B. Balinov, O. Söderman, NMR Self-Diffusion Studies of the Water and the Oil Components in a W/O/W Emulsion, J. Colloid Interface Sci. 192 (1997) 66–73. doi:10.1006/jcis.1997.4966.

[54] L. Vermeir, P. Sabatino, M. Balcaen, A. Declerck, K. Dewettinck, J.C. Martins, G. Guthausen, P. Van der Meeren, Effect of molecular exchange on water droplet size analysis as determined by diffusion NMR: The W/O/W double emulsion case, J. Colloid Interface Sci. 475 (2016) 57–65. doi:10.1016/j.jcis.2016.04.029.

[55] A. Lamprecht, U. Schäfer, C.-M. Lehr, Structural analysis of microparticles by confocal laser scanning microscopy, AAPS PharmSciTech. 1 (2000) 10–19. doi:10.1208/pt010317.

[56] S. Schuster, R. Bernewitz, G. Guthausen, J. Zapp, A.M. Greiner, K. Köhler, H.P. Schuchmann, Analysis of W1/O/W2 double emulsions with CLSM: Statistical image processing for droplet size distribution, Chem. Eng. Sci. 81 (2012) 84–90. doi:10.1016/j.ces.2012.06.059.

[57] C.A. Coulaloglou, L.L. Tavlarides, Description of interaction processes in agitated liquid-liquid dispersions, Chem. Eng. Sci. 32 (1977) 1289–1297. doi:10.1016/0009-2509(77)85023-9.

[58] Theodore Vermeulen, Interfacial area in liquid-liquid and gas-liquid agitation, Chem. Eng. Progr. 51 (1955) 85F-94F.

[59] P. Julian Becker, F. Puel, H.A. Jakobsen, N. Sheibat-Othman, Development of an improved breakage kernel for high dispersed viscosity phase emulsification, Chem. Eng. Sci. 109 (2014) 326–338. doi:10.1016/j.ces.2014.02.008.

Chapter 3. Modeling of Double Emulsions Using Population Balance Equations

Double emulsions are widely spread in a number of applications, such as food, cosmetics and pharmaceutics. They are usually prepared in two steps, comprising the preparation of a first emulsion that is in a second step introduced in an external continuous phase. A number of phenomena may occur during the second step including breakage, coalescence, and escape that is aimed to be reduced to keep high the encapsulation efficiency. Suitable models of these phenomena are proposed in this chapter and incorporated into a population balance model (PBM) to allow predicting the evolution of the droplet size distribution (DSD) of the external macro-droplets as well as the release rate. During the considered short preparation time and the slow molecular diffusion of the encapsulated salt, the release rate was assumed to be mainly governed by the leakage of internal droplets, i.e. their release due to the breakage of the macro-droplets. The proposed leakage model is thus described as a function of the breakage rate of the macro-droplets. The model parameters involved in the different sub-models of the PBMs (breakup and coalescence kernels, leakage) were identified in experiments of W/O/W double emulsions prepared using a rotor stator. Then, the model was validated under various key process conditions, such as the internal water fractions (10 - 40 %) and stirring rate. The dependence of the leakage parameter on the concentration of salt was also investigated. The macro-DSD was measured by Laser diffraction while the leakage rate was monitored by conductivity measurements.
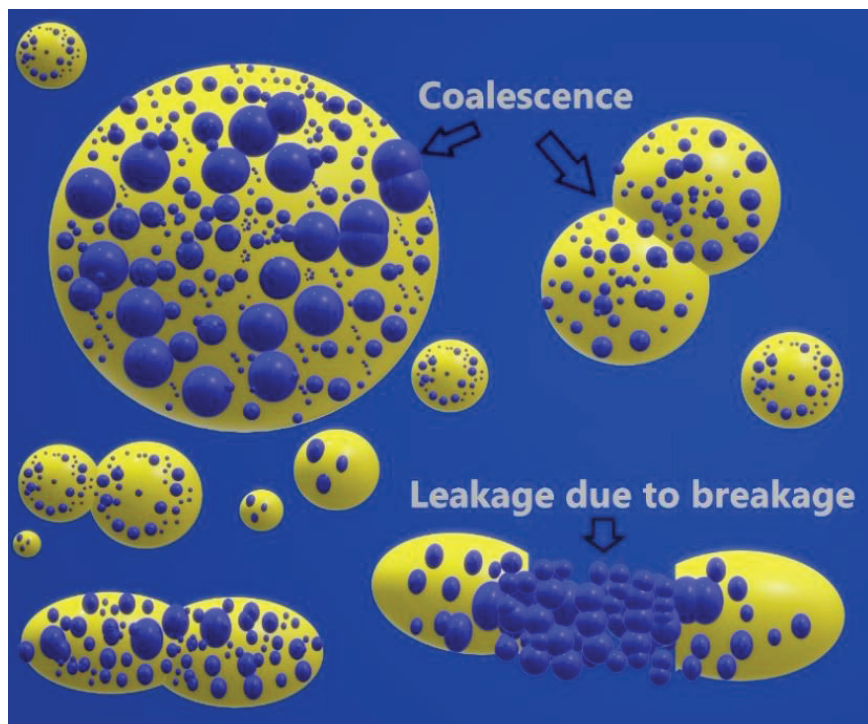
3.1. Introduction

Different destabilization pathways may occur during the second preparation step of double emulsions, as well as during storage, such as macro- (i.e., outer) droplet breakage and coalescence, Ostwald ripening, swelling or shrinkage, leakage of micro- (i.e., inner) droplets (i.e. escape due to breakage) [1–7], and over-swelling (leading to breakdown). Such a high number of simultaneous phenomena taking place in the system represent the main difficulty in modeling this system. Another difficulty is related to the lack of experimental methods allowing to accurately measure the internal DSD. Finally, both the micro- and macro-droplets are usually distributed in size.

In terms of modeling the evolution of the droplet size, a number of works have been performed regarding single emulsions, either using stationary models that describe only a mean diameter [8–10] or using PBM [11,12]. Some stationary correlations were also applied to model double emulsions [13–16].

In terms of modelling the extraction rate from double emulsions, few works concerned the escape in the absence of breakage, which would be interesting during storage but is not sufficient during the preparation of the double emulsion. For instance, Ho et al. (1982) [17] developed a diffusion model assuming micro- and macro-droplets to be of uniform size and in the absence of breakage and over-swelling/explosion of macro-droplets. Kang et al. (2016) [18] developed an escape model based on the dewetting phenomenon during storage of double emulsions. Pays et al. (2001) [19] and Chávez-Páez et al. (2012) [1] proposed an escape model during storage based on the coalescence of micro-droplets with the external aqueous phase. Few other works concerned modelling escape during preparation. For instance, Klahn et al. (2002) [20] proposed a model to describe micro-droplet escape in simple shear flow regime. Mukhopadhyay et al. (2008) [21] proposed a model to describe osmotic and occlusion modes of swelling of double-emulsions assumed to have a core-shell structure, and a leakage model of the internal phase that was assumed proportional to the thickness of the membrane. Okazaki (1992) [22] proposed a leakage correlation as a function of the energy dissipation rate, viscosity and osmotic pressure. Shere and Cheung (1988) [6] proposed a model to describe leakage assuming macro-droplet rupture to be the main mechanism responsible for micro-droplet leakage, while the internal substance was assumed to have negligible diffusivity through the membrane during the preparation time. A summary of some models describing the release rate during preparation can be found in table 3.1.

The objective of this work is to develop a model that describes micro-droplet leakage during the second preparation step of the double emulsion, where the micro-and macro-droplets are not of uniform size and where macro-droplets may undergo breakage and coalescence. These phenomena can be described by considering population balance models (PBM) of the internal and external droplets. In turbulent systems, these phenomena are the consequence of the mechanical operating conditions, such as the energy dissipation rate, and physical properties like viscosity, density and the interfacial tension. However, while a number of kernels were proposed to describe breakage and coalescence of simple emulsions in turbulent systems [11,12], a specific attention is required when applying these kernels to double emulsions, as a

number of properties of the dispersed phase change when the dispersed phase itself becomes an emulsion, such as its density, viscosity and surface tension [15,23]. Finally, the escape model is required to be combined to breakage and coalescence of the macro-droplets within the population balance model.

In this work, rotor stator is used in the first and second emulsification steps to prepare W/O/W double emulsions. A number of key process parameters were investigated during the preparation of the double emulsions, namely, the fraction of internal water, the stirring rate in the second preparation step and the fraction of salt. The size of macro-droplets was monitored offline by laser diffraction and the release of salt by conductivity measurements.

Table 3.1. *Correlations for the release rate in double emulsions during preparation*

The release rate in double emulsions	Reference
Simple shear flow regime $$\frac{dn_m}{dt} = \frac{-2P}{t_c\,\alpha_{cr}}\left(n_m - (1-\alpha_{cr})n_{m0}\right)$$ Coalescence probability: $P = \left(\dfrac{\pi\,\sigma\,r_m^2}{2\,A_H}\right)^{-\frac{4}{9\,\pi\,t_{cir}}\left(1+\frac{\mu_M}{\mu_{ex}}\right)}$ Volume fraction of critical region: $\alpha_{cr} = 1 - \exp\left(-\dfrac{r_m}{r_M}\left[2.22 + 1.51\left(\dfrac{\mu_M}{\mu_{ex}}\right)^{-0.57}\right]\right)$ where A_H is Hamaker constant and t_{cir} total circulation time	Klahn et al. (2002) [20]
Turbulent regime in core-shell morphology $$\frac{d\theta}{dt} = K_{Br}(1-\theta)$$ $\theta = \dfrac{(C_{ex}(t) - C_{ex}(t_0))V_{ex}}{C_m\,V_m}$ $\begin{cases} K_{Br} = 3\times10^{-19}\,\delta^{-1}\,\mu_M^{-0.8}\,\varepsilon^{(2.2\times10^{-8}\,\Delta\Pi+0.8)}\,\Delta\Pi^{0.9}, \Delta\Pi > 1\times10^6 \\ K_{Br} = 8\times10^{-13}\,\delta^{-1}\,\mu_M^{-0.8}\,\varepsilon^{0.8} \qquad\qquad\quad, \Delta\Pi < 1\times10^6 \end{cases}$ Where Π is osmotic pressure and $\delta = r_m(\phi_m^{-1/3} - 1)$ is the membrane thickness.	Okazaki et al. (1992) [22]
Turbulent regime $\ln\left(\dfrac{n_M(t)}{n_M(t_f)}\right) = \ln\left(\dfrac{n_M(t_0)}{n_M(t_f)}\right)e^{-kt}$ $\ln\left(\dfrac{L(t_f)}{L(t)}\right) = a_m \ln\left(\dfrac{n_M(t_f)}{n_M(t_0)}\right)e^{-(k_m+k)t}$ $L = \dfrac{(C_{ex}(t)-C_{ex}(t_0))(1-\phi_m)\,100}{C_{in}\,\phi_m\phi_M}$ is the leakage fraction and k, k_m and a_m are constants	Shere & Cheung (1988) [6]

3.2. Materials and experimental methods

3.2.1. Materials

The materials used to prepare the W/O/W double emulsions are Mineral oil (Fisher Scientific^TM), Span 80 (Alfa Aesar) as hydrophobic internal emulsifier, Tween 80 (Fisher Scientific^TM) as hydrophilic external emulsifier, Sodium Chloride as tracer and regulator of osmotic pressure and Millipore water (resistivity $\approx 18.2\ m\,\Omega.cm$).

3.2.2. Double emulsion preparation

W/O/W double emulsions were prepared at room temperature using a two-step method (see Fig. 1.1). In the first step, the NaCl aqueous solution was dispersed in the oil phase - consisting of oil in which Span 80 is dissolved - and mixed using an IKA T 25 digital ULTRA-TURRAX® at 12 000 rpm for 4 min. In the second step, this primary emulsion was dispersed in an external aqueous phase - consisting of water in which Tween 80 is dissolved - and mixed using the ULTRA-TURRAX® at 3 400 rpm for 1-16 min. The fractions of these materials are shown in Table 3.2. The employed ULTRA-TURAX was equipped with the dispersing elements S25N-10G and S25N-18G for mixing the first and second emulsions respectively.

Table 3.2. Experimental conditions

| | First step of preparation[1] | | | | | | Second step of preparation[2] | | | | |
| | Fractions (wt. %) | | | | Operating parameters | | Fractions (wt. %) | | | Operating parameters | |
	Water	Mineral oil	NaCl	Span 80	t_1 (min)	N_R (rpm)	Primary emulsion[3]	Water	Tween 80	t_2 (min)	ω_R (rpm)
Set 1: Internal water fraction effect	40 / 30 / 20 / 10	50 / 60 / 70 / 80	0.05	9.95	4	12000	10	89	1	16	3400
Set 2: Stirring rate effect	10	80	0.05	9.95	4	12000	10	89	1	16	3400 / 5600 / 6800
Set 3: Salt fraction effect	40	50	0.01 / 0.03 / 0.05 / 0.14 / 0.19 / 0.23	9.95	4	12000	10	89	1	4	3400

[1] These values are weight percentages of the total first step (primary, or internal emulsion)
[2] These values are weight percentages of the total double emulsion
[3] The primary emulsion consists of the emulsion produced in the first step
The total volume is 250 ml for sets 1 and 2, and 150 for set 3

3.2.3. Droplet size measurement

The size of micro- (i.e, inner) droplets was measured right after the first step of preparation by means of dynamic light scattering (Malvern Zetasizer Nano ZS®). Then, samples were taken every one minute during the second preparation step and the size distribution of the macro- (i.e., outer) droplets was analyzed using laser diffraction (Malvern Mastersizer 3000®).

3.2.4. Conductivity measurements

The released amount of NaCl was monitored by measuring the conductivity of the samples, taken every one minute during the second preparation step, using a CDM210 Conductivity Meter (MeterLab®). The released amount was estimated based on a predetermined calibration curve. Two calibration methods were evaluated and found equivalent, either by dispersing different salt concentrations in pure water or by dispersing the salt in a single O/W

emulsion instead of water, thus indicating no effect of the oil on the measurement in the employed concentration range.

3.3. Modeling

Double emulsions consist of an emulsion inside another emulsion. Thus, there are two dispersed phases. The internal dispersed phase consists of water droplets dispersed into the oil phase, and will be referred to as micro-droplets hereafter. The external dispersed phase consists of the first emulsion dispersed into water, and will be referred to as macro-droplets. Each of these dispersions is distributed in size, and can thus be described by a population balance.

3.3.1. Population balance models

The general PBM of size distributed systems [24,25] can be applied for both the macro- and micro-droplets during the second preparation step of the double emulsion. On one hand, macro-droplets might undergo breakage, coalescence and swelling that might lead to over-swelling-breakdown, which leads to the following balance of the number density distribution of macro-droplets, n_M (number per m^{-3} of macro-droplet size):

$$\frac{\partial n_M(t,v)}{\partial t} + \frac{\partial \left(S_M(t,v)n_M(t,v)\right)}{\partial x} = \Re_{Br} + \Re_{Co} + \Re_{OSB} \qquad 3.1$$

On the other hand, micro-droplets can be assumed to undergo mainly leakage, as the external mixing is supposed to cause no breakage and very little coalescence within the considered preparation time and energy [26,27]. Thus, the number density of micro-droplets (n_m) can be obtained by:

$$\frac{\partial n_m(t,v)}{\partial t} + \frac{\partial \left(S_m(t,v)n_m(t,v)\right)}{\partial x} = \Re_{Co}^m - \Re_{Leak} \qquad 3.2$$

Where v is the droplet volume, $\mathbb{S}$ the swelling or shrinkage rates due to osmotic pressure difference or diffusion by Oswald ripening, $\Re_{Br}$ the breakage rate, $\Re_{Co}$ the coalescence rate, $\Re_{OSB}$ the breakge rate (due to over-swelling) and $\Re_{Leak}$ is the internal droplet leakage rate (number.m^{-3}.s^{-1}). The indices m and M refer to micro- and macro-droplets respectively.

The second terms on the LFHs of eq. 3.1 and eq. 3.2 represent the swelling or shrinkage of micro- and so of macro-droplets which cause the change in the number of micro-droplets leading to decrease the size of macro-droplets. Due to the short time of the second step of the double emulsion preparation, swelling of micro- or macro-droplets can be considered to be negligible, and therefore over-swelling breakdown is negligible. Oswald ripening is also negligible during the preparation period due to the low solubility of each phase in the other. With these assumptions, Eqs. (3.1 and 3.2) become:

$$\frac{\partial n_M(t,v)}{\partial t} = B_{Br}(t,v) - D_{Br}(t,v) + B_{Co}(t,v) - D_{Co}(t,v) \qquad 3.3$$

$$\frac{\partial n_m(t,v)}{\partial t} = -\Re_{Leak} \qquad 3.4$$

Where the birth (B) and death (D) terms for breakage and coalescence are as follows [24,25]:

$$B_{\mathrm{Br}}(t,v) = \int_v^\infty b(v,\varepsilon)\,\Gamma(t,\varepsilon)\,n(t,\varepsilon)\,d\varepsilon \qquad\qquad 3.5$$

$$D_{\mathrm{Br}}(t,v) = \Gamma(v)\,n(t,\varepsilon) \qquad\qquad 3.6$$

$$B_{\mathrm{Co}}(t,v) = \tfrac{1}{2}\int_0^v \beta(v,v-\varepsilon)\,n(t,v-\varepsilon)\,n(t,\varepsilon)\,d\varepsilon \qquad\qquad 3.7$$

$$D_{\mathrm{Co}}(t,v) = n(t,v)\int_0^\infty \beta(v,\varepsilon)\,n(t,\varepsilon)\,d\varepsilon \qquad\qquad 3.8$$

3.3.2. Leakage rate

The leakage is defined as the escape of micro-droplets upon breakage of the macro-droplets. The leakage causes a decrease in the volume of the encapsulated micro-droplets and so in the macro-droplets' volume. Considering a constant micro-droplet volume fraction in the macro-droplets, independently of their size, one may write $\frac{dV_M}{dt} = \frac{dV_m}{dt}$, with $V_M = V_m + V_{\mathrm{oil}}$. The leakage of micro-droplets leads to the release of salt that they contain. This mechanism is assumed to represent the main mechanism of release of salt, since the diffusion of salt into the oil phase is slow. Therefore, when escape occurs, only the total volume of micro-droplets (V_m) decreases while the concentration of salt in the micro-droplets (C_m) remains constant (i.e. $\frac{dC_m}{dt} = 0$). Therefore, the material balance of salt in the micro-droplets becomes:

$$\frac{d(V_m C_m)}{dt} = C_m \frac{dV_m}{dt} = -\,C_m Q_L \qquad\qquad 3.9$$

Where Q_L is the volumetric flowrate of micro-droplet given by:

$$Q_L = -\frac{dV_m}{dt} = -\frac{dV_M}{dt} = \int_0^\infty \Re_{\mathrm{Leak}}(t,v_m)v_m dv_m \qquad\qquad 3.10$$

Based on experimental observations, it can be assumed that micro-droplet escape is governed by the breakage rate of the macro-droplets, as also reported by [6,28,29]. This assumption is valid only during the preparation of macro-droplet, as during storage the escape may occur via other pathways mentioned above, like diffusion or swelling-breakdown. It is therefore reasonable to write the leakage rate as a function of the change in the surface of macro-droplets and the volume fraction of the internal phase, as follows:

$$Q_L = k_L \frac{V_m}{V_M}\int_0^\infty \pi r_M^2 \Re_{\mathrm{Br}}(t,v_M)dv_M \qquad\qquad 3.11$$

Where k_L is the leakage rate coefficient (in meter) and r_M is the macro-droplet radius.

By substitution into equation 3.9, the number of moles of salt in the micro-droplets ($N_m = V_m C_m$) can be calculated by:

$$\frac{dN_m}{dt} = -\,k_L \frac{N_m}{V_M}\int_0^\infty \pi r_M^2.\,\Re_{\mathrm{Br}}(t,v_M)dv_M \qquad\qquad 3.12$$

3.3.3. Energy dissipation in high shear devices

The energy dissipation rate is one of the key process parameters that is required in the breakage and coalescence kernels. In rotor-stator devices like ULTRA-TURRAX® the energy dissipation in the continuous phase can be calculated using the power equation, similarly to stirred tanks [10]:

$$\varepsilon_c = \frac{N_{\mathrm{P}} \, \omega_{\mathrm{R}}{}^3 \, D_{\mathrm{R}}^5}{V}$$

3.13

Where $\omega_{\mathrm{R}} \, [rps]$ is the rotational speed of the rotor, D_R the rotor diameter, N_P the power number and V is the volume of the mixed media.

In turbulent flow regime, the power number of high shear rotor stator mixers is constant and is in the range of $1.4 - 3$ for different geometries [10]. In this work, a power number equal to 1.7 was used, as determined by Padron (2001) [31].

It is to be noted that the mean energy dissipation rate used here is the average value, and its accuracy can be enhanced by using local values being calculated via such methods as the compartmental method of Alopaeus et al. [30] that is to be solved via a coupled CFD modeling framework which requires more calculation time and effort. Here, the mean value provides a straightforward approximation to focus on the main objective in this chapter.

3.3.4. Breakage kernel

During the second step of double emulsion preparation, a high shear rate is employed by means of Ultra-Turrax, and therefore the fluid dynamics are in a turbulent flow regime. The breakage and coalescence kernels developed for turbulent flows should therefore be used. The turbulent energy is thus the driving force for breakage of the macro-droplets while the viscous and surface forces are the driving forces for stabilization. In this regard, Alopaeus et al. [30] proposed a breakage kernel that they employed on a compartmentalized stirred tank reactor:

$$\Gamma(v) = C_1 \varepsilon_{eff}^{\frac{1}{3}} \, \mathrm{erfc} \left(\sqrt{ \frac{C_2 \sigma_{\mathrm{disp}}}{\rho_c \, \varepsilon_{\mathrm{eff}}^{\frac{2}{3}} v^{\frac{5}{9}}} + \frac{C_3 \, \mu_{\mathrm{disp}}}{\sqrt{\rho_c \, \rho_{disp}} \, \varepsilon_{\mathrm{eff}}^{\frac{1}{3}} \, v^{\frac{4}{9}}} } \right)$$

3.14

Where C_1, C_2 and C_3 are the breakage rate coefficients, v the droplet volume, σ the interfacial tension, $\varepsilon_{\mathrm{eff}}$ the effective energy dissipation rate of the dispersion, μ_{disp} and μ_c are the dispersed and continues phase viscosities respectively, ρ_{disp} and ρ_c are the dispersed and continues phase densities respectively and erfc stands for the complementary error function. This kernel was used by Qin et al. [32] to model the emulsification in a rotor-stator mixer, within a coupled CFD-PBM framework.

To model the daughter size distribution, the normal distribution was selected [33]:

$$b(v_i, v_j) = \frac{2c}{v_j \sqrt{2\pi}} \exp\left(-\frac{(v_i - 0.5 \, v_j)^2 (2c)^2}{2v_j^2} \right)$$

3.15

Where c is a constant which is equal to 3.

3.3.5. Coalescence kernel

Binary coalescence of two droplets of volumes v_i and v_j can be defined as the product of collision frequency, $h(v_i, v_j)$, and coalescence efficiency, $\lambda(v_i, v_j)$ [34]:

$$\beta(v_i, v_j) = h(v_i, v_j)\lambda(v_i, v_j)$$

3.16

The collision frequency depends on the shear during preparation while it depends on the Brownian motion during storage. Coulaloglou and Tavlarides [34] proposed a binary collision frequency for turbulent conditions, that was later-on slightly revised as follows (see for instance [35–38]):

$$h(V_i, V_j) = C_4 \varepsilon_{\text{eff}}^{\frac{1}{3}} \left(v_i^{1/3} + v_j^{1/3}\right)^2 \left(v_i^{2/9} + v_j^{2/9}\right)^{1/2}$$

(3.17)

To describe the coalescence efficiency, Coulaloglou and Tavlarides [34] proposed to use the film drainage theory:

$$\lambda(v_i, v_j) = \exp\left(-\frac{t_d}{t_c}\right) = \exp\left[-\frac{C_5 \, \mu_c \, \rho_c \, \varepsilon_{\text{eff}}}{\sigma_{\text{disp}}^2} \left(\frac{v_i^{1/3} v_j^{1/3}}{v_i^{1/3} + v_j^{1/3}}\right)^4\right]$$

(3.18)

Where t_d is the drainage time and t_c the contact time.

It can be seen that the coalescence efficiency depends on the surface tension. However, an excess amount of surfactant is employed in this work, thus ensuring full coverage of the micro- and macro-droplets' surface area during all the preparation stages. Therefore, the surface tension was the same in all experiments.

3.3.6. Properties of the dispersion

It is important to take into account the effect of the presence of the dispersed phase on the properties of the dispersion and to use these apparent properties in the population balance, rather than using those of the pure phases.

For instance, the apparent viscosity of the liquid-liquid dispersion can be obtained by the model of Vermeulen (1955) [39]:

$$\mu_{\text{disp}} = \frac{\mu_c}{1 - \phi_m} \left(1 + 1.5 \, \phi_m \frac{\mu_d}{\mu_d + \mu_c}\right)$$

(3.19)

Similarly, the density of macro-droplet changes due to the presence of micro-droplets dispersion by the model of Miller and Mann (1944) [40]:

$$\rho_{\text{disp}} = \phi_m \, \rho_d + (1 - \phi_m) \, \rho_c$$

(3.20)

Also, the increase in the dispersed phase fraction is known to damp the continues phase energy dissipation [34]:

$$\varepsilon_{\text{eff}} = \frac{\varepsilon_c}{(1 + \phi_{\text{M}})^3}$$

(3.21)

Finally, the interfacial tension of the macro-droplets may also be affected by the presence of micro-droplets, as the change in the work required to strain a pure-oil droplet may be different from the required work for a droplet containing other droplets [23]. However, the experimental and simulation results indicated a negligible effect, so the interfacial tension between water and oil droplet – not containing micro-droplets – was implemented hereafter.

3.3.7. Numerical solution

The finite volume discretization scheme was used to solve the population balance equations. This method was firstly developed by Filbet and Laurençot (2004) [41] for pure coalescence in

which the PBM was reformulated into a mass distribution, $g(t,v) = v\, n(t,v)$. Then, Kumar et al. [42] extended the model for combined breakage and coalescence.

$$\frac{\partial g(t,v)}{\partial t} = -\frac{\partial}{\partial v}\left(\int_0^v \int_{v-u}^{v_{max}} u\,\beta(u,v)n(t,u)n(t,v)dv\,du\right) +$$
$$\frac{\partial}{\partial v}\left(\int_v^\infty \int_0^v u\,b(u,v')\Gamma(v')n(t,v')du\,dv'\right)$$

3.22

By discretizing the mass balance across the cell boundaries $[i+\frac{1}{2}, i-\frac{1}{2}]$:

$$\frac{\Delta g_i}{\Delta t} = -\frac{\left(J_{i+\frac{1}{2}}^{Co} + J_{i+\frac{1}{2}}^{Br} - J_{i-\frac{1}{2}}^{Co} - J_{i-\frac{1}{2}}^{Br}\right)}{v_{i+1/2} - v_{i-1/2}}$$

3.23

With the mass fluxes:

$$J_{i+\frac{1}{2}}^{Br} = -\sum_{k=i+1}^{I} g_k \int_{\Lambda_k} \frac{\Gamma(v)}{v}\,dv \int_0^{v_{i+1/2}} u\,b(u,v_k)du$$

3.24

$$J_{i+\frac{1}{2}}^{Co} = \sum_{k=1}^{i}\left(\sum_{j=\alpha_{i,k}}^{I} \int_{\Lambda_j} \frac{\beta(u,\,v_k)}{u}\,du\,g_i + \int_{v_{i+1/2}-v_k}^{v_{\alpha_{i,k}-1/2}} \frac{\beta(u,v_k)}{u}\,du\,g_{\alpha_{i,k}-1}\right)$$

Where $\alpha_{i,k}$ represents the index of each cell, such that $v_{i+1/2} - v_k \in \Lambda_{\alpha_{i,k}-1}$.

3.4. Results and discussions

Different process parameters were investigated during the preparation of double emulsions and the model robustness was evaluated. These parameters include the internal water fraction, the stirring rate and time and the salt concentration (see Table 3.2).

For each experiment, the double emulsion was first shaken by hand to make a uniform premix and a sample was taken to measure the initial DSD, which is used as an input for the simulations. Then, mixing by the rotor stator was employed following the stirring rate and times indicated in the table 3.2, and samples were taken every one minute to measure the macro-DSD and the conductivity. A typical optical image of the double emulsion just after preparation is shown in Fig. 3.1 that clearly indicates the presence of internal droplets. Fig. 3.1B shows that some of the micro-droplets can reach a diameter up to 6 µm.

Using Nano-ZS, the DSD of micro-droplets measured just after the first step, i.e., the primary emulsion (Fig. 3.2). The mean droplet diameter was around 1 µm, however the figure shows that the droplet size can be as high as 1.5 µm. Therefore, the microscopic image is showing comparable results to the DSD obtained by Nano-ZS, but slightly higher sizes could be detected. This may indicate the occurrence, during the second step, of either some coalescence as previously reported by Hindmarsh et al. [27], or swelling, but that seem to be minor.
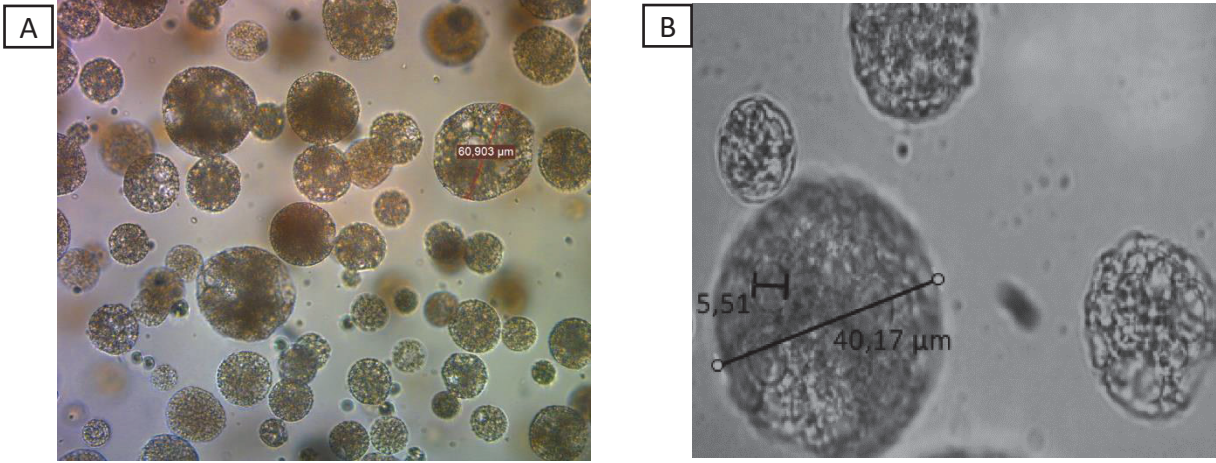
Fig. 3.1. *Optical microscopic image of the double emulsion taken just after preparation, with two different zooms ($\phi_m = 40\%$, 3400 rpm, $\phi_M = 10\%$, 2nd step mixing time = 4 min).*
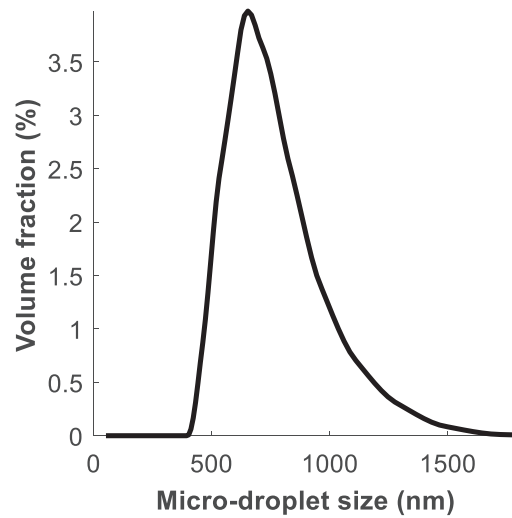
Fig. 3.2. *Example of the droplet size distribution of micro-droplets measured by NanoZS.*

3.4.1. Parameter identification

The optimization procedure was done using the following objective function, and by employing the nonlinear solvers "lsqnonlin" and "fmincon" in a "MultiStart class" global optimization function of Matlab®, where the solver attempts to find multiple local solutions to a problem by starting from various points:

$$\min_{C_1, C_2, C_3, C_4, C_5, K_L} J \qquad\qquad 3.25$$

with

$$J = \sum_{\text{2 experiments}} \left(\sum_{\substack{\text{sample n° (t=1,2,3,4,16 min)}}} \left| n_M^{\text{Model}}(t, v) - n_M^{\text{Exp}}(t, v) \right| + \left| C_m^{\text{Model}} - C_m^{\text{Exp}} \right| \right)$$

with $[C_1, C_2, C_3, C_4, C_5, K_L] \in [0, \infty]$.

Two experiments, with different energy dissipation rates (3 400 and 5 600 rpm) and internal water fractions (ϕ_m = 20 % and 10 %, respectively), were used to identify the model

parameters. Then, the obtained parameters were used to predict the evolution of the DSD of macro-droplets as well as the leakage rate while varying the process operating conditions.

The initial guess of the breakage and coalescence kernels (C_1-C_5) was obtained by optimization of these coefficients alone without considering leakage. The obtained results were then used in order to optimize all the coefficients together (C_1-C_5, K_L), including the leakage phenomena. This way was found to give a more robust parameter identification.

The obtained parameters are given in table 3.3 and compared to some values from the literature. The breakage parameters C_2 and C_3 are respectively related to the ratio of surface tension and dispersed phase viscosity to the inertia. Increasing these parameters decreases the breakage probability. Lower values are obtained in the Ultra-Turrax compared to the stirred tank, thus indicating a higher breakage efficiency. This might be due to the higher energy dissipation and the induced shear on the droplets surface. Concerning the ratio of C_3 to C_2 (revealing the relative impact of the droplets viscosity), then it is much higher for Ultra-Turrax than for stirred tanks. This can be due to the smaller droplets produced in this case. Indeed, from Hinze (1955) [9] it can be deduced that for big droplets, the breakage phenomenon depends only on the ratio of energy dissipation to the surface force (i.e., C_2), while for smaller droplets it also depends on the dispersed phase viscosity (i.e., C_3), as also supported by data from Narsimhan et al. [43] and Coulaloglou & Tavlarides (1977) [34]. Concerning the value of C_1, it is within the same range as for stirred tanks.

Regarding the coalescence parameters, higher values of C_4 are obtained with the Ultra-Turrax, thus indicating a higher collision frequency, due to the higher energy dissipation. Concerning C_5, the higher its value the lower is the coalescence efficiency (very high values of C_5 lead to a probability of zero). It appears that a higher coalescence efficiency is obtained in Ultra-Turrax, which can be due to the high shear, as for the breakage efficiency. The identifiability of C_5 was however argued for a low coalescence rate. Ribeiro et al. (2011) [44] indicated that when the overall coalescence rate is low, the parameter C_5 has a negligible influence, which justified the fact that different values were identified when changing the initial guess.

Table 3.3. *Identified parameters for the different models compared to literature values*

Breakage			Coalescence		Leakage	K_L model (eq. 3.26)		Geometry	Ref.
C_1 ($m^{-2/3}$)	C_2	C_3	C_4	C_5 (m^{-2})	K_L (m)	K_{L0} (m)	α		
0.719	3.76×10^{-5}	0.0018	0.913	5.66	1.74×10^{-9}	8.77×10^{-6}	54	UltraTurrax	**This work**
			1.5×10^{-4}	1.83×10^{13}				Stirred tank	[34]
0.986	8.92×10^{-4}	0.2	4.33×10^{-4}					Stirred tank	[30]
6	0.04	0.01	4.6	6×10^9				Stirred tank	[45]
0.657	0.021	0.402	2.3×10^{-6}	1.2×10^9				Stirred tank	[11]
			3.6×10^{-4} to 9.2×10^{-4}	12.5 to 640				Stirred tank	[44]

3.4.2. Effect of the internal water fraction

The effect of the internal water fraction was investigated in the first set of experiments over the range of 10 %, 20 %, 30 % and 40 % (Set 1 in table 3.2). Fig. 3.3 shows an example of the model predictions of the DSD compared to the experimental results (Fig. 3.3A) and the leakage rate (Fig. 3.3B) that is represented by the fraction of the released salt. The figure indicates a good prediction capability of both models.
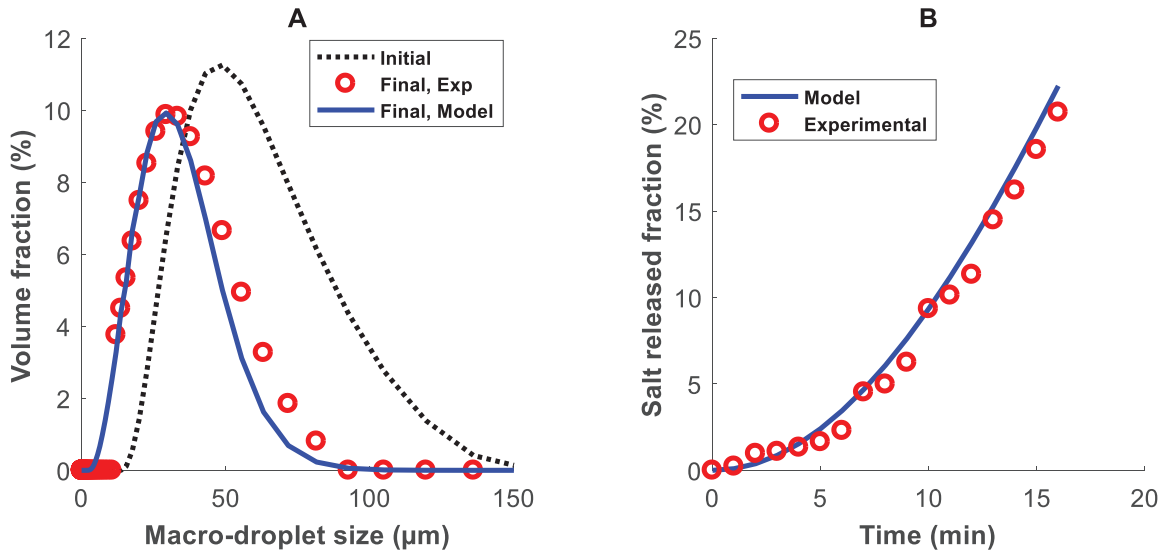
Fig. 3.3. *Experimental and modelling results for ϕ_m = 40 %, ϕ_M = 10 %, 3400 rpm, showing (A) the macro-DSD, and (B) the leakage rate.*
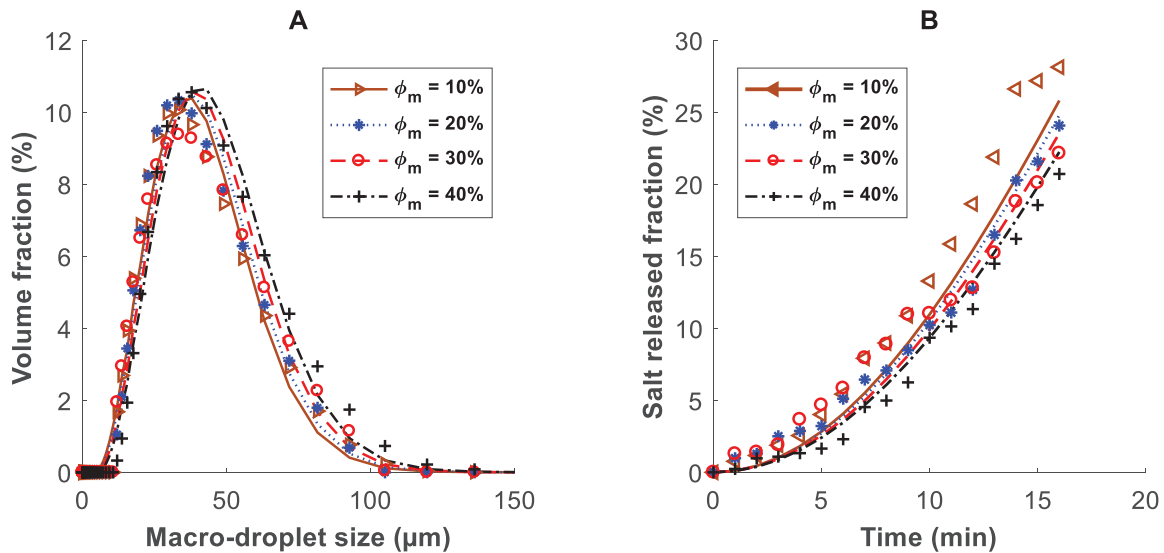
Fig. 3.4. *Effect of internal phase fraction, in the experiments of set 1, on (A) the evolution of macro-DSD, and (B) salt leakage. The lines indicate the model predications and the symbols the experimental results.*

When plotting the different experiments of Set 1 together (Fig. 3.4), it can be seen that when increasing the internal water fraction, the DSD moved towards bigger sizes while the leakage rate decreased slightly. This observation cannot be related to an enhanced coalescence phenomena, as the coalescence phenomena would not reduce the leakage rate. On the

contrary, this seems to be due to a reduced breakage rate. Indeed, when increasing the internal water fraction, the viscosity of the macro-droplets is increased, following Vermeulen's relation (Eq. 3.19). This leads to a decrease in the breakage rate, following experimental observations and as expected from the used model (Eq. 3.14) [30].With the decreased breakage rate, the leakage is also decreased, as observed by Fig. 3.4B. It should be noted that the size of the internal droplets might also have an effect on the apparent viscosity of the globule (macro-droplet), but this parameter was not investigated in this work. In summary, increasing the internal water fraction leads to an increase in the macro-droplets viscosity, which decreases both the breakage and leakage rates. So, the observed effect seems to be due to a change in the effective viscosity of the globules.

As an example of the model accuracy, Fig. 3.5 shows the parity plot of the Fig. 3.4A. It can be seen that the model is mostly capable of the predictions below 20% of error.
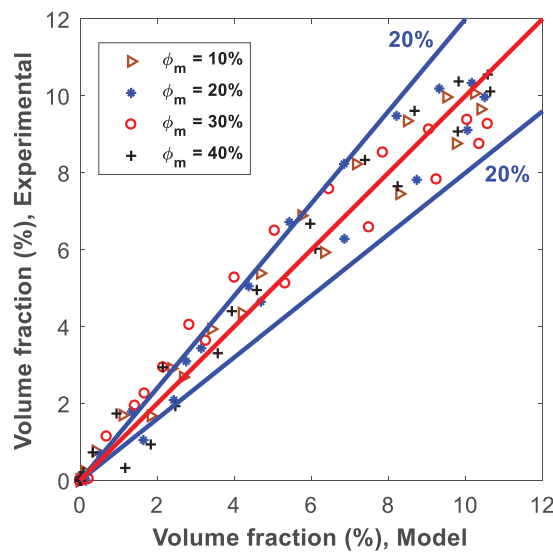
Figure 3.5. *Parity plot for the results of the effect of internal phase fraction shown in Fig. 3.4A.*

3.4.3. Effect of the stirring rate

The stirring rate, as well as the type of rotor stator and the properties of the continuous phase all have a direct effect on the energy dissipation rate. In this section, the effect of the stirring rate on energy dissipation, and therefore on the breakage and leakage rates, is investigated (Set 2 in table 3.2). Using equation 3.13, the mean energy dissipation rate was calculated in these experiments to be ε_c=0.405, 1.8 and 3.23 W.kg^{-1} for mixing rates of 3 400, 5 600 and 6 800 rpm respectively. It is to be noted that the energy dissipation in the region between the rotor and stator is orders of magnitudes higher than these mean values, but only the average values are used in the kernel.

Fig. 3.6 shows the model predictions compared to the experimental results when changing the energy dissipation. A good prediction of both the DSD and leakage rate is obtained under these conditions. It can be seen (Fig. 3.6A) that when increasing the stirring rate the macro-droplet's size is decreased until equilibrium between breakage and coalescence is reached where no more decrease is observed. This is due to the fact that both phenomena are proportional to the energy dissipation rate.
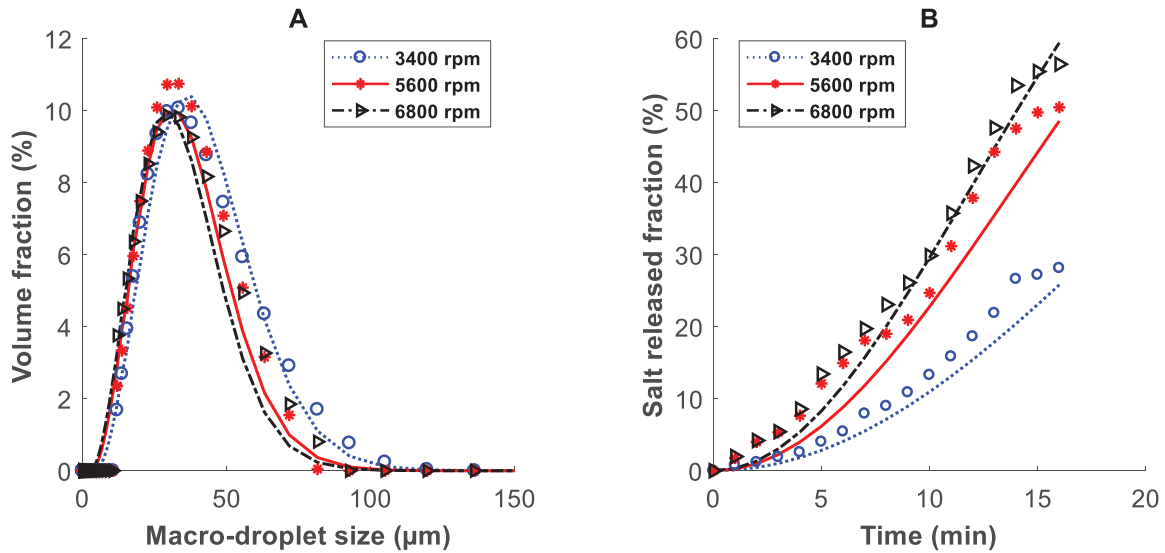
Fig. 3.6. *Effect of energy dissipation rate, in the experiments of set 2, on (A) the evolution of macro-DSD, and (B) salt leakage. The lines indicate the model predications and the symbols the experimental results.*

Concerning the leakage fraction (Fig. 3.6B), it increases when increasing the stirring rate, independently of the observed equilibrium in terms of droplet size. Indeed, even if equilibrium between breakage and coalescence is reached, leakage continues to occur proportionally to the breakage rate. This confirms the hypothesis of relating the leakage to the breakage rate, and not only to the macro-droplet size.

Fig. 3.7 shows the typical evolution of the DSD with time in two experiments, with ϕ_m=10 %: Fig. 3.7A at 3 400 rpm and Fig. 3.7B at 5 600 rpm. It can be seen that the equilibrium is reached very quickly in both cases, but smaller droplets are obtained when mixing at 5 600 rpm.
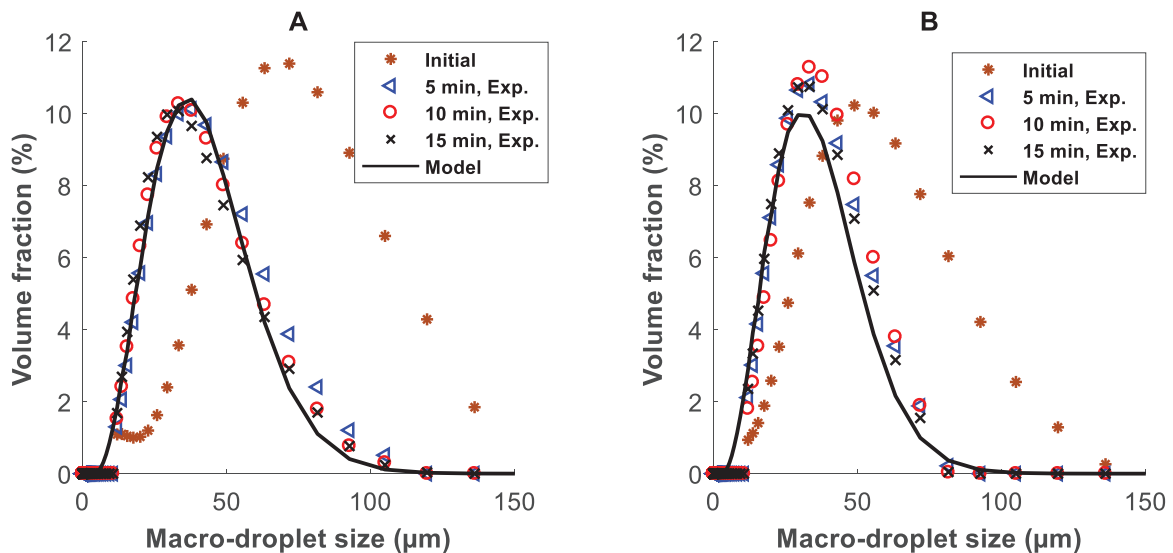
Fig. 3.7. *Evolution of the macro-DSD with time (ϕ_m = 10%) (A) at 3400 rpm (Exp. 1.3) and (B) 5600 rpm (Exp. 2.2). The lines indicate the model predications and the symbols the experimental results.*

3.4.4. Effect of the salt concentration on leakage

As the salt concentration is expected to modify the osmotic pressure and thus the stability of micro-droplets against leakage, then the leakage rate coefficient, k_L, is dependent on the salt concentration. It would thus be interesting to write this coefficient as a function of the concentration of salt, in order to generalize the proposed leakage model over a wide range of salt fractions, which can be done by defining k_L as eq. 3.26 and fitting it to the experimental data (set 3 in Table 3.2) while using eqs. 3.1 and 3.4:

$$k_L = k_{L0} \; C_m^{-\alpha} \tag{3.26}$$

Where k_{L0} and α are the model parameters, that are supposed to be constant.

The effect of salt on leakage was investigated by changing the salt fraction over the range of 0.01 % to 0.23 % (Set 3 in table 3.2). Using the experimental leakage rate, the model parameters were identified to be $k_{L0} = 8.77 \times 10^{-6}$ m and $\alpha = 2.54$.

Note that the presence of salt may also affect the physical stability of the macro-droplets, and thus the breakage or coalescence rates, as the Laplace pressure curvature can be counterbalanced by the salt as a result of osmotic pressure [46]. In this case, the salt contributes to the surface force. This effect was not considered in the model, as the surface tension was approximated to be the same in all experiments. Also, the difference between osmotic and Laplace pressure due to the addition of salt can lead to swelling of the micro- and macro-droplets, but this requires longer time periods to become significant, for instance during storage [46].

Fig. 3.8A shows the fraction of leaked number of micro-droplets as a function of the salt concentration, both experimentally and by the model. The double emulsions becomes more stable and better opposes leakage when increasing the salt concentration. A burst drop in leakage fraction is observed when increasing the salt concentration until reaching a negligible effect at the salt concentration of 20 mol m^{-3} ($\phi_{salt} = 0.05$ %). Okazaki et al. (1992) also observed that the osmotic pressure, or salt concentration, have an effect on leakage only over a specific concentration range of salt [22]. Fig. 3.8B shows the DSD of micro-droplets for different salt fractions. It can be seen that increasing the salt concentration leads to an increase in the micro-droplet size until a specific concentration limit, beyond which the droplets size decreases. This can be due to the salt effect on the spreading of surfactant on the interface, and thus on its stabilization potential. Note that the size of internal droplets is accounted for in the proposed leakage model.
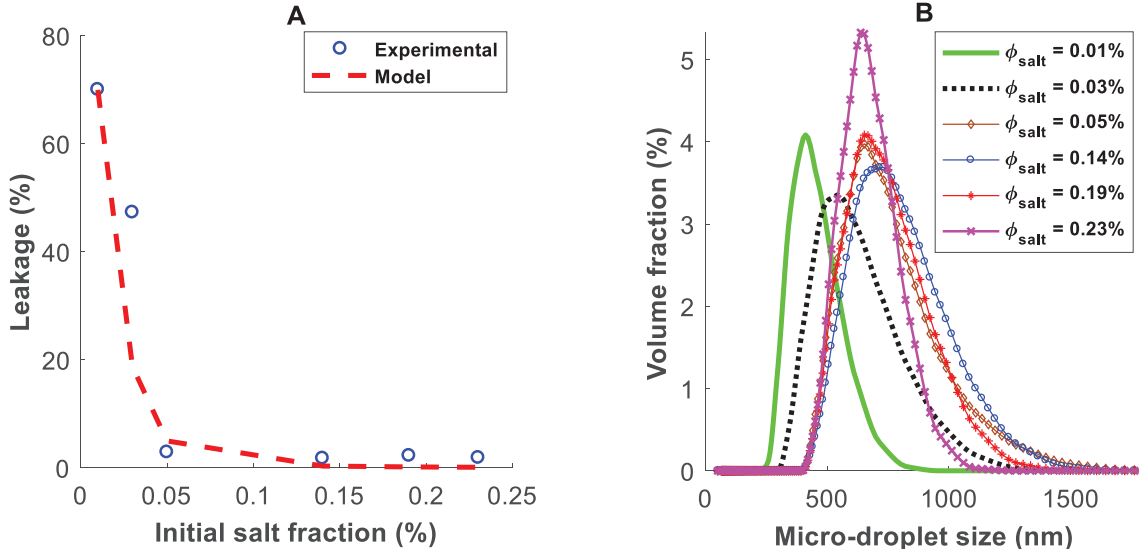
Fig. 3.8. *Effect of the initial salt concentration on (A) the leakage rate during the second step of preparation, the dashed line is the model (Eq. (3.26)), and (B) on the DSD of micro-droplets.*

3.4.5 Comparison to equilibrium correlation

As an evaluation of the methodology, the obtained mean diameter by PBM was compared to the Kolmogorov-Hinze correlation at equilibrium:

$$d_{32} \propto \mathrm{We}^{-0.6} \tag{3.27}$$

where d_{32} is the Sauter mean diameter and $\mathrm{We} = \frac{\omega_R^2 D_R^3 \rho_c}{\sigma}$ is the Weber number.

Fig. 3.9 shows that the evolution of d_{32} is proportional to $\mathrm{We}^{-0.6}$, as suggested by Kolmogorov-Hinze. This is because the kernel of Alopaeus et al. relies on similar assumptions as suggested by Kolmogorov and Hinze. The Weber number changes when changing the stirring rate and at $\mathrm{We}^{-0.6} = 0.1$ different experiments were realized with different macro-droplet viscosities, where the macro-droplets contain different fractions of internal phases. It can be seen that the viscosity of the dispersed phase changes the slope, and it is required to be accounted for in the correlation. Note that while this correlation is simple to use, it is valid only at equilibrium and it only predicts a mean size, while the population balance allows for predicting the whole DSD as a function of time.
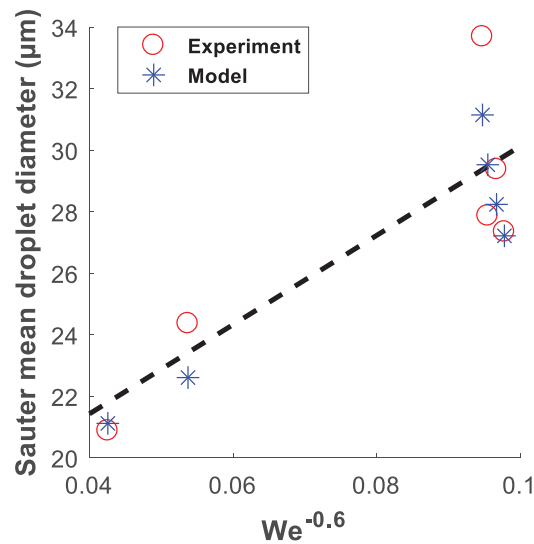
Fig. 3.9. *Relation between the d_{32} of macro-droplets (experimental and using PBM) and the Weber number*

3.5. Conclusions

A combined population balance and leakage model is developed in order to predict the evolution of the macro-DSD and the leakage rate during the preparation of double emulsions. The methodology includes the adaptation of the breakage and coalescence kernels for double emulsions in order to account for the changes in the dispersion properties, such as the apparent density and viscosity. Moreover, a leakage model is proposed by assuming the breakage rate of macro-droplets to be the driving force for leakage. Finally, the leakage coefficient was described as a function of the salt concentration in order to generalize the model over a wide range of salt concentrations.

The obtained experimental results demonstrate the model validity over a wide range of experimental conditions. An effect of the internal phase fraction was observed on the viscosity of the macro-droplets which showed a direct effect on the breakage rate as well as the leakage fraction. A fast convergence of the macro-DSD to an equilibrium point between coalescence and breakage rates was observed. Increasing the stirring rate in the second step of preparation, and thus the energy dissipation, showed an increase in the leakage of salt, but a negligible effect on the macro-DSD that quickly reached equilibrium. The increase of the salt concentration was found to have an effect on the micro-DSD in a nonlinear way, which may be explained by an effect of salt on the stabilizer spreading. Increasing the salt fraction was also found to decrease the leakage rate until the volume fraction of $\phi_{salt} = 0.05$ %, beyond which no more effect of salt on the leakage rate could be observed.

The DSD and the leakage rate in double emulsions are the key parameters determining the final product properties. This study showed that an accurate estimation of these parameters can be achieved by using PBM and by employing operational and physical parameters which in turn helps to define an accurate leakage model. Such models are useful in different domains of double emulsions, such as food, cosmetics and pharmaceutical industries, where increasing the encapsulation efficiency and ensuring the physical stability of droplet are of high

importance. Double emulsions may also be employed as liquid membranes for solvent extraction, for instance in waste water treatment, where the proposed leakage model can be used. Finally, the methodology can be extended to other mixing devises by modifying the energy dissipation. It should be noted that the use of mean energy dissipation rate may cause the recalibration of the model constants when one extends the model to other mixing devices. To avoid such rework and improve the accuracy of the model, the use of local energy dissipation rate is suggested.

Nomenclature

b: Daughter size distribution $[-]$

B: Birth term $[-]$

C_m, C_{ex}: Salt concentration in the micro-droplets or in the external phase respectively $[\text{mol.m}^{-3}]$

$C_1 \left[\text{m}^{-\frac{2}{3}}\right], C_2[-], C_3[-]$: Breakage rate constants

$C_4[-], C_5[\text{m}^{-2}]$: Coalescence rate constants

d: Droplet diameter $[\text{m}]$

d_{32}: Sauter mean diameter $[\text{m}]$

D: Death term in the PBM $[-]$

D_R: Rotor diameter or stirrer diameter $[\text{m}]$

$g(t,v)$: Size distribution in volume density $[\text{m}^3\,\text{m}^{-3}]$

h: Collision frequency $[\text{s}^{-1}]$

I: Total number of grid cells $[-]$

J: Volumetric flux across cell boundary $[\text{s}^{-1}]$

K_L, K_{L0}: Leakage rate constants $[\text{m}]$

$n(t,v)$: number density $[\text{number per m}^{-3} \text{ of droplet size}]$

N_m: Number of moles of salt in the micro-droplets $[\text{mol}]$

N_P: Stirrer power number $[-]$

Q_L: Volumetric leakage flow rate $[\text{m}^3\text{s}^{-1}]$

r: Droplet radius $[\text{m}]$

$\Re$: Rate $[\text{number m}^{-3}\text{s}^{-1}]$

Γ: Breakage kernel $[\text{s}^{-1}]$

$\mathbb{S}$: Swelling rate $[\text{m}^3\text{s}^{-1}]$

t_c: Contact time $[\text{s}]$

t_d: Film drainage time $[\text{s}]$

t_1, t_2 : Mixing time of the first and second steps $[\text{min}]$

u and v: Droplet volume $[\text{m}^3]$

V: Volume $[\text{m}^3]$

We: Weber number $[-]$

Greek letters

ω_R: Rotational speed of the rotor, $[\text{rps}]$ in the equations, and $[\text{rpm}]$ in table 3.2

β: Coalescence kernel $[\text{s}^{-1}]$

ε: Energy dissipation rate $[\text{W kg}^{-1}]$

λ: Coalescence efficiency $[-]$

μ: Viscosity $[\text{Pa. s}]$

ρ: Density $[\text{kg m}^{-3}]$

σ: Interfacial tension $[\text{N m}^{-1}]$

ϕ: Volume fraction $[-]$

Subscripts

Br: Breakage

c: Continues phase

Co: Coalescence

d: Dispersed phase (single emulsion)

disp: Dispersed phase (multiple emulsion)

eff: effective

Leak: Leakage

m: Micro-droplet

M: Macro-droplet

References

[1] M. Chávez-Páez, C.M. Quezada, L. Ibarra-Bracamontes, H.O. González-Ochoa, J.L. Arauz-Lara, Coalescence in Double Emulsions, Langmuir. 28 (2012) 5934–5939. doi:10.1021/la205144g.

[2] W.S.W. Ho, K.K. Sirkar, eds., Membrane Handbook, Springer US, Boston, MA, 1992. doi:10.1007/978-1-4615-3548-5.

[3] N. Jager-Lezer, I. Terrisse, F. Bruneau, S. Tokgoz, L. Ferreira, D. Clausse, M. Seiller, J.-L. Grossiord, Influence of lipophilic surfactant on the release kinetics of water-soluble molecules entrapped in a W/O/W multiple emulsion, J. Controlled Release. 45 (1997) 1–13. doi:10.1016/S0168-3659(96)01507-6.

[4] R. Mezzenga, B.M. Folmer, E. Hughes, Design of Double Emulsions by Osmotic Pressure Tailoring, Langmuir. 20 (2004) 3574–3582. doi:10.1021/la036396k.

[5] T. Schmidts, D. Dobler, C. Nissing, F. Runkel, Influence of hydrophilic surfactants on the properties of multiple W/O/W emulsions, J. Colloid Interface Sci. 338 (2009) 184–192. doi:10.1016/j.jcis.2009.06.033.

[6] A.J. Shere, H.M. Cheung, MODELING OF LEAKAGE IN LIQUID SURFACTANT MEMBRANE SYSTEMS, Chem. Eng. Commun. 68 (1988) 143–164. doi:10.1080/00986448808940403.

[7] F. Wolf, L. Hecht, H.P. Schuchmann, E.H. Hardy, G. Guthausen, Preparation of W_1/O/W_2 emulsions and droplet size distribution measurements by pulsed-field gradient nuclear magnetic resonance (PFG-NMR) technique, Eur. J. Lipid Sci. Technol. 111 (2009) 730–742. doi:10.1002/ejlt.200800272.

[8] J.T. Davies, Drop sizes of emulsions related to turbulent energy dissipation rates, Chem. Eng. Sci. 40 (1985) 839–842. doi:10.1016/0009-2509(85)85036-3.

[9] J.O. Hinze, Fundamentals of the hydrodynamic mechanism of splitting in dispersion processes, AIChE J. 1 (1955) 289–295. doi:10.1002/aic.690010303.

[10] J. Zhang, S. Xu, W. Li, High shear mixers: A review of typical applications and studies on power draw, flow pattern, energy dissipation and transfer properties, Chem. Eng. Process. Process Intensif. 57–58 (2012) 25–41. doi:10.1016/j.cep.2012.04.004.

[11] P.J. Becker, F. Puel, R. Henry, N. Sheibat-Othman, Investigation of Discrete Population Balance Models and Breakage Kernels for Dilute Emulsification Systems, Ind. Eng. Chem. Res. 50 (2011) 11358–11374. doi:10.1021/ie2006033.

[12] Y. Liao, D. Lucas, A literature review on mechanisms and models for the coalescence process of fluid particles, Chem. Eng. Sci. 65 (2010) 2851–2864. doi:10.1016/j.ces.2010.02.020.

[13] T. Kataoka, T. Nishiki, Dispersed mean drop sizes of (W/O)/W emulsions in a stirred tank., J. Chem. Eng. Jpn. 19 (1986) 408–412. doi:10.1252/jcej.19.408.

[14] T. Ohtake, T. Hano, K. Takagi, F. Nakashio, Effects of viscosity on drop diameter of W/O emulsion dispersed in a stirred tank., J. Chem. Eng. Jpn. 20 (1987) 443–447. doi:10.1252/jcej.20.443.

[15] R. Rautenbach, O. Machhammer, Modeling of liquid membrane separation processes, J. Membr. Sci. 36 (1988) 425–444. doi:10.1016/0376-7388(88)80034-6.

[16] T. Gallego-Lizon, E.S. Pérez de Ortiz, Drop Sizes in Liquid Membrane Dispersions, Ind. Eng. Chem. Res. 39 (2000) 5020–5028. doi:10.1021/ie000016y.

[17] W.S. Ho, T.A. Hatton, E.N. Lightfoot, N.N. Li, Batch extraction with liquid surfactant membranes: A diffusion controlled model, AIChE J. 28 (1982) 662–670. doi:10.1002/aic.690280419.

[18] Z. Kang, P. Zhu, T. Kong, L. Wang, A Dewetting Model for Double-Emulsion Droplets, Micromachines. 7 (2016) 196. doi:10.3390/mi7110196.

[19] K. Pays, J. Giermanska-Kahn, B. Pouligny, J. Bibette, F. Leal-Calderon, Coalescence in Surfactant-Stabilized Double Emulsions, Langmuir. 17 (2001) 7758–7769. doi:10.1021/la010735x.

[20] J.K. Klahn, J.J.M. Janssen, G.E.J. Vaessen, R. de Swart, W.G.M. Agterof, On the escape process during phase inversion of an emulsion, Colloids Surf. Physicochem. Eng. Asp. 210 (2002) 167–181. doi:10.1016/S0927-7757(02)00376-X.

[21] S. Mukhopadhyay, S.K. Ghosh, V.A. Juvekar, Mathematical model for swelling in a liquid emulsion membrane system, Desalination. 232 (2008) 110–127. doi:10.1016/j.desal.2008.01.009.

[22] S. Okazaki, M. Imai, M. Shimizu, Leakage Suppressing Oe W/O Emulsion Using High Viscous Solvent, in: Process Metall., Elsevier, 1992: pp. 1487–1492. doi:10.1016/B978-0-444-88677-4.50064-7.

[23] F. Michaut, P. Perrin, P. Hébraud, Interface Composition of Multiple Emulsions: Rheology as a Probe, Langmuir. 20 (2004) 8576–8581. doi:10.1021/la048715t.

[24] D. Ramkrishna, A.W. Mahoney, Population balance modeling. Promise for the future, Chem. Eng. Sci. 57 (2002) 595–606. doi:10.1016/S0009-2509(01)00386-4.

[25] D. Ramkrishna, Population balances: theory and applications to particulate systems in engineering, Academic Press, San Diego, CA, 2000.

[26] I. Lönnqvist, B. Håkansson, B. Balinov, O. Söderman, NMR Self-Diffusion Studies of the Water and the Oil Components in a W/O/W Emulsion, J. Colloid Interface Sci. 192 (1997) 66–73. doi:10.1006/jcis.1997.4966.

[27] J.P. Hindmarsh, J. Su, J. Flanagan, H. Singh, PFG–NMR Analysis of Intercompartment Exchange and Inner Droplet Size Distribution of W/O/W Emulsions, Langmuir. 21 (2005) 9076–9084. doi:10.1021/la051626b.

[28] L. Boyadzhiev, T. Sapundzhiev, E. Bezenshek, Modeling of Carrier-Mediated Extraction, Sep. Sci. 12 (1977) 541–551. doi:10.1080/00372367708068466.

[29] L. Zeng, Y. Zhang, C. Bukirwa, W. Li, Y. Yang, Study of mean diameter and drop size distribution of emulsion drops in a modified rotating disc contactor for an emulsion liquid membrane system, RSC Adv. 5 (2015) 89959–89970. doi:10.1039/C5RA16267J.

[30] V. Alopaeus, J. Koskinen, K. I. Keskinen, J. Majander, Simulation of the population balances for liquid–liquid systems in a nonideal stirred tank. Part 2—parameter fitting and the use of the multiblock model for dense dispersions, Chem. Eng. Sci. 57 (2002) 1815–1825. doi:10.1016/S0009-2509(02)00067-2.

[31] Gustavo A. Padron, Measurement and comparison of power draw in batch rotor-stator mixers, Doctoral dissertation, University of Maryland, 2001.

[32] C. Qin, C. Chen, Q. Xiao, N. Yang, C. Yuan, C. Kunkelmann, M. Cetinkaya, K. Mülheims, CFD-PBM simulation of droplets size distribution in rotor-stator mixing devices, Chem. Eng. Sci. 155 (2016) 16–26. doi:10.1016/j.ces.2016.07.034.

[33] K.J. Valentas, O. Bilous, N.R. Amundson, Analysis of Breakage in Dispersed Phase Systems, Ind. Eng. Chem. Fundam. 5 (1966) 271–279. doi:10.1021/i160018a019.

[34] C.A. Coulaloglou, L.L. Tavlarides, Description of interaction processes in agitated liquid-liquid dispersions, Chem. Eng. Sci. 32 (1977) 1289–1297. doi:10.1016/0009-2509(77)85023-9.

[35] M.A. Hsia, L.L. Tavlarides, A simulation model for homogeneous dispersions in stirred tanks, Chem. Eng. J. 20 (1980) 225–236. doi:10.1016/0300-9467(80)80007-4.

[36] P.M. Bapat, L.L. Tavlarides, G.W. Smith, Monte carlo simulation of mass transfer in liquid-liquid dispersions, Chem. Eng. Sci. 38 (1983) 2003–2013. doi:10.1016/0009-2509(83)80104-3.

[37] C. Tsouris, L.L. Tavlarides, Breakage and coalescence models for drops in turbulent dispersions, AIChE J. 40 (1994) 395–406. doi:10.1002/aic.690400303.

[38] V. Alopaeus, J. Koskinen, K.I. Keskinen, Simulation of the population balances for liquid–liquid systems in a nonideal stirred tank. Part 1 Description and qualitative validation of the model, Chem. Eng. Sci. 54 (1999) 5887–5899. doi:10.1016/S0009-2509(99)00170-0.

[39] Theodore Vermeulen, Interfacial area in liquid-liquid and gas-liquid agitation, Chem. Eng. Progr. 51 (1955) 85F-94F.

[40] S.A. Miller, C.A. Mann, Agitation of Two-Phase Systems of Immiscible Liquids, Trans. Am. Inst. Chem. Engrs. (1944) 709–743.

[41] F. Filbet, P. Laurençot, Numerical Simulation of the Smoluchowski Coagulation Equation, SIAM J. Sci. Comput. 25 (2004) 2004–2028. doi:10.1137/S1064827503429132.

[42] J. Kumar, G. Warnecke, M. Peglow, S. Heinrich, Comparison of numerical methods for solving population balance equations incorporating aggregation and breakage, Powder Technol. 189 (2009) 218–229. doi:10.1016/j.powtec.2008.04.014.

[43] G. Narsimhan, J.P. Gupta, D. Ramkrishna, A model for transitional breakage probability of droplets in agitated lean liquid-liquid dispersions, Chem. Eng. Sci. 34 (1979) 257–265. doi:10.1016/0009-2509(79)87013-X.

[44] M.M. Ribeiro, P.F. Regueiras, M.M.L. Guimarães, C.M.N. Madureira, J.J.C. Cruz_Pinto, Optimization of Breakage and Coalescence Model Parameters in a Steady-State Batch Agitated Dispersion, Ind. Eng. Chem. Res. 50 (2011) 2182–2191. doi:10.1021/ie100368t.

[45] M. Laakkonen, V. Alopaeus, J. Aittamaa, Validation of bubble breakage, coalescence and mass transfer models for gas–liquid dispersion in agitated vessel, Chem. Eng. Sci. 61 (2006) 218–228. doi:10.1016/j.ces.2004.11.066.

[46] J. Jiao, D.J. Burgess, Rheology and stability of water-in-oil-in-water multiple emulsions containing Span 83 and Tween 80, AAPS PharmSci. 5 (2003) 62–73. doi:10.1208/ps050107.

Chapter 4. Theoretical and experimental investigations of double emulsion preparation by ultrasonication

Double emulsion preparation by ultrasonication is investigated in order to optimize the outer droplet size and the encapsulation efficiency. The effects of the sonication time, the oil viscosity, and the fractions of salt and primary emulsion are studied. A correlation is developed in order to predict the mean droplet diameter as a function of these parameters. The model is valid in the dissipation energy subrange. It accounts for the effects of salt within the surface force group, and the oil viscosity within the viscous group, the primary fraction through energy damping and allows the prediction of the transitionary change in size with time. The properties of the outer droplets, such as the viscosity and density, take into account the presence of inner droplets. Based on this model, a leakage model is proposed where the rate increases proportionally with breakage, but continues at a constant rate once the size reaches equilibrium.

$$d_{mean} = f(\varepsilon, \rho_c, \rho_d, \mu_c, \mu_d, \sigma, t)$$
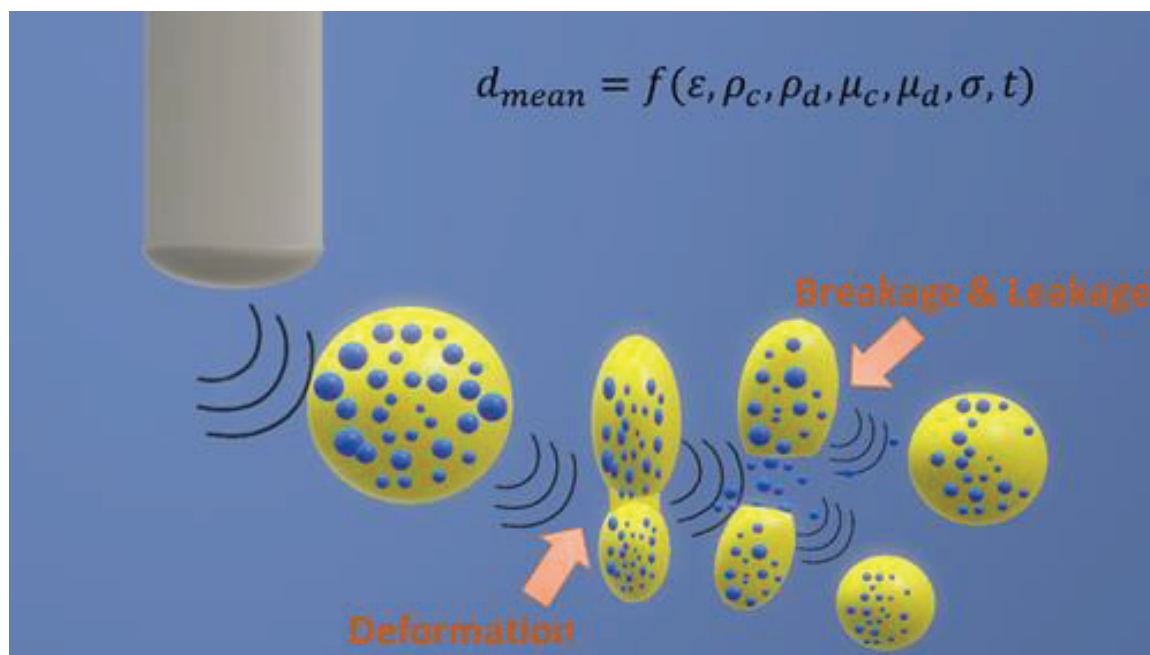
4.1. Introduction

During this second preparation step, different phenomena may occur, which are governed by physical-chemical parameters and the energy dissipation by the emulsification device that need to be optimized in order to maximize the encapsulation rate and ensure a longer physical stability of the double emulsion.

Schuch et al. [1] investigated the preparation of double emulsions in different devices and deduced that the encapsulation efficiency was proportional to the outer droplet size, independently of the type of device. Lindenstruth et al. (2004) [2] proposed that the encapsulation rate was governed by the size ratio between inner and outer droplets, which should be reduced in order to increase the yield. They also indicated a reduction of the encapsulation efficiency during preparation due to the escape of inner droplets that accompanies the breakage of outer droplets, hereafter called "leakage". For this reason, the mixing energy and time of the second step are generally lowered in order to increase the yield, which leads to big outer droplets compared to the inner droplets. Nevertheless, fine outer droplets may induce other advantages like preventing creaming, thus enhancing the stability during storage[3–5] or increasing the transparence of the final product [6]. Therefore, there is a compromise to be determined between droplet size and encapsulation rate [1].

Emulsions, and so double emulsions, can be produced using different emulsification devices, such as impellers, high speed rotor-stators, high pressure homogenizers, microfluidic devices, membranes, and ultrasonicators [1,4,7]. Among these techniques, ultrasonication allows producing very fine emulsions within a short emulsification time, and it constitutes an easy and clean process[8]. Ultrasonic waves transmitted through a liquid induce acoustic cavitation, which consists of the nucleation, growth, and collapse of gaseous bubbles in the fluid [9–11]. When applied on a two-phase interface, the interfacial waves caused by the propagation of ultrasound erupt the dispersed phase into the continuous phase in the form of droplets. Then, the acoustic cavitation causes intense physical shearing within the continuous phase, which generates turbulent eddies and allows gradual breakage of the droplets [7,12]. During this process, part of the acoustic energy is degraded into heat under the effect of viscous friction [7,9–12].

Ultrasonication has been widely used for the preparation of nanometric single emulsions[6,13–16] and it represents a topic of growing interest for double emulsions, for instance for pharmaceuticals [17] and food [18]. The process parameters affecting the yield and mixing efficiency, or droplet size, are the sonication time and energy level. While increasing their levels would allow for a better mixing and the production of smaller droplets, it may destroy the double emulsion leading to total leakage of the inner droplets [19]. Another disadvantage of increasing the sonication time or power is related to the associated increase in temperature and pressure which may cause the degradation of the encapsulated ingredient, the emulsifier or the organic phase [7]. Therefore, there are optimal conditions to be determined. The encapsulation efficiency was reported to decrease when increasing the sonication time [17,20]. This observation was confirmed by Tang et al., who also found the addition of gelatin in the inner phase reduces droplet coalescence due to the formation of an interfacial rigid film, and investigated the effect of the concentration of surfactants [21,22].

The minimal power amplitude ensuring the production of cavitation was theoretically examined by Tal-Figiel [23]. Leong et al. indicated that increasing the sonication power led to a decrease in the droplet size. The encapsulation efficiency was found to increase when decreasing the fraction of the internal water phase and when increasing the fraction of the primary emulsion; However the fraction of the primary emulsion had no effect on the outer droplet's size, except for extremely low, or extremely high sonication powers [3]. They also investigated other parameters such as the fraction of surfactant [24,25].

For a better comprehension and optimization of the process, different modelling approaches were proposed in order to predict the encapsulation efficiency and the outer droplet size during the preparation of double emulsions in different devices. Okazaki et al. [26] proposed a correlation to estimate the leakage rate in a stirred tank as a function of energy dissipation, viscosity, and osmotic pressure over a specific salt concentration range. Concerning the mean droplet size, a number of correlations were proposed for single emulsions produced in stirred tanks [27–30], which were then used for double emulsions [31–34]. For single emulsions preparation using sonication, the mean droplet diameter was predicted by semi empirical correlations [6,23,35,36] or based on fundamental investigations, such as Nazarzadeh and Sajjadi [37] and Gupta et al., [38] who investigated the preparation in the dissipation subrange. These correlations will be investigated in this work and adapted for double emulsions. Indeed, some physical parameters of the emulsion change when the dispersed phase becomes itself an emulsion, i.e., during the second step of double emulsion preparation. A model is then developed to predict the release rate based on the breakage. The model needs to take into account the parameters that were found to affect the droplet size and the encapsulation efficiency in the literature review presented above.

The objective of this work is to investigate the effect of different operating conditions in ultrasonic emulsification on the yield and the outer droplet size and to propose correlations to estimate the leakage rate and outer droplet size as a function of the sonication time. W/O/W double emulsions are produced using ultrasonication in both steps. Different operating parameters were investigated, namely the sonication time of the second step, the oil viscosity, the internal fraction and the salt concentration.

4.2. Experimental Section

4.2.1. Materials

Different types of mineral oils were used to prepare the W/O/W double emulsions: white mineral oil (Fisher Scientific), fluid paraffin oil (Cooper), Marcol 82 (ExxonMobil) and Marcol 52 (ExxonMobil). The used emulsifiers were Span 80 (Alfa Aesar) as hydrophobic emulsifier and Tween 80 (Fisher Scientific) as hydrophilic emulsifier. Sodium chloride was used as tracer. Millipore water with resistivity ≈ 18.2 mΩ.cm was used all over the work.

4.2.2. Double Emulsion Preparation

Sonication was done using an ultrasonic processor (UP400S 400 W, 24 kHz) equipped with a Sonotrode H7 (tip diameter = 7 mm) manufactured by Hielscher Ultrasonics GmbH.

Table 4.1. *Weight Fractions and Operating Conditions*

Set	Effect of	μ_{oil} (mPa.s)	First preparation step[1] Fractions (wt. %) water	NaCl	Span 80	Oil	Second preparation step[1] Fractions (wt. %) Primary	water	Tween 80	Operating parameters t_2 (s)	ΔT (K)	P (W)
1	t_2	45	10	0.05	9.95	80	10	89	1	5 / 10 / 15 / 20	1.5 / 3.5 / 5.5 / 7.5	9.4 / 11 / 11.5 / 11.76
2	μ_{oil}	6 / 22 / 32 / 45	10	0.05	9.95	80	10	89	1	10	3.5	11
3	ϕ_{NaCl}	45	10	0.025 / 0.05 / 0.1 / 0.15	9.95	80	10	89	1	10	3.5	11
4	ϕ_{Macro}	45	10	0.05	9.95	80	10 / 20 / 30 / 40	89 / 79 / 69 / 59	1	10	3.5	11

[1]The total masses used in the first and second steps are 10 and 7.5 g, respectively.

W/O/W double emulsions were prepared using a two-step method, at room temperature, similarly to Leong et al. [3]. In the first step, the NaCl solution was dispersed in the oil phase – consisting of oil in which Span 80 was dissolved. A total mass of 10 g was placed in a 20 mL bottle and the Sonotrode tip was fixed at the interface of the aqueous and oil phases to help the interfacial waves to act immediately [7]. The sonication time of this first emulsification step was 30 s at amplitudes of 20 %. In the second step, part of the primary emulsion was dispersed in an external aqueous phase – consisting of water in which Tween 80 was dissolved – and emulsified with the same ultrasound device for 5-20 s, giving a total mass of 7.5 g of double emulsion. The calculated calorimetric power (P) [36,39] of the first sonication step was 16 W and in the second step P = 9.4 – 11.76 W. Table 4.1 shows the conditions and fractions of the used materials.

4.2.3. Droplet Size Measurements

The inner droplet size distribution was measured right after the first preparation step by means of dynamic light scattering (Malvern Zetasizer Nano ZS). Before the measurement, the samples were diluted approximately 1:1000 (similar to refs [3] and [9]) in mineral oil. The analysis was performed twice for each sample, and every time three measurements were repeated, each of consisting of 11 runs. The Z-average ($d_{Z-average} \approx \frac{\sum d_i^6}{\sum d_i^5}$) was considered as the mean diameter of inner droplets. The outer droplets' size distribution was analyzed using laser diffraction (Malvern Mastersizer 3000). The refractive index of the outer droplets was considered to be that of oil (i.e., 1.467), which represents the main component of these droplets, especially close to the surface. Schmidts et al. [41] made the same assumption and

validated the Mastersizer measurements of the outer droplets by optical microscopic observations. The De Broukere mean diameter, d_{43}, was considered for outer droplets.

4.2.4. Conductivity Measurements

The released amount of NaCl was monitored by measuring the conductivity of the samples, taken after the second preparation step, using a CDM210 conductivity Meter (MeterLab). The released amount was estimated based on a predetermined calibration curve. Two calibration methods were evaluated and found equivalent, either by dispersing different salt concentrations in pure water or by dispersing the salt in a single O/W emulsion instead of water.

4.2.5. Methods

A preliminary study was conducted in order to determine the optimal sonication time and internal water fraction of the primary emulsion. First, the optimal sonication time of the primary emulsion was varied over the range of 30, 60, 90, and 120 s. The internal weight fraction was 20 %. The obtained mean inner droplet diameters (Z-average) were d_{μ}= 540, 425, 394, and 360 nm. The emulsification time of the primary emulsion was fixed at 60 s, since beyond this limit the inner droplets did not show an important decrease in their size and the emulsions were stable with 60 s emulsification. Second, the internal fraction was varied over the range of 10, 20, 30, and 40 %. It was found that different energy levels would be required in order to ensure uniform emulsification of the different fractions. In order to allow a straightforward comparison between the different experimental sets, the internal fraction was maintained at 10 % with the energy level at 20 % amplitude (i.e., P = 16 W).

Thereafter, different key process parameters were investigated during the preparation of the double emulsions, including the sonication time of the second step, the primary emulsion fraction, the oil viscosity, and the salt fraction (see Table 4.1). The inner and outer droplet sizes were measured as well as the conductivity at the end of the emulsification. The mean dissipation energy by ultrasound was determined using the equation $\varepsilon = C_{\mathrm{P}}\dfrac{\mathrm{d}T}{\mathrm{d}t}$, where C_{P} is the specific heat capacity of the liquid and T is its temperature [3,36,42].

4.3. Modeling

The outer droplet size and the encapsulation efficiency, or the escape of inner droplets during preparation, are the two main process variables that are interesting to model and predict during the emulsification by ultrasonication as a function of the different operating conditions that were found in the literature review to affect these variables.

4.3.1. Mean Droplet Diameter

In the turbulent regime, the Kolmogorov length scale of the smallest vortices is $\eta = \left(\dfrac{\nu^3}{\varepsilon}\right)^{1/4}$, where ν is the kinematic viscosity and ε the energy dissipation [43]. At high Reynolds numbers, (i.e. a turbulence Reynolds number $Re_L > 8630$ [44]), the universal equilibrium range is divided into two subranges with regard to the eddy/vortex size (λ):

(1) The first is the inertial subrange, $60\,\eta \ll \lambda \ll L/6$, in which the motion is dominated merely by the energy dissipation rate, thus the mean velocity fluctuation of an eddy of size λ is given by $\overline{u_\lambda^2} \propto \varepsilon^{\frac{2}{3}} \lambda^{\frac{2}{3}}$, where L is the scale of largest vortices;

(2) The second is dissipation or viscous subrange, $\eta \ll \lambda \ll 60\,\eta$, where the motion is dominated by both the energy dissipation rate and the kinematic viscosity, thus the velocity is given by $\overline{u_\lambda^2} \propto \dfrac{\varepsilon \lambda^2}{\nu}$.

The limits of the inertial subrange, L/6 and 60η, are valid only at high Reynolds number, while for moderate Reynolds they can reach L/2 and 15η [54,55]. In this study, the outer droplet mean diameters are in the range 10 to 60 µm, thus below the limit between the inertial and viscous subranges (70–280 µm assuming 15η–60η). The main correlations proposed to estimate the droplet size in this subrange (i.e., dissipation) are given in Table 4.2. They will be modified to account for the properties of the different phases (i.e., fractions, viscosities), in analogy with the methodologies developed for the inertial subrange, shown in Table 4.2.

Table 4.2. *Mean Diameter Correlations for Single Emulsions, at Equilibrium, under Turbulent Conditions*

mean (or maximum) diameter correlation	range	ref
$d \propto \varepsilon^{-\frac{2}{5}} \left(\dfrac{\sigma}{\rho_c}\right)^{\frac{3}{5}}$ Or, $d/D_I \propto We^{-\frac{3}{5}}$, with $We = \dfrac{\rho_c \overline{u_d^2} d}{\sigma}$, $\overline{u_d^2} \approx \overline{u_\lambda^2}$ (with D_I the impeller diameter)		Kolmogorov [45] Hinze [27]
To account for the dispersed phase fraction, ϕ: $d/D_I \propto (1 + a\,\phi)\, We^{-\frac{3}{5}}$ With a =3.75 for Calderbank (1958). Other values of a are available[29,46,47].	inertial $\overline{u_\lambda^2} \propto \varepsilon^{\frac{2}{3}} \lambda^{\frac{2}{3}}$	Calderbank [48]
To account for the dispersed phase viscosity, μ_d: $d \propto \varepsilon^{-\frac{2}{5}} \left(\dfrac{\sigma + \mu_d \overline{u_d}/4}{\rho_c}\right)^{\frac{3}{5}}$		Davies [49]
To account for the viscosity ratio (with D the static mixer diameter): $d/D \propto W_e^{-\frac{3}{4}} \left(\dfrac{\mu_d}{\mu_c}\right)^{0.18}$		Chen & Libby [50]
$\dfrac{\mu_c d}{\sigma} \dfrac{\partial \overline{u_\lambda}}{\partial \lambda} = \underbrace{f\left(\dfrac{\mu_d}{\mu_c}\right)}_{\text{or } Ca_{crit}}$ which gives $d \propto \sigma (\varepsilon \rho_c \mu_c)^{-\frac{1}{2}} Ca_{crit}$	dissipation $\overline{u_\lambda^2} \propto \dfrac{\varepsilon \lambda^2}{\nu}$	Taylor [51,52] Shinnar [53]
$d \propto \rho_d^{-\frac{1}{6}} (\varepsilon \rho_c \mu_c)^{-\frac{5}{12}} \sigma^{\frac{2}{3}} \mu_d^{\frac{1}{3}}$		Gupta et al. [38]

Table 4.3. *Mean Outer Droplet Diameter Correlations in Double Emulsions*

$d/D_I \propto \left(1 + 2\phi_\mu\right)^{1.2} \left(1 + 2\,\phi_M\right)^{1.2} We^{-0.6}(1 + 4.08 N_{vi})^{\frac{3}{5}}$ With $N_{vi} = \left(\dfrac{\rho_c}{\rho_d}\right)^{1/2} \dfrac{\mu_d\, \varepsilon^{-1/3} d^{1/3}}{\sigma} \left(1 + 2\,\phi_\mu\right)^{-1}(1 + 2\phi_M)^{-1}$	inertial	Sharma et al.[56]
$d/D_I \propto We^{-0.6} \phi_M^{0.136} \left(\dfrac{\mu_M}{\mu_c}\right)^{0.11} \left(1 + F^{SW}\right)^{\frac{1}{3}}$ With $F^{SW} = \dfrac{d^3 - (d^0)^3}{(d^0)^3}$		Gallego-Lizon & Pérez de Ortiz [34]
$d = K_1(\varepsilon \rho_c \mu_c)^{-\frac{1}{2}} \left(\dfrac{\mu_M}{\mu_c}\right)^{\beta} \left(1 + 2.5\phi_M\right)^{\frac{3}{2}}\left(\sigma_M + K_2 \phi_\mu C_{salt} RTd\right)(1 + K_3 e^{-K_4 t})$	dissipation	This work (eq 4.8)
$d = C_1(\varepsilon \rho_c \mu_c)^{-\frac{5}{12}} \left(\dfrac{\mu_M}{\mu_c}\right)^{\beta-\frac{1}{3}}\left(1 + 2.5\phi_M\right)^{\frac{5}{4}}\left(\sigma_M + C_2 \phi_\mu C_{salt} RTd\right)^{\frac{2}{3}}(1 + K_3 e^{-K_4 t})\rho_M^{-\frac{1}{6}}\mu_M^{\frac{1}{3}}$		This work (eq 4.9)

The correlations used for simple emulsions were also used in double emulsions, with some adaptations, mainly the effect of internal phase fraction [56] and adding a swelling factor [34] (Table 4.3). The equations proposed in the present work for double emulsions appear in Table 4.3, and they will be developed in the following section.

4.3.1.1. Effect of The Dispersed Phase Viscosity

Taylor Basis. Based on Taylor's theory of droplet deformation, there exists a critical generalized Weber group, $N_{We} = \frac{\tau d}{\sigma}$, below which breakup does not occur, where d is the droplet diameter, σ is the interfacial tension, and τ is the external force per unit area (i.e., the stress) acting on the surface of the droplet[27]. In the inertial subrange, τ represents the dynamic pressure $\tau = \rho_c \overline{u_\lambda^2}$, from which the original Weber number can be obtained, $N_{We} = We = \frac{\rho_c \overline{u_d^2} d}{\sigma}$, thus allowing the derivation of the Kolmogorov droplet size correlation for the inertial subrange (Table 4.2) [27]. For the viscous subrange, which is of interest here, τ is a viscous stress $\tau = \mu_c \frac{\partial \overline{u_\lambda}}{\partial \lambda}$, which gives the capillary number[51,52], $N_{We} = Ca = \frac{\mu_c d}{\sigma} \frac{\partial u_\lambda}{\partial \lambda}$ (below which the droplets will not break). By applying the Kolmogorov velocity of the dissipation subrange into this equation, the following correlation can be obtained for the maximum droplet size at equilibrium [27, 53, 57]: $d_{max} \propto \sigma (\varepsilon \rho_c \mu_c)^{-\frac{1}{2}} Ca_{crit}$. The critical capillary number can be described as a function of the viscosity ratio [58, 59], i.e., $Ca_{crit} \propto \left(\frac{\mu_d}{\mu_c}\right)^\beta$, where β is a constant, which gives:

$$d_{max} \propto \sigma (\varepsilon \rho_c \mu_c)^{-\frac{1}{2}} \left(\frac{\mu_d}{\mu_c}\right)^\beta \qquad \qquad 4.1$$

where ρ and μ are respectively the density and viscosity, and the subscripts "d" and "c" are indicators of the dispersed and continuous phases, respectively. The curve of Ca_{crit} against the viscosity ratio $\frac{\mu_d}{\mu_c}$ is known to first decrease with this ratio up to $\frac{\mu_d}{\mu_c} \approx 1$ (i.e., β is negative) and then Ca_{crit} increases with the viscosity ratio (i.e., β becomes positive), approximately when $\frac{\mu_d}{\mu_c} > 7$ (Grace curve)[27, 59–61]. Nazarzadeh and Sajjadi [37] implemented the values of the critical Capillary of Bentley and Leal (1986) [61] and fitted equation 4.1 in ultrasound emulsification operating in the viscous subrange, in which they observed a decrease then an increase in the mean droplet size with the viscosity ratio.

Hinze Basis. Hinze [27] suggested that besides the generalized Weber group, the viscosity group that accounts for the viscosity of the droplet (i.e. the Ohnesorge number $Oh = \frac{\mu_d}{\sqrt{\rho_d \sigma d}}$), also controls the droplet deformation. Following this suggestion, the critical capillary number is defined as $Ca_{crit} = C \left(1 + f(Oh)\right)$. Based on this, Gupta at al. [38] developed a correlation for the dissipation subrange with C as a constant. However, in the suggestion of Hinze [27], C is a function of the viscosity ratio $\frac{\mu_d}{\mu_c}$. In this case, the following correlation can be proposed:

$$d_{max} \propto \sigma^{\frac{2}{3}} (\varepsilon \rho_c \mu_c)^{-\frac{5}{12}} \left(\frac{\mu_d}{\mu_c}\right)^{\beta_2} \rho_d^{-\frac{1}{6}} \mu_d^{\frac{1}{3}} \qquad \qquad 4.2$$

This correlation is valid for large Oh values, where the high viscous stresses inside the droplet necessitate higher inertial stress to break it.

Equations 4.1 and 4.2 will constitute the two main model bases, in which other properties of the double emulsions will be incorporated. In order to have a comparable effect of the viscosity of the dispersed phase in both models, we assume $\beta_2 = \beta - \frac{1}{3}$ (as eq 4.2 contains a separate term $\mu_d^{1/3}$). However, the power of the viscosity ratio will still be different in the two models.

4.3.1.2. Effect Of The Dispersed Phase Fraction (Damping Effect)

Calderbank [48] and Brown and Pitt [28] included the damping effect of the dispersed phase volume fraction (ϕ) on energy dissipation, $d^\phi \propto d^0(1 + a\,\phi)$, with "a" equal to 3.75 and 3.14, respectively. Based on series expansion, Doulah (1975) [46] estimated $a = 3$ for the inertial subrange. By analogy, we can make the same development for the dissipation subrange. Based on the Kolmogorov length scale, the ratio of energy dissipation between the damped and nondamped system is $\frac{\varepsilon_0}{\varepsilon_\phi} = \left(\frac{\nu_\phi}{\nu_0}\right)^3$. By approximating the viscosity ratio using Einstein's equation, $\mu_\phi = \mu_0\left(1 + \frac{5}{2}\phi\right)$, one obtains $\mathrm{d}^\phi \propto d^0(1 + 2.5\phi)^q$ with $q = 3 \times (-p)$, where p is the power of ε in the correlation of d^0. Doulah[46] used $p = 0.4$ in the inertial subrange. In the dissipation subrange, one should use $q = 3/2$ and $5/4$ for equations 4.1 and 4.2, respectively.

4.3.1.3. Effect Of Time, Transitionary State

The available droplet size correlations are usually valid for stationary state, thus giving the equilibrium droplet size. For continuous emulsifications, it was suggested that the droplet diameter depends on the residence time, for instance $d \propto \tau^{-0.3}$ [62], or $d \propto E_v^{-b}$ with $E_v = \varepsilon\tau$ being the energy density and $b \sim 0.4$ for turbulent breakage [35]. In order to predict the evolution of the droplet size with time in the present system, the following correlation is proposed:

$$d = d_{eq}(1 + K_3 e^{-K_4 t}) \tag{4.3}$$

Where K_4 is the breakage frequency and d_{eq} is the equilibrium diameter that can be obtained from the stationary correlations, for instance using eqs 4.1 and 4.2. When t $\to \infty$, $e^{-K_4 t} \to 0$, which allows to get the stationary value, d_{eq}.

4.3.1.4. Adaptations To Double Emulsions

In double emulsions the dispersed phase is itself an emulsion, which requires specific correlations to calculate the outer droplet viscosity (μ_M) and density (ρ_M). Moreover, the presence of salt may lead to swelling of the outer droplets, thus affecting their size and the escape rate. The properties of the inner (micro) and outer (macro) phases/droplets are distinguished and indicated with the indices "μ" and "M", respectively.

Viscosity and density. The apparent viscosity and density of a liquid-liquid dispersion (i.e. outer droplets here) can be obtained by the models of Vermeulen [63] and Miller and Mann [64], respectively:

$$\mu_M = \frac{\mu_c}{1-\phi}\left(1 + 1.5\,\phi\,\frac{\mu_d}{\mu_d + \mu_c}\right) \qquad\qquad 4.4$$

$$\rho_M = \phi\,\rho_d + (1-\phi)\,\rho_c \qquad\qquad 4.5$$

The subscripts "d" and "c" refer to the dispersed (i.e., internal water) and continuous (i.e., oil) phases, respectively.

Effect of Salt. The concentration difference of salt between the internal and external phases creates a force on the surface of inner and outer droplets (i.e., osmotic pressure). The work required to strain a droplet containing other droplets is thus modified compared to the work required to strain a pure droplet [65]. This force can be added into the surface force group, and therefore the balance between the Laplace and osmotic pressures gives [66–68]:

$$\Delta P = \frac{4\,\sigma}{d} - \mathcal{O}_{reflx}\,i\,C_{salt}RT \qquad\qquad 4.6$$

Where C_{salt} is the salt concentration in the inner droplets, R is the ideal gas constant, T is the temperature, i is the van't Hoff factor, and $\mathcal{O}_{reflx}$ is the reflection coefficient of the membrane. Assuming the surface of the inner droplet to play the role of a membrane during release, it may be considered that $\sigma_\mu \propto d_\mu\,\mathcal{O}_{reflx}\,i\,C_{salt}RT$. Thus, the effective surface tension can be calculated:

$$\sigma_{M,eff} = \sigma_M + K_2\,\phi_\mu\,C_{salt}RT\,d_M \qquad\qquad 4.7$$

where K_2 is a parameter regrouping the different unknown constants (i.e., $\mathcal{O}_{reflx}$ and i) or deviations from an ideal behavior, and σ_M is the surface tension of the outer droplets having no salt (in this work considered as the oil-water surface tension, i.e. with $\phi_\mu = 0$).

4.3.1.5. Complete Droplet Size Correlation For Double Emulsions In Ultrasonication

The different properties of the double emulsion discussed above were included into eqs 4.1 and 4.2, which gives, based on the Taylor approach (eq 4.1):

$$d = K_1(\varepsilon\rho_c\mu_c)^{-\frac{1}{2}}\left(\frac{\mu_M}{\mu_c}\right)^{\beta}(1 + 2.5\phi_M)^{\frac{3}{2}}\left(\sigma_M + K_2\phi_\mu C_{salt}RTd\right)(1 + K_3 e^{-K_4 t}) \qquad 4.8$$

By incorporating the Hinze suggestion into Taylor's approach, through Gupta's development (eq 4.2), the correlation becomes:

$$d = C_1(\varepsilon\rho_c\mu_c)^{-\frac{5}{12}}\left(\frac{\mu_M}{\mu_c}\right)^{\beta-\frac{1}{3}}(1 + 2.5\phi_M)^{\frac{5}{4}}\left(\sigma_M + C_2\phi_\mu C_{salt}RTd\right)^{\frac{2}{3}}(1 + K_3 e^{-K_4 t})\,\rho_M^{-\frac{1}{6}}\mu_M^{\frac{1}{3}} \qquad 4.9$$

Where K_1, K_2, K_3, K_4, C_1, C_2 and β are constants to be determined by fitting to the experimental data. The breakage frequency K_4 and the pre-exponential factor K_3 should have the same values in both models. The main differences between these correlations mainly lay in the powers of different terms.

4.3.2. Leakage

During the preparation by ultrasound, molecular diffusion of salt can be neglected due to the low solubility of the used salt in the oil phase and the short preparation time. Similarly, the escape of the inner droplets by diffusion is slow and can be neglected during preparation. Therefore, the main phenomenon responsible for the release is inner droplet leakage, which

is defined as the escape of inner droplets joining the breakage of outer droplets. The leakage rate can thus be correlated to the breakage rate, i.e., eqs 4.8 and 4.9.

The leakage rate is also proportional to the concentration of encapsulated salt. The concentration of salt in the outer droplets, C_{salt}, can be obtained from the following balance (here the release is measured by conductivity) [26]:

$$\frac{dC_{salt}}{dt} = -K_L \, C_{salt} \qquad\qquad 4.10$$

The leakage constant is suggested to be correlated to the droplet diameter d (determined from es 4.8 or 4.9) as follows:

$$K_L = \frac{K_{L0}}{d} \qquad\qquad 4.11$$

where K_{L0} is a tuning parameter. By this way, the leakage rate is related to the same phenomena governing breakage. Moreover, when the droplet size reaches equilibrium between breakage and coalescence, the leakage continues at a constant rate until emptying the outer droplets from the inner droplets. The encapsulation efficiency (EE) fraction, therefore, can be obtained by $EE(\%) = \frac{C_{salt}(t)}{C_{salt}\,(t=0)} \times 100 = \exp(-K_L \, t) \times 100$.

4.4. Results And Discussions

The De Brouckere mean diameter, d_{43}, was considered in fitting eqs 4.8 and 4.9 because it represents the mean diameter over volume. However, any other mean diameter can be used if preferred in some applications [69,70]. The unknown constants in eqs 4.8, 4.9 and 4.11, were identified using a least square minimization in MatLab environment (Table 4.4). It was found that both correlations 4.8 and 4.9 give similar curves in general (but with different constant values). Therefore, only the results of eq 4.8 are shown in the following figures, except for the case with fractions of salt higher than 0.21 %, where a deviation is observed.

Table 4.4. Constants of the Mean Droplet Diameter and Leakage Correlations

constants of the mean diameter correlations							leakage
model 1 (eq 4.8)		model 2 (eq 4.9)		both models			eq 4.11
K_1	K_2	C_1	C_2	β	K_3	K_4	K_{L0}
0.0034	0.0095	0.0116	0.018	0.116	12.18	0.0864 s^{-1}	2.8×10^{-7}

4.4.1. Sonication Time of The Second Step

The sonication time of the second step was varied over the range 5, 10, 15, and 20 s, and its effect on the droplet size and leakage was investigated (set 1, Table 4.1). The primary emulsion was prepared with 60 s of sonication and 20 % energy amplitude (16 W). The size distribution of the internal emulsion is presented in Figure 4.1A giving a mean diameter of 425 nm. This primary emulsion was stable over several hours, thus giving safely enough time for the preparation of the double emulsion.
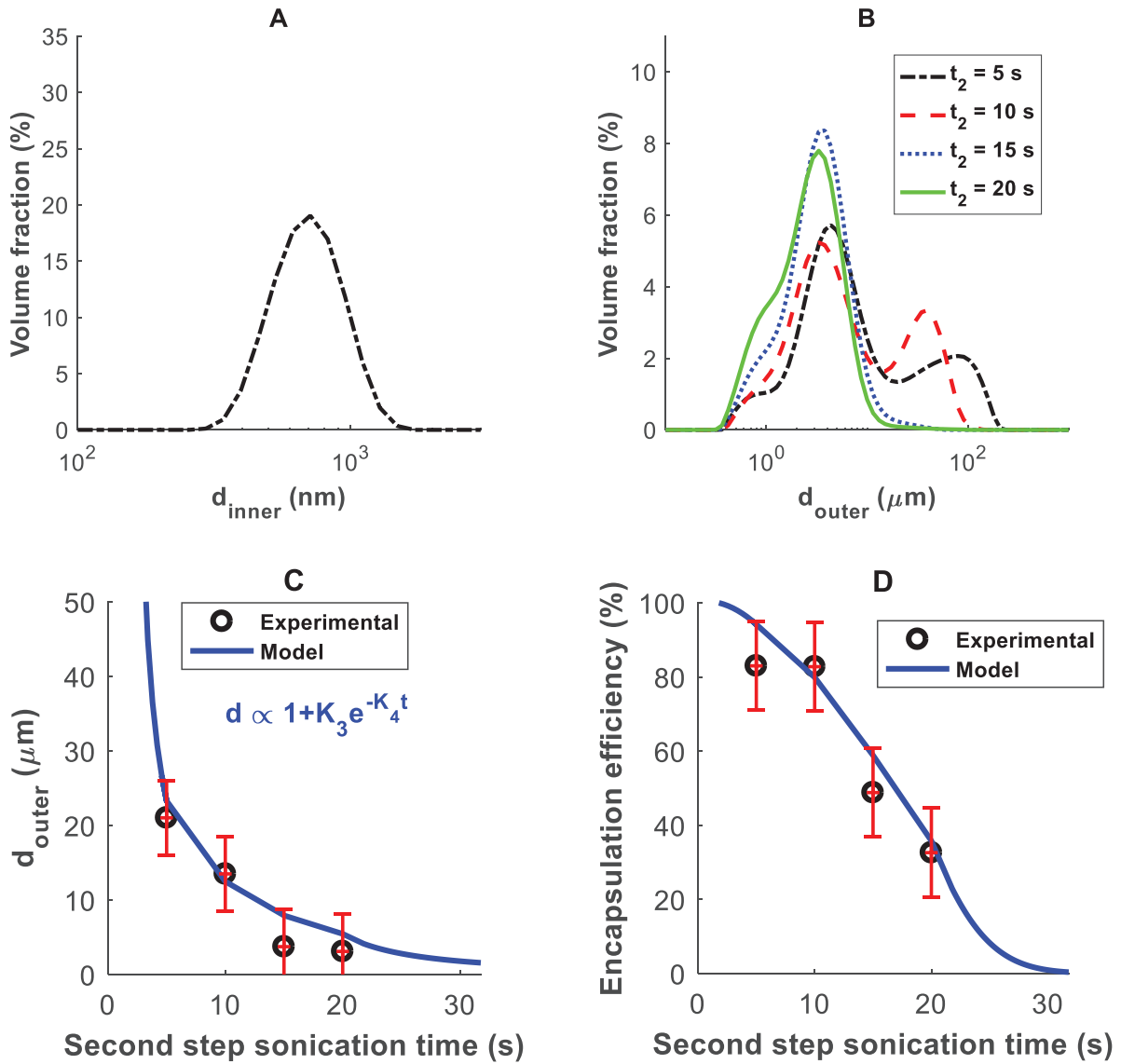
Figure 4.1. *Effect of the sonication time in the second emulsification step. (A) Size distribution of inner droplets, (B) size distribution of outer droplets, (C) mean diameter of outer droplets, and (D) encapsulation efficiency. The model curve is obtained by eq 4.8 for the droplet diameter (giving similar results as eq 4.9 here) and using eqs 4.10–4.11 for the yield.*

Figures 4.1B and 4.1C show the outer droplet size distribution and the mean diameter respectively. It can be seen that increasing the sonication time leads to the production of smaller outer droplets, until reaching an equilibrium between breakage and coalescence approximately after 15 s where further sonication a negligible effect. The encapsulation rate (Figure 4.1D) indicates that increasing the second step emulsification time leads to a higher leakage and thus to a lower yield. Indeed, in each breakage event, a number of inner droplets can leak out to the outer droplets due to the generated surface and the kinetic energy gained by the outer droplets. This confirms the fact that leakage is directly correlated to breakage. Consequently, bigger outer emulsions are recommended as they ensure a higher encapsulation efficiency, as far as these double emulsions are physically stable during storage and induce the final desired properties (e.g. transparence).

The models of the mean droplet diameter (equation 4.8) and the yield (eqs 4.10–4.11) are shown in Figure 4.1. The part of the mean diameter correlation that accounts for the

sonication (emulsification) time of the second step is: $1 + K_3 e^{-K_4 t}$. It can be seen that the proposed correlations allow a good prediction of the tendencies as well as the final steady state of the outer droplet size. Note that even after reaching the equilibrium droplet size, the escape of inner droplet continues. Indeed, at equilibrium the breakage rate equals the coalescence rate, but breakage events persist, thus leading to inner droplet escape. In the next sections, the second emulsions will be prepared in 10 s, which provides a good compromise between outer droplet size and encapsulation rate (around 80 %).

It is to be noted that the sonication causes an increase in the temperature that may affect the viscosity of the different phases and their interfacial properties [7] or may lead to degradation of some materials, such as proteins or surfactants [4]. In this first set of experiments, the temperature increased from 23 to 30.5 °C when the sonication time was the highest (20 s). However, the increase of 7.5 °C was found to have a negligible effect on the viscosity. Indeed, the viscosity-temperature correlation of Stanciu [71] was used and its parameters were identified for mineral oil, giving: $\mu = 0.0018 + 8.22 \times 10^4 \exp\left(-T/20.47\right)$. Using this correlation, the viscosities were predicted to be: 45 mPa.s at 23 °C, 42 mPa.s at 24.5 °C, 34.8 mPa.s at 28.5 °C, and 31.7 mPa.s at 30.5 °C. When implementing this viscosity change in the proposed models (eqs 4.8 and 4.9), only a slight effect could be perceived on the final size and the leakage fraction. As mentioned above, in the following sets of experiments, the emulsification time is fixed at 10 s, therefore, the increase in temperature is 3.5 °C, which makes the change in viscosity negligible. Therefore, the viscosity of the oil at room temperature can reasonably be considered in both models, and any change due to the increase in temperature can be neglected. Nevertheless, in order to prevent any undesired side effects in case of a big thermal increase, a cooling jacketed system may help to maintain the temperature constant during emulsification by sonication [4].

4.4.2. Effect Of The Oil Viscosity

In order to investigate the effect of the oil phase viscosity, four paraffin oils with different viscosities were used: $\mu_{\text{Macrol 52}} = 6$ mPa.s., $\mu_{\text{Macrol 82}} = 22$ mPa.s., $\mu_{\text{Fluid Paraffin oil}} = 32$ mPa.s., and $\mu_{\text{Mineral oil}} = 45$ mPa.s. As in the previous section, the primary emulsions were sonicated with 20 % energy amplitude for 60 s (16 W).

Figure 4.2A shows the size distribution of the inner droplets obtained with the different oil viscosities. While similar sonication energies and times were employed for all oils, bigger water inner droplets were produced when the oil viscosity was increased. These primary emulsions were then used to produce double emulsions by sonication at an energy amplitude of 20 % for 10 s (11 W). Figure 4.2B shows the size distribution of the outer droplets of different oil viscosities. It can be seen that increasing the oil viscosity leads to the production of slightly bigger outer droplets, except for the distribution obtained with the oil of 6 mPa.s which is wider.

Figure 4.2. *Effect of the oil viscosity. (A) Size distribution of inner droplets, (B) size distribution of outer droplets, (C) mean size of outer droplets, and (D) encapsulation efficiency. The estimated size is given by eq 4.8, both for $\beta = 0$ (with $K_1 = 0.0053$, $K_2 = 0.0146$) and $\beta = 0.116$ (with the parameters of Table 4.4), and the encapsulation efficiency is obtained by eqs 4.10–4.11.*

In order to explain these observations, the critical capillary number is investigated for both the internal and external emulsions. For the primary emulsion, where water constitutes the dispersed phase and oil the continuous phase, the range of viscosity ratios $\left(\frac{\mu_d}{\mu_c} = \frac{\mu_{water}}{\mu_{oil}}\right)$ is 0.02, 0.028, 0.04 and 0.15 (corresponding to oil viscosities of 45, 32, 22, and 6 mPa.s), thus less than unity. Based on the Taylor theory [37], the critical capillary decreases with $\frac{\mu_d}{\mu_c}$ when $\frac{\mu_d}{\mu_c} < 1$. Therefore, the primary emulsions have bigger sizes when the oil viscosities are higher (i.e. lower viscosity ratios) (Figure 4.2A). For the external emulsions, the range of viscosity ratios is 6.7–55. The critical capillary number starts to increase with $\frac{\mu_d}{\mu_c}$ when $\frac{\mu_d}{\mu_c} > 7$. Therefore, the outer droplets move toward bigger sizes (Figure 4.2B,C), i.e., the turbulent disrupting force needs to overcome interfacial forces besides an increasing viscous force. With

an oil viscosity of 6 mPa.s, the viscosity ratio is in the intermediate range, i.e. $1 < \frac{\mu_d}{\mu_c} < 7$, where a small effect of the viscosity ratio is observed on the size, and β starts changing of sign. In other words, the factor β in $\left(\frac{\mu_d}{\mu_c}\right)^{\beta}$, is negative for the inner droplet and positive for the outer droplets in this study. This allows the prediction of the droplet size over the whole region of $\frac{\mu_d}{\mu_c}$, considering updating the parameter β. Nazarzadeh and Sajjadi [37], studied the effect of viscosity ratio between 0.4 and 100 on the size of emulsions prepared with ultrasound and observed a similar decrease, followed by an almost constant range, then an increase in the droplet size for $\frac{\mu_d}{\mu_c} < 1$, $1 < \frac{\mu_d}{\mu_c} < 7$, and $\frac{\mu_d}{\mu_c} > 7$, respectively.

The model results for the outer droplet size and encapsulation efficiency are shown in Figures 4.2C and 4.2D respectively. In order to demonstrate the interest of incorporating the viscosity ratio in the model, equation 4.8 is plotted with the optimized value of β as well as with $\beta = 0$, thus assuming C to be constant in $Ca_{\text{crit}} = C\left(1 + f(Oh)\right)$, as done by Gupta model [38]. It can be seen that accounting for the viscosity ratio leads to a better agreement. However, a different values of β would be required for oil viscosities lower than 6 mPa.s, as explained above.

4.4.3. Effect Of Nacl Fraction

The primary emulsions were sonicated during 60 s with 20 % energy amplitude (16 W) using different NaCl fractions, ϕ_{NaCl}: 0.025 %, 0.05 %, 0.1 %, and 0.15 % (Set 3, Table 4.1). Figure 4.3A shows a slight increase in the size of the inner droplets when the salt fraction is increased, however the minimal size is obtained using $\phi_{\text{NaCl}} = 0.05$ %. The presence of ions is known to have an effect on the adsorption of surfactant or its spreading on the interface, thus increasing the interfacial tension. This leads to a lower breakage rate, and so to the formation of bigger droplets. Kent and Saunders (2001) similarly indicated that the presence of salt generated higher interfacial tension that was justified by a possible delay in the absorption of surfactant at the oil-water interface [72].

Double emulsions were then sonicated with an energy amplitude of 20 % for 10 s (11 W). The part of equations 4.8 and 4.9 that accounts for the effect of salt fraction is described by $\left(\sigma_M + K_2\phi_\mu C_{\text{salt}}RTd\right)$ or $\left(\sigma_M + C_2\phi_\mu C_{\text{salt}}RTd\right)^{2/3}$ respectively. Accordingly, an increase in the outer droplet size is expected when increasing the salt fraction.

Figure 4.3B,C indicates an increase in the outer droplet size and Figure 4.3D shows a higher encapsulation efficiency, when increasing the salt in the internal phase. The observed lower breakage rate when increasing the salt concentration is a consequence of the increased effective interfacial tension term that includes the osmotic pressure. It can be seen that the model allows describing accurately this phenomena. Indeed, using eq 4.7, $\sigma_{M,\text{eff}}$ is found to be equal to 0.008, 0.009, 0.013, and 0.02 N.m^{-1} for ϕ_{NaCl} 0.025, 0.05, 0.1, and 0.15 %, respectively, while the measured σ_M is 0.007 N.m^{-1}.

Note that while the two models predict similar mean diameters over the investigated range of salt fractions (up to $\phi_{\text{NaCl}} = 0.15$ %), when extrapolating to higher salt fractions the models deviate from each other (Figure 4.3C). Usually the salt fraction is never so high, but if required,

this region should be investigated experimentally to check which model would be more appropriate in regions with extremely high salt fractions.
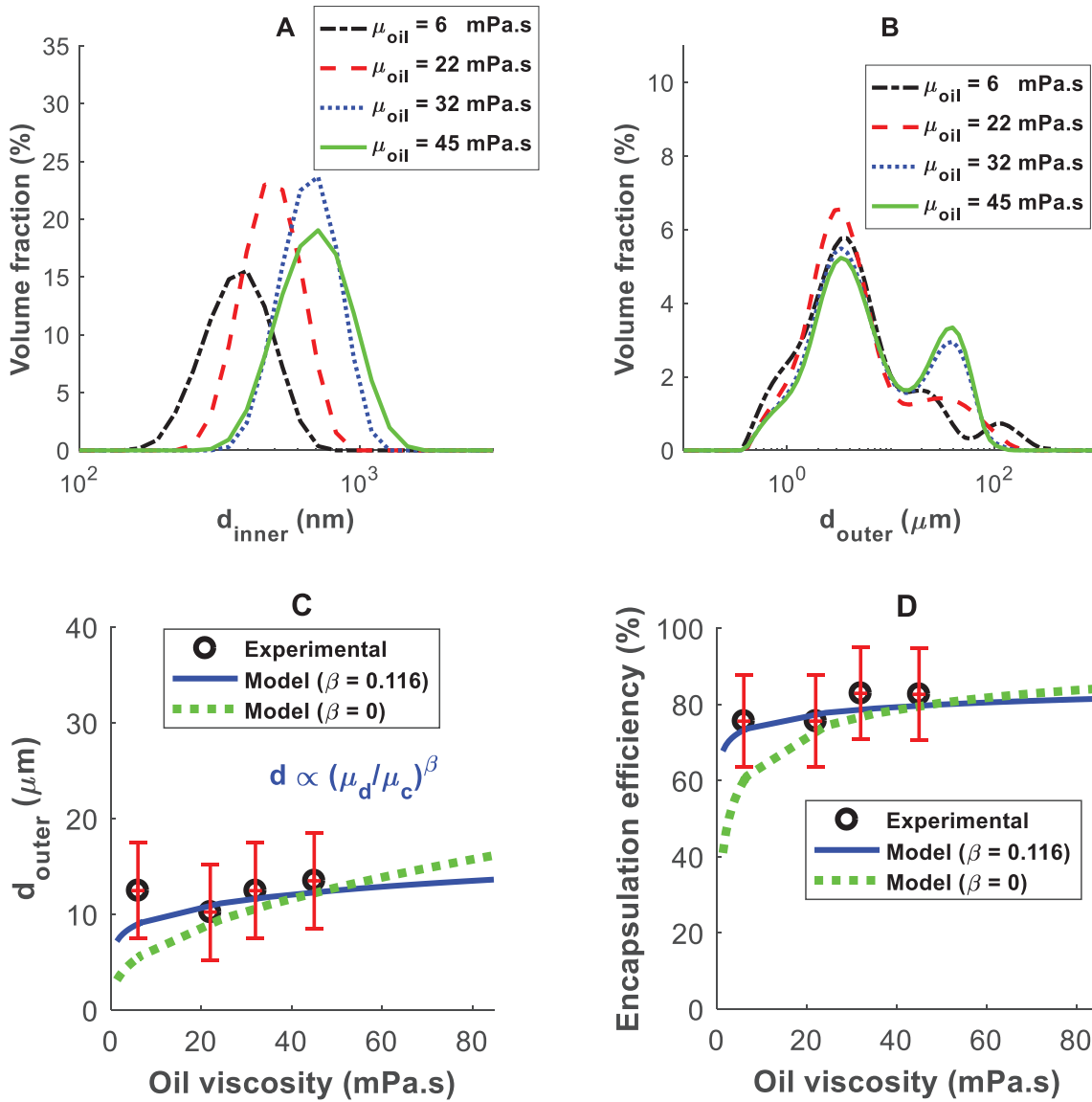

Figure 4.3. *Effect of the NaCl fraction. (A) Size distribution of inner droplets, (B) size distribution of outer droplets, (C) mean size of outer droplets, and (D) encapsulation efficiency. The model curve is based on eqs 4.8 and 4.9 for the droplet diameter and eqs 4.10–4.11 for the yield.*

4.4.4. Effect Of Primary Emulsion Fraction

A primary emulsion was prepared as previously, with 60 s of sonication and 20 % energy amplitude (16 W). The size distribution of the inner droplets is presented in Figure 4.4A. Then, the double emulsions were sonicated with an energy amplitude 20 % (11 W) during 10 s using different fractions of the primary emulsion, ϕ_M: 10, 20, 30, and 40 %.

The terms accounting for the fraction of the dispersed phase in the droplet correction are given by $(1 + 2.5\phi_M)^{3/2}$ and $(1 + 2.5\phi_M)^{5/4}$ for eqs 4.8 and 4.9, respectively. This term indicates a damping effect, where increasing ϕ_M lowers the energy dissipation rate and thus hinders the breakage of outer droplet. Part B and C of Figure 4.4 show respectively the size distribution of the outer droplets and their mean diameters as a function of the fraction of the primary emulsion. A general increase in the outer droplet size can be observed when

increasing ϕ_M. This can be due to a decreased breakage rate (due to the energy dissipation damping) or to an enhanced coalescence rate (due to the higher collision frequency when increasing the dispersed phase fraction). However, Figure 4.4D indicates that the encapsulation efficiency increases slightly with ϕ_M, as observed by Leong et al. [3].
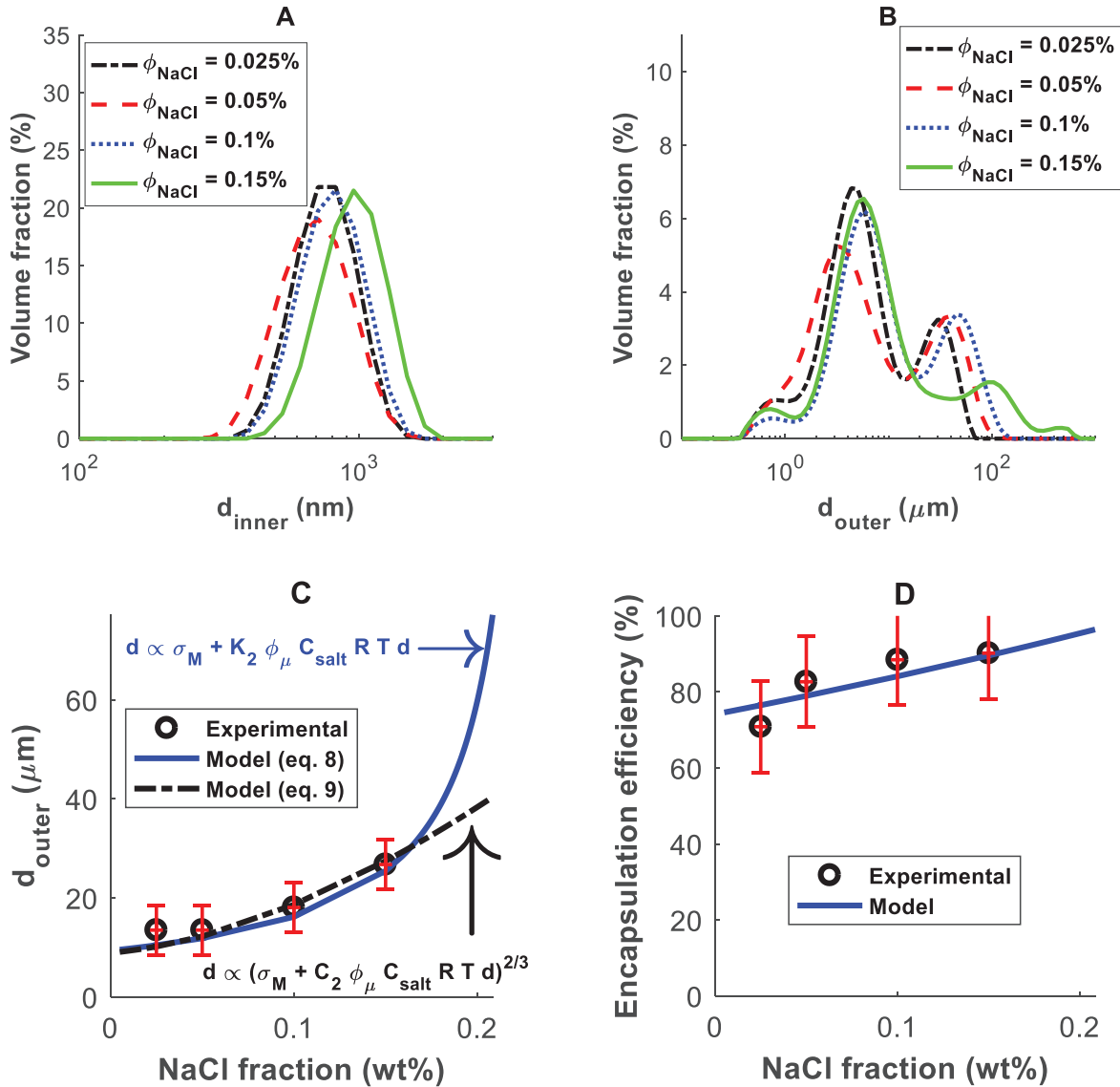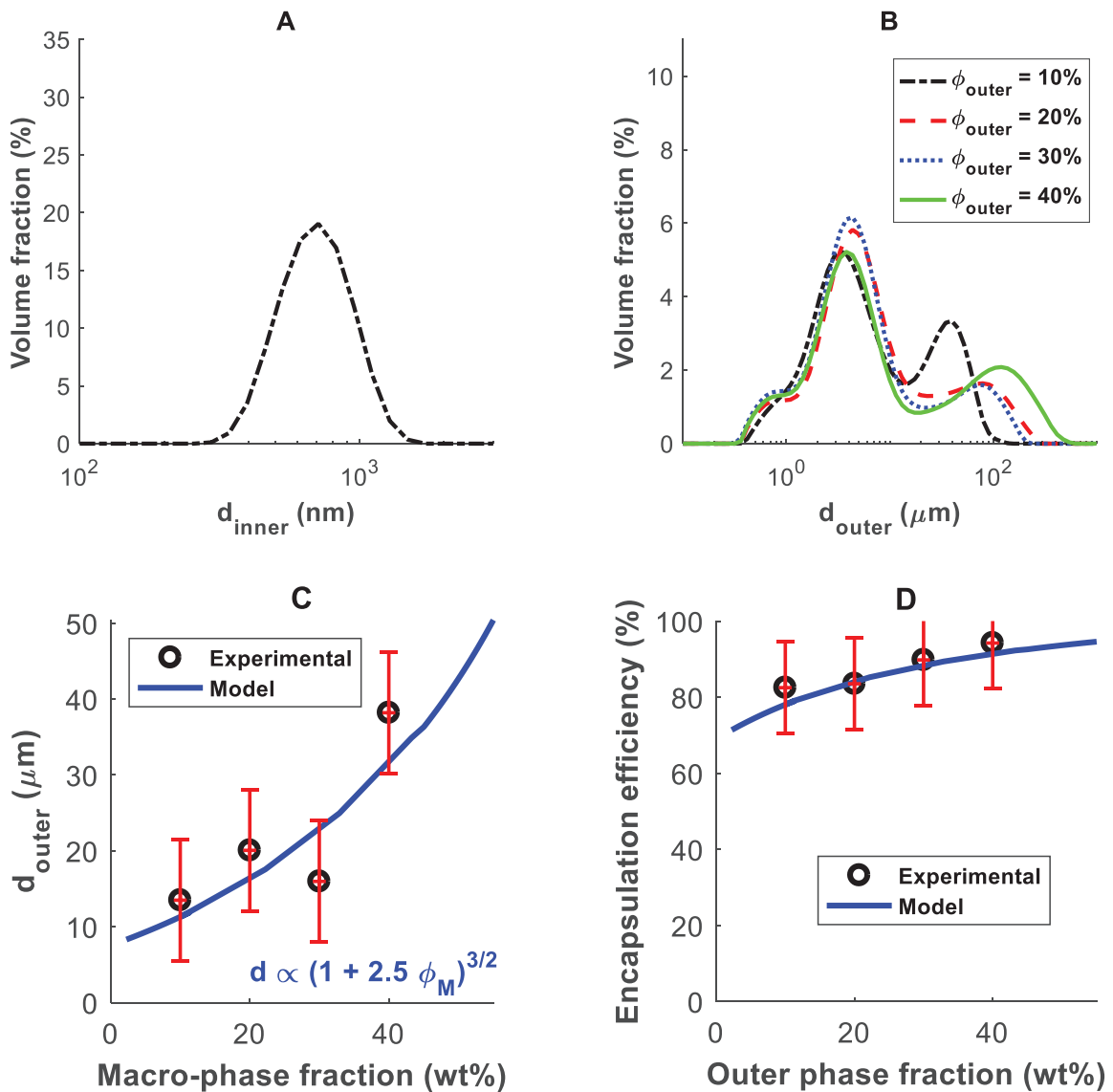

Figure 4.4. *Effect of the primary emulsion fraction. (A) size distribution of inner droplets, (B) size distribution of outer droplets, (C) mean size of outer droplets, and (D) encapsulation efficiency. The model is based on eq 4.8 for the droplet diameter and eqs 4.10–4.11 for the yield.*

From these combined observations, it can be concluded that when increasing the fraction of the primary emulsion, the effective energy imposing on the surface of the outer droplets is damped, leading to a decrease in the breakage and so leakage. Indeed, outer droplet coalescence would not have a direct effect on the encapsulation efficiency and cannot explain both observations. As the model takes into account the damping effect for dissipation subrange, by an analogical derivation of the method of Doulah [46], it shows a good agreement with the experimental data. Leong et al. [3] did not observe an effect of ϕ_M (varied up to 20 %) on the outer droplet size, except when employing extremely low calorimetric

power of 2 W or extremely high power of 26 W, where an increase in the outer droplet size was increased with ϕ_M.

4.5. Conclusions

The droplet size and encapsulation efficiency are key parameters of the final product properties of double emulsions. The effect of the process variables on these parameters were investigated experimentally and by modelling. Two correlations for the outer droplet mean diameter were proposed based on fundamental developments for the dissipation energy subrange and accounting for different properties, including the interfacial tension, the viscosities and densities of both phases, the fraction of salt and the sonication time and energy. A correlation is also proposed to estimate the leakage rate.

- Increasing the second step sonication time was found to create smaller outer droplets and consequently higher leakage, until reaching the equilibrium size. At equilibrium, the breakage rate is equal to the coalescence rate, and therefore the size does not evolve but the inner droplet leakage continues at a constant rate.
- Increasing the oil viscosity of W/O/W double emulsions was found to form bigger inner droplets (where water represents the dispersed phase) and bigger outer droplets (where the water-oil dispersion represents the dispersed phase) and to lower the leakage rate. This could be explained by the capillary critical, $\left(\frac{\mu_d}{\mu_c}\right)^{\beta}$, where β is negative for the inner droplets and positive for the outer droplets.
- Increasing the salt fraction was found to hinder the breakage, and leakage, and thus to form bigger outer droplets. This phenomenon is driven by the osmotic pressure that adds a force to the droplets interface.
- Increasing the fraction of the primary emulsion was found to dampen the effective energy dissipation rate and thus to form bigger outer droplets and less leakage.

As a perspective, there is still a need to account for the inner droplet size and fraction in the breakage rate, for instance through the outer droplet viscosity and cohesion forces. It would be interesting to implement a PBM to predict the the droplet size distribution with time.

References

[1] A. Schuch, J. Wrenger, H.P. Schuchmann, Production of W/O/W double emulsions. Part II: Influence of emulsification device on release of water by coalescence, Colloids Surf. Physicochem. Eng. Asp. 461 (2014) 344–351. doi:10.1016/j.colsurfa.2013.11.044.

[2] K. Lindenstruth, B.W. Müller, W/O/W multiple emulsions with diclofenac sodium, Eur. J. Pharm. Biopharm. 58 (2004) 621–627. doi:10.1016/j.ejpb.2004.04.003.

[3] T.S.H. Leong, M. Zhou, N. Kukan, M. Ashokkumar, G.J.O. Martin, Preparation of water-in-oil-in-water emulsions by low frequency ultrasound using skim milk and sunflower oil, Food Hydrocoll. 63 (2017) 685–695. doi:10.1016/j.foodhyd.2016.10.017.

[4] T.S.H. Leong, G.J.O. Martin, M. Ashokkumar, Ultrasonic encapsulation – A review, Ultrason. Sonochem. 35 (2017) 605–614. doi:10.1016/j.ultsonch.2016.03.017.

[5] H. Lamba, K. Sathish, L. Sabikhi, Double Emulsions: Emerging Delivery System for Plant Bioactives, Food Bioprocess Technol. 8 (2015) 709–728. doi:10.1007/s11947-014-1468-6.

[6] T.S.H. Leong, T.J. Wooster, S.E. Kentish, M. Ashokkumar, Minimising oil droplet size using ultrasonic emulsification, Ultrason. Sonochem. 16 (2009) 721–727. doi:10.1016/j.ultsonch.2009.02.008.

[7] T.S.H. Leong, S. Manickam, G.J.O. Martin, W. Li, M. Ashokkumar, Ultrasonic Production of Nano-emulsions for Bioactive Delivery in Drug and Food Applications, Springer International Publishing, Cham, 2018. doi:10.1007/978-3-319-73491-0.

[8] S. Mahdi Jafari, Y. He, B. Bhandari, Nano-Emulsion Production by Sonication and Microfluidization—A Comparison, Int. J. Food Prop. 9 (2006) 475–485. doi:10.1080/10942910600596464.

[9] M.K. Li, H.S. Fogler, Acoustic emulsification. Part 1. The instability of the oil-water interface to form the initial droplets, J. Fluid Mech. 88 (1978) 499. doi:10.1017/S0022112078002232.

[10] M.K. Li, H.S. Fogler, Acoustic emulsification. Part 2. Breakup of the large primary oil droplets in a water medium, J. Fluid Mech. 88 (1978) 513. doi:10.1017/S0022112078002244.

[11] A. Shanmugam, M. Ashokkumar, Ultrasonic Preparation of Food Emulsions, in: M. Villamiel, A. Montilla, J.V. García-Pérez, J.A. Cárcel, J. Benedito (Eds.), Ultrasound Food Process., John Wiley & Sons, Ltd, Chichester, UK, 2017: pp. 287–310. doi:10.1002/9781118964156.ch10.

[12] T. Leong, M. Ashokkumar, S. Kentish, The fundamentals of power ultrasound-A review, (2011).

[13] E. Tornberg, A.-M. Hermansson, FUNCTIONAL CHARACTERIZATION OF PROTEIN STABILIZED EMULSIONS: EFFECT OF PROCESSING, J. Food Sci. 42 (1977) 468–472. doi:10.1111/j.1365-2621.1977.tb01524.x.

[14] S. Kentish, T.J. Wooster, M. Ashokkumar, S. Balachandran, R. Mawson, L. Simons, The use of ultrasonics for nanoemulsion preparation, Innov. Food Sci. Emerg. Technol. 9 (2008) 170–175. doi:10.1016/j.ifset.2007.07.005.

[15] S.G. Gaikwad, A.B. Pandit, Ultrasound emulsification: Effect of ultrasonic and physicochemical properties on dispersed phase volume and droplet size, Ultrason. Sonochem. 15 (2008) 554–563. doi:10.1016/j.ultsonch.2007.06.011.

[16] J.R. Rajian, M.L. Fabiilli, J.B. Fowlkes, P.L. Carson, X. Wang, Drug delivery monitoring by photoacoustic tomography with an ICG encapsulated double emulsion, Opt. Express. 19 (2011) 14335. doi:10.1364/OE.19.014335.

[17] C.-K. Kim, S.-C. Kim, H.-J. Shin, K.M. Kim, K.-H. Oh, Y.-B. Lee, I.-J. Oh, Preparation and characterization of cytarabine-loaded w/o/w multiple emulsions, Int. J. Pharm. 124 (1995) 61–67. doi:10.1016/0378-5173(95)00074-S.

[18] N.P. Aditya, S. Aditya, H. Yang, H.W. Kim, S.O. Park, S. Ko, Co-delivery of hydrophobic curcumin and hydrophilic catechin by a water-in-oil-in-water double emulsion, Food Chem. 173 (2015) 7–13. doi:10.1016/j.foodchem.2014.09.131.

[19] L. Zeng, Y. Zhang, C. Bukirwa, W. Li, Y. Yang, Study of mean diameter and drop size distribution of emulsion drops in a modified rotating disc contactor for an emulsion liquid membrane system, RSC Adv. 5 (2015) 89959–89970. doi:10.1039/C5RA16267J.

[20] S.S. Davis, A.S. Burbage, The Particle Size Analysis of Multiple Emulsions (Water-in-Oil-in-Water), in: Part. Size Anal., Heyden & Son, University of Salford, 1977: p. 395.

[21] S.Y. Tang, M. Sivakumar, Design and evaluation of aspirin-loaded water-in-oil-in-water submicron multiple emulsions generated using two-stage ultrasonic cavitational emulsification technique: SUBMICRON W/O/W MULTIPLE EMULSIONS OF ASPIRIN BY ULTRASONIC CAVITATION, Asia-Pac. J. Chem. Eng. 7 (2012) S145–S156. doi:10.1002/apj.664.

[22] S.Y. Tang, M. Sivakumar, B. Nashiru, Impact of osmotic pressure and gelling in the generation of highly stable single core water-in-oil-in-water (W/O/W) nano multiple emulsions of aspirin assisted by two-stage ultrasonic cavitational emulsification, Colloids Surf. B Biointerfaces. 102 (2013) 653–658. doi:10.1016/j.colsurfb.2012.08.036.

[23] B. Tal-Figiel, The Formation of Stable W/O, O/W, W/O/W Cosmetic Emulsions in an Ultrasonic Field, Chem. Eng. Res. Des. 85 (2007) 730–734. doi:10.1205/cherd06199.

[24] H. Ghasemi, H. Mazloomi, H. Hajipour, Stabilization of multiple emulsions using natural surfactants, ArXiv170508296 Cond-Mat. (2017). http://arxiv.org/abs/1705.08296 (accessed December 18, 2018).

[25] T.S.H. Leong, M. Zhou, D. Zhou, M. Ashokkumar, G.J.O. Martin, The formation of double emulsions in skim milk using minimal food-grade emulsifiers – A comparison between ultrasonic and high pressure homogenisation efficiencies, J. Food Eng. 219 (2018) 81–92. doi:10.1016/j.jfoodeng.2017.09.018.

[26] S. Okazaki, M. Imai, M. Shimizu, Leakage Suppressing Oe W/O Emulsion Using High Viscous Solvent, in: Process Metall., Elsevier, 1992: pp. 1487–1492. doi:10.1016/B978-0-444-88677-4.50064-7.

[27] J.O. Hinze, Fundamentals of the hydrodynamic mechanism of splitting in dispersion processes, AIChE J. 1 (1955) 289–295. doi:10.1002/aic.690010303.

[28] H.C. Brinkman, Brownian motion in a field of force and the diffusion theory of chemical reactions, Physica. 22 (1956) 29–34. doi:10.1016/S0031-8914(56)80006-2.

[29] Y. Mlynek, W. Resnick, Drop sizes in an agitated liquid-liquid system, AIChE J. 18 (1972) 122–127. doi:10.1002/aic.690180122.

[30] C.A. Coulaloglou, L.L. Tavlarides, Drop size distributions and coalescence frequencies of liquid-liquid dispersions in flow vessels, AIChE J. 22 (1976) 289–297. doi:10.1002/aic.690220211.

[31] T. Kataoka, T. Nishiki, Dispersed mean drop sizes of (W/O)/W emulsions in a stirred tank., J. Chem. Eng. Jpn. 19 (1986) 408–412. doi:10.1252/jcej.19.408.

[32] T. Ohtake, T. Hano, K. Takagi, F. Nakashio, Effects of viscosity on drop diameter of W/O emulsion dispersed in a stirred tank., J. Chem. Eng. Jpn. 20 (1987) 443–447. doi:10.1252/jcej.20.443.

[33] R. Rautenbach, O. Machhammer, Modeling of liquid membrane separation processes, J. Membr. Sci. 36 (1988) 425–444. doi:10.1016/0376-7388(88)80034-6.

[34] T. Gallego-Lizon, E.S. Pérez de Ortiz, Drop Sizes in Liquid Membrane Dispersions, Ind. Eng. Chem. Res. 39 (2000) 5020–5028. doi:10.1021/ie000016y.

[35] H. Karbstein, H. Schubert, Developments in the continuous mechanical production of oil-in-water macro-emulsions, Chem. Eng. Process. Process Intensif. 34 (1995) 205–211. doi:10.1016/0255-2701(94)04005-2.

[36] J. O'Sullivan, B. Murray, C. Flynn, I. Norton, Comparison of batch and continuous ultrasonic emulsification processes, J. Food Eng. 167 (2015) 114–121. doi:10.1016/j.jfoodeng.2015.05.001.

[37] E. Nazarzadeh, S. Sajjadi, Viscosity effects in miniemulsification via ultrasound, AIChE J. 56 (2010) 2751–2755. doi:10.1002/aic.12133.

[38] A. Gupta, H.B. Eral, T.A. Hatton, P.S. Doyle, Controlling and predicting droplet size of nanoemulsions: scaling relations with experimental validation, Soft Matter. 12 (2016) 1452–1458. doi:10.1039/C5SM02051D.

[39] T. Kimura, T. Sakamoto, J.-M. Leveque, H. Sohmiya, M. Fujita, S. Ikeda, T. Ando, Standardization of ultrasonic power for sonochemical reaction, Ultrason. Sonochem. 3 (1996) S157–S161.

[40] T. Schmidts, D. Dobler, C. Nissing, F. Runkel, Influence of hydrophilic surfactants on the properties of multiple W/O/W emulsions, J. Colloid Interface Sci. 338 (2009) 184–192. doi:10.1016/j.jcis.2009.06.033.

[41] T. Schmidts, D. Dobler, A.-C. Guldan, N. Paulus, F. Runkel, Multiple W/O/W emulsions—Using the required HLB for emulsifier evaluation, Colloids Surf. Physicochem. Eng. Asp. 372 (2010) 48–54. doi:10.1016/j.colsurfa.2010.09.025.

[42] S. Zhao, Z. Dong, C. Yao, Z. Wen, G. Chen, Q. Yuan, Liquid-liquid two-phase flow in ultrasonic microreactors: Cavitation, emulsification, and mass transfer enhancement, AIChE J. 64 (2018) 1412–1423. doi:10.1002/aic.16010.

[43] A.N. Kolmogorov, The local structure of turbulence in incompressible viscous fluid for very large Reynolds numbers, in: Dokl Akad Nauk SSSR, 1941: pp. 299–303.

[44] R.O. Fox, Computational Models for Turbulent Reacting Flows, Cambridge University Press, Cambridge, 2003. doi:10.1017/CBO9780511610103.

[45] Andrey Kolmogorov, On the breakage of drops in a turbulent flow, Dokl Akad Navk SSSR. 66 (1949).

[46] M.S. Doulah, An Effect of Hold-up on Drop Sizes in Liquid-Liquid Dispersions, Ind. Eng. Chem. Fundam. 14 (1975) 137–138. doi:10.1021/i160054a015.

[47] DR. BROWN, K. Pitt, Drop break-up in a stirred liquid-liquid contactor, BRITISH CHEMICAL ENGINEERING. 16 (1971) 525.

[48] P.H. CALDERBANK, Physical Rate Processes in Industrial Fermentations Part I : The Interfacial Area in Gas-Liquid Contacting with Mechanical Agitation, Trans Inst Chem Engrs. 36 (1958) 443–463.

[49] J.T. Davies, Drop sizes of emulsions related to turbulent energy dissipation rates, Chem. Eng. Sci. 40 (1985) 839–842. doi:10.1016/0009-2509(85)85036-3.

[50] S. J. Chen, D. R. Libby, Gas-liquid and liquid-liquid dispersions in a Kenics mixer, in: 1978.

[51] G.I. Taylor, The Viscosity of a Fluid Containing Small Drops of Another Fluid, Proc. R. Soc. Math. Phys. Eng. Sci. 138 (1932) 41–48. doi:10.1098/rspa.1932.0169.

[52] G.I. Taylor, The Formation of Emulsions in Definable Fields of Flow, Proc. R. Soc. Math. Phys. Eng. Sci. 146 (1934) 501–523. doi:10.1098/rspa.1934.0169.

[53] R. Shinnar, On the behaviour of liquid dispersions in mixing vessels, J. Fluid Mech. 10 (1961) 259. doi:10.1017/S0022112061000214.

[54] S.B. Pope, Turbulent Flows, Cambridge University Press, Cambridge, 2000. doi:10.1017/CBO9780511840531.

[55] M. Karimi, R. Andersson, An exploratory study on fluid particles breakup rate models for the entire spectrum of turbulent energy, Chem. Eng. Sci. 192 (2018) 850–863. doi:10.1016/j.ces.2018.08.016.

[56] A. Sharma, A.N. Goswami, B.S. Rawat, Drop size prediction in liquid membrane systems, J. Membr. Sci. 60 (1991) 261–274. doi:10.1016/S0376-7388(00)81539-2.

[57] J.M.H. Janssen, H.E.H. Meijer, Droplet breakup mechanisms: Stepwise equilibrium versus transient dispersion, J. Rheol. 37 (1993) 597–608. doi:10.1122/1.550385.

[58] G.I. Taylor, Conical free surfaces and fluid interfaces, in: H. Görtler (Ed.), Appl. Mech., Springer Berlin Heidelberg, Berlin, Heidelberg, 1966: pp. 790–796. doi:10.1007/978-3-662-29364-5_104.

[59] E.J. Hinch, A. Acrivos, Long slender drops in a simple shear flow, J. Fluid Mech. 98 (1980) 305. doi:10.1017/S0022112080000171.

[60] J.M. Rallison, A numerical study of the deformation and burst of a viscous drop in general shear flows, J. Fluid Mech. 109 (1981) 465. doi:10.1017/S002211208100116X.

[61] B.J. Bentley, L.G. Leal, An experimental investigation of drop deformation and breakup in steady, two-dimensional linear flows, J. Fluid Mech. 167 (1986) 241. doi:10.1017/S0022112086002811.

[62] B. Koglin, J. Pawlowski, H. Schnöring, Kontinuierliches Emulgieren mit Rotor/Stator-Maschinen: Einfluß der volumenbezogenen Dispergierleistung und der Verweilzeit auf die Emulsionsfeinheit: Kontinuierliches Emulgieren mit Rotor/Stator-Maschinen: Einfluß der volumenbezogenen Dispergierleistung und der Verweilzeit auf die Emulsionsfeinheit, Chem. Ing. Tech. 53 (1981) 641–647. doi:10.1002/cite.330530813.

[63] Theodore Vermeulen, Interfacial area in liquid-liquid and gas-liquid agitation, Chem. Eng. Progr. 51 (1955) 85F-94F.

[64] S.A. Miller, C.A. Mann, Agitation of Two-Phase Systems of Immiscible Liquids, Trans. Am. Inst. Chem. Engrs. (1944) 709–743.

[65] F. Michaut, P. Perrin, P. Hébraud, Interface Composition of Multiple Emulsions: Rheology as a Probe, Langmuir. 20 (2004) 8576–8581. doi:10.1021/la048715t.

[66] A. Aserin, ed., Multiple emulsions: technology and applications, Wiley-Interscience, Hoboken, N.J, 2008.

[67] K.S. Spiegler, O. Kedem, Thermodynamics of hyperfiltration (reverse osmosis): criteria for efficient membranes, Desalination. 1 (1966) 311–326. doi:10.1016/S0011-9164(00)80018-1.

[68] M.V. Voinova, The theory of membrane "vitrification," Thermochim. Acta. 280–281 (1996) 465–477. doi:10.1016/0040-6031(95)02657-6.

[69] F.B. Sprow, Distribution of drop sizes produced in turbulent liquid—liquid dispersion, Chem. Eng. Sci. 22 (1967) 435–442. doi:10.1016/0009-2509(67)80130-1.

[70] G.A. Farzi, N. Rezazadeh, A.P. Nejad, Droplet Formation Study in Emulsification Process by KSM using a Novel In Situ Visualization System, J. Dispers. Sci. Technol. 37 (2016) 575–581. doi:10.1080/01932691.2015.1052144.

[71] I. Stanciu, A new viscosity-temperature relationship for mineral oil SAE 10W, Analele Univ. Ovidius Constanta - Ser. Chim. 23 (2012) 27–30. doi:10.2478/v10310-012-0003-8.

[72] P. Kent, B.R. Saunders, The Role of Added Electrolyte in the Stabilization of Inverse Emulsions, J. Colloid Interface Sci. 242 (2001) 437–442. doi:10.1006/jcis.2001.7792.

Chapter 5. Modeling droplets swelling and escape in double emulsions using population balance equations

Monitoring the physical stability of double emulsions is considered in this chapter. A coupled population balance equation model for the inner and outer droplets is developed. The model involves a sub-model of swelling of the inner, and so of the outer, droplets and a sub-model describing the escape of the inner droplets. The swelling phenomena is governed by the osmotic and Laplace pressure gradients while the inner droplets' escape rate is governed by balance of the surface and viscous forces of the droplets. Experimental investigations demonstrated the usefulness of the model and its capability to describe the evolution of the inner and outer droplets' size distributions and the release rate during storage of the double emulsions.
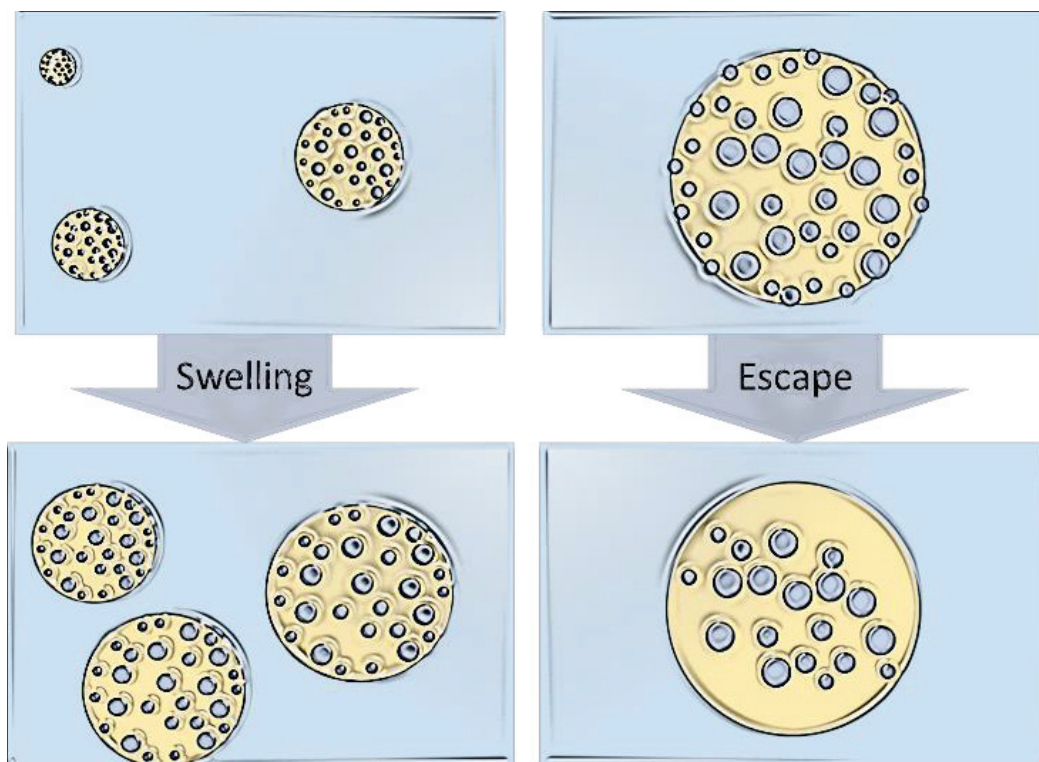
5.1. Introduction

During storage, the phenomena that may take place are inner or outer droplets coalescence, Ostwald ripening leading to droplets growth, shrinkage or swelling of the inner droplets and thus of the outer droplets [1–6] and the release of the encapsulated substance [6–12]. Concerning the release, on one hand, it may occur at the inner droplet level, also called escape. This phenomena is described by the coalescence of inner droplets with the external continuous phase through the surface of the outer droplets. The release may on the other hand take place at a molecular level by diffusion of the encapsulated substance until reaching the external phase, without causing film rupture. Concerning the shrinkage or the swelling phenomena, they take place due to the osmotic gradient. The swelling phenomena may ultimately lead to swelling-breakdown, i.e. the expulsion of the inner droplets out of the outer droplet [6]. This phenomenon takes place either gradually, or more abruptly leading to the disintegration of the outer droplet [13], herein called "over-swelling breakdown". In this chapter, both the swelling and escape phenomena (i.e., the release by coalescence) will be investigated experimentally and theoretically, until the onset of the over-swelling breakdown phenomena.

The first phenomenon of interest is the escape of inner droplets as a consequence of the coalescence of the inner droplet with the external continuous phase, i.e., by drainage of the film between the inner droplet and the boundary of the outer droplet. Different approaches were proposed in the literature to model this phenomenon and will be investigated in detail in the modelling section. For instance, Pays et al. (2001) [14] assumed the escape rate to be proportional to the number of adsorbed inner droplets on the surface of the outer droplets times a coalescence frequency. They proposed an adsorption isotherm to predict the number of adsorbed inner droplets based on Fowler and Guggenheim model (1939) [15], while the escape frequency was determined by fitting to experimental data. Klahn et al. (2002) considered the escape rate to be proportional to the escape frequency times the escape probability and a critical region concerned by the escape phenomenon [16]. The escape frequency was determined from the circulation time on streamlines formed within an outer droplet present in a simple shear flow, the escape probability was obtained from the film drainage theory, while the fraction of the critical region was obtained by fitting to experimental data. Chávez-Páez et al. (2012) [7] conducted 3D simulations to describe the inner droplets Brownian motion and to estimate their collision frequency with the surface of outer droplet. The escape rate was then considered to be proportional to the collision frequency times a coalescence probability to be determined elsewhere. Kang et al. (2016) [17] considered that the droplets' movement can be approximated by a Stokes flow. Based on this, they developed a model to calculate the dewetting time in double emulsions, or equivalently the escape time, based on momentum and energy conservation.

The second phenomena of interest is droplets' swelling. One of the earliest researches regarding the swelling phenomena in W/O/W double emulsions was performed by Matsumoto et al. [5,18–20]. By handling experiments in an optical microscope, the authors measured the swelling rate of W/O/W double emulsions and stated that it was not affected by the fraction of the inner droplets (ϕ_μ) (see Table 5.1). Their viscosity measurements of the

double emulsions showed an increase with the osmotic pressure in the internal phase (which is controlled by the fraction of ions ϕ_{ions}) until a point above which it decreased. They calculated the permeability of different hydrocarbon oils using the membrane permeability model [19,21], but without including the effect of Laplace pressure (for inner droplets of 1-2 µm). They suggested that the physical state of the oil layer, its rheology, and so the permeation coefficient, is altered by the presence of ions [20]. Garti et al. (1985) [22] applied the same methodology to double emulsions undergoing shrinkage and estimated an increase in the permeability coefficient when increasing the fraction of the internal emulsifier ($\phi_{\text{emulsifier}}^{\text{in}}$) that was explained by possible micellar transport. The same phenomenon was observed by Yan and Pal (2001) [23] but they explained it by the diffusion of hydrated surfactant that facilitates transport. They also observed a slight decrease in the permeability when increasing the internal aqueous phase fraction (ϕ_μ) that was explained by a reduced free space for swelling. Jager-Lezer (1997) found that increasing the lipophilic surfactant fraction ($\phi_{\text{emulsifier}}^{\text{in}}$) increased the swelling capacity and delayed the release. They indicated that increasing the amount of lipophilic emulsifier enhances the stability of the double emulsions while an excess would destabilize the emulsion [6]. These papers thus highlight opposing effects of the internal emulsifier on the swelling and release that are the increased viscosity (reducing permeability) and the diffusion of hydrated surfactant or potential micellar transport (increasing permeability). Similarly, a complex effect of the presence of ions on the rheology of the oil layer and the physical state of the surfactants is revealed. Besides the swelling capacity and permeation, a latent period was also underlined in the literature. In a single drop-in-drop emulsion Bahtz et al. (2015) [24] investigated the initial stage of swelling and distinguished a lag period during which water migration was very slow. This lag period was found to be independent of the osmotic gradient over the range of 2.7–13.3 bar, and it was shorter for less viscous oil phases. For instance a lag period of ~10 min was found for an oil viscosity of 40 mPa.s. Jager-Lezer (1997) explained the latent period by the production of small inner droplets for which the Laplace counter pressure was higher, thus delaying the aqueous flow driven by the osmotic pressure [6]. Table 5.1 summarizes the effects of the different parameters on the swelling rate and permeability.

From the literature review it appears that swelling is mainly studied as the direct effect of osmotic pressure gradient while the Laplace pressure was neglected, which can be justified only if the inner droplets are big. Consequently, the combined effect of the osmotic and Laplace pressure gradients needs to be considered if smaller droplets are produced. Moreover, modeling both the swelling and the escape phenomena during storage were done by considering a mean inner and outer droplets size. However, in practice, double emulsions are polydisperse and using the mean diameter may fail to give the full understanding of the system. In order to allow for a thorough understanding of the double emulsion stability, it is required to consider the full droplet size distribution of both the inner and outer droplets by incorporating the individual models of the swelling and escape phenomena into population balance models (PBM) of both phases. In a previous work, we proposed a population balance model for the preparation step of double emulsions involving breakage, coalescence and leakage (using one PBM for the outer droplets) [25], and in the present work we will be

interested in the storage period, involving swelling and escape, where coupled inner and outer droplets PBMs are required.

Table 5.1. Effect of some process parameters on the swelling rate, permeability and lag time

	Effect on swelling / shrinkage rate	Effect on L_p	Effect on lag time	Reference
$\uparrow \phi_\mu$	-	No effect	-	Matsumoto et al. [19]
	$\downarrow$	$\downarrow$	-	Yan and Pal [23]
	No effect	-	$\downarrow$	Bahtz et al. (2015) [24]
$\uparrow \phi_{ions}$	$\uparrow$	~No effect	No effect	Bahtz et al. (2015) [24]
(or $\uparrow \Delta\Pi$)	$\uparrow$	$\downarrow$	-	Matsumoto & Kohda [25]
$\uparrow \phi_{emulsifier}^{in}$	-	$\downarrow$	-	Matsumoto et al.[14, [19]
	-	$\uparrow$	-	Yan & Pal [23]
				Garti et al. (1985) [22]
	$\uparrow$	-	$\uparrow$	Jager-Lezer (1997) [6]
$\uparrow$ Oil viscosity	$\downarrow$	-	$\uparrow$	Bahtz et al. (2015) [24]
	$\downarrow$	$\downarrow$	-	Matsumoto et al. [26]
$\uparrow$ Temperature	$\uparrow$	No effect	$\downarrow$	Bahtz et al. (2015) [24]

The objective of this study is therefore to develop a coupled PBM for the inner and outer droplet size distributions (DSD) of W/O/W double emulsions undergoing escape and swelling during storage. The escape and swelling models are developed respectively based on the dewetting model of Kang et al. (2016) [17] and the permeability model of membranes including the Laplace pressure. The release rate is monitored using conductivity and the evolution of the outer DSD using laser diffraction. The DSD of inner droplets is measured right after the first step of preparation using dynamic light scattering. A number of key operating parameters are varied: the internal water fraction, the stirring rate in the second preparation step, the salt fraction, and the fraction of the primary emulsion.

5.2. Experimental

The constituents used for double emulsion preparation are mineral oil (Fisher Scientific™), Span 80 (Alfa Aesar) as hydrophobic internal emulsifier, Tween 80 (Fisher Scientific™) as hydrophilic external emulsifier, sodium chloride as tracer and Millipore water (resistivity $\approx$ 18.2 $m\,\Omega.cm$).

Double emulsions were prepared in two steps. Table 5.2 shows the fractions used in the different experiments. In the first step, the NaCl solution was dispersed in the oil phase (composed of mineral oil and Span 80, at 0.314 mol L^{-1}) to produce the primary W/O emulsion using an IKA T 25 digital ULTRA-TURRAX® at 12 000 rpm for 4 min. In the second step, the primary emulsion was dispersed in an external aqueous phase (composed of water and Tween 80, at 0.0078 mol L^{-1})) to produce the W/O/W double emulsion. The second step was done in

a 1-L stirred tank, equipped with four baffles, and stirring was done at 300-500 rpm for 70 min using a three-bladed stainless-steel impeller.

Right after the preparation of the primary emulsion, the DSD of the inner droplets was measured by using dynamic light scattering (Malvern Zetasizer Nano ZS®). The outer droplets DSD was measured after the second step of preparation as well as during storage by means of Laser diffraction (Mastersizer 3000®).

Table 5.2. Experimental conditions

	First preparation step						Second preparation step					Right after preparation
	Operating parameters		Fractions (wt. %)				Operating parameters		Fractions (wt. %)			Encapsulation efficiency (%)
	t_1^* (min)	ω_{R1}^{**} (rpm)	Water	Mineral oil	NaCl	$Span_{80}$	t_2^* (min)	ω_{R2}^* (rpm)	Primary	Water	$Tween_{80}$	
Set 1 ϕ_M	4	12000	40	50	0.05	9.95	70	400	1 2 3 4	98 97 96 95	1	92.5 94.7 95.44 95.5
Set 2 ϕ_{NaCl}	4	12000	40	50	0.05 0.14 0.19 0.24	9.95	70	400	1	98	1	92.5 96.1 96.4 96.4
Set 3 ϕ_μ	4	12000	10 20 30 40	80 70 60 50	0.05	9.95	70	400	1	98	1	51.2 67 82.2 92.5
Set 4 ω_R	4	12000	40	50	0.05	9.95	70	300 350 400 500	1	98	1	94.1 93.3 92.5 88.1

[*]t_1 and t_2 are the mixing times of the first and second step respectively.

[**]ω_{R1} and ω_{R2} are mixing rates of the first and second emulsions respectively.

The total mass in the second step is 1 kg.

A CDM210 Conductivity Meter (MeterLab®) was used to measure the conductivity of the samples, right after the second preparation step and during storage, in order to determine the released amount of encapsulated NaCl. A predetermined calibration curve was prepared either by dissolving different NaCl concentrations in O/W emulsion or in pure water. No effect

of the oil was observed on the calibration curve in the studied concentration range, thus both methods were found equivalent.

5.3. Modeling

During storage, the inner (i.e. the micro-) droplets may undergo coalescence and swelling/shrinkage, or may escape. In the considered system, the inner salt concentration is higher than the outer concentration, and therefore the inner droplets would rather swell than shrink. The outer (i.e. the macro-) droplets may also undergo coalescence and swelling (due to inner droplets' swelling) that may ultimately lead to breakdown due to over-swelling. Since double emulsions are dilute and a high amount of stabilizer is used, the rate of coalescence was found to be negligible during storage. The objective of this work is thus to model swelling and escape until the onset of overswelling-breakdown. These phenomena need to be implemented in population balance models for both the inner and outer droplets [26,27]. The two PBMs are coupled and should be solved simultaneously.

5.3.1. Coupled population balance models

The PBM representing the evolution of the number density function of the inner droplets, n_μ (m^{-3}, i.e. per inner droplet's size), undergoing only swelling and escape is:

$$\frac{\partial n_\mu(t,v_\mu)}{\partial t} + \frac{\partial\left(\mathbb{S}_\mu(t,v_\mu)n_\mu(t,v_\mu)\right)}{\partial v_\mu} = \mathfrak{R}_{es,\mu}\left(t,v_\mu\right) \qquad 5.1$$

The PBM representing the evolution of the number density function of the outer droplets, n_M (m^{-3}, i.e. per outer droplet's size) is:

$$\frac{\partial n_M(t,v_M)}{\partial t} + \frac{\partial\left(\left[\mathbb{S}_M(t,v_M)+Q_{es,M}(t,v_M)\right]n_M(t,v_M)\right)}{\partial v_M} = 0 \qquad 5.2$$

where v (m^3) is the droplets volume and the properties of the inner and outer droplets are indicated by the indices μ and M, respectively. The source term in eq. 1, $\mathfrak{R}_{es,\mu}$ (m^{-3} s^{-1}), is the escape rate of inner droplets, which causes a change in the outer droplets volume represented by $Q_{es,M}$ (m^3 s^{-1}). $\mathbb{S}_\mu$ (m^3 s^{-1}) is the volumetric swelling rate of the inner droplets that leads to swelling of the outer droplets, represented by $\mathbb{S}_M$ (m^3 s^{-1}). The second terms on the LHS of eqs. 5.1 and 5.2 represent the growth or shrinkage respectively of the inner and outer droplets. The growth (i.e. when $\mathbb{S}_\mu > 0$, $\mathbb{S}_M > 0$) or shrinkage (i.e. $\mathbb{S}_\mu < 0$, $\mathbb{S}_M < 0$) are due to the osmotic pressure gradient which may lead to water diffusion in (i.e. swelling) or out (i.e. shrinkage) of the droplets. The escape of inner droplets may also cause shrinkage of the outer droplets. With only the growth/shrinkage term present in a population balance and a source terms equal to zero, the total number of droplets would be conserved and only their size may change. This is the case of the outer droplets which conserve a constant number, while the number of inner droplets reduces due to their escape. The models of droplets escape and swelling, required in the PBMs, are investigated in the following sections.

5.3.2. Swelling of inner and outer droplets

By analogy to Fick's law of diffusion and according to Starling's hypothesis, the net fluid flow through a membrane can be assumed to be proportional to the difference between the

osmotic and the hydrostatic pressure gradients [21,28]. Thus, swelling of the inner droplets is driven by the osmotic pressure gradient ($\Delta\Pi$) and it is countered by the Laplace pressure (ΔP) [6]. The Laplace pressure is commonly neglected while modelling swelling in the literature, but it will be accounted for in this work as the model will be applied to submicronic inner droplets where the Laplace effect is not negligible. Considering the oil phase as an ideally selective membrane (i.e., permeable only to solvent), the volumetric swelling rate of an inner droplet, $\mathbb{S}_\mu$ (m³ s⁻¹), can be written as follows:

$$\mathbb{S}_\mu(t, v_\mu) = \frac{dv_\mu}{dt} = L_p A_\mu(v_\mu)\big(\Delta\Pi - \Delta P(v_\mu)\big) \qquad 5.3$$

Where L_p (m² s kg⁻¹) is the permeability coefficient of the membrane and A (m²) the droplet's surface area. By this equation, when the osmotic pressure gradient is exactly counterbalanced by the Laplace pressure, equilibrium is reached and no mass transfer (swelling or shrinkage) occurs. The osmotic pressure gradient between the internal and external aqueous phases, $\Delta\Pi$ (Pa), is [29,30]:

$$\Delta\Pi = \Pi_{in} - \Pi_{out} = i\,R\,T\,(C_{in} - C_{out}) \qquad 5.4$$

Where i is the van't Hoff factor estimated to be 2 for NaCl [29], R (J K⁻¹ mol⁻¹) the universal gas constant, T (K) temperature and C (mol m⁻³) the concentration of salt (in and out stand for the inner and outer water phases, respectively). The Laplace pressure of inner droplets, ΔP (Pa), is:

$$\Delta P(v_\mu) = \frac{4\,\sigma_{\mu,M}}{d_\mu} \qquad 5.5$$

Where d (m) is the droplets diameter and σ (N m⁻¹) the interfacial tension (here between inner and outer droplets).

As a consequence of inner droplets' swelling, the volume of the outer droplets will increase. Considering the inner droplets to be evenly distributed among the outer droplets, the swelling rate of the outer droplets, $\mathbb{S}_M$ (m³ s⁻¹), can be obtained by integrating the swelling rates of the encapsulated inner droplets:

$$\mathbb{S}_M(t, v_M) = \frac{dv_{M,swelling}}{dt} = \frac{v_M}{V_M(t)} \int_0^\infty n_\mu(t, v_\mu)\, \mathbb{S}_\mu(t, v_\mu)\, dv_\mu \qquad 5.6$$

where V_M is the total volume of the outer droplets. Eq. 5.6 indicates for instance that increasing the number of inner droplets in an outer droplet increases the swelling rate of the outer droplet.

Concerning the mechanism of diffusion of water through the oil layer, two mechanisms were suggested in the literature. Garti et al. (1985) [22] explained the water transfer based on the micellar transport and Yan and Pal (2001) [23], on the other hands, explained it by the diffusion of hydrated surfactant that facilitates water transport.

It is also to be noted that in this model swelling of the outer droplets is totally governed by the swelling of the inner droplets, and the external interfacial tension does not appear in the model to oppose the osmotic pressure gradient. The literature regarding modeling of double emulsions did not point out an effect of the outer interfacial tension on swelling. If such an effect is present, it would be lumped into the parameter L_p (the permeability coefficient of

the membrane) in the present model. This parameter includes the different molecular phenomena (e.g., effects of both surfactants, thickness of the layer, etc....) responsible for the resistance force.

5.3.3. Escape of inner droplets

Escape rate. The inner droplets may escape if they get close to the outer droplet's surface. Different approaches were considered in the literature to model the escape rate (Table 5.3).

Table 5.3: Coalescence-driven escape models of inner droplets, with: $\frac{dn_\mu}{dt} = -\Omega_{es}\, n_\mu^{cr}\, P$.

Pays et al. (2001) [14]**: Based on an adsorption isotherm**
Only droplets adsorbed on the surface (n_μ^{cr}) may escape, evaluated using the isotherm: $$\frac{\Theta}{1-\Theta} = \frac{1}{4}\pi d_\mu^2 \tau k_B T\, \frac{(n_\mu - n_\mu^{cr})}{\sqrt{2\pi m_\mu k_B T}} \exp\left(\frac{u_a + 4\,u_l\,\Theta}{k_B T}\right)$$ With $\Theta = \frac{n_\mu}{n_0}$, $n_0 = d_M^2/(d_\mu^2 v_M)$, $u_a = \frac{1}{12 l_s}A_H d_\mu$ and $u_l \approx \frac{1}{24\, l_s}A_H d_\mu$. The escape frequency Ω_{es} is fitted to experimental data. The escape probability is $P = 1$.
Klahn et al. (2002) [16]**: Double emulsions in simple shear flow**
The escape probability is assumed equal to the coalescence probability and is given by: $$P = \exp\left(\frac{t_d}{t_i}\right) \approx \left(\frac{\pi\sigma_{\mu,M}}{6A_H}\right)^{-\frac{4}{9\pi\tau_c}\left(1+\frac{\eta_M}{\eta_{out}}\right)}$$ The volume fraction (with $n_\mu^{cr} = \alpha_{cr}\,n_\mu$) is obtained by fitting to experimental data, giving: $$\alpha_{cr} = 1 - \exp\left(-\frac{d_\mu}{d_M}\left[2.22 + 1.51\left(\frac{\eta_M}{\eta_{out}}\right)^{-0.57}\right]\right)$$ The escape frequency is obtained from the circulation time in a simple shear flow ($\tau_c = \frac{\dot\gamma}{4\pi}t_c$): $$\Omega_{es} = \frac{2}{t_c}$$
Chávez-Páez et al. (2012) [7]**: Based on 3D Brownian dynamics**
The global frequency of collisions of inner droplets with the surface of outer droplets (i.e. $\Omega_{es}\,n_\mu^{cr}$) is determined by the equation of motion: $$r_i(t + \Delta t) = r_i(t) + \beta\,D_i\,F_i(t)\Delta t + R_i$$ The interaction between particles is modelled by a short-range repulsive potential: $$\beta u_{ij}(r) = \varepsilon\exp(-z\,(r - L_{ij})), \text{ with } \beta = (k_B T)^{-1}$$ The coalescence probability, P, is assumed to be determined by another source.
Kang et al. (2016) [17]**: Based on momentum and energy conservation**
The escape frequency is calculated from the dewetting time (See equations 9-13).

Pays et al. (2001) assumed that the escape may only concern the inner droplets adsorbed on the surface of outer droplets and used an adsorption isotherm to evaluate the amount of adsorbed droplets [14]. In a simple shear flow, Klahn et al. (2002) considered that the escape may concern droplets present in a critical region close to the surface, of volume fraction α_{cr} [16]. In this case, the change in the number density of inner droplets n_μ with time is proportional to their change in the critical region, with $n_\mu^{cr} = \alpha_{cr}\,n_\mu$. This concept can be assumed to be valid in general. The escape rate can therefore be written as, $\Re_{es,\mu}$(m^{-3} s^{-1}):

$$\Re_{es,\mu}(t, v_\mu) = -\alpha_{cr}\,n_\mu(t, v_\mu)\,\frac{1}{N_M}\int_0^\infty \Omega_{es}(v_\mu, v_M)n_M(t, v_M)\,dv_M \qquad 5.7$$

Where N_M is the total number of outer droplets, $\Omega_{es} = 1/t_{es}(v_\mu, v_M)$ (s^{-1}) is the escape frequency with t_{es} (s) the escape time. From eq. 5.7 it can be seen for instance that increasing the number of inner droplets would increase the escape frequency.

The overall escape rate of inner droplets from each outer droplet then causes a decrease in the volume of the outer droplet, $Q_{es,M}$ (m^3 s^{-1}), as follows:

$$Q_{es,M}(t, v_M) = \frac{dv_{M,escape}}{dt} = \frac{v_M}{V_M(t)} \int_0^\infty \Re_{es,\mu}(t, v_\mu)\, v_\mu\, dv_\mu \qquad 5.8$$

Escape frequency. Klahn et al. [16] estimated the escape frequency of double emulsions undergoing a simple shear from the circulation time (Table 5.3). For emulsions under storage, droplets move only due to Brownian motion. In this case, Chávez-Páez et al. (2012) [7] considered the escape frequency to be governed by the collision frequency of inner droplets with the surface of the outer droplet which is driven by their Brownian motion. They employed 3D simulations to calculate this frequency.

Kang et al. (2016) proposed to calculate the escape time from the coalescence or dewetting time of inner droplets through the surface of the outer droplets [17,31]. This approach is applicable to double emulsions under storage, and does not require heavy calculations, compared to 3D simulations. The methodology is based on balancing the force caused by the interfacial tension and the viscous force. First, the escape time can be obtained by integrating the speed function over the crossed distance l (m) as follows:

$$t_{es}(v_\mu, v_M) = \int_{0.01}^{L_{eq}} \frac{1}{u_\mu(v_\mu) + u_M(v_M)}\, dL \qquad 5.9$$

Where u (m s^{-1}) is the velocity, $L = 2\, l/d_\mu$ a dimensionless position and L_{eq} the final position of the inner droplet at equilibrium with $L_{eq} = 2$ for complete separation/escape (i.e., when $l = d_\mu$). The lower bound of the integral corresponds to 0.5 % of d_μ considered as a threshold of dewetting.

The velocities are calculated based on momentum and energy conservations. If the viscosity of the continuous phase is small compared to the globules, the momentum conservation of the inner and outer droplets can be written as:

$$m_\mu\, u_\mu(v_\mu) = m_M\, u_M(v_M) \qquad 5.10$$

Where m (kg) is the droplet's mass.

During the dewetting phenomenon, on one hand, the driving force of separation (F_S) is governed by the interfacial tensions across the three phases: the inner droplet with outer droplet ($\sigma_{\mu,M}$), the outer droplet with the outer continuous phase ($\sigma_{M,out}$) and the inner droplet with the outer continuous phase ($\sigma_{\mu,out}$, null in the present work). Kang et al. defined this force as [17]:

$$F_S(v_\mu, v_M) = \pi\, d_\mu\, L(2 - L)\sigma_{\mu,M}\left(1 - \frac{\sigma_{\mu,out}}{\sigma_{\mu,M}} + \frac{\sigma_{M,out}}{\sigma_{\mu,M}}\frac{1}{K}\right) \qquad 5.11$$

Where $K = \frac{d_M}{d_\mu}$.

On the other hand, the resistance force to escape (F_V) is governed by the viscosity of the outer droplet, as the viscosity of the continuous phase is negligible compared to the outer droplet. Kang et al. defined this force by:

$$F_V(v_\mu, v_M) = \frac{3}{2}\pi\, d_\mu \eta_M \left[u_\mu(v_\mu) + u_M(v_M)\right](2 - L) \qquad 5.12$$

The energy conservation implies:

$$\int_{0.01}^{L} \left[F_S(v_\mu, v_M) - F_V(v_\mu, v_M)\right]dL = \frac{1}{2}m_\mu u_\mu^2(v_\mu) + \frac{1}{2}m_M u_M^2(v_M) \qquad 5.13$$

The velocities are calculated by solving equations 5.10–5.13 analytically (see appendix A2). This allows to calculate the dewetting time (eq. 5.9), and thus the escape frequency.

Fig. 5.1A shows the calculated escape frequency for different inner and outer droplets' diameters. The escape frequency decreases for bigger outer droplets and in this case the size of the inner droplets has a negligible effect. For smaller outer droplets, the escape frequency is higher, and the impact of the size of the inner droplet is very important. Indeed, smaller inner droplets have a higher velocity. Fig. 5.1B shows that higher oil viscosities lead to much lower escape frequencies. Indeed, the viscosity has a great impact on the speed of the inner droplets, which affects their escape frequency.
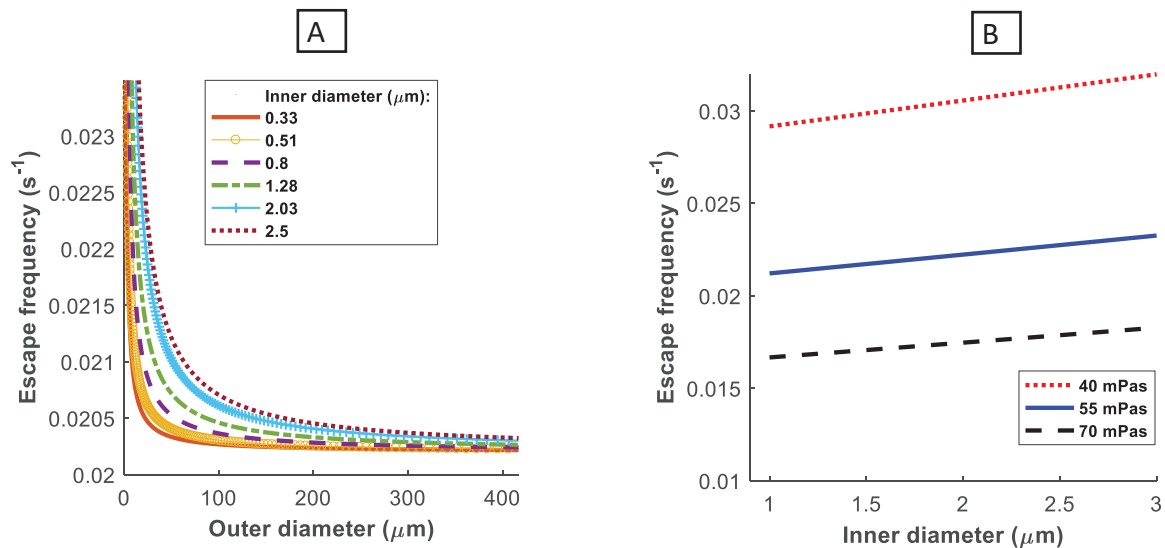
Fig. 5.1. *The escape frequency calculated by the dewetting model for: A) Different inner droplets' diameters using η_M = 55 mPa s and $\sigma_{\mu,M}$ = 5 × 10^{-3} N m^{-1}, and B) Different outer phase viscosities using $\sigma_{\mu,M}$ = 5 × 10^{-3} N m^{-1} and d_M = 20 μm.*

5.3.4. Numerical solution

The semi-discrete finite volume scheme is adapted to solve a population balance involving a growth (or swelling) term, G (m^3 s^{-1}) (Qamar and Warnecke 2007 [32], Kumar and Warnecke (2010) [33]). In the finite volume method, the PBM is reformulated into a mass balance, $g(t, v) = v\, n(t, v)$. By discretizing the flux across the cell boundaries $[i + \frac{1}{2}, i - \frac{1}{2}]$ and setting $\tilde{G} = \frac{G}{v}$ one obtains:

$$\frac{dg_i(t,v)}{dt} = -\frac{v_i}{\Delta v_i} \left[\left(\tilde{G} \, g \right)_{i+\frac{1}{2}} - \left(\tilde{G} \, g \right)_{i-\frac{1}{2}} \right] \qquad 5.14$$

with:

$$\left(\tilde{G} \, g \right)_{i+\frac{1}{2}} = \tilde{G}_{i+\frac{1}{2}} \left[g_i + \frac{\Delta v_i}{2\Delta v_{i-\frac{1}{2}}} \, \Phi(r_i^+) \, (g_{i+1} - g_i) \right] \qquad 5.15$$

In which $\Phi(r_i^+) = \frac{|r_i^+| + r_i^+}{1 + |r_i^+|}$ is the flux limiting function with $r_i^+ = \frac{g_i - g_{i-1} + \epsilon}{g_{i+1} - g_i + \epsilon}$ and the parameter ϵ is a small number used to avoid the division by zero [33,34].

5.4. Results and discussions

The developed models for inner droplets' escape and swelling were incorporated into the PBMs of the inner and outer droplets and solved simultaneously using the semi-discrete finite volume numerical scheme [33]. The evolution of the release rate and the size distribution of the outer droplets were monitored during storage of the double emulsions. Different parameters were varied to evaluate the robustness of the combined models, including the fraction of the primary emulsion, the fraction of salt, the fraction of the internal phase, and the effect of the stirring rate in the second step of preparation through its effect on the outer droplets size and the encapsulation efficiency (Table 5.2).

5.4.1 Observation of the swelling and escape phenomena

Few microscopic images of double emulsions are shown in Fig. 5.2 at different storage times. At day 0, right after the preparation, inner droplets (of 800 nm in diameter, as measured by the NanoZS) clearly appear to be encapsulated within the outer droplets (mean diameter of 40 μm). This image confirms that the inner droplets size did not sensibly evolve during the second preparation step either through inner-inner droplet coalescence or swelling. After 6 days, both the inner and outer droplets have bigger sizes than initially, revealing either swelling or coalescence of these droplets during storage. After 20 days, the outer droplets have a smaller size than day 0, and many outer droplets appear to be almost empty from the inner droplets. This last observation clearly reveals an over-swelling breakdown phenomenon.

In order to investigate the cause of outer droplet growth (shown at day 6 in Fig. 5.2), whether it is due to droplets' swelling or coalescence, a single O/W emulsion was prepared using the same oil phase (i.e., mineral oil + Span 80) without salt and stored under similar conditions as the double emulsions. Note that it is hard to produce a single emulsion that has exactly the same properties of the double emulsion in terms of size, viscosities, densities and surface tension. However, the oil fraction ($\phi_{oil+Span\,80} = 1$ %) was equivalent to the primary emulsion fraction in the double emulsions (ϕ_M), and similar external emulsifier concentrations ($\phi_{emulsifier}^{out} = 1$ %), stirring rate (ω_R = 400 rpm) and duration were employed. Under these conditions, the obtained mean droplets' size distribution right after the preparation of the single emulsion (Fig. 5.3A) was comparable to the outer droplets' size in the double emulsion (Fig. 5.3B). So the single and double emulsions may be assumed to undergo similar coalescence rates.
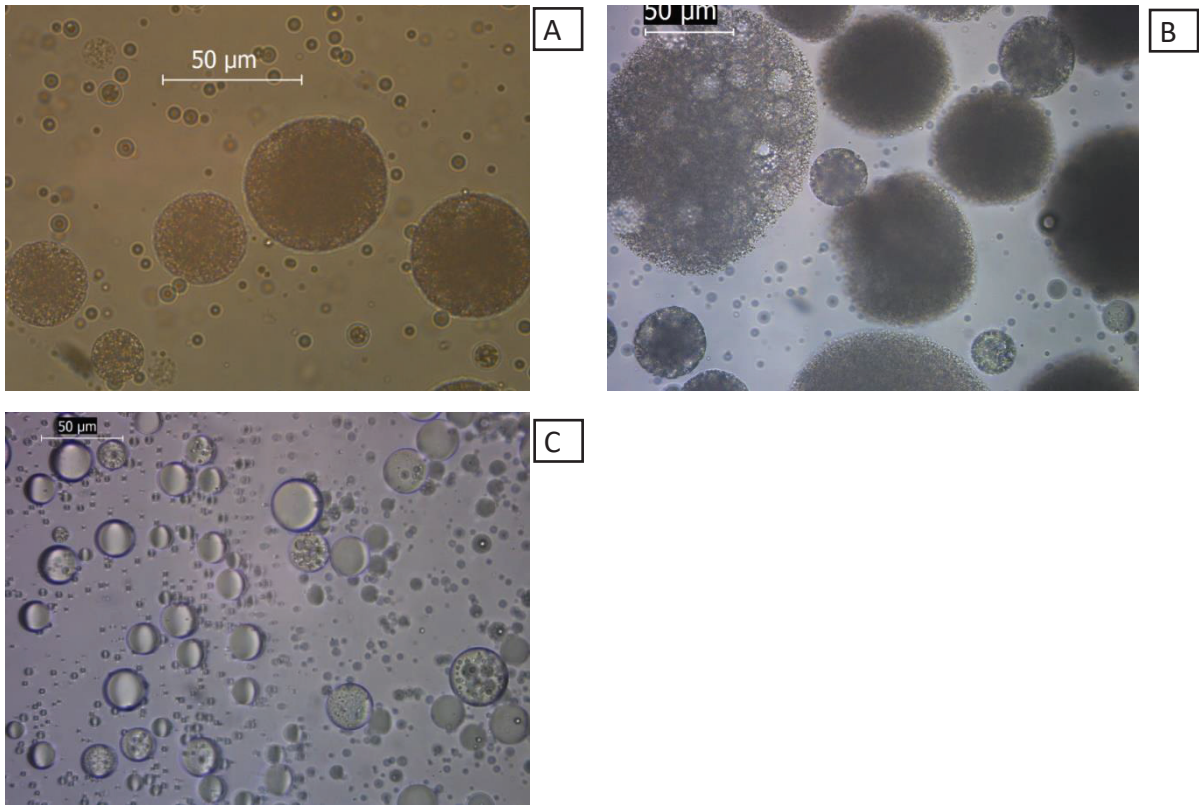
Fig. 5.2. *Microscopic images of the double emulsion prepared with $\phi_\mu = 40$ %, $\phi_M = 1$ %, and $\omega_R = 400$ rpm: A) day 0, so right after preparation, B) day 8 and C) day 20.*
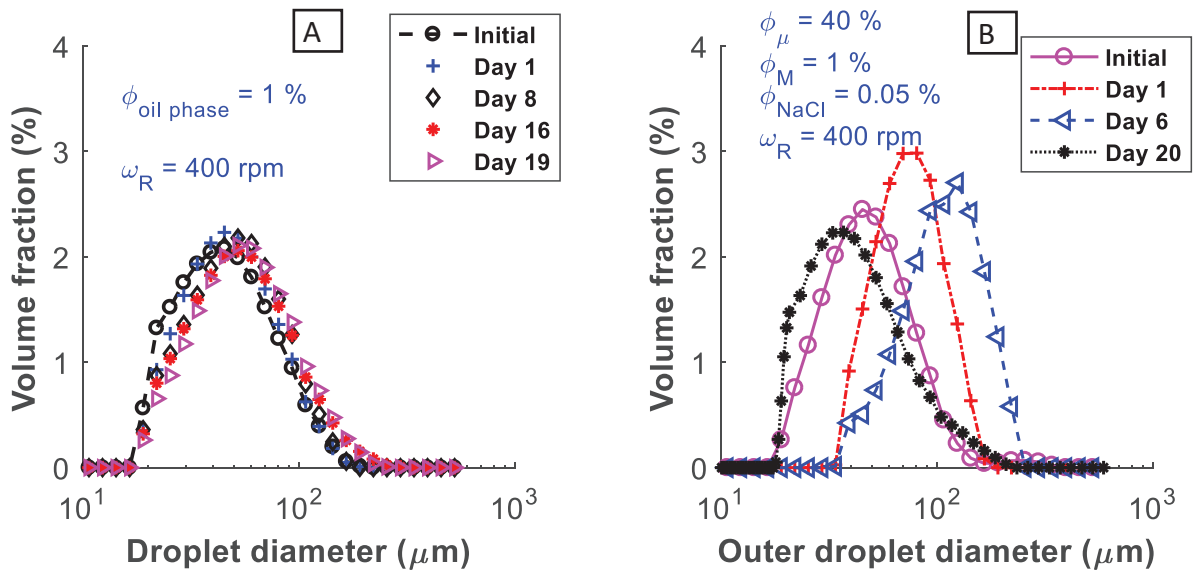
Fig. 5.3. *A) The DSD of a single O/W emulsion. B) The DSD of a double emulsion W/O/W. In both cases, similar fractions and mixing rates were employed, and the oil phase consists of mineral oil and Span 80, and the water phase consists of water and Tween 80.*

However, Fig. 5.3A shows that the single emulsion undergoes only slight coalescence during 19 days of storage while Fig. 5.3B shows that the size of the outer droplets in the double emulsion increases importantly during the first week, which is in agreement with the microscopic images (Fig. 5.2). It can thus be deduced that the observed growth of the outer droplets in the case of the double emulsion is mainly due to swelling due to the osmotic

pressure gradient, which is a well-known phenomenon in double emulsions containing ions [5,6,18,19,23,24].

The maximum swelling was found to occur after around one week of storage (6-8 days) for most samples, after which the double emulsions endured over-swelling breakdown (Fig. 5.2C and Fig. 5.3B). Thus, the predictions of swelling and release are done over one week in the following sections.

5.4.2. Parameter identification

Two model parameters that need to be identified for the present system are the volume fraction of the critical region, α_{cr}, and the permeability coefficient, L_P. Three experiments were chosen among the experiments presented in Table 5.2 for parameter identification. The selected experiments were chose in the way to include the most variation in the system and were prepared at 400 rpm stirring rate but have different compositions: a) $\phi_M = 4\,\%$, $\phi_{NaCl} = 0.05\,\%$, $\phi_\mu = 40\,\%$; b) $\phi_M = 1\,\%$, $\phi_{NaCl} = 0.24\,\%$, $\phi_\mu = 40\,\%$; and c) $\phi_M = 1\,\%$, $\phi_{NaCl} = 0.05\,\%$, $\phi_\mu = 40\,\%$. The "MultiStart class" global optimization function of MATLAB® was used while employing "fmincon" nonlinear solver to perform the identification:

$$\min_{L_p,\alpha_{cr}} J \tag{5.16}$$

with

$$J = \sum_{3\ \text{experiments}} \left(\sum_{\text{sample n°}} \left| n_M^{Model}(t,v) - n_M^{Exp}(t,v) \right| + \left| C_m^{Model} - C_m^{Exp} \right| \right)$$

with $[L_p] \in [1 \times 10^{-16}, 1 \times 10^{-14}], [\alpha_{cr}] \in [0,1]$.

Table 5.4. Identified parameters compared to literature values

Hydraulic permeability coefficient	Volume fraction of the critical region, α_{cr}	Conditions	Reference
2.75×10^{-15}	3.6×10^{-5}	Storage ($P = 1$)	This work
$2.27 \times 10^{-15} - 2.27 \times 10^{-14}$	-	Storage	Matsumoto & Kohda (1980) [25]
$2.27 \times 10^{-15} - 4.78 \times 10^{-15}$	-	Storage	Garti et al. (1985) [22]
$0.3 \times 10^{-15} - 5.87 \times 10^{-15}$	-	Storage	Yan & Pal (2001) [23]
$2.2 \times 10^{-14} - 2.72 \times 10^{-14}$	-	Storage	Bahtz et al. (2015) [24]
-	≈ 0.57	Storage (high escape rate, $P = 1$)	Pays et al. [14]
-	≈ 0.2	Simple Shear flow (with a probability term)	Klahn et al. [16]

P_0: Permeation coefficient (m s^{-1}), $L_p = \frac{P_0 V_w^*}{R\,T}$, V_w^*: Molar volume of pure water (m^3 mol^{-1})

The identified parameters are given in Table 5.4. The identified permeability coefficient, L_{p}, is compared to the literature values, and it can be seen that it is of the same order of magnitude. The permeability coefficient was found in the literature to depend on the oil viscosity and the fraction of internal emulsifier [6,18,19,22,23]. In this work, the oil type and the emulsifier concentration were maintained the same in all experiments. Therefore, it was possible to fit a unique value of L_{P} for the three experiments used for the identification, $L_{\mathrm{p}} = 2.75 \times 10^{-15}$. This value, as well as the identified value of the critical region, $\alpha_{\mathrm{cr}} = 3.6 \times 10^{-5}$, will be kept constant in the model to predict the evolution of the other experiments. It is worthy to note however that the viscosity of the outer droplet evolves with time, due to swelling and release, which might lead to an evolution of the permeability, but this effect was not modelled.

Concerning the critical fraction α_{cr}, Klahn et al. [16] estimated a decreasing value of α_{cr} when increasing $d_{\mathrm{M}}/d_{\mathrm{\mu}}$, (for instance, $\alpha_{\mathrm{cr}} = 0.2$ for $d_{\mathrm{M}}/d_{\mathrm{\mu}} = 10$). However, their operating conditions and modelling approach favors the estimation of higher critical fractions than the present work ($\alpha_{\mathrm{cr}} = 3.6 \times 10^{-5}$). First of all, they applied simple shear flow to the double emulsions, while in our case the double emulsions were stored under stagnant conditions. Second, in our case $d_{\mathrm{M}}/d_{\mathrm{\mu}} \approx 50$, which should lead to lower fractions. Finally, they calculated the escape probability to be $P \approx 0.06$ while in our work P is regrouped with α_{cr} as in Pays et al. (i.e. $P = 1$). In the work of Pays et al. [14], the fraction of the adsorbed droplets (here regarded as α_{cr}) was not indicated, but it could be estimated to be around $\alpha_{\mathrm{cr}} = n_{\mathrm{\mu}}^{cr}/n_{\mathrm{\mu}} = 0.57$ (see Table 5.3). This is reasonable as in their study the escape was faster, and the outer droplet was empty from inner droplets within 20 hours. Chávez-Páez et al. (2012) [7] simulated full escape in 1 second when employing an arbitrary escape probability of $P = 1 \times 10^{-3}$ and indicated that real probabilities should be lower.
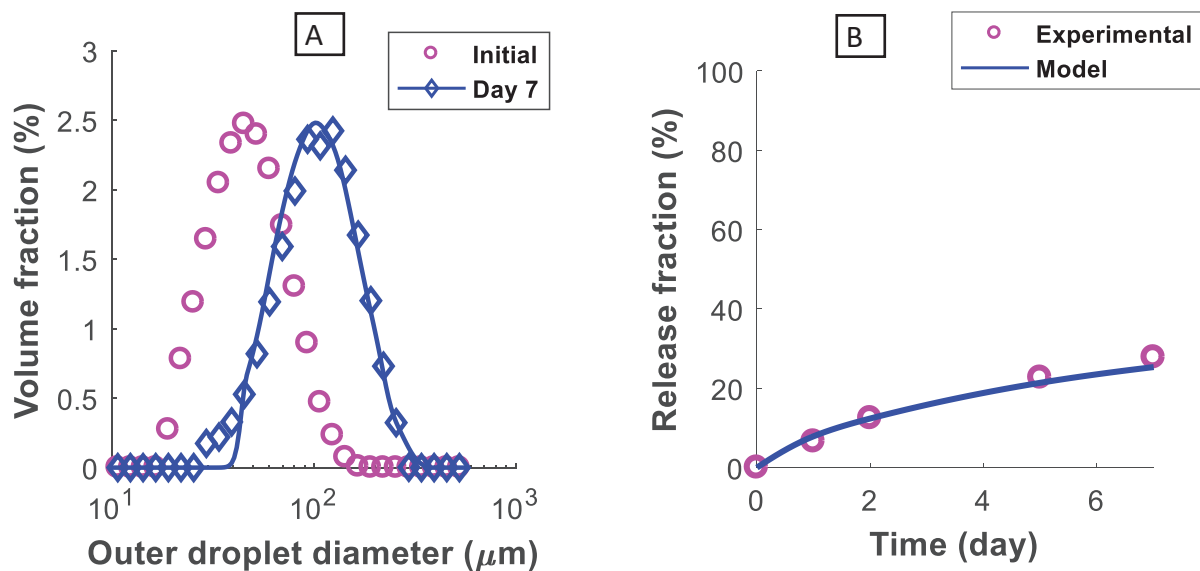

Fig. 5.4. Experimental (represented by the symbols) and modelling results (continuous lines) of the double emulsion prepared with ϕ_{μ} = 40%, ϕ_M = 4%, and ω_R = 400 rpm: A) The outer DSD. B) The released fraction due to inner droplets' escape.

5.4.3. Effect of the primary emulsion fraction (ϕ_M)

The effect of the primary emulsion fraction was investigated over the range of ϕ_M = 1 %, 2 %, 3 % and 4 % (set 1 in Table 5.2). Fig. 5.4 shows the model predictions compared to the experimental results for one of the experiments (with ϕ_M = 4 %), both for the outer DSD (Fig. 5.4A) and the released fraction of NaCl (Fig. 5.4B). It can be seen that the model predictions are in good agreement with the experimental results for both variables. In this experiment, the encapsulation efficiency measured right after preparation was 95.5 % (Table 5.2).

The plotted released fraction represents the amount released during storage only (so the released amount is 0 at time 0). To have the cumulative released fraction one needs to add the fraction released initially during preparation. In this experiment, after seven days, we obtain a released fraction of 28 % during storage and a cumulative released fraction of 31.24 %.
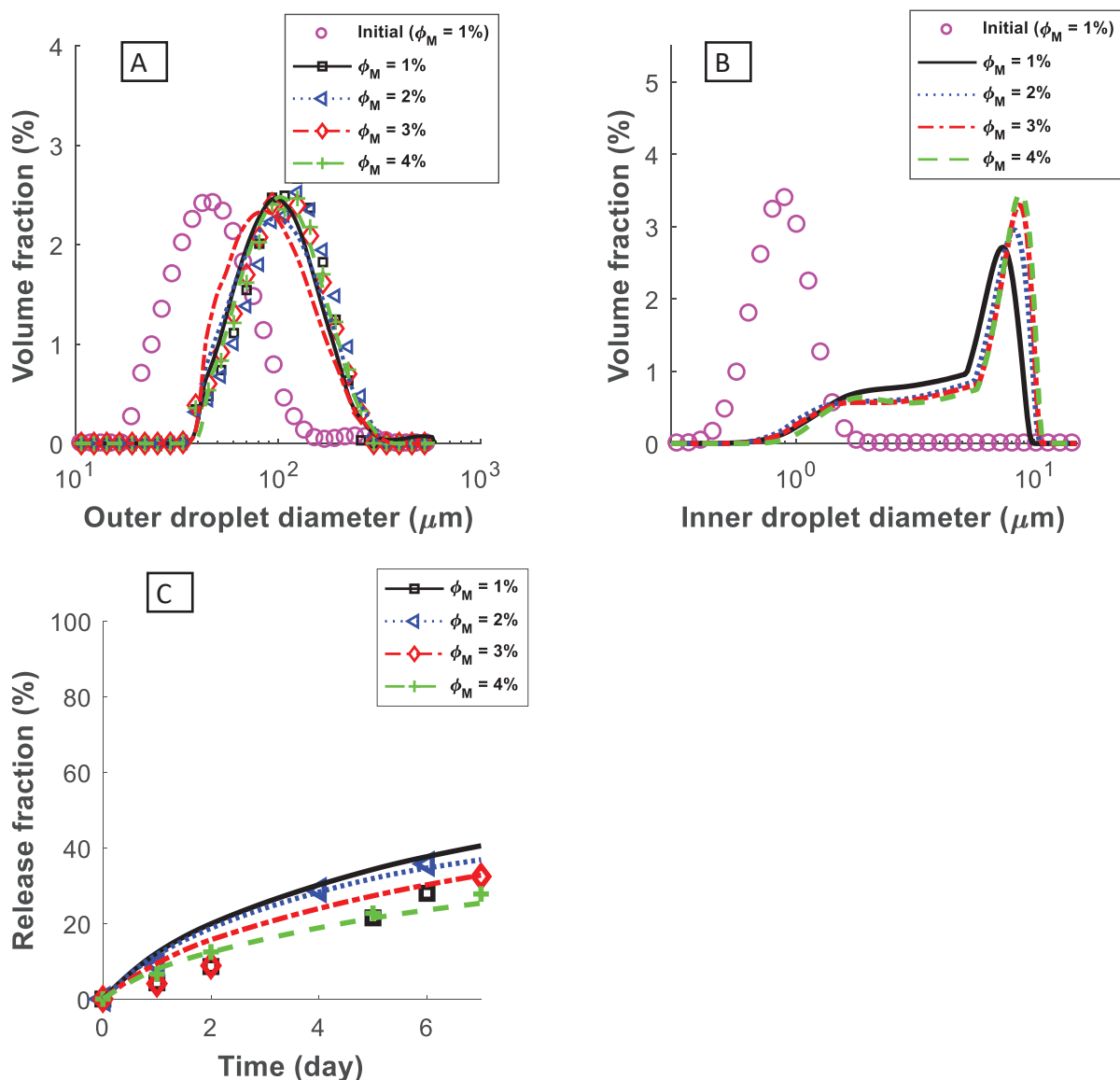

Fig. 5.5. Effect of the primary emulsion fraction (ϕ_M). A) The outer DSD at day 0 and after one week of storage. B) The inner DSD at day 0 and after one week of storage. C) The released fraction over one week of storage. The lines indicate the model predictions and the symbols the experimental measurements.

Fig. 5.5 shows the evolutions of the outer and inner DSD and the escape rate during storage of all the experiments in set 1, where the volume fraction of the primary emulsion ϕ_M was varied. As the initial DSDs are similar for all the experiments of this set, only one initial DSD is depicted on the figure for both the inner and outer droplets. The theoretical concentration of salt is the same in all the experiments of this set, but a slightly higher encapsulation efficiency was obtained when increasing ϕ_M ($EE = 92.5 - 95.5$ %), which is in line with the results reported by Matsumoto et al. [35]. As the differences in the encapsulation efficiencies are small, the experiments are comparable in terms of osmotic pressure gradients (which represents the driving force for swelling), and therefore they undergo similar swelling rates. Only a slightly higher swelling is observed in the inner DSD when increasing ϕ_M (Fig. 5.5B). Note that the inner droplets' size changes only due to swelling and is not affect by the escape phenomenon. Concerning the outer DSD (Fig. 5.5A), it changes as a consequence of both swelling, as a primary factor, and escape, but at a much lower extent. In Fig. 5.5C, it can be seen that a slightly lower escape rate is observed for higher primary fractions ϕ_M. As a global result, the measured outer DSDs are similar for the different fractions.

Fig. 5.5B shows that the DSD of inner droplets gets deformed with time and deviates from its initial Gaussian distribution. This is explained by the fact that the swelling rate is governed by $\mathbb{S}_\mu(t, v_\mu) \propto [\Delta\Pi - \Delta P(v_\mu)]$. Therefore, within the droplets of the distribution, smaller droplets have a higher Laplace pressure, and may attain $\Delta P \geq \Delta\Pi$, and consequently stop swelling, before bigger droplets. As a consequence, only a very small number of the inner droplets continues to swell to the size of about 10 µm (estimated by the model to be less than 5 % in number in all experiments). Quantitative measurement of the inner droplet's size distribution represents a big challenge [12], but a qualitative confirmation could be obtained by microscopy. This simulation shows the advantage compared to models neglecting the Laplace pressure. Indeed, if the Laplace pressure is neglected, all the droplets would continue to swell until reaching osmotic equilibrium ($\Delta\Pi = 0$), as no other force is opposing swelling.

5.4.4. Effect of the salt fraction (ϕ_{NaCl})

The ions fraction controls the osmotic pressure gradient, which represents the driving force for swelling. In this section, the effect of this key parameter is investigated over the range of ϕ_NaCl = 0.05 %, 0.14 %, 0.19 % and 0.24 % (set 2 in Table 5.2). The encapsulation efficiency was found to slightly increase when increasing the salt fraction: $EE = 92.5 - 96.4$ %. Note that the change in the salt fraction led to a change in the measured interfacial tension from 4 mN.m^{-1} to 5 mN.m^{-1}, respectively. Such change was not found to impact the calculation and therefore a constant value of 5 mN.m^{-1} was implemented for the double emulsion.

Concerning the inner droplets, Fig. 5.6A shows the measured inner DSD after the preparation of the first emulsion for the different experiments in the set. It can be seen that the inner droplets' size increases when increasing the salt fraction over the range of $\phi_\text{NaCl} = 0.05 - 0.19$ %, but much smaller sizes are obtained with the highest salt fraction ($\phi_\text{NaCl} = 0.24$ %). It is known that the ions may affect the surfactant spreading and oil viscosity leading to a complex effect on the stability and release during preparation, which may lead to this optimal point [25,36,37]. During storage (Fig. 5.6B), the model predicts that the swelling of the inner

droplets increases when increasing the salt fraction. As the experiment with $\phi_{NaCl} = 0.24$ % had initially the smallest droplets' size, it remains smaller than two experiments with higher salt fractions ($\phi_{NaCl} = 0.14$ and 0.19 %) but exceeds the size of the experiment with $\phi_{NaCl} = 0.05$ %.
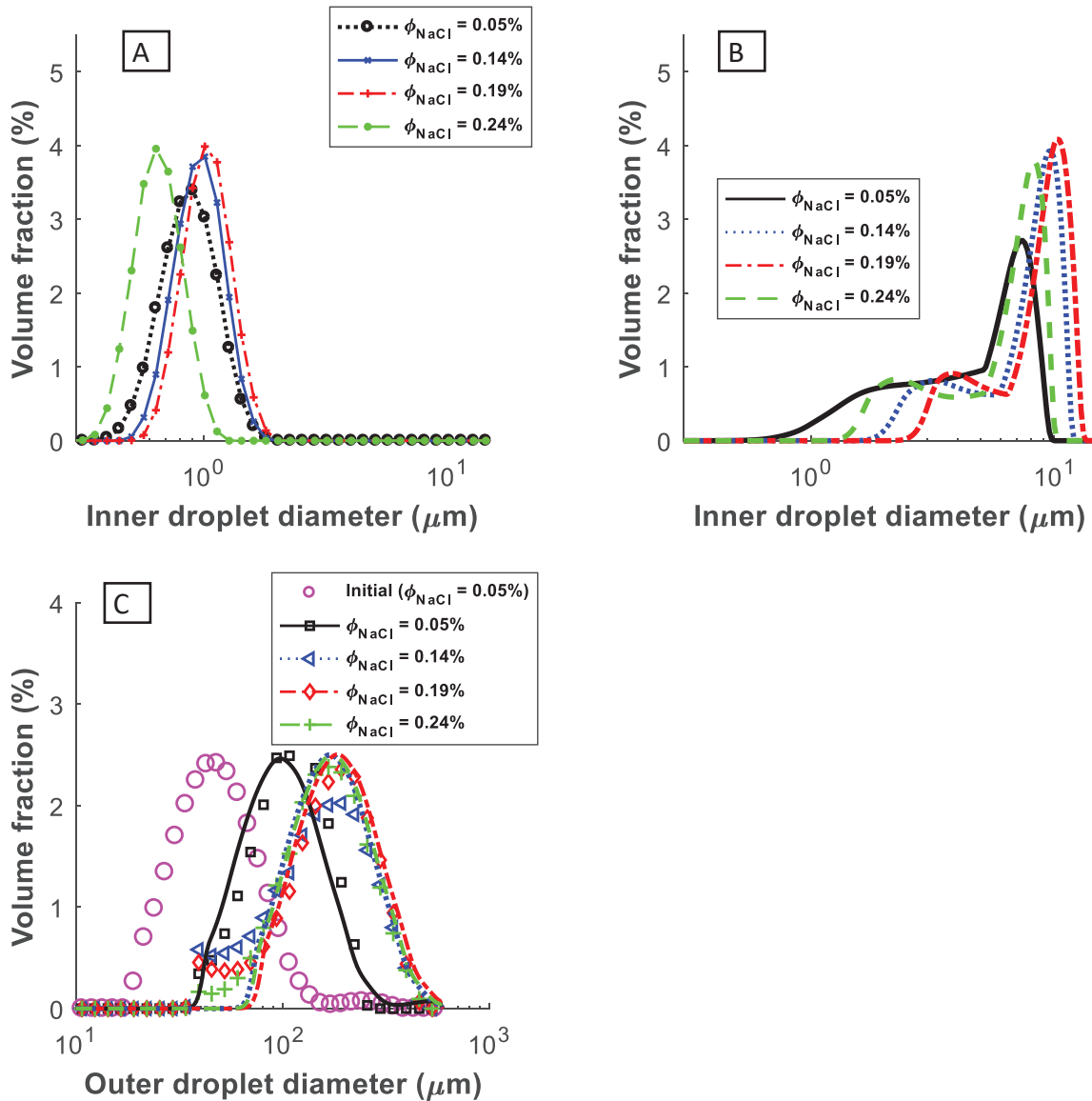
Fig. 5.6. *Effect of the salt fraction (ϕ_{NaCl}). A) The measured initial inner DSD (after the 1st preparation step). B) The model prediction of the inner DSD after one week of storage. C) The outer the DSD (initial and after one week of storage) by the model (represented by the continuous lines) and experimentally (symbols).*

Concerning the outer droplets, Fig. 5.6C shows that the model predictions of the outer DSD after one week are in good agreement with the experimental measurements for all concentrations. Besides, it can be seen that increasing the salt fraction has a negligible effect on the outer DSD when the salt fraction is high ($\phi_{NaCl} \geq 0.14$ %). Indeed, the double emulsions in the different experiments seem to swell up to a maximum swelling capacity where the fraction of salt has no effect. For a lower salt fraction ($\phi_{NaCl} = 0.05$ %), the droplets reach much smaller sizes after one week, which can be due to a lower inner droplets' swelling rate combined to higher inner droplets' escape. Indeed, a negligible fraction was released

109

after one week in the experiments with high salt fractions ($\phi_{NaCl} \geq 0.14$ %), while for the experiment with $\phi_{NaCl} = 0.05$ % the release was approximately 40 % (see experiment $\phi_M = 1$ % in Fig. 5.5C). The difference in the escape rates can be explained by the differences in the sizes of the inner droplets, as explained in Fig. 5.1., a higher escape contributes to a reduction in the osmotic pressure gradient, which leads to less swelling. This is in line with the literature, where a higher swelling rate is observed for higher osmotic pressure gradients [18,23,24]. Moreover, Jager-Lezer (1997) reported in general a lower release for higher swelling [6], as observed here.

It is to be noted that in the employed model the salt fraction affects the escape rate indirectly through its effect on the size. The salt fraction is not considered in the dewetting model proposed by Kang et al. (2016) [17]. It might be considered that the salt has a direct effect on the escape rate through its influence on the surface or viscosity forces [38]. This would require to account for the complex effects of salt on the surfactant and rheological behavior of the double emulsion. In the present work, the proposed model fits well the experimental data and has the advantage of being easy to implement. But, the identified parameters would be inaccurate if some phenomena are neglected.

5.4.5. Effect of the internal phase fraction (ϕ_μ)

The internal phase was varied over the range of $\phi_\mu = 10$ %, 20 %, 30 % and 40 % (set 3 in Table 5.2). The amount of salt was maintained constant and only the fraction of water to oil was varied. Therefore, when increasing ϕ_μ, the osmotic pressure gradient between the inner and outer water theoretically decreases.

The encapsulation efficiency was found to importantly increase when increasing ϕ_μ: $EE = 51.2 - 92.5$ %. As a result, the real osmotic gradient remained lower when increasing ϕ_μ. The increase in the encapsulation efficiency with ϕ_μ can be explained by an increased viscosity of the outer droplets, following the viscosity model of Vermeulen (1955) [39]. A higher apparent viscosity leads to a decrease in the escape rate during preparation. Indeed, the escape rate during preparation is mainly due to leakage of the inner droplets during the breakage of the outer droplets [11,25,40]. The higher the internal phase fraction, the higher the viscosity of the outer droplets, which leads to a reduced breakage rate [41] and to a higher encapsulation efficiency [25].

Fig. 5.7A shows the initial DSD of the outer droplets measured just after preparation for the different experiments of this set. A slight increase in the outer droplets' size is observed when increasing ϕ_μ, which confirms the reduction in the breakage, and therefore the leakage rate.

Fig. 5.7B shows the predictions of the evolution of the inner DSD after one week of storage. A slightly higher swelling is observed for the emulsions with lower ϕ_μ, which can be explained by the higher osmotic pressure gradient. Yan and Pal (2001) [23] also observed a slight decrease in droplets' swelling for higher ϕ_μ up to 40 %, beyond which they observed a sharper decrease. Bahtz et al. [24] observed a negligible effect on the swelling rate when increasing ϕ_μ up to 30 %.

Fig. 5.7C shows the evolution of the outer DSD during storage, experimentally and by the model. It can be seen that increasing ϕ_μ leads to a very slight increase in the outer droplet's size, which is partly due to their different initial sizes (Fig. 5.7A). Concerning the released fraction, it was approximately 40% for the experiment with $\phi_\mu = 40\%$ (experiment $\phi_M = 40\%$ in Fig. 5.5C), and around 15 % for the other experiments after one week of storage. This is in line with previous investigations where higher swelling rates imply lower release rates [6].
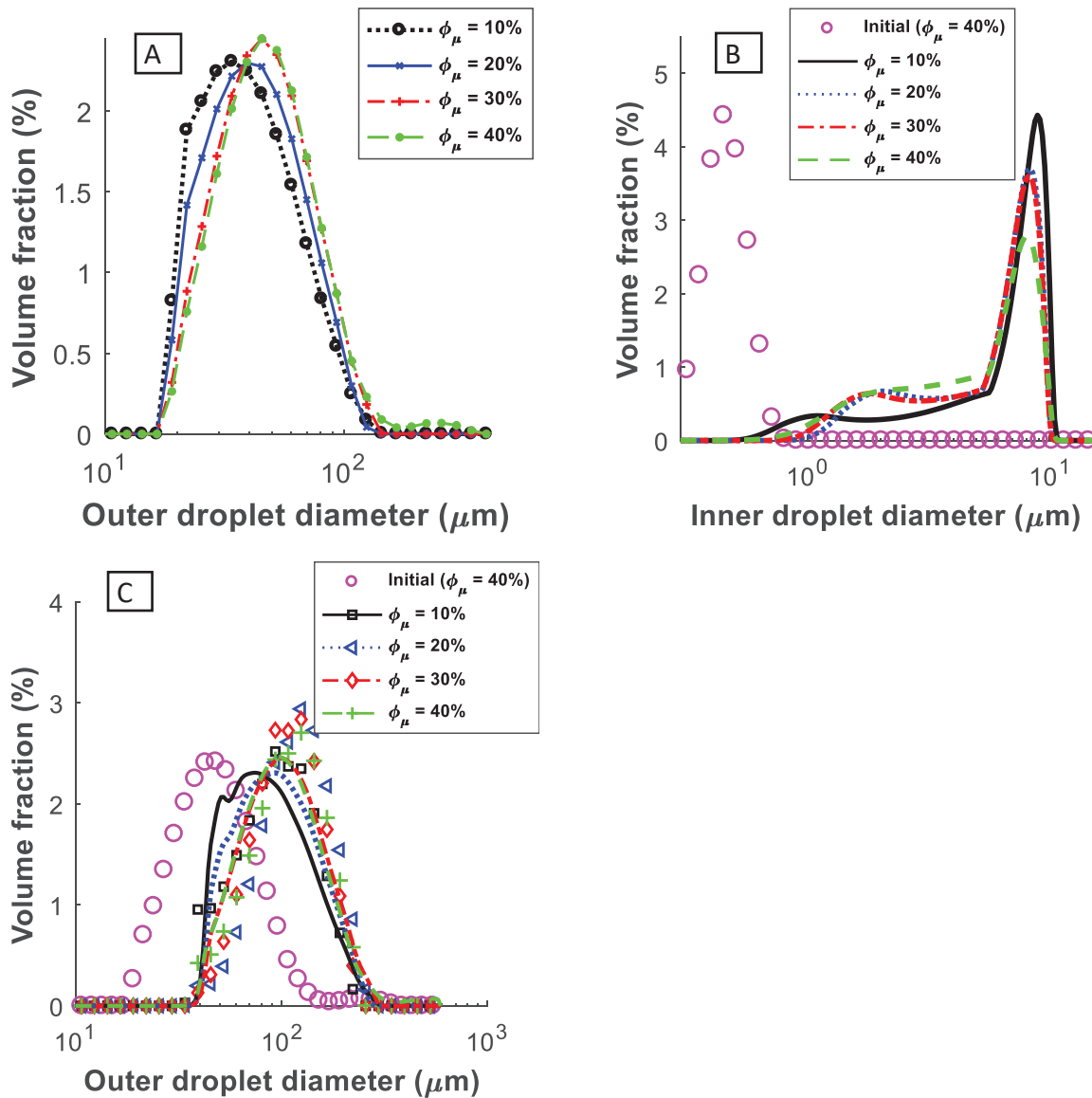
Fig. 5.7. *Effect of the internal phase fraction (ϕ_μ). A) The measured outer DSD at day 0 (after the 2nd preparation step). B) The initial experimental inner DSD and the predicted ones after one week. C) The outer DSD (initial and after one week), where the lines indicate the model predictions and the symbols the experimental measurements.*

5.4.6. Effect of the stirring rate

Changing the stirring rate during the preparation of the double emulsion has a direct effect on the outer droplets' size and the encapsulation efficiency, which may affect droplets' swelling and escape during storage. The stirring rate was varied over the range of 300, 350,

400 and 500 rpm (set 4 in Table 5.2) leading respectively to mean Sauter diameters of d_{32} =29.4, 26, 24.5 and 24 μm and encapsulation efficiencies of 94.1 %, 93.3 %, 92.5 % and 88.1 %. It is known that a higher stirring leads to more breakage, which causes more leakage of the inner droplets and therefore to a lower encapsulation efficiency [25]. Fig. 5.8A shows the DSD of the outer droplets measured right after preparation. As expected, smaller droplets are produced when increasing the stirring rate.
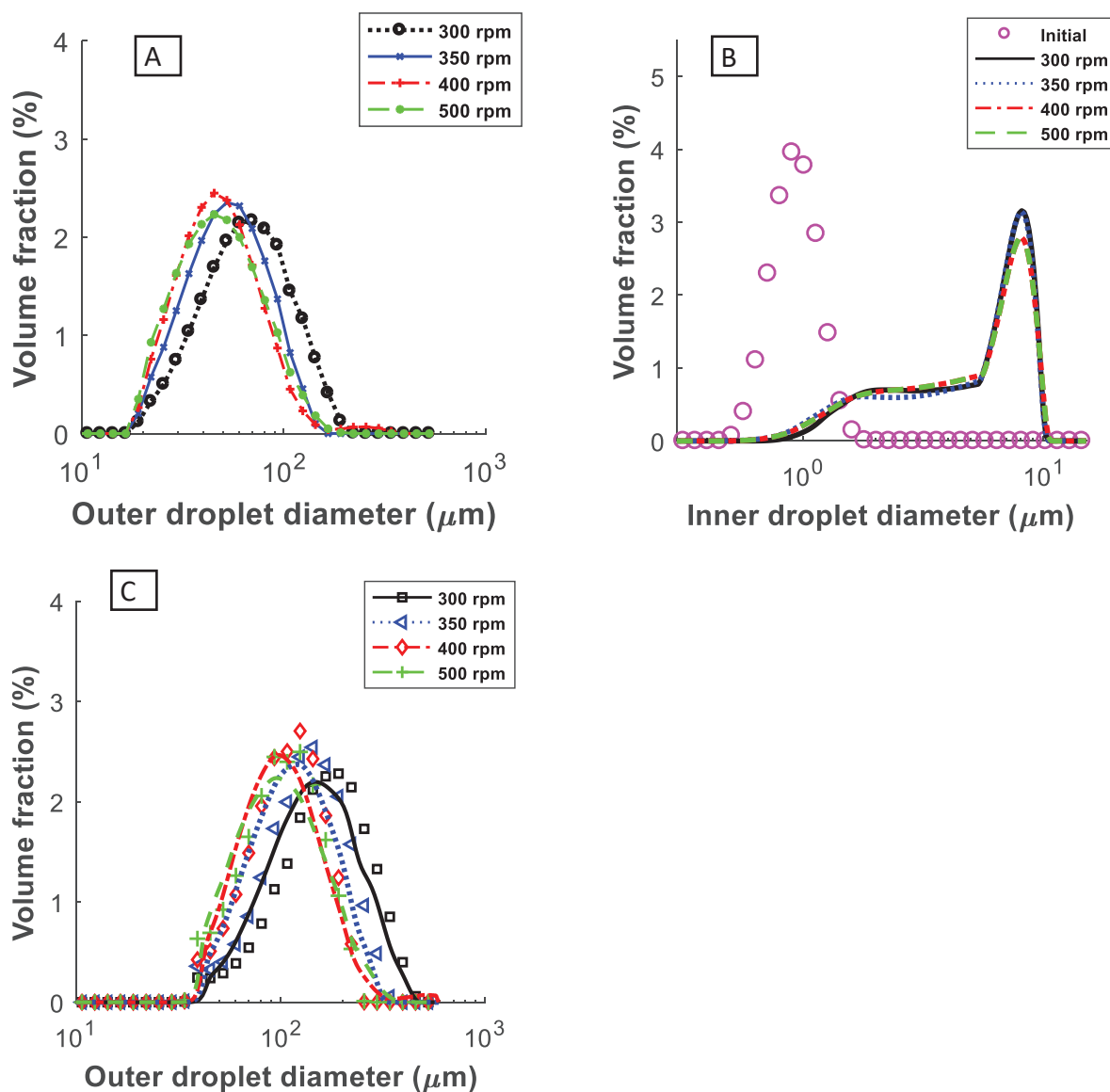
Fig. 5.8. *Effect of the stirring rate (ω_R) in the 2nd preparation step. A) The measured outer DSD at day 0. B) The inner DSD (initial-experimental; and after one week storage-model). C) The outer DSD after one week of storage, where the continuous lines indicate the model predictions and the symbols the experimental measurements.*

The internal emulsion was prepared under the same conditions in all the experiments of this set, and therefore only one initial experimental DSD is shown on Fig. 5.8B. The figure also shows the predictions of the swelling effect on the size of the inner droplets during storage which appears to be identical for all experiments. The size distribution of the outer droplets of the different experiments of this set after one week of storage are shown in Fig. 5.8C. The experiments conserve the same order of size as initially (Fig 8A), where the biggest droplets

measured after one week correspond to the experiment done with the lowest stirring rate. The released fraction after one week in all the experiments was found to be around 40%, which is due to the fact that the inner sizes and salt fractions are identical.

5.4.7. Evolution of the pressure gradients with time

The Laplace pressure counterbalances the osmotic pressure and should be overcome to lead the droplets to swell. Fig. 5.9A shows the evolution of the osmotic pressure gradient at different time steps and the Laplace pressure gradient as a function of the size of the inner droplets. There is only one curve for the Laplace pressure as it depends on the droplet size and the surface tension which is assumed not to change with time. In contrast, the osmotic pressure decreases with time due to droplets' swelling, and therefore a selection of few time steps was made and plotted in the figure. The osmotic pressure is independent of the droplet size. The swelling is conditioned by $\Delta\Pi > \Delta P(v_\mu)$, and only the fraction of droplets that have their sizes in the region where the osmotic pressure is higher than the Laplace pressure would swell. The size of the critical inner droplets corresponding to the intersection between $\Delta\Pi$ and ΔP becomes bigger with time, because $\Delta\Pi$ decreases due to swelling (that decreases C_{in}) and due to escape (that slightly increases C_{out}).

Fig. 5.9B shows the swelling rates at the selected time steps as a function of the inner droplets' size. The curves were forced to go to zero in the region of sizes where no droplets exist or when $\Delta\Pi \leq \Delta P(v_\mu)$. As the swelling rate is $\mathbb{S}_\mu(t, v_\mu) \propto [\Delta\Pi - \Delta P(v_\mu)]$, it increases when the difference between the osmotic and Laplace pressure gradients increases. As $\Delta P(v_\mu)$ decreases with the droplet size, a global increase in the swelling rate is observed over the size. Finally, the curves move towards bigger sizes with time, due to the creation of bigger droplets and the disappearance of small ones by swelling.

Fig. 5.9C shows the evolution of the inner DSD at different times. The swelling phenomenon clearly leads to an increase in the size of the inner droplets. As explained above, the change in the form of the distribution from normal to bimodal is due to the fact that part of the droplets become smaller than the critical size bellow which no swelling occurs. Actually, only a small number fraction of the inner droplets (here 2.67 %) is estimated to continue to swell up to 5-10 μm.

Fig. 5.9D shows the DSD of the outer droplets at the different times. The outer droplets quickly attain a big size and only undergo a little change afterwards. This is due to the fact that the main part of the inner droplets stops swelling when the osmotic pressure gradient is counterbalanced by the Laplace pressure gradient. The model is fitting the experimental data very well at day six, but there is a slight difference at day one. This may be due to an evolution of the permeation coefficient with time, due to swelling and escape which affect for instance the rheology of the double emulsion. This difference is in line with the lag time of swelling reported in the literature, for instance by Bahtz et al. (2015) [24], that is not accounted for by the model. Indeed, it is preferable to have a unique permeation coefficient with time, as estimating different values would render the model empirical. The evolution in the rheology should be described by a fundamental model and allow an automatic evolution of the permeation coefficient, which may constitute an improvement of this model. Experimental

results of Fig. 5.9D also shows some tails on the small sizes which the model could not predict. This can be an unknown phenomenon related to the swelling of the outer droplets.
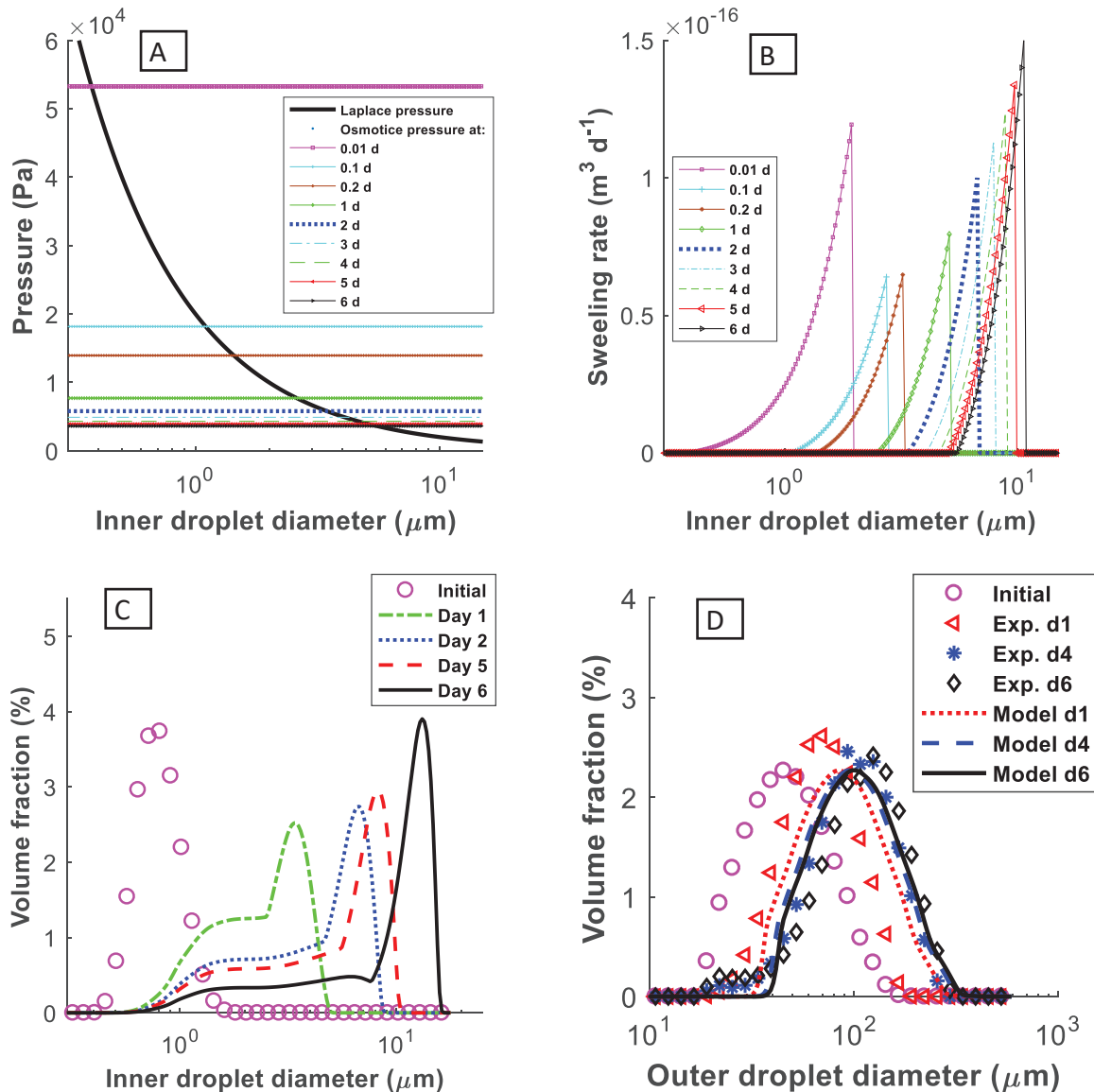
Fig. 5.9. *Swelling during storage (sample prepared with ϕ_μ = 40 %, ϕ_M =2 %, and ω_R=400 rpm). A) The osmotic and Laplace pressure gradients. B) The swelling rate (eq. 5.3) of the inner droplets (if $n_\mu = 0$ or $\Delta\Pi < \Delta P(v_\mu)$, then $\mathbb{S}_\mu = 0$). C) The inner DSD. D) The outer DSD. The lines indicate the model predictions and the symbols the experimental measurements.*

5.5. Conclusions

The escape and swelling rates of the inner droplets and the swelling of the outer droplets were incorporated into the population balances of the inner and outer droplets in order to predict the evolution of the droplets' size and the release rate during storage of double emulsions. The PBMs allow the prediction of the full size distribution of the droplets. The Laplace pressure gradient was accounted for in the swelling model. The model parameters were identified and validated for a wide range of operating conditions.

It was found that the main growth of the outer droplets during storage is due to the swelling of the inner droplets, due to osmotic pressure gradients. The extent of coalescence was found negligible, and the effect of inner droplets' escape on the outer droplets' diameter is minor

compared to the swelling effect. The effect of the Laplace pressure gradient is essential and leads to stopping the swelling of the inner droplets before osmotic equilibrium.

The two models were found to give good predictions over a wide range of conditions. The change in the fraction of the primary phase (1–4%) was found to cause a slight increase in the inner droplets' swelling and a slightly lower escape rate, while almost no effect could be measured on the outer droplets. Increasing the salt fraction was found to have a complex effect on the inner droplets' size during preparation and led to a higher swelling rate and lower escape during storage. Increasing the internal phase fraction led to bigger outer droplets due to their higher apparent viscosities and during storage the DSD showed a slight increase in the inner droplets' swelling due to the higher ions fraction. Higher stirring rates led to smaller outer droplets but no effect on the swelling rate was observed. Most emulsions seem to reach a kind of maximum size during swelling. This could be explained by the fact that most of the inner droplets stop swelling when the osmotic pressure gradient decreases, mainly due to swelling, which become compensated by the Laplace pressure gradient.

The developed model still needs to be evaluated on a wider range of operating conditions, mainly for different inner and outer surfactant types and different oils (with different viscosities, densities, interfacial tension). This work has put the basis of the coupled PBMs of inner and outer droplets to describe the stability of double emulsions during storage that should be able incorporate new parameters without big difficulty.

Nomenclature

A surface area of the droplet [m^2]

A_H Hamaker constant [J] (Table 3)

C salt concentration [mol m^{-3}]

d diameter of the droplet [m]

D_i diffusion coefficient of particle i [m^2 s^{-1}] (Table 3)

F_i total force acting on particle i [N] (Table 3)

F_S driving force of separation [N]

F_V resistance force to escape [N]

g size distribution in volume density [m^3 m^{-3}]

G growth or shrinkage [m^3 s^{-1}]

i van't Hoff factor [-]

K ratio of the outer to inner droplet diameter, $K = \frac{d_M}{d_\mu}$, [-]

k_B Boltzman constant [m^2 kg s^{-2} K^{-1}]

l inner droplet crossed distance [m]

l_s average length of surface tails [m] (Table 3)

L dimensionless position [-]

L_{ij} distance between particles i and j [m] (Table 3)

L_{p} permeability coefficient of membrane [m^2 s kg^{-1}]

m mass of the droplet [kg]

n number density [m^{-3}, i.e. per droplet's size]

n_0 total number density of available sites for adsorption (Table 3)

N_{M} total number of the droplets

P escape probability [-]

P_0 permeation coefficient [m s^{-1}]

$Q_{\mathrm{es,M}}$ rate of change in outer droplets volume due to escape of inner droplets [m^3 s^{-1}]

r_i position [m] (Table 3)

r_i^+ upwind ratio of two consecutive solution gradients [-]

R universal gas constant [J K^{-1} mol^{-1}]

R_i random displacement [m] (Table 3)

$\mathfrak{R}_{\mathrm{es,\mu}}$ escape rate of inner droplets [m^{-3} s^{-1}]

$\mathbb{S}$ swelling rate [m^3 s^{-1}]

t time [s]

T temperature [K]

u velocity of the droplet [m s^{-1}]

u_{a} adsorption energy [J] (Table 3)

u_{l} latent energy of interaction between droplets [J] (Table 3)

v volume of the droplet [m^3]

V total volume of the droplets [m^3]

V_{w}^* molar volume of pure water [m^3 mol^{-1}]

z screening constant [-] (Table 3)

Greek letters

α_{cr} volume fraction of the critical region of escape [-]

$\dot{\gamma}$ shear rate [s^{-1}] (Table 3)

ΔP Laplace pressure [Pa]

ε dimensionless energy parameter [-] (Table 3)

ϵ a small number (e.g., $\epsilon = 10^{-10}$) to avoid the division by zero

η viscosity [Pa s]

Θ fraction of occupied sites [-] (Table 3)

Π osmotic pressure [Pa]

σ interfacial tension [N m^{-1}]

τ time spent by an inner droplet on the surface of the outer droplet [s] (Table 3)

Φ flux limiting function [-]

Ω_{es} escape frequency [s^{-1}]

Subscripts

c   circulation (Table 3)

d   drainage (Table 3)

eq   equilibrium

es   escape

i   interaction (Table 3)

in   inner phase

M   outer (or Macro-) droplet

out   outer (external) phase

μ   inner (or micro-) droplet

References

[1]   L. Zeng, Y. Zhang, C. Bukirwa, W. Li, Y. Yang, Study of mean diameter and drop size distribution of emulsion drops in a modified rotating disc contactor for an emulsion liquid membrane system, RSC Advances. 5 (2015) 89959–89970. doi:10.1039/C5RA16267J.

[2]   J. Yan, R. Pal, Isotonic swelling behavior of W/O/W emulsion liquid membranes under agitation conditions, Journal of Membrane Science. 213 (2003) 1–12. doi:10.1016/S0376-7388(02)00501-X.

[3]   R.M. Pfeiffer, A.L. Bunge, W. Navidi, Leakage and Swell in Emulsion Liquid-Membrane Systems: Batch Experiments, Separation Science and Technology. 38 (2003) 519–539. doi:10.1081/SS-120016649.

[4]   S. Mukhopadhyay, S.K. Ghosh, V.A. Juvekar, Mathematical model for swelling in a liquid emulsion membrane system, Desalination. 232 (2008) 110–127. doi:10.1016/j.desal.2008.01.009.

[5]   S. Mataumoto, W.W. Kang, FORMATION AND APPLICATIONS OF MULTIPLE EMULSIONS, Journal of Dispersion Science and Technology. 10 (1989) 455–482. doi:10.1080/01932698908943184.

[6]   N. Jager-Lezer, I. Terrisse, F. Bruneau, S. Tokgoz, L. Ferreira, D. Clausse, M. Seiller, J.-L. Grossiord, Influence of lipophilic surfactant on the release kinetics of water-soluble molecules entrapped in a W/O/W multiple emulsion, Journal of Controlled Release. 45 (1997) 1–13. doi:10.1016/S0168-3659(96)01507-6.

[7]   M. Chávez-Páez, C.M. Quezada, L. Ibarra-Bracamontes, H.O. González-Ochoa, J.L. Arauz-Lara, Coalescence in Double Emulsions, Langmuir. 28 (2012) 5934–5939. doi:10.1021/la205144g.

[8]   W.S.W. Ho, K.K. Sirkar, eds., Membrane Handbook, Springer US, Boston, MA, 1992. doi:10.1007/978-1-4615-3548-5.

[9]   R. Mezzenga, B.M. Folmer, E. Hughes, Design of Double Emulsions by Osmotic Pressure Tailoring, Langmuir. 20 (2004) 3574–3582. doi:10.1021/la036396k.

[10]   T. Schmidts, D. Dobler, C. Nissing, F. Runkel, Influence of hydrophilic surfactants on the properties of multiple W/O/W emulsions, Journal of Colloid and Interface Science. 338 (2009) 184–192. doi:10.1016/j.jcis.2009.06.033.

[11]   A.J. Shere, H.M. Cheung, MODELING OF LEAKAGE IN LIQUID SURFACTANT MEMBRANE SYSTEMS, Chemical Engineering Communications. 68 (1988) 143–164. doi:10.1080/00986448808940403.

[12]   F. Wolf, L. Hecht, H.P. Schuchmann, E.H. Hardy, G. Guthausen, Preparation of W_1/O/W_2 emulsions and droplet size distribution measurements by pulsed-field gradient nuclear magnetic resonance (PFG-NMR) technique, European Journal of Lipid Science and Technology. 111 (2009) 730–742. doi:10.1002/ejlt.200800272.

[13]   A.T. Florence, D. Whitehill, Some features of breakdown in water-in-oil-in-water multiple emulsions, Journal of Colloid and Interface Science. 79 (1981) 243–256. doi:10.1016/0021-9797(81)90066-7.

[14]   K. Pays, J. Giermanska-Kahn, B. Pouligny, J. Bibette, F. Leal-Calderon, Coalescence in Surfactant-Stabilized Double Emulsions, Langmuir. 17 (2001) 7758–7769. doi:10.1021/la010735x.

[15]   S.R. Fowler, E.A. Guggenheim, Statistical thermodynamics, University Press: Cambridge, 1939.

[16]   J.K. Klahn, J.J.M. Janssen, G.E.J. Vaessen, R. de Swart, W.G.M. Agterof, On the escape process during phase inversion of an emulsion, Colloids and Surfaces A: Physicochemical and Engineering Aspects. 210 (2002) 167–181. doi:10.1016/S0927-7757(02)00376-X.

[17] Z. Kang, P. Zhu, T. Kong, L. Wang, A Dewetting Model for Double-Emulsion Droplets, Micromachines. 7 (2016) 196. doi:10.3390/mi7110196.

[18] S. Matsumoto, M. Kohda, The viscosity of W/O/W emulsions: an attempt to estimate the water permeation coefficient of the oil layer from the viscosity changes in diluted systems on aging under osmotic pressure gradients, Journal of Colloid and Interface Science. 73 (1980) 13–20.

[19] S. Matsumoto, T. Inoue, M. Kohda, K. Ikura, Water permeability of oil layers in W/O/W emulsions under osmotic pressure gradients, Journal of Colloid and Interface Science. 77 (1980) 555–563.

[20] S. Matsumoto, P. Sherman, A PRELIMINARY STUDY OF W/O/W EMULSIONS WITH A VIEW TO POSSIBLE FOOD APPLICATIONS, Journal of Texture Studies. 12 (1981) 243–257. doi:10.1111/j.1745-4603.1981.tb01234.x.

[21] O. Kedem, A. Katchalsky, Thermodynamic analysis of the permeability of biological membranes to non-electrolytes, Biochimica et Biophysica Acta. 27 (1958) 229–246.

[22] N. Garti, S. Magdassi, D. Whitehill, Transfer phenomena across the oil phase in water-oil-water multiple emulsions evaluated by Coulter counter: 1. Effect of emulsifier 1 on water permeability, Journal of Colloid and Interface Science. 104 (1985) 587–591.

[23] J. Yan, R. Pal, Osmotic swelling behavior of globules of W/O/W emulsion liquid membranes, Journal of Membrane Science. 190 (2001) 79–91.

[24] J. Bahtz, D.Z. Gunes, E. Hughes, L. Pokorny, F. Riesch, A. Syrbe, P. Fischer, E.J. Windhab, Decoupling of Mass Transport Mechanisms in the Stagewise Swelling of Multiple Emulsions, Langmuir. 31 (2015) 5265–5273. doi:10.1021/acs.langmuir.5b01138.

[25] B. Khadem, N. Sheibat-Othman, Modeling of double emulsions using population balance equations, Chemical Engineering Journal. 366 (2019) 587–597. doi:10.1016/j.cej.2019.02.092.

[26] D. Ramkrishna, A.W. Mahoney, Population balance modeling. Promise for the future, Chemical Engineering Science. 57 (2002) 595–606. doi:10.1016/S0009-2509(01)00386-4.

[27] D. Ramkrishna, Population balances: theory and applications to particulate systems in engineering, Academic Press, San Diego, CA, 2000.

[28] J.R. Pappenheimer, Passage of molecules through capillary walls, Physiological Reviews. 33 (1953) 387–423.

[29] O. Karnland, Bentonite swelling pressure in strong NaCl solutions. Correlation between model calculations and experimentally determined data, Swedish Nuclear Fuel and Waste Management Co., 1997.

[30] T.S.H. Leong, M. Zhou, N. Kukan, M. Ashokkumar, G.J.O. Martin, Preparation of water-in-oil-in-water emulsions by low frequency ultrasound using skim milk and sunflower oil, Food Hydrocolloids. 63 (2017) 685–695. doi:10.1016/j.foodhyd.2016.10.017.

[31] B. Khadem, N. Sheibat-Othman, Modeling stability of double emulsions, in: Computer Aided Chemical Engineering, Elsevier, 2017: pp. 493–498.

[32] S. Qamar, G. Warnecke, Numerical solution of population balance equations for nucleation, growth and aggregation processes, Computers & Chemical Engineering. 31 (2007) 1576–1589.

[33] J. Kumar, G. Warnecke, A note on moment preservation of finite volume schemes for solving growth and aggregation population balance equations, SIAM Journal on Scientific Computing. 32 (2010) 703–713.

[34] B. Van Leer, Towards the ultimate conservative difference scheme. II. Monotonicity and conservation combined in a second-order scheme, Journal of Computational Physics. 14 (1974) 361–370.

[35] S. Matsumoto, Y. Kita, D. Yonezawa, An attempt at preparing water-in-oil-in-water multiple-phase emulsions, Journal of Colloid and Interface Science. 57 (1976) 353–361. doi:10.1016/0021-9797(76)90210-1.

[36] T. Schmidts, D. Dobler, P. Schlupp, C. Nissing, H. Garn, F. Runkel, Development of multiple W/O/W emulsions as dermal carrier system for oligonucleotides: Effect of additives on emulsion stability, International Journal of Pharmaceutics. 398 (2010) 107–113. doi:10.1016/j.ijpharm.2010.07.037.

[37] P. Kent, B.R. Saunders, The Role of Added Electrolyte in the Stabilization of Inverse Emulsions, Journal of Colloid and Interface Science. 242 (2001) 437–442. doi:10.1006/jcis.2001.7792.

[38] F. Michaut, P. Perrin, P. Hébraud, Interface Composition of Multiple Emulsions: Rheology as a Probe, Langmuir. 20 (2004) 8576–8581. doi:10.1021/la048715t.

[39] Theodore Vermeulen, Interfacial area in liquid-liquid and gas-liquid agitation, Chem. Eng. Progr. 51 (1955) 85F-94F.

[40] S. Okazaki, M. Imai, M. Shimizu, Leakage Suppressing Oe W/O Emulsion Using High Viscous Solvent, in: Process Metallurgy, Elsevier, 1992: pp. 1487–1492. doi:10.1016/B978-0-444-88677-4.50064-7.

[41] P. Julian Becker, F. Puel, H.A. Jakobsen, N. Sheibat-Othman, Development of an improved breakage kernel for high dispersed viscosity phase emulsification, Chemical Engineering Science. 109 (2014) 326–338. doi:10.1016/j.ces.2014.02.008.

Chapter 6. PFG-NMR to predict the size of inner droplets

This work was done in collaboration with Dr. Andrew Parrott and Dr. Alison Nordon from the University of Strathclyde, partners of the ModLife project. In this work we develop a procedure to estimate the size distribution of the inner droplets of double emulsions using pulsed field gradient nuclear magnetic resonance (PFG-NMR). The results from PFG-NMR are then compared with the results from the coupled swelling and escape PBM models presented in chapter 5.

Behnam Khadem[a], Andrew Parrott[b], Alison Nordon[b], Nida Sheibat-Othman[a]

[a]Univ Lyon, Université Claude Bernard Lyon 1, CNRS, LAGEP UMR 5007, F-69100, Villeurbanne, France.
[b]West CHEM,Department of Pure and Applied Chemistry and Centre for Process Analytics and Control Technoloy, University of Strathclyde, Glasgow, G11XL, United Kingdom.

6.1. Introduction

The measurement of the inner droplet size distribution, after the preparation of the second emulsion, represents a real challenge. The fact that the inner droplets are encapsulated within the outer droplets makes them difficult to measure by a quantitative method like conventional laser diffraction which will be almost only sensitive to the outer droplets. Also, the inner droplets have a submicronic size, which requires a high resolution in order to observed them by microscopy, which represents though a qualitative measurement. Indeed, optical microscopic visualization is limited to the droplets with sizes bigger than 1 μm for light microscopes and bigger than 750 nm for confocal fluorescence microscopes (CLSM) [1]. CLSM represents one of the methods employed to observe qualitatively the inner droplets with success [81,82,86].

Another method that was proposed to measure the inner droplets is pulsed-field gradient nuclear magnetic resonance (PFG-NMR). This method is based on the molecular displacements due to diffusion that provides the signal attenuation of a specific matter [1–7]. However, this method measures a spectrum that requires a mathematical treatment to predict the droplet size distribution. Three modelling approaches were suggested to treat the measured signal attenuation in order to estimate the size distribution of the inner droplets within double emulsions [1–7], which are short gradient pulse (SGP), Gaussian Phase Distribution (GPD) and block gradient pulse approximation (BGP) [1,8]. These methods were compared and validated by different authors [1–7], all showing an acceptable size estimation. In this section, the Gaussian Phase Distribution (GPD) is selected to predict the inner size distribution of W/O/W double emulsions. The mathematical treatment is extended to the bimodal distribution. The method is employed to estimate the change in the size of inner droplets during storage of a double emulsion prepared with high speed rotor-stator and stored at room temperature. The obtained experimental results by PFG-NMR combined with the GPD mathematical treatment are compared with the results using the swelling model presented in chapter 5.

6.2. Theoretical background

In the GPD approach, which is described by Murday and Cotts [1,9], a Gaussian Phase Distribution is assumed along the time of diffusion with the logarithmic signal attenuation as [1]:

$$\ln\big(E(\delta, g, \Delta, R)\big) = -\frac{2(\gamma g)^2}{D} \sum_{m=1}^{\infty} \frac{\alpha_m^{-4}}{\alpha_m^2\, R^2 - 2} \left\{ 2\delta - \frac{1}{\alpha_m^2\, D}\left(2 + \exp\big(-\alpha_m^2\, D\, (\Delta - \delta)\big) - 2\exp(-\alpha_m^2\, D\, \delta) - 2\exp(-\alpha_m^2\, D\, \Delta) + \exp\big(-\alpha_m^2\, D\, (\Delta + \delta)\big)\right) \right\}$$

<div align="right">6.1</div>

where δ is the gradient pulse duration (s), g the gradient amplitude (T/m), Δ the gradient pulse delay or the diffusion time (s), R the droplet radius (m), γ the gyromagnetic ratio (1/(Ts)), and α_m is the mth roots of the equation $\frac{1}{\alpha R}\, \mathcal{J}_{\frac{3}{2}}(\alpha R) = \mathcal{J}_{\frac{5}{2}}(\alpha R)$ in which $\mathcal{J}_n$ is the nth order Bessel function.

In order to convert the normalized observed NMR signal attenuation – $b(\delta, g, \Delta, R)$ – into a droplet size distribution – $P(R)$ – the following equation is typically used [1,2,8]:

$$b(\delta, g, \Delta, R) = \frac{\int_0^\infty R^3\, P(R)\, E(\delta, g, \Delta, R)\, dR}{\int_0^\infty R^3 P(R)\, dR}$$

<div align="right">6.2</div>

Finally, the size distribution can be described by a logarithmic normal distribution:

$$P(R) = \frac{1}{\sqrt{2\pi}\, R\sigma}\, \exp\left(-\frac{\left(ln\left(\frac{2R}{d_{33}}\right)\right)^2}{2\, \sigma^2}\right)$$

<div align="right">6.3</div>

Where, d_{33} is the volume-weighted geometric mean diameter and σ the standard deviation, which are the fitting parameters when solving equations 6.1–6.3 simultaneously.

6.3. Materials and methods

The materials used to prepare the W/O/W double emulsions are Mineral oil (Fisher Scientific™), Span 80 (Alfa Aesar) as hydrophobic internal emulsifier, Tween 80 (Fisher Scientific™) as hydrophilic external emulsifier, Sodium Chloride as tracer and regulator of osmotic pressure and Millipore water (resistivity $\approx 18.2\ m\,\Omega.cm$).

The primary emulsion – i.e., dispersion of NaCl aqueous solution (wt. = 30 %) in the oil phase having Mineral oil (wt. = 60 %) plus Span 80 (wt. = 10 %) – was produced using ULTRA-TURRAX operating at 12 000 rpm for 4 min. Right after this step, the droplet size of the primary emulsion was measured using Malvern Zetasizer Nano ZS.

In the second step, the double emulsion was prepared by dispersing the primary emulsion (wt. = 10%) into an external aqueous phase (wt. = 89 %) containing Tween 80 (wt. = 1 %) using ULTRA-TURRAX® operating at 3 400 rpm for 4 min. The produced double emulsion was, then, stored at room temperature. Right after preparation and during storage, the outer droplet size was measured using Mastersizer 3000. Right after preparation, the encapsulation efficiency was found to be 29.4 % using conductivity measurements. The NMR measurement was done at the University of Strathclyde. Table 6.1 shows the NMR operating conditions.

Table 6.1. *Values of NMR parameters*

NMR parameter	Value(s)	Unit
Gradient pulse duration	4	ms
Gradient pulse delay and diffusion time	50, 100, 150, 200, 300 and 500	ms
gradient amplitude	12–155	mT/m
Number of steps	16 or 32	-
Number of scans	4 or 8	-

6.4. Results and discussions

The GPD approach as well as the swelling model, presented in chapter 5, are applied to the experiment here and compared.

In Fig. 6.1, the shift of the size distribution of outer droplets to the right side of x-axis indicates that outer droplets grow in size mainly due to swelling as discussed in chapters 4 and 5. The maximum swelling occurred at day 7, after which the outer droplets underwent overswelling-breakdown and, thus, decreased in size (not shown here). It can be seen that, the prediction of the swelling model – using the same values of L_p = 2.75 × 10^{-15} and α_{cr} = 3.6 × 10^{-5} that were identified in chapter 5 – is in good agreement with the experimental measurement, by laser diffraction.
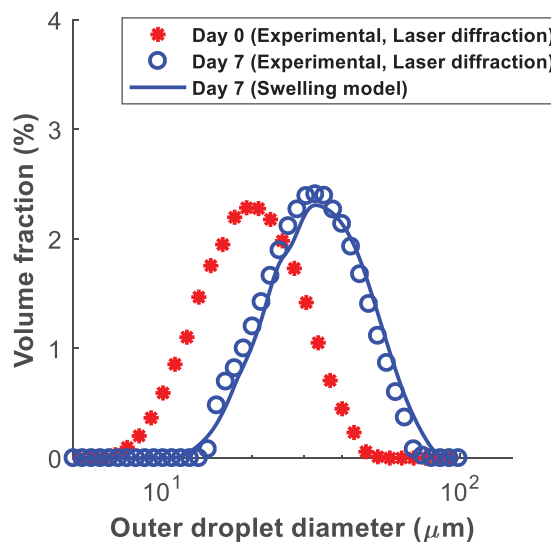

Fig. 6.1. *Evolution of the size distribution of the outer droplets during the first week of storage, for a double emulsion prepared with ϕ_{inner} = 30 % and ϕ_{outer} = 10 %.*

Predictions of the inner droplet size distribution using a monomodal distribution. After one week of storage, which corresponds to the time where the maximum swelling of the outer droplets was observed, the NMR measurement was performed to validate the evolution in the size of the inner droplets observed by the swelling model by employing the GPD approach. Note that NMR measurement can also be checked for day 0, which was not necessary in this

123

work. By using equations 6.1 – 6.3, the signal attenuation from the model was fitted to the measured values. By doing so, σ and d_{33} were identified to be 0.25 and 7.5 µm, respectively.
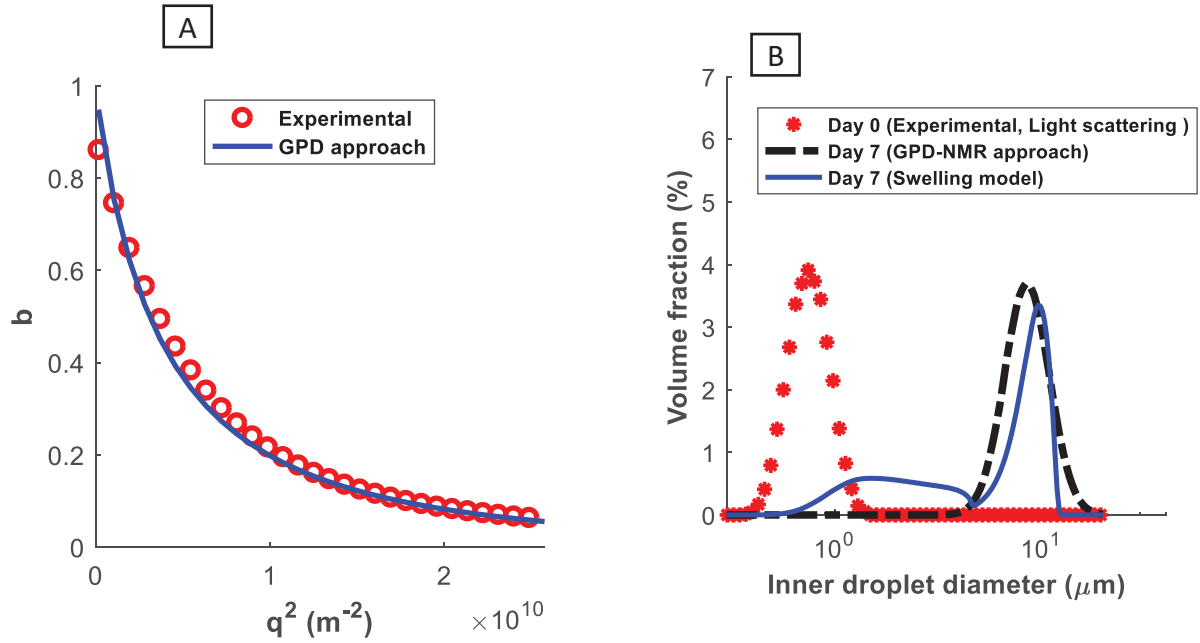

Fig. 6.2. *A) Normalized signal attenuation as a function of $q^2 = (\gamma g \delta)^2$. B) Size distribution of the inner droplets. The double emulsion is prepared with ϕ_{inner} = 30 % and ϕ_{outer} = 10 %. The fit of the GPD approach is done using eq.s 6.1–6.3: σ = 0.25 and d_{33}= 7.5 µm.*

The fit of the model to measurements can be seen in Fig. 6.2A in which quit good fit of the signal attenuation is obtained. The size distribution of the inner droplets is plotted in Fig. 6.2B. It can be seen that the inner droplets have a bi-model distribution, as predicted by the swelling model. This was explained by the fact that part of the droplets stop swelling as they reach the equilibrium between Osmotic pressure gradient and Laplace pressure and only part continues to grow (approximated by the swelling model to be less than 5 % in number of the inner droplets). The GPD approach allows a good prediction of the big population of the inner droplets, which should have a higher impact on the measurement due to their bigger volume fraction. It can be observed that even though the GPD approach does not predict the small ranges of inner droplets, both the swelling model and GPD approach are confirming each other for the part of the distribution belonging to the big sizes. The source of difference between the two predictions can be due to the employment of a monomodal lognormal distribution in the GPD approach, which can only provide one peak while the swelling model predicts two peaks (i.e., a bimodal distribution).

Model improvement - Predictions of the inner droplet size distribution using a bi-modal distribution. The swelling model predicts accurately the outer size distributions, which is also encouraging to believe that the predictions of the inner droplet size distribution is well predicted, as both PBMs are related. However, it appears from the model predictions that the inner droplet size distribution becomes bimodal after one week of storage. Thus, a bimodal distribution (i.e., eq. 6.4) consisting of two lognormal distributions would be better to use instead of eq. 6.3 in order to reconstruct the inner droplet size distribution, as follows:

124

$$P_{Bimodal}(R) = \frac{p_{mixing}}{\sqrt{2\pi}\,R\sigma_1}\exp\left(-\frac{\left(ln\left(\frac{2R}{d_{33,1}}\right)\right)^2}{2\,\sigma_1^2}\right) + \frac{1-p_{mixing}}{\sqrt{2\pi}\,R\sigma_2}\exp\left(-\frac{\left(ln\left(\frac{2R}{d_{33,2}}\right)\right)^2}{2\,\sigma_2^2}\right) \qquad 6.4$$

where p_{mixing} is the is the mixing proportion (between 0 and 1) of each lognormal distribution.

By fitting this model following the GPD approach to the NRM measurements while using equation 6.4 instead of 6.3, the new parameters were identified to be p_{mixing} = 0.96, σ_1 = 0.95, $d_{33,1}$ = 0.45 µm, σ_2 = 0.16, and $d_{33,2}$ = 8.4 µm. As it can be seen in Fig. 6.3, both the fit of the signal attenuation (part A of Fig. 6.3) as well as the prediction of the inner size distribution (part B of Fig. 6.3) are improved and the distribution of the small sizes can be estimated more precisely. The GPD predictions are now in line with the predictions of the swelling model, i.e. bimodal, with a good estimate of both amplitudes. Besides, a better prediction of the amplitude of the big population is obtained compared to Fig. 6.2B that is based on a monomodal distribution.

This strategy was validated for two double emulsions prepared under different conditions (in terms of the internal phase fraction) and similar results were obtained.
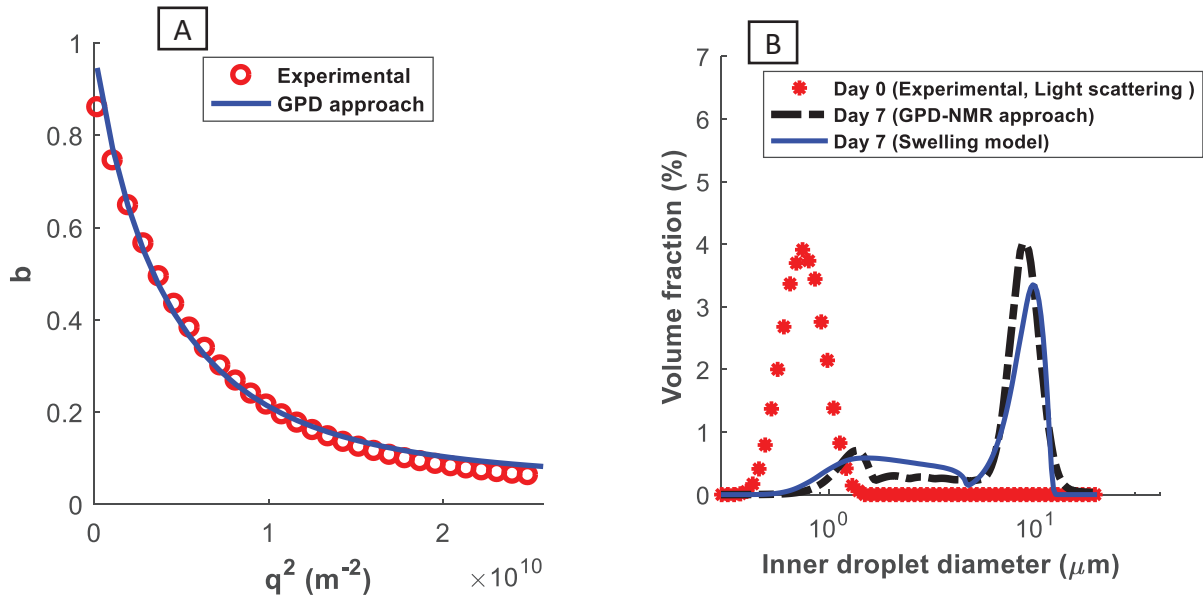

Fig. 6.3. *A) Normalized signal attenuation as a function of $q^2 = (\gamma g\delta)^2$. B) Size distribution of the inner droplets. The double emulsion is prepared with ϕ_{inner} = 20 % and ϕ_{outer} = 10 %. The fit of the GPD approach is done using eqs. 6.1, 6.2, and 6.4: p_{mixing} = 0.96, σ_1 = 0.95, $d_{33,1}$ = 0.45 µm, σ_2 = 0.16, and $d_{33,2}$ = 8.4 µm.*

The swelling model can predict the evolution of the inner DSD over the storage period, where swelling and escape occur, while the direct evaluation of inner DSD found to be a challenge. The proposed methodology thus allows the validation of the swelling model. One of the major parameters used in the swelling model is the interfacial tension of the outer droplets with the internal phase. This parameter governs the Laplace pressure, which is the force that counterbalances the Osmotic pressure gradient. It thus determines the fraction of droplets that continue swelling. However, measuring the interfacial tension of the outer droplets might be subject to error due to combined phases and the use of a mixture of hydrophilic and hydrophobic emulsifiers. Fig. 6.4 shows that when making +/- 20 % of error in the interfacial tension, the population of big inner droplets is not well predicted. The NMR measurement

and the proposed GPD approach thus allow validating the swelling model and the employed parameters.
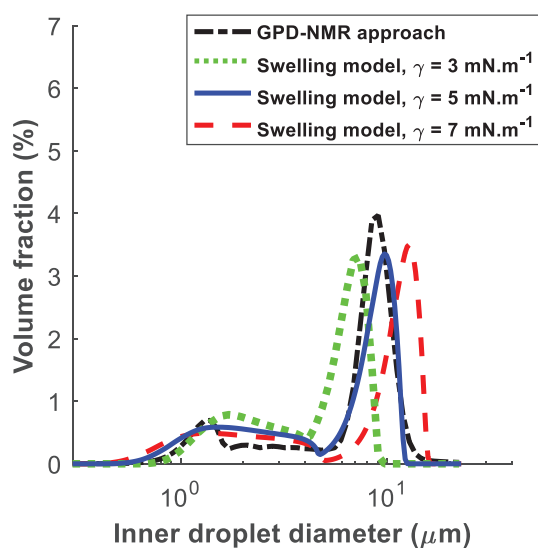

Fig. 6.4. *Effect of interfacial tension (γ) on inner size distribution obtained by swelling model.*

6.5. Conclusions

An attempt was done to estimate the inner droplet size distribution of double emulsions using the PFG-NMR technique while employing the validated existing approach of Gaussian Phase Distribution to NMR parameters. The technique was improved by implementing a bimodal distribution instead of the monomodal distribution. The results, shown here, can pave the way for further investigations in double emulsion systems. An example of which can be a full set of experiments covering the variation of different parameters and their effects on both the swelling model and GPD approach. By doing so, the pros and cons of both models can be more clear leading to improve the inner size determination of double emulsions.

References

[1] F. Wolf, L. Hecht, H.P. Schuchmann, E.H. Hardy, G. Guthausen, Preparation of W$_1$/O/W$_2$ emulsions and droplet size distribution measurements by pulsed-field gradient nuclear magnetic resonance (PFG-NMR) technique, Eur. J. Lipid Sci. Technol. 111 (2009) 730–742. doi:10.1002/ejlt.200800272.

[2] J.P. Hindmarsh, J. Su, J. Flanagan, H. Singh, PFG–NMR Analysis of Intercompartment Exchange and Inner Droplet Size Distribution of W/O/W Emulsions, Langmuir. 21 (2005) 9076–9084. doi:10.1021/la051626b.

[3] X. Guan, K. Hailu, G. Guthausen, F. Wolf, R. Bernewitz, H.P. Schuchmann, PFG-NMR on W1/O/W2-emulsions: Evidence for molecular exchange between water phases, Eur. J. Lipid Sci. Technol. 112 (2010) 828–837. doi:10.1002/ejlt.201000022.

[4] R. Bernewitz, F. Dalitz, K. Köhler, H.P. Schuchmann, G. Guthausen, Characterisation of multiple emulsions by NMR spectroscopy and diffusometry, Microporous Mesoporous Mater. 178 (2013) 69–73. doi:10.1016/j.micromeso.2013.02.049.

[5] R. Bernewitz, U.S. Schmidt, H.P. Schuchmann, G. Guthausen, Structure of and diffusion in O/W/O double emulsions by CLSM and NMR–comparison with W/O/W, Colloids Surf. Physicochem. Eng. Asp. 458 (2014) 10–18. doi:10.1016/j.colsurfa.2014.01.002.

[6] L. Vermeir, P. Sabatino, M. Balcaen, A. Declerck, K. Dewettinck, J.C. Martins, G. Guthausen, P. Van der Meeren, Effect of molecular exchange on water droplet size analysis as determined by diffusion NMR: The W/O/W double emulsion case, J. Colloid Interface Sci. 475 (2016) 57–65. doi:10.1016/j.jcis.2016.04.029.

[7] I. Lönnqvist, B. Håkansson, B. Balinov, O. Söderman, NMR Self-Diffusion Studies of the Water and the Oil Components in a W/O/W Emulsion, J. Colloid Interface Sci. 192 (1997) 66–73. doi:10.1006/jcis.1997.4966.

[8] M.A. Voda, J. van Duynhoven, Characterization of food emulsions by PFG NMR, Trends Food Sci. Technol. 20 (2009) 533–543. doi:10.1016/j.tifs.2009.07.001.

[9] J.S. Murday, Self-Diffusion Coefficient of Liquid Lithium, J. Chem. Phys. 48 (1968) 4938. doi:10.1063/1.1668160.

7. Closing remarks

7.1 Conclusions

The objective of this work was to theoretically investigate the phenomena occurring during the two main stages of double emulsion stability, which are preparation and storage. The evolution of the size and release were taken into account as the key parameters to follow the stability of the system.

7.1.1. Second Step Of Preparation

Different devices operating in different volume scales and turbulent subranges were considered to advance the full development of the models for W/O/W double emulsion system.

Stirred Vessel. Experimental investigation of dilute double emulsions in a 1-L stirred vessel provided the following pivotal points as the bases for model developments:

- Online monitoring of the outer droplets, using *in situ* video probe, verified the results of the laser diffraction technique.

- Higher encapsulation efficiency and bigger outer droplet size were observed when the internal phase was increased showing the alteration of the properties of the outer droplets due to the presence of the inner droplets.

- Bigger outer droplet and higher encapsulation efficiency were found when the salt fraction in the internal phase was increased.

- More stirring rate caused further breakage in the system resulting in smaller outer droplets and lower release rate, which shows that the release and breakage during preparation are interwoven.

Rotor Stator. Since the release during preparation was found to be a direct consequence of the breakage of the outer droplets, the PBM of the outer droplets was combined with the leakage of the inner phase. Breakage as the mutual phenomenon was used to develop an original model of leakage. In addition, the alteration of the viscosity and density of the outer droplets due to the presence of the inner phase was taken into account in order to adopt the breakage and coalescence kernels of the inertial subrange of single emulsions to double emulsions. The model was capable of good estimations of the outer droplet size and encapsulation efficiency, such as the correct account for the internal phase fraction, increasing which make more viscous outer droplets that resist more against breakage. The strong dependency of the leakage to breakage rate (the base of the model development) was precise, since the leakage continues to increase when the breakage and coalescence were at

equilibrium. The correlation of the leakage constant as a function of the salt concentration, which is necessary for systems in different salt ranges, was proposed as well.

Ultrasound Device. Fine inner and outer droplets produced with sonication emulsification allowed the investigation of double emulsion systems in dissipation subrange, where very small droplets are typically formed in order for producing higher quality products. In this subrange, two theoretically developed correlations for droplet size and one proposed model for the leakage, which was connected to size correlations, were investigated. The sub models were found to be of high predicting capability of the experimental results when being incorporated into the general correlations.

The effect of the transitionary state was added originally and found to well predict the experimental results, where smaller outer droplets and higher release were observed by increasing the sonication time of the second step until reaching an equilibrium at which the size did not evolve, but the leakage continues to occur at a constant rate.

The accuracy of the model was further discussed when the oil viscosity was varied. While oil was once the outer phase (i.e., for primary emulsion) and the other time the dispersed phase (i.e., for double emulsion), it caused the formation of both bigger inner and outer droplets.

The original sub model that takes into account the specific effect of the salt concentration for double emulsions, based on the balance of the osmotic and Laplace pressure, showed very precise estimations of bigger outer droplets and lower release for high salt fractions.

The damping effect of the dispersed phase is generally considered in the models of the inertial subrange. While it was missing for the dissipation subrange, by theoretical analogy to inertial subrange, a sub model was developed to accurately predict bigger formed outer droplets with higher encapsulation efficiency for the samples with higher primary emulsion fraction.

7.1.2. Storage

Storage Timeframes. Two periods were observed during the storage of dilute double emulsions. The inner, and thus the outer, droplets were found to swell until a maximum swelling capacity (period one), beyond which the overswelling-breakdown occurs (period 2). During the first period, the release generally occurs via the coalescence of the inner droplets to the external phase. During the second period, the release is mainly due to the breakage of the outer droplets as a consequence of the overswelling. Escape of inner droplets causes the outer droplets to decrease in size. Swelling makes an increase in the sizes of the inner and outer droplets, while overswelling results in the breakage of the outer droplets at the expense of the escape of the inner phase. The smaller real size of the outer droplets in comparison to the expected calculated one (i.e., considering only escape) indicated the occurrence of the breakage of the outer droplets due to overswelling. It was found that breakdown is delayed when the fraction of the primary emulsion is increased, and bigger initial outer droplets swelled more while the breakdown was not delayed.

Modelling The Storage. A coupled population balance model of inner and outer droplets is developed consisting of escape and swelling of inner droplets, both of which cause the change

in the size of the outer droplets. The effect of the Laplace pressure, which was missing in the literature, was taken into account in the swelling model. The escape and swelling models were adjusted over the full distributions. The coupled PBM was validated to the experimental data over the first period of the storage (i.e., before the occurrence of the overswelling-breakdown). The main results can be summarized as follows:

- A slight increase in swelling of inner droplets and a slight decrease in escape was observed when the primary emulsion was increased from 1 to 4%.

- Higher salt fraction causes more swelling and less escape rate.

- Inner droplets were found to be slightly more swollen when the inner phase was higher.

The coupled PBM of inner and outer droplets showed a high capability for the accurate predictions of the size and encapsulation efficiency.

Finally, the size estimation of the inner droplets using PFG-NMR was improved by using a bimodal distribution instead of the monomodal one in GPD approach.

7.2 Perspectives

Despite the long history behind the investigations of double emulsions, the theoretical investigations, which are of high importance, were among minorities. In this thesis, an attempt was done to model the main phenomena of the system that can lay the foundations for further investigations in double emulsion processes.

Some suggestions that can be considered are listed below:

- Adoptation of the proposed models of preparation to continuous emulsification systems (e.g., static mixers). In such systems, the energy dissipation is more uniform than in stirred vessels and is much higher, with a much shorter preparation time (of the order of seconds)

- Developing one sole PBM of outer droplets, for the system during preparation, including the concentration of the inner phase and the size of the outer droplets as two coordinates over time. This approach can be useful to model the preparation step where the inner droplets do not evolve in size, and only their number changes (by escape). This allows outer droplets of different size to have different concentrations of inner droplets, which is not the case in the approach of the present work. However, the one bi-variate PBM approach does not allow to predict the increase in the size of inner droplets by swelling during storage.

- Developing a PBM model for ultrasonication using breakage and coalescence kernels that are valid within the dissipative subrange of turbulence.

- Coupling the kernels (or the mean diameter correlations) of the inertial subrange with those of the dissipation subrange to accurately predict the droplet size when both subranges can be found within the distribution. Indeed, as shown in the Overview, part of the droplets fall within the dissipation subrange. This can be done by using the full spectrum of turbulence [1].

- Investigating the effect of the inner droplet size on the rheological properties of the outer droplets, such as viscosity. Only the inner droplet fraction was accounted for in this work.

- Developing a breakage kernel for the outer droplets undergoing overswelling-breakdown in order to predict their final size distribution. The leakage due to overswelling-breakdown can then be modeled implementing the same leakage model proposed in the third chapter of this thesis.

- Developing the model of the dependency of the permeability coefficient on time over the initial stage of swelling phenomenon.

- Monitoring the motion of a single droplet of double emulsion using high speed camera. This may give insight into the breakage, swelling and coalescence phenomena of double emulsions.

- Developing a model of the escape probability based on the film drainage theory, considering the driving and resistance forces of escape (presented in chapter 6) in the equation of the drainage rate and the adsorption force between inner and outer droplets to determine the contact time.

- Modelling the motion of inner droplets, when outer droplets are under turbulent flow regime, in order to find the possible coalescence rates between inner droplets in systems where inner-inner coalescence is not negligible.

- Improving the escape model by accounting for the effect of the salt on either the escape frequency or the volume fraction of the critical region.

- Model-based experimental analysis of double emulsion during preparation.

- Sensitivity analysis and parameter identification of the proposed models of double emulsion in order to test the validity of the identified parameters and the robustness of the model leading to generalize the models.

References

[1] S. Carrillo De Hert, T.L. Rodgers, On the steady-state drop size distribution in stirred vessels. Part II: Effect of continuous phase viscosity, AIChE J. (2018).

Appendices

Three appendices are presented consisting of further investigations, which are listed below:

Appendix 1. Modelling Pure Escape In A Silicone Oil Double Emulsion.

Appendix 2. An Analytical Solution To Dewetting Model.

Appendix 3. Model-Based Experimental Analysis Of Double Emulsion During Preparation

Appendix 1. Modelling pure escape in a silicone oil double emulsion

This work is regarding the escape of inner droplets to the external phase during the storage of W/O/W double emulsions prepared using different viscosities of silicon oil in a rotor-stator system. The difference with respect to chapter 5 is that here only the escape model is developed without a need of PBM, so the model can only predict the release rate with time (via the number of inner droplets). In chapter 5, the model also predicts the swelling of inner and outer droplets, therefore 2 PBMs were coupled. Second, we use silicone oil here while mineral oil was used in chapter 6. The two systems, mineral oil and silicone oil differ in terms of viscosities, densities and surface tension. For instance the viscosity of the used mineral oil is 45 mPa.s while the viscosity of the silicon oils are 50, 100 and 350 mPa.s. Therefore, bigger droplets are obtained here and they appear to be more stable. Indeed, a slight release is observed over the first week, then equilibrium is reached.

Behnam Khadem[a], Nida Sheibat-Othman[a]

[a]Univ Lyon, Université Claude Bernard Lyon 1, CNRS, LAGEP UMR 5007, F-69100, Villeurbanne, France

Double emulsions are of high potential for drug delivery of active ingredients. They consist of small droplets of one fluid suspended in larger droplets of a second immiscible fluid. The product properties in double emulsions are governed by the droplet size distribution (DSD) of both the internal and external emulsions. During storage, the internal emulsion can undergo coalescence, Ostwald ripening (leading to increase in inner droplet size) and droplet escape (leading to mass transfer to the external phase). The external DSD may evolve due to external droplet coalescence and Oswald ripening. In this work, droplet escape from the inner emulsion to the external continuous phase is investigated experimentally and theoretically. The escape rate is monitored by conductivity measurements, after encapsulating salt in the inner emulsion. A model is proposed to describe the escape rate based on dewetting phenomena.

Keywords: Double emulsion, escape rate, modeling, droplet size distribution.

A1.1. Introduction

Predicting the escape rate requires the estimation of: i) the frequency of escape as well as ii) the region concerned by the escape phenomena at any time. In the literature, either the first or the second parameter is usually theoretically modeled, and the second is fitted to experimental data. For instance, Klahn et al. [1] proposed a model for the escape during the preparation of a double emulsion in a simple shear device. The escape frequency was theoretical and the critical region was a correlation derived by fitting with experimental

results. Pays et al. [2] proposed a model to predict escape from internal droplets during storage. Their model estimates the critical region of escape based on the energy for adsorption using the model of Fowler and Guggenheim [3]. They fitted the frequency of escape in order to make the model match their experimental data. Another escape model was proposed by Chávez-Páez et al. [4]. They predicted the critical region based on 3D simulations of Brownian motion of the internal droplets. They indicated the necessity to estimate the probability of escape based on surface properties and by fitting it to experimental data. Kang et al. [5] recently proposed a model to calculate the dewetting time in double emulsions by considering Stokes flow, momentum conservation of the internal droplet and the globule as well as energy conservation. This dewetting time is equivalent to the escape time and thus allows calculating the escape frequency.

The objective of this work is to propose a model to predict droplet escape in double emulsions during storage for different conditions: viscosity of the oil phase and size of the internal droplets and external globules. The method proposed by Kang et al. [5] was employed to calculate the escape frequency. The critical region was fitted to experimental results. A comparable recipe as the one proposed by Schmidts et al. [6] was used.

A1.2. Model

Internal droplet may only escape from a critical region, α_{cr}, surrounding the surface of the globule. The change in the number of internal droplets (n_μ) with time is thus proportional to n_μ^{cr}, times the escape frequency (Ω_{es}) as follows:

$$\frac{dn_\mu}{dt} = \frac{dn_\mu^{cr}}{dt} = -\Omega_{es}\, n_\mu^{cr} \qquad\qquad \text{A1.1}$$

Where n_μ^{cr} is the number of droplets in the critical region from which the droplets can escape (coalesce with external aqueous phase). As $n_\mu^{cr} = \alpha_{cr}\, n_\mu$, the solution of eq A1.1 is:

$$n_\mu^{cr} = \alpha_{cr}\, n_{\mu 0} e^{-\alpha_{cr}\, \Omega_{es}\, t} \qquad\qquad \text{A1.2}$$

Where $n_{\mu 0}$ is the initial number of internal droplets.

The dewetting model of [5] was used to calculate the escape frequency ($\Omega_{es} = \frac{1}{t_{dewetting}}$) as follows:

$$t_{dewetting} = \int_{0.01}^{L_{eq}} \frac{1}{u_\mu + u_M}\, dL \qquad\qquad \text{A1.3}$$

Where $L = l/R_\mu$, R_μ is the internal droplet radius, l is the distance that the internal droplet travels during the dewetting process, and u_μ and u_M are the velocities of the internal droplet and the globule, respectively. These velocities are calculated based on momentum conservation of the inner and outer phase ($m_\mu u_\mu = m_M u_M$) as follows:

$$\int_0^{L_{eq}} (F_S - F_V) dL = \frac{1}{2} m_\mu u_\mu^2 + \frac{1}{2} m_M u_M^2 \qquad\qquad \text{A1.4}$$

With

$$F_\text{V} = 3\pi\eta_\text{M}u_\mu R_\mu \left(1 + \frac{1}{\frac{\rho_\text{M}}{\rho_\mu}\left(\frac{R_\text{M}}{R_\mu}\right)^3}\right)(2-L) \qquad\qquad \text{A1.5}$$

$$F_\text{S} = 2\pi\sigma_{\mu,\text{M}}R_\mu L(2-L)\left(1 - \frac{\sigma_{\mu,\text{out}}}{\sigma_{\mu,\text{M}}} + \frac{\sigma_{\text{M,out}}}{\sigma_{\mu,\text{M}}}\frac{1}{K}\right) \qquad\qquad \text{A1.6}$$

Where $\sigma_{\mu,\text{M}}$ is the interfacial tension between the internal droplets and the continuous phase in the primary emulsion (i.e., the oil phase), "out" stands for the external water, η_M is the viscosity of globules, ρ_M is the globule density, ρ_μ is the inner phase density, $K = 0.5\left(8(R_\text{M}/R_\mu)^3 + 8 - 6L^2 + 2L^3\right)^{1/3}$, and L_{eq}, which is the equilibrium value of L, is obtained by Gibbs energy as:

$$\frac{1}{2}\left[\frac{L^2-2L}{K} + \frac{L^2-2L+4KL-4K}{2\sqrt{K^2-2L+L^2}} + \frac{(L^2-2L)\sqrt{K^2-2L+L^2}}{2K^2}\right] = \frac{\sigma_{\mu,\text{M}}-\sigma_{\mu,\text{out}}}{\sigma_{\text{M,out}}} \qquad \text{A1.7}$$

A1.3. Emulsion preparation

Double emulsions were produced in two steps (Table A1.1). First, the NaCl solution was dispersed in the oil phase—consisting of oil with some Span 80—and mixed with Ultra-Turrax at 12000 rpm for 4 min. The size of the internal droplet was measured by means of dynamic light scattering. In the second step, this primary emulsion was dispersed in an external aqueous phase—consisting of deionized water with some Tween 80—by mixing with Ultra-Turrax at 3200 rpm for 8, 10, 12, and 14 min. The size of the globules was measured by laser diffraction (Mastersizer 3000, Malvern Instruments Ltd.) and the released amount of salt was measured by conductivity over one month storage at ambient temperature. The double was observed by an optical microscope, Leica DM2000 LED.

Two parameters were investigated: the viscosity of silicone oil (50, 100 and 350 mPa.s) and the effect of the size off the globules, which was varied by varying the mixing time of the second preparation step (8, 12 and 14 min). In this second series, the oil viscosity was 50 mPa.s. It is worthy to mention that by following the DSD of a single O/W emulsion similar to the double emulsions composition, the physical stability of globules has been confirmed over the storage time. This indicates that the evolution of the DSD in the case of double emulsions can be attributed only to escape of the internal droplets.

Table A1.1. *Composition of double emulsions in volume percent*

Ingredient	Role	Volume fraction
0.02 M NaCl Solution	Internal aqueous phase	4%
Silicon Oil (50, 100 and 350 $mPa.s$)	Oil	4.5%
Span 80	Lipophilic surfactant	1.5%
Deionized water	External aqueous phase	89.5%
Tween 80	Hydrophilic surfactant	0.5%

A1.4. Results and Discussion

Fig. A1.1a shows the DSD of the internal droplets (measured before the preparation of 2$^\text{nd}$ emulsion). The oils (thus the continuous phase) with viscosities of 50 and 100 mPa.s give

similar inner droplets, while the oil with 350 mPa.s leads to smaller inner water droplets. An image of the double emulsion can be seen on Fig. A1.1b that validates the formation of the double emulsion, and confirms the measured inner droplet size. Fig. A1.2 shows the globule size distribution. It can be seen that similar DSD were obtained in the experiments with different oil viscosity (Fig. A1.2a), showing a negligible effect on the globule size for the considered viscosity range. Fig. A1.2b shows that when increasing the mixing time of the external emulsion a slight decrease in the globule size occurs, which agrees with the expectations.
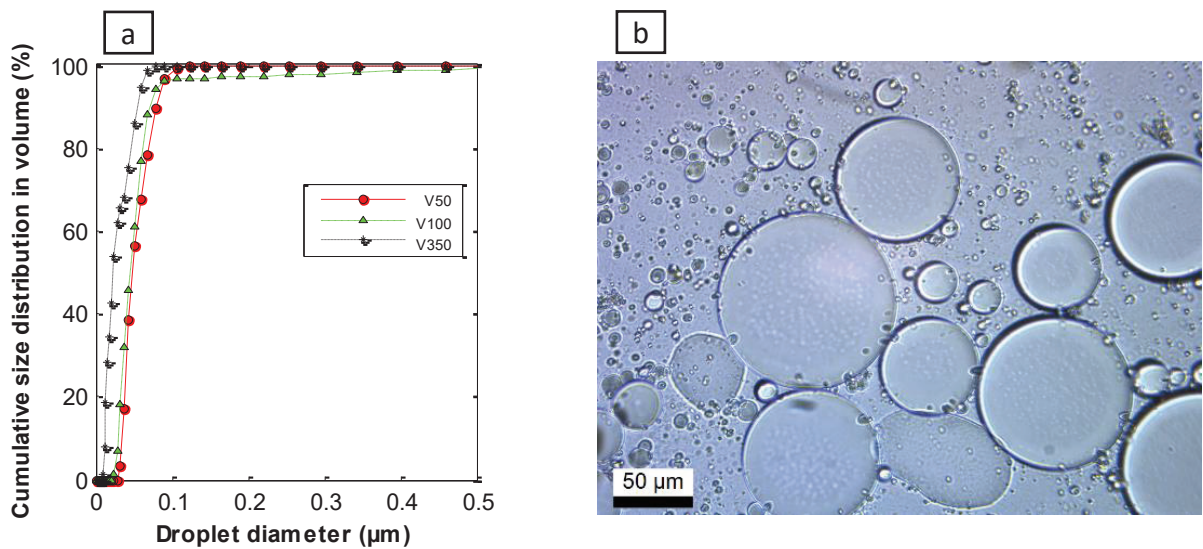

Fig. A.1.1. *a) Cumulative size distribution of internal water droplets prepared into silicone oil with different viscosities (initial, right after the second preparation step). b) An image of the double emulsion using a microscope (right after the second preparation step).*
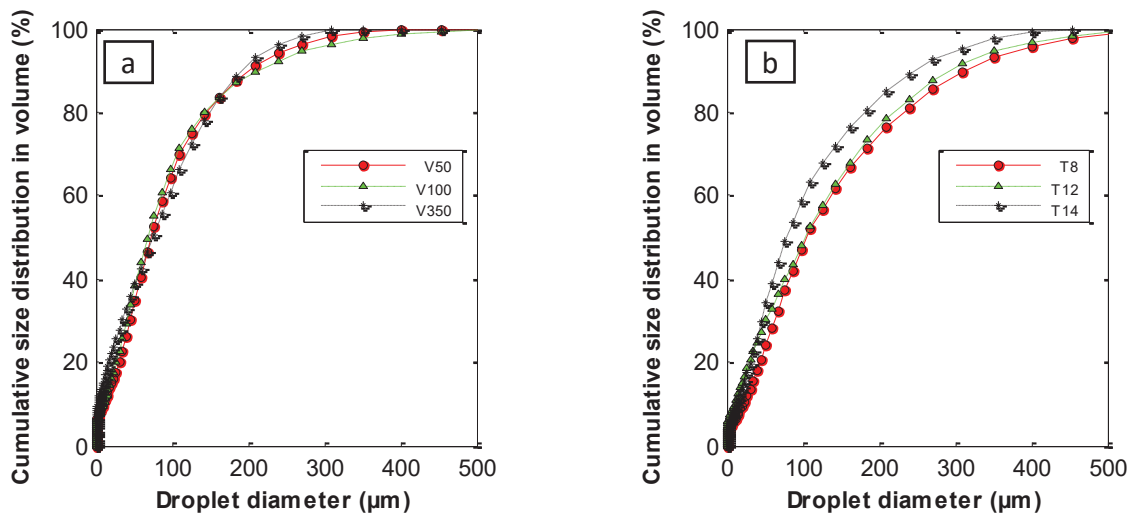

Fig. A1.2. *Size distribution of globules* (initial, right after the second preparation step) *for: (a) Different viscosities of silicone oil. (b) Different mixing time of the second emulsin globule size (using V50).*

The modelling results of the escape rate with time are shown in Fig. A1.3 and Table A1.2. First of all, the dewetting time was calculated using the model proposed above for the specific emulsion properties underhand (droplet size, viscosity). The results are shown in Table A1.2.

It can be seen that increasing the oil viscosity decreases the escape frequency. This result can be explained by the slower film drainage in a more viscous phase, which is coherent. For the experiments realized at different mixing times, similar escape frequencies were obtained. In the dewetting model, increasing the globule size generally leads to a decrease in the escape frequency until a specific limit where the globule size has a negligible effect on Ω_{es}. In the experiments underhand, the obtained globules are big, and the effect of their size on Ω_{es} becomes negligible.

Table A1.2. *Fitted values of f_e and α_{cr} for different viscosities and different globule sizes*

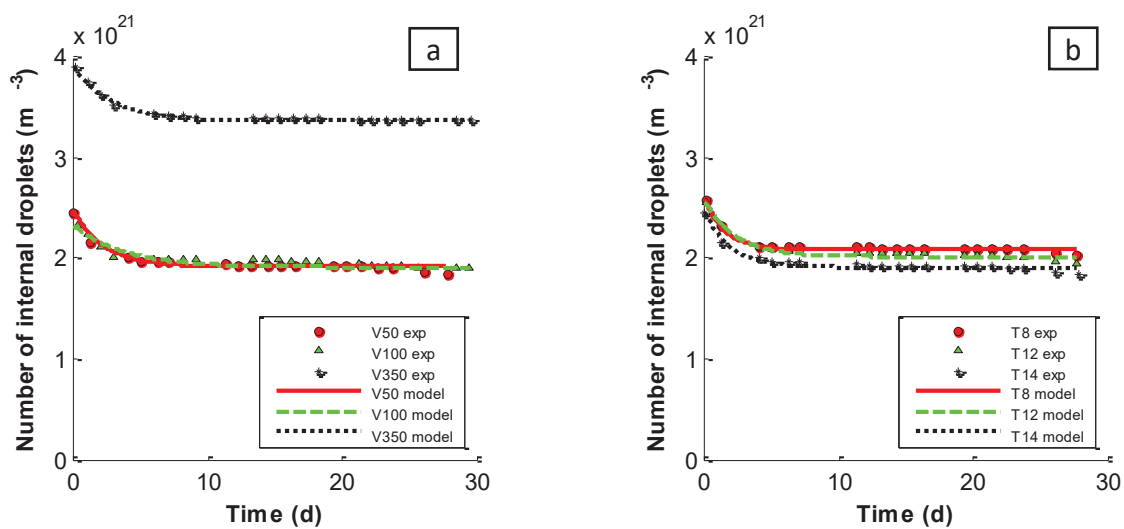| Experiment	V50	V100	V350	T8	T12	T14
Ω_{es} $(s^{-1}) \times 10^4$	15	12	6	15	15	15
α_{cr} $(-) \times 10^4$	42	26	65	47	42	39

Fig. A1.3. *Reduction in number of internal droplets during storage of double emulsions with: (a) Different silicone oils. (b) Different mixing time (with V50).*

In a second step, the estimated frequencies were used in the escape model to predict the critical region concerned by the escape phenomena. Fig. A1.3 shows the fitting results of the model compared to experimental data, and Table A1.2 shows the fitted values of α_{cr}.

Fig. A1.3a shows the effect of the oil viscosity. As the oil V350 led to smaller inner droplets, their number is higher than V50 and V100 that give similar initial droplet number. Also, the experimental results seem to reach a plateau indicating that the release regime slows down after a first burst effect. The final released amount was estimated from the plateau of the experimental release curve over 30 days, and was used as an input to the model. A different slope might be required for the following periods. Over the first 30 days, a good fitting of the model can be observed. Concerning the values of α_{cr} obtained for this series of experiments, it does not follow a specific tendency. However, the global release rate was comparable for the different oil viscosities.

Fig. A1.3b shows the effect of the globule size (or mixing time of the external emulsion). It can be seen that the initial inner droplet number is similar for all experiments, as the same oil was used, thus leading to similar inner droplet size. Thereafter, it can be seen that the release was

faster for the smaller globules. This is due to the larger contact surface area between the globules and the external continuous phase. Similar results were experimentally observed by [7]. Concerning α_{cr} obtained for this series of experiments, it slightly decreases with the droplet size. This is contradictory to the results obtained by [1]. However, the differences between the identified values are very small, and may be considered to be comparable.

A1.5. Conclusion

A model was proposed to predict the escape rate of internal droplets from double emulsions and to describe the long-term stability of the emulsion. The escape frequency was found to decrease with the oil viscosity and not to be affected by the globule size for the range of sizes considered in the present paper. The identified critical region concerned by the escape phenomena was not found to be affected by the viscosity and to slightly decrease with the globule size. α_{cr} is the only parameter that still needs to be fitted with experimental data. An empirical correlation can be proposed to avoid the fitting step, which requires realising a bigger number of experiments under various conditions in order to predict a comprehensive correlation.

References

[1]   J.K. Klahn, J.J.M. Janssen, G.E.J. Vaessen, R. de Swart, W.G.M. Agterof, On the escape process during phase inversion of an emulsion, Colloids Surf. Physicochem. Eng. Asp. 210 (2002) 167–181. doi:10.1016/S0927-7757(02)00376-X.

[2]   K. Pays, J. Giermanska-Kahn, B. Pouligny, J. Bibette, F. Leal-Calderon, Coalescence in Surfactant-Stabilized Double Emulsions, Langmuir. 17 (2001) 7758–7769. doi:10.1021/la010735x.

[3]   S.R. Fowler, E.A. Guggenheim, Statistical thermodynamics, University Press: Cambridge, 1939.

[4]   M. Chávez-Páez, C.M. Quezada, L. Ibarra-Bracamontes, H.O. González-Ochoa, J.L. Arauz-Lara, Coalescence in Double Emulsions, Langmuir. 28 (2012) 5934–5939. doi:10.1021/la205144g.

[5]   Z. Kang, P. Zhu, T. Kong, L. Wang, A Dewetting Model for Double-Emulsion Droplets, Micromachines. 7 (2016) 196. doi:10.3390/mi7110196.

[6]   T. Schmidts, D. Dobler, C. Nissing, F. Runkel, Influence of hydrophilic surfactants on the properties of multiple W/O/W emulsions, J. Colloid Interface Sci. 338 (2009) 184–192. doi:10.1016/j.jcis.2009.06.033.

[7]   A. Schuch, P. Deiters, J. Henne, K. Köhler, H.P. Schuchmann, Production of W/O/W (water-in-oil-in-water) multiple emulsions: droplet breakup and release of water, J. Colloid Interface Sci. 402 (2013) 157–164. doi:10.1016/j.jcis.2013.03.066.

Appendix 2. An analytical solution of the dewetting model

The procedure to determine the escape time based on the analytical solution of the dewetting model of Kang et al. [1] is presented here, and a comparison with a numerical resolution by iteration is shown.

A2.1. Analytical solution

The aim is to analytically solve the integration below (copied from chapter 5):

$$\int_0^L \left[F_S(v_\mu, v_M) - F_V(v_\mu, v_M)\right]dL = \frac{1}{2}m_\mu u_\mu^2(v_\mu) + \frac{1}{2}m_M u_M^2(v_M) \qquad \text{A2.1}$$

Where F_S and F_V are the driving force of separation and the resistance force to escape respectively, which are defined by Kang et al. [1] as:

$$F_S(v_\mu, v_M) = \pi \, d_\mu \, L(2 - L)\sigma_{\mu,M}\left(1 - \frac{\sigma_{\mu,out}}{\sigma_{\mu,M}} + \frac{\sigma_{M,out}}{\sigma_{\mu,M}}\frac{1}{K}\right) \qquad \text{A2.2}$$

$$F_V(v_\mu, v_M) = \frac{3}{2}\pi \, d_\mu \eta_M \left[u_\mu(v_\mu) + u_M(v_M)\right](2 - L) \qquad \text{A2.3}$$

Where $K = \frac{d_M}{d_\mu}$.

From the momentum conservation of inner and outer droplets (eq. A2.1) the velocity of outer droplets can be considered to be: $u_M(v_M) = \frac{m_\mu}{m_M} u_\mu(v_\mu)$.

By writing $\bar{a} = \pi \, d_\mu \sigma_{\mu,M}\left(1 - \frac{\sigma_{\mu,out}}{\sigma_{\mu,M}} + \frac{\sigma_{M,out}}{\sigma_{\mu,M}}\frac{1}{K}\right)$ in F_S (eq. A2.2), it becomes:

$$F_S(v_\mu, v_M) = 2\bar{a}\, L - \bar{a}\, L^2 \qquad \text{A2.4}$$

Similarly by writing $\bar{b} = \frac{3}{2}\pi \, d_\mu \eta_M \left[1 + \frac{m_\mu}{m_M}\right]$ in F_V (eq. A2.3) while using $u_M(v_M) = \frac{m_\mu}{m_M} u_\mu(v_\mu)$ gives:

$$F_V(v_\mu, v_M) = 2\bar{b}\, u_\mu - \bar{b}\, L\, u_\mu \text{ s} \qquad \text{A2.5}$$

Substituting u_M as well as eqs. A2.4 and A2.5 into eq. A2.1, one can write:

$$\int_0^L \left[4\bar{a}\, L - 2\bar{a}\, L^2 - 4\bar{b}\, u_\mu + 2\bar{b}\, L\, u_\mu\right]dL = \left(m_\mu + \frac{m_\mu^2}{m_M}\right) u_\mu^2(v_\mu) \qquad \text{A2.6}$$

Integrating over L gives:

$$2\bar{a}\, L^2 - 2\bar{a}\frac{L^3}{3} - 4\bar{b}\, u_\mu L + \bar{b}\, L^2\, u_\mu = \left(m_\mu + \frac{m_\mu^2}{m_M}\right) u_\mu^2(v_\mu) \qquad \text{A2.7}$$

Regrouping the coefficients over u_μ leads to the following equation:

$$\underbrace{\left(m_\mu + \frac{m_\mu^2}{m_M}\right)}_{\bar{A}} u_\mu^2(v_\mu) + \underbrace{\left(\bar{b}\, L^2 - 4\bar{b}\, L\right)}_{\bar{B}} u_\mu + \underbrace{2\bar{a}\, L^2 - 2\bar{a}\frac{L^3}{3}}_{\bar{C}} = 0 \qquad \text{A2.8}$$

Eq. A2.8 is a quadratic equation of the form $\bar{A}\, u_\mu^2(v_\mu) + \bar{B}\, u_\mu + \bar{C} = 0$, which can be solved employing the "roots" function in MatLab. Using the positive root of this equation (u_μ) in

$u_\mathrm{M}(v_\mathrm{M}) = \frac{m_\mu}{m_\mathrm{M}} u_\mu(v_\mu)$, the velocities of inner and outer droplets can be determined, and so the dewetting or escape time, t_es, and the escape frequency $\Omega_\mathrm{es} = 1/t_\mathrm{es}$.

The abovementioned procedure is valid when $\frac{d_\mathrm{M}}{d_\mu} \approx \frac{d_\mathrm{M}^0}{d_\mu}$, where d_M^0 is the outer droplet diameter before the separation (or escape). The numerical solution showed that when $d_\mu \ll d_\mathrm{M}$ then $\frac{d_\mathrm{M}}{d_\mu}$ is close to $\frac{d_\mathrm{M}^0}{d_\mu}$. This relation is defined by Kang et al. [1] as:

$$K = \frac{d_\mathrm{M}}{d_\mu} = 0.5 \left[8 \left(\frac{d_\mathrm{M}^0}{d_\mu} \right)^3 + 8 - 6L^2 + 2L^3 \right]^{1/3} \qquad \text{A2.9}$$

Indeed, $8 \left(\frac{d_\mathrm{M}^0}{d_\mu} \right)^3$ is of the order of $O(10^5)$ and $(8 - 6L^2 + 2L^3)$ is of the order of $O(10^0)$ that makes a negligible change in the value of $\frac{d_\mathrm{M}}{d_\mu}$. Thus, it can safely be assumed that $K \approx \frac{d_\mathrm{M}^0}{d_\mu}$, so independent of L which allows to solve the equation analytically.

Fig. A2.1 shows a comparison between the analytical and numerical solutions for two different conditions. It can be seen that the analytical solution is in good agreement with the numerical one. Thus, the analytical solution that has the advantage of faster simulation is used in this work.
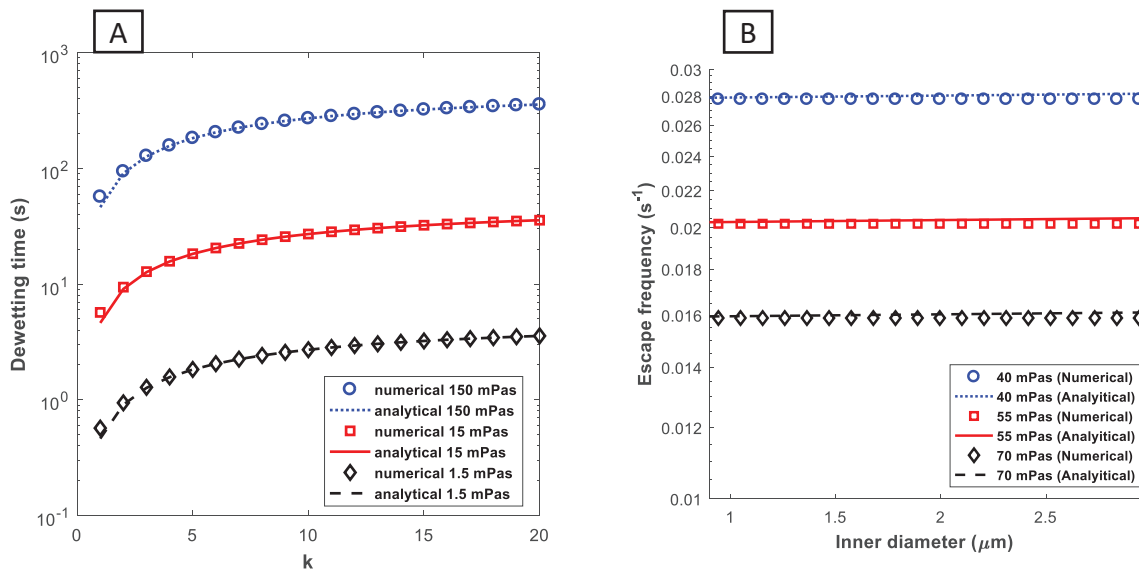

Fig. A2. 1. *Comparison between analytical and numerical solutions. A) d_μ = 0.1 mm, $k = \frac{d_M^0}{d_\mu}$, $\sigma_{\mu,M}$ = 15.4 mN.m^{-1}, $\frac{\sigma_{\mu,out}}{\sigma_{\mu,M}}$ = 0.916, $\frac{\sigma_{M,out}}{\sigma_{\mu,M}}$ = 0.779, ρ_μ = 1020 kg.m^{-3}, and ρ_M = 816 kg.m^{-3}. B) d_M = 200 μm, $\sigma_{\mu,M}$ = 5 mN.m^{-1}, $\frac{\sigma_{\mu,out}}{\sigma_{\mu,M}}$ = 0, $\frac{\sigma_{M,out}}{\sigma_{\mu,M}}$ = 1, ρ_μ = 1000 kg.m^{-3}, and ρ_M = 850 kg.m^{-3}.*

Reference

[1]   Z. Kang, P. Zhu, T. Kong, L. Wang, A Dewetting Model for Double-Emulsion Droplets, Micromachines. 7 (2016) 196. doi:10.3390/mi7110196.

Appendix 3. Model-based experimental analysis of double emulsion during preparation

Behnam Khadem[a], Adel Mhamdi [b], Eduardo Schultz [b], Nida Sheibat-Othman[*a]

[a]Univ Lyon, Université Claude Bernard Lyon 1, CNRS, LAGEP UMR 5007, F-69100, Villeurbanne, France.
[b] AVT-Process Systems Engineering, RWTH Aachen University, D-52064 Aachen, Germany.

This appendix presents a short description of the work done during one month of secondment at RWTH Aachen University to collaborate with Eduardo Schultz (MSc.) and Dr.-Ing. Adel Mhamdi. In this work, it is aimed to apply the model of double emulsion preparation – presented in chapter 3 – within a dynamic optimization strategy to determine the ideal operating conditions that ensure the desired product quality. Since the model presented in chapter 3 is valid over a wide range of experimental data (i.e., effects of the emulsification time and energy and fractions of inner phase and/or salt), it can be used to predict the optimal conditions required to produce the desired product. The quality of the double emulsion was defined as the encapsulation rate (to be maximized) and the outer droplet size (to be minimized in order to ensure the physical stability of the double emulsion during storage). The operating conditions that may be manipulated to control these outputs were defined as the mixing energy and time, the internal phase fraction and the salt concentration.

To do so, a dynamic optimization procedure, the package of the functions of which is provided by RWTH Aachen University, was considered. In order to employ the combined PBM of outer droplets and leakage model into the mentioned package, it was required to, firstly, transform and validate the model to Modelica programming language. The objective function of the optimization is to minimize the size of outer droplets while maximizing the encapsulation efficiency, which are both critical in qualifying the final product quality and stability. This is done by manipulating the control inputs (i.e. the mixing energy and time, the internal phase fraction and the salt concentration). This secondment has thus put the basis of the optimization strategy of this system.

The full optimization of the model and its experimental validation is a promising work that is worthy to continue, which is of interest for food, cosmetics and pharmaceutical industries. Other investigations were also discussed with Aachen or DTU, partners of the ModLife project, regarding sensitivity analysis (necessary to ensure the validity of the identified parameters and to develop a generalized model) and model-based experimental analysis, which represent a good to continue.